HIGH ANGULAR RESOLUTION STUDIES OF PROTOPLANETARY DISCS

HIGH ANGULAR RESOLUTION STUDIES

OF PROTOPLANETARY DISCS

Proefschrift

Promotiecommissie

Promotor: Prof. dr. E.F. van Dishoeck

Co-promotor: Dr. M. R. Hogerheijde

Overige leden: Dr. I. Kamp   (Rijksuniversiteit Groningen)
                      Prof. dr. K. Kuijken
                      Prof. dr. A. I. Sargent   (California Institute of Technology)
                      Prof. dr. A. G. G. M. Tielens
                      Dr. D. Wilner (Harvard-Smithsonian Center for Astrophysics)

The great use of life is to spend it for something that will outlast it.
WILLIAM JAMES

Contents

CHAPTER 1

Introduction

THROUGHOUT our lives, we unknowingly observe the final stage of circumstellar disc evolution: our planet orbiting the Sun. The origin of planets and the uniqueness of Earth have been the motivation to explore beyond the Solar system and into our Milky Way Galaxy, which we can see stretched across a cloudless night sky. In the youngest regions of the Galaxy, where stars like our Sun are being born, we look for answers to how the planets, gaseous giants like Jupiter or small rocky planets like Earth, form. It is in these star-forming regions that we find evidence that the planets of the Solar system all formed in a single disc of gas and dust, extending from near the central star to hundreds of times the Earth orbit. This thesis relies on data from instruments often used in the media as examples of human technological achievement: interferometric arrays of antennas operating in the submillimetre wavelength regime (Figure 1.1), that are able to observe the structure of young proto-planetary discs hundreds of light years away. It focuses on constraining the mass of dust and gas that discs are made of, and how this material is distributed from the star outwards. The underlying physics that is studied in this thesis touches on processes of direct interest to planet formation: dust grain growth and migration, gas dispersal, as well as on the presence of planets or other bodies within these discs suggested by disc asymmetry. Future instruments, in particular the Atacama Large Millimeter Array, consisting of 66 antennas at 5000 m elevation in the Chilean Andes and being built through a joint worldwide effort including Europe, will allow a major leap forward in our understanding of discs and how planets are formed within them.

Figure 1.1: Submillimeter Array, Mauna Kea, Hawaii

1.1 HOW IT ALL BEGINS

Low-mass star formation begins in *molecular clouds* made of molecular gas and dust, regions of low density ($\approx 10^3$ particles per cm^{-3}), that can be more than 100 pc in size (e.g. Alves 2004). Some of the nearest and most studied star-forming regions are Taurus-Auriga, Orion and Ophiuchus. The temperature in these regions is dominated by the interstellar radiation field and cosmic ray ionisation and can be as low as 10 K. Molecular clouds are readily observed in the submillimetre, via rotational transitions of CO (e.g. Ungerechts & Thaddeus 1987) or dust extinction (e.g. Lada et al. 2007). Parts of clouds undergo a collapse to form denser regions, the process led by gravity and regulated by the cloud turbulence and other factors. In about 10^5 yr, ten to hundred times denser and much smaller regions ($\approx 10^4$ AU), called dense clouds, are formed. First discovered by W. Herschel in 1784 as regions where stellar light was lacking, or as 'holes in heavens' as he exclaimed, these clouds were later identified in interstellar extinction maps as regions of high-extinction and reddening, seen in silhouette against the background light (e.g., Barnard 68, Alves et al. 2001). The dense clouds with no central object, which often exhibit evidence of an ongoing contraction seen in the submillimetre mapping of the lines of CO and other molecular species (e.g. Tafalla et al. 1998; Caselli et al. 2002), are believed to be on the way to form protostars and are called *pre-stellar cores*. Their temperature is ≈ 10 K, due to their higher density with respect to the molecular clouds. The process of contraction is led by gravity and regulated by the 'magnetic breaking' through ambipolar diffusion (Shu 1977; Mouschovias & Ciolek 1999) and/or the dissipation of turbulence via shocks (e.g. Mac Low & Klessen 2004). The central object is formed, and it begins to heat the surrounding core by radiating away the excess gravitational energy released during contraction. At this stage the density and temperature conditions in the core make it rich in chemistry, with an increase in abundance of complex molecules. Eventually, a *young stellar object* (YSO) is

formed, embedded in the envelope material (commonly called 'Class 0' stage). The material close to the star is accreted through a dense and hot disc, and funneled onto the star along the magnetic field lines. The envelope material is being accreted onto the disc as the disc viscously spreads outwards, processes dominated by the angular momentum, gravity and the magnetic field. YSOs are identified by a notable infrared emission, while the stellar photospheric emission is heavily obscured by the surrounding envelope. The embedded stage in which the envelope dominates the spectral energy distribution of the object ('Class 0' and 'Class I') lasts about 0.5 Myr (Evans et al. 2009) and often exhibits outflows that partially clear away the envelope. In the following, 'Class II' stage, the viscous accretion disc (Hartmann et al. 1998) extends several hundreds of AU from the star, with the outer edge determined by photoevaporation due to the interstellar radiation field or truncation by a companion. The envelope mass is small with respect to the disc mass, and no longer obscures the young star. The stellar photospheric emission is observed, as well as the excess emission in the infrared and submillimetre, arising from the disc. The work presented here concerns this last stage.

1.2 DISC PHYSICAL PROPERTIES

The discs around young stars extend up to 1000 AU in radius and consist primarily of molecular gas, with H_2 being the most abundant molecule followed by CO. About 99% of the disc mass is in the molecular gas. It rotates around the star in slightly sub-Keplerian motion due to gas pressure and viscosity[1]. The remaining 1% of the mass is contained in dust. Dust is generally well coupled to the gas and thus in sub-Keplerian rotation, with the exception of particles large enough to decouple from the gas and which may consequently drift inward. The disc is heated primarily by the radiation field of the central star, which is absorbed in the inner rim and surface disc layers where the optical extinction $A_V \leq 1$ mag. Almost all of the energy is absorbed and reprocessed by the dust, and these processes determine the disc gas temperature throughout the disc, except in the uppermost disc surface layers where gas and dust are decoupled, and the densest midplane layers in the inner few AU where viscous heating may be a dominant process. In turn, the gas provides pressure that maintains the disc vertical structure enabling the dust to be exposed to the stellar light. Almost every major process involving one of the two components, dust or gas, affects the other significantly. Dust coagulation and settling toward the disc midplane disables the photoelectric heating process and may lead to a decrease of the gas temperature in the surface layers. Vertical mixing within the disc stirs the dust up along with the gas and opposes the dust settling. When dust drifts inward due to the loss of angular momentum to the sub-Keplerian gas, the outermost disc regions remain exposed to the interstellar radiation field and the gas may be photodissociated more efficiently there. Gas ionisation enhances the influence of the magnetic field on the disc. This causes

---

[1]This is not the viscosity in its conventional definition, but a parametrisation of the energy dissipation mechanism, necessary for the accretion of matter through the disc.

turbulence and allows magneto-rotational instability.

It is because of the mutual dependence of gas and dust in shaping the disc that both these components need to be observed, modelled and analysed simultaneously when studying disc structure. This thesis shows how this approach yields results that could not be obtained by investigating the two components independently.

During the evolution of the disc, the gas is largely accreted onto the star, but also thought to be dispersed and photoevaporated (Alexander et al. 2006a,b, and references therein), while the dust in the inner disc dissipates typically within 10 Myr (Hillenbrand 2008). The dust settles to the disc midplane and coagulates, and the dust growth process is most efficient in the dense midplane where the largest particles may drift radially, against the gas pressure (Whipple 1972; Weidenschilling 1977; Brauer et al. 2008). All these processes change the appearance of the discs: young discs are gas-rich and their dust is well mixed with the gas, while old discs have very little gas, with dust that has already grown to significant sizes and is no longer dominated by gas pressure. However, the age of the star does not seem to be a good indicator of the evolutionary stage of the disc. This implies that the disc evolution is a more intricate matter, and depends on the environment in which the star and disc are born: their initial masses, angular momentum, and magnetic field for example. In this sense it is interesting to study discs of all types, gas rich or not, to try to disentangle the possible evolutionary trends.

Based on the mass of the central star, the discs around young pre-main sequence stars have different nomenclatures. The low-mass young stars, with $M \leq 1$ M$_\odot$ and spectral types from late F to early M, are called T Tauri stars, their prototype being the famous young variable star T Tau. The discs attributed to T Tauri stars are observed to be typically a few hundred AU in size, have the gas + dust mass 10^{-3}-10^{-1} M$_\odot$, and are relatively cold due to the low stellar luminosity. The intermediate mass stars, with mass 1.5-8 M$_\odot$, are called Herbig AeBe stars after their definition given in Herbig (1960). As the name suggests, they have A and B spectral types. Their discs are observationally similar to those around T Tauri stars (Beckwith et al. 1990) but warmer. Stars of higher masses with discs are not frequent but a few examples are found in the literature (Alonso-Albi et al. 2009). These discs are believed to evolve rapidly due to the strong stellar radiation field. This thesis focuses on the discs around T Tauri and Herbig Ae stars, both formed by the same low-mass star formation mechanism as outlined in Section 1.1.

1.3   FEEDBACK FOR PLANET FORMATION

An ever growing number of the newly discovered extra-solar planets and planetary systems provide evidence that a possible outcome of disc evolution is a planetary system (e.g. Udry & Santos 2007), and there is an ongoing effort to understand which conditions in discs are necessary to form a habitable planet like Earth. The distribution of mass with distance from the star in the extra-solar planetary systems and in our own Solar system may carry some imprint of how the mass in the planet-forming regions of their predecessor discs was distributed. Some information about the chemical compo-

sition of gas and dust in the pre-solar nebula is encrypted into the cometary material which we can observe and study. However, an important part in understanding planet formation is looking back in time, to the earliest phases of planet formation, and this is done through the observations of discs around young stars.

It is observationally challenging to probe the physical conditions in the planet-forming regions of discs directly (a few tens of AU from the star), as these observations require subarcsecond spatial resolution. Furthermore, the emission of gas and dust arising from these regions (in the near- and mid-infrared wavelength regime) is optically thick and does not probe beyond the surface of the disc. However, a number of physical processes that influence the planet formation leave their signatures in the disc structure at larger scales that can be probed via optically thin dust and molecular gas tracers. Also, planets themselves can leave a signature on the larger scale disc structure in the form of gaps, inner cavities, and clumps.

The disc is formed through the accretion process of circumstellar material from the proto-stellar envelope. This material is distributed spherically at scales of several thousands of AU, and accretes on to the plane of rotation at relatively small distances from the star (a few to a hundred AU). The subsequent viscous spreading of the accretion disc until its final size of typically 200 AU or more (Hartmann et al. 1998) determines the overall disc structure. The amount of mass in the envelope and the initial angular momentum play a major role in how the mass is accreted on to the disc, while the disc's viscous properties, linked to the effect of magnetic field on the turbulence within the disc along with the disc density, shape the disc as it spreads. Irradiated accretion disc models and passive irradiated disc models provide disc structures consistent with the broad-band spectral energy distibutions of discs (Dullemond et al. 2001; Calvet et al. 2004; Dent et al. 2006, Chapter 2 of this thesis) and spatially resolved dust millimetre interferometer observations (Chapter 6 of this thesis), and are widely used. The densest, planet-forming regions (disc midplane up to few tens of AU from the star), are not directly probed, because emission arising from these regions is optically thick, and their properties are extrapolated from the model fits to the outer disc or other indirect methods.

Physical parameters like the radial distribution of material, gas-to-dust mass ratio and the reservoir of gas available for the formation of gas giants, are essential for the understanding of these disc regions. They need to be extrapolated from the studies of larger-scale disc structure. Viscous acretion disc models (see the database of accretion disc models in D'Alessio et al. 2005), suggest a surface density distribution (the vertical column density) $\Sigma \propto R^{-p}$, with $p \approx 1$ throughout the disc. This value is consistent with the measurements of p in the outer disc of some sources (Pinte et al. 2008; Wilner et al. 2000; Andrews & Williams 2007). and suggests that the slope is likely to be steeper in the inner regions where the turbulence and viscosity are expected to be lower than in the outer disc.

1.4   OBSERVATIONS OF PROTOPLANETARY DISCS

The observational properties of young low-mass stars, like ultraviolet and infrared excess or flaring activity, encouraged the idea that young stars may be surrounded by circumstellar discs (Lynden-Bell & Pringle 1974). In the near-infrared speckle interferometric observations of (Beckwith et al. 1984), compact elongated infrared emission is detected towards two young stars, and associated with circumstellar discs. Sub-millimetre interferometry followed shortly with more evidence for circumstellar discs (Beckwith et al. 1986; Sargent & Beckwith 1987), until developing its full potential in the last ten years and resolving disc structure with instruments mentioned in Sect. 1.5. The first images of discs taken with the Hubble Space Telescope (HST) (Burrows et al. 1996), marked the beginning of intensive and ever growing research over the past decade focusing on discs around young stars, their structure and implications this may have for planet formation. Other observational methods like scattered light imaging with HST have contributed greatly to our understanding of disc structure (see Padgett et al. 1999; Grady et al. 1999, and later work by these authors). This thesis uses a range of observational methods, with an emphasis on the submillimetre interferometry at high angular resolution, to study the disc structure and compare the dust and gas components in discs.

Due to the range of temperatures found in them, discs can be observed at wavelengths from the near-infrared to millimetre. This fact has enabled the disc modelling based on their spectral energy distribution (SED). An example of an SED is shown in the bottom-left panel of Fig. 1.2, for the star DoAr 21 studied in Chapter 4 of this thesis. The observed fluxes (symbols) beyond 10 μm exceed the stellar photosphere, represented by the full line, and this excess is attributed to the circumstellar material. Although the continuum fluxes are due entirely to the dust emission, which is a minor fraction of the disc mass, general characterisation of the disc is possible, distinguishing between flat and flared disc structures (Dullemond & Dominik 2004a,b), with or without an inner cavity (Brown et al. 2008) - all generally indicative of the evolutionary state of the disc. However, the SED is only sensitive to the inner few hundred AU which is not necessarily the entire disc. Some information about the disc size and inclination can be derived in discs based on their spatially unresolved low-J ^{12}CO line spectra (Chapters 5, 6 and 7), particularly when the line is optically thick. Yet, an image is worth a thousand words, and at least as many spectra as the number of the resolution units in it. An example of the spatially resolved dust emission is seen in the bottom-left panel of Fig. 1.2 where the warm dust imaging in the mid-infrared of the same source provides insights into the spatial extent of the circumstellar material. In this case, the disc is highly asymmetric, has a large inner hole and the emission extends to 200 AU or 1″6. To probe the radial distribution of material and disc dust mass, optically thin millimetre continuum emission is perfectly suited. Spatially resolved observations can be obtained using millimetre interferometry (see Sect. 1.5). An example of the spatially resolved millimetre continuum emission from the disc around IM Lup (Chapter 3) is given in the bottom-middle panel of Fig. 1.2. These observations are indicative of the disc radius, but in order to probe the disc extent fully, observations of cold molecular gas are necessary. The upper-middle panel of Fig. 1.2 shows observations of the low-

energy rotational transition of ^{12}CO of the same disc. The comparison with the dust continuum shows how the relatively compact dust emission may be deceiving. Only with the ^{12}CO observations, we were able to probe the entire disc structure and unveil an interesting structural discontinuity in this large disc (Chapter 3). Furthermore, the molecular gas lines provide kinematical information that can be used for determination of the mass of the central star in sources at sufficiently high inclination (Chapter 3). Observations of the molecular line transitions of different optical depth, like ^{12}CO, ^{13}CO and C^{18}O J=2–1, allow us to probe the disc vertical structure and test the SED models as shown in Chapters 2 and 3. In the discs at late stages of evolution, with a low amount of material, these lines may be too weak to observe, and there the near-infrared imaging of the main gas component H$_2$ is an interesting prospect. This new method of tracing disc surface and geometry, discussed in Chapter 4, has allowed us to probe the surprising arc structure around DoAr 21 as seen in the upper-left panel of Fig. 1.2.

Other observational methods that are not used in this thesis, but are worth mentioning, are scattered light imaging, infrared interferometry, observations of the 10 μm silicate feature, and spectroastrometry, all having contributed greatly to our understanding of discs over the past few decades.

1.5   SUBMILLIMETRE INTERFEROMETRY

With the advent of the submillimetre interferometer facilities, like the Submillimeter Array shown in Fig. 1.1 (SMA), Plateau de Bure Interferometre (PdBI), Combined Array for Millimeter Astronomy (CARMA), and others, it has become possible to investigate the outer regions and global structure of the discs around young stars through various molecular line tracers and study the dust grain growth through the thermal continuum emission of the dust. The advantage of these observations over spatially unresolved observations is that the disc emission is successfully separated from the more extended envelope or cloud emission and that the disc radial and vertical structure can be probed. The submillimetre emission, more than at any other wavelength, probes the full extent of the discs, from the hot inner disc regions at several tens of AU from the star to the cold outermost regions up to a 1000 AU from the star.

The principle of submillimetre interferometry is in its essence similar to the interferometry at any other wavelength. Individual telescopes are distributed over an area and linked together to overcome the technical difficulty of building a single extremely large telescope, and to obtain an equivalent spatial resolution. The signal from the source is correlated for each pair of antennas, taking into account the delay with which the wavefront meets the individual antennas. The correlation obtained (correlated flux) is associated with a (u,v) coordinate describing the distance between the two antennas and its orientation, projected onto a plane normal to the direction of the source, i.e., the plane of the wavefront. Due to the Earth rotation, a static spatial distribution of interferometre elements provides a sampling of the (u,v) plane in the course of an observing run (typically several hours). In principle, small (u,v) distances probe emission coming from a larger spatial scale while greater (u,v) distances probe emission on small scales.
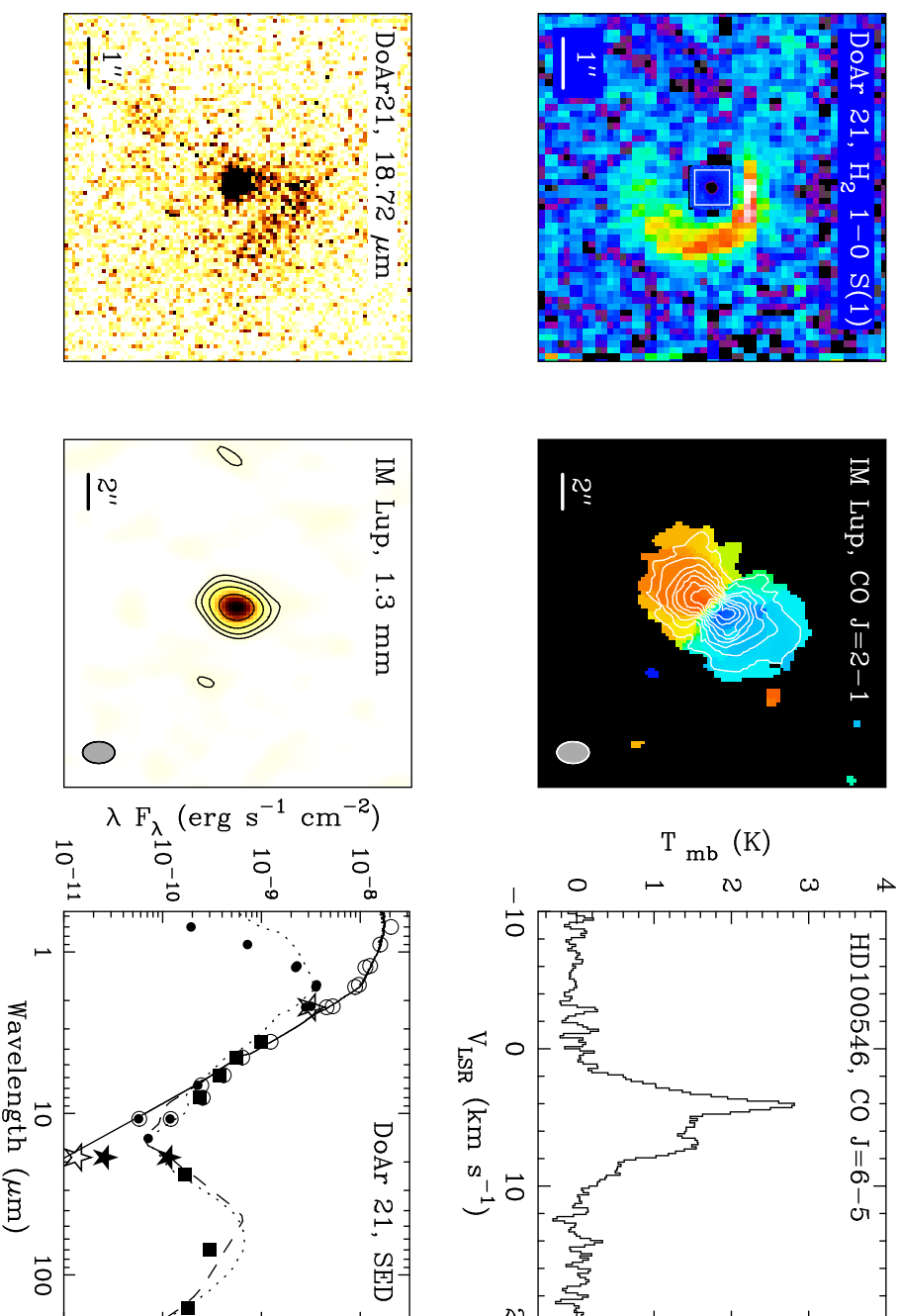
Figure 1.2: Some of the observations of circumstellar discs presented in this thesis. Upper row shows gas observations and the lower row dust observations. Clockwise: Spatially resolved imaging of the fluorescent H$_2$ 2.1 μm line emission towards DoAr 21 (Chapter 4); Millimetre interferometric imaging of the ^{12}CO $J=2$–1 line in the disc around IM Lup (Chapter 3); Single dish observations of the ^{12}CO $J=2$–1 line spectrum toward HD 179614 (Chapter 5); Wide-band spectral energy distribution of DoAr 21 (Chapter 4); Dust thermal continuum image of the disc around IM Lup (Chapter 3); Warm dust imaging at 18 μm towards DoAr 21 (Chapter 4). The distances to these sources are 100-200 pc. See the respective chapters for detailed description.
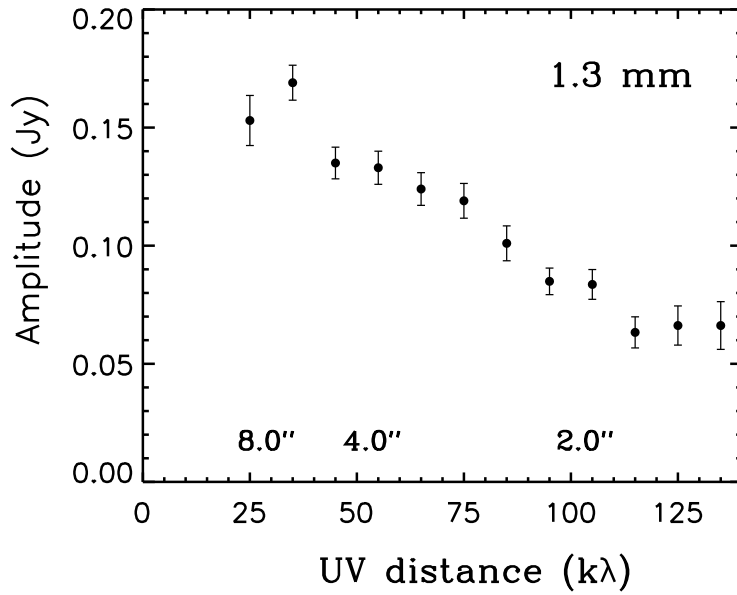
Figure 1.3: Correlated flux as function of uv-distance of the thermal continuum emission at 1.3 mm (230 GHz) towards the disc around HD 169142. The corresponding spatial scale probed by these fluxes is shown on the horizontal axis. See Chapter 2 for details.

This is best seen when the correlated flux is plotted as a function of (u,v) distance as shown in Fig. 1.3.

For the typical distance to the nearby star-forming regions (140 pc) the resolution as high as 0.3″ (50 AU) provided by current interferometers is sufficient to resolve the structure of the discs, objects typically a few arcseconds (a few hundreds of AU) in size.

Because the sampling of the (u,v) plane is never complete, the visibility data need to be processed in order to (re)construct the image of the source starting from the Fourier transformed, partial source brightness distribution. The ASP publication *Synthesis imaging in radio astronomy* (1999) is a good reference for the details of the complex process of interferometer data reduction. For the scope of understanding the data presented in this Thesis, it is sufficient to note that the visibility data are true measurements of the signal from the source, probing large scales at short baselines and smaller scales at longer baselines. The spectral lines and two-dimensional images are a reconstruction (model) of the source emission based on the visibility data and these representations may differ depending on the particular schemes used in the data reduction process. For all the interferometer data presented in this Thesis, both the visibility data and the processed images are shown and compared to the results from the disc modelling.

1.6   THIS THESIS

With the recent advance in observational facilities in the submillimetre and the increased interest in the early stages in star and planet formation, the study of circum-

stellar discs over the last decade has grown substantially (e.g. Guilloteau & Dutrey 1994; Koerner & Sargent 1995; Qi et al. 2003; Piétu et al. 2005; Isella et al. 2007; Brown et al. 2007; Hughes et al. 2009). These studies focus on some key questions regarding the physical processes that involve both planet formation and the disc structure at a larger scale. For example, the very first stage of planet formation is the growth of dust to mm sized grains. This is the process that takes place in the dense disc midplane. The thermal dust emission at millimetre wavelengths increases as the grains grow and thus we see these discs bright in the millimetre. It will be very important in the coming years, with the advent of ALMA (see Section 1.7), to measure and spatially resolve the long-wavelength disc emission in order to quantify the grain growth ongoing in different disc regions. Another example is the later stage of planet formation, where the planets perturb the disc content. This process can cause gaps in disc gas and dust distribution or disc inner holes. Planet resonances can also cause disc material to clump and appear axially asymmetric. These features can be spatially resolved using a range of instruments.

The underlying theme throughout this thesis is the relative distribution of gas and dust in discs and consequently the main method used here are submillimetre interferometer observations sensitive to the disc density and temperature structure, both radial and vertical, resolved at scales $\geq$100 AU.

In this thesis, we address the following questions:

- How can we measure the gas mass in discs, and what constraints on the gas-to-dust mass ratio can be derived?

- How does the large scale (100 AU) disc structure probed with millimetre interferometry compare to the disc models based on the spectral energy distribution (SED)?

- Does disc modelling, based on the dust observations alone (SED, scattered light imaging, millimetre continuum imaging, silicate feature), provide a good description of the regions dominating the cold molecular gas emission?

- What are the typical temperatures and sizes of discs around intermediate-mass young (Herbig AeBe) stars and can we use these sources to measure disc gas masses?

- Should the SED be modelled from inside-out (starting from the near-infrared) or outside-in (starting from the submillimetre)?

- Can we derive reliable constraints on the stellar mass from the disc kinematics seen in submillimetric images of molecular gas?

- Can we test the radial drift models observationally?

- How can we probe the gas and dust spatial distribution in low-mass gas-poor discs at late stages of evolution?

- For what aspects of the study of disc mass and structure are submillimetre observations of gas essential?

1.6.1 Disc modelling approach proposed by this thesis

This thesis merges diverse observational methods to study disc structure, with a special focus on the submillimetre interferometry. Its complementarity with other observations, spatially resolved or not, is investigated in depth. Another important aspect of the work presented here is the joint analysis of dust and gas, in which the relative amounts and spatial distribution of these two components are investigated. The molecular excitation and radiative transfer code RATRAN (Hogerheijde & van der Tak 2000) is used throughout the thesis as an essential tool to model and interpret the molecular line emission arising from circumstellar discs. Figure 1.4 gives a overview of the methods and the observational constraints they provide. The methods are listed in a sequence designed to minimise the uncertainties in the analysis, with each method building on the input received from the previous one. The most basic prerequisites for the modelling of disc structure are the constraints on the main geometric properties, the disc size R_{out} and inclination i. As mentioned in Section 1.4, the best way to derive these parameters are the spatially resolved submillimetre interferometric observations of the rotational ^{12}CO emission. Where these are not available, other imaging methods sensitive to the outermost disc regions, like the scattered light, mid-infrared or fluorescent H_2 imaging can provide some indication of R_{out} and i. The fluorescent H_2 imaging in the near-infrared is a surprising new observational method, discussed in Chapter 4. As shown in Chapter 5, even the ^{12}CO spectrum may be used to place constraints on R_{out} and i, thanks to the kinematic information it contains. As we show in Chapter 5, prior knowledge of R_{out} and i is essential for the SED modelling, otherwise the SED may be misinterpreted due to parameter degeneracy between i and the inner radius, and between R_{out} and the density distribution. Next step is the simple SED modelling, e.g., through comparison with the 'ready-made' SEDs in the D'Alessio et al. (2005) database of irradiated accretion disc models. The disc temperature structure can be assesed, particularly in the cold midplane regions, which are not directly illuminated by the central star and thus are less sensitive to the exact stellar radiation field and disc geometry. Given the midplane temperature structure at large ($\approx$100 AU) radii, R_{out} and i, this is sufficient information for the interpretation of the spatially resolved interferometric observations of the thermal dust emission at millimetre wavelengths. In this way, the minimum dust mass can be derived and some information about the radial density structure can be obtained (see Chapters 2, 3 and 6). The detailed dust disc structure is derived in the following step, the simultaneous modelling of the SED, millimetre interferometric data, scattered light image and the silicate feature, probing, respectively, the inner disc, the outer disc midplane, the disc surface and the properties of the dust in the surface of the inner disc. The diverse observational constraints combined in this way allow to determine disc geometry, dust growth and settling as illustrated in Pinte et al. (2008). With the detailed knowledge of the dust distribution and properties, and in particular the disc temperature structure (dominated by dust),

low-J CO spectrum [5, 6, 7]	Scattered light imaging
Fluorescent H_2 imaging [4]	Mid-infrared continuum imaging [4]

Geometrical disc properties: R_{out}, i

SED [4]

Midplane temperature structure

Interferometric millimetre dust continuum observations [2, 3, 6]

Density structure: M_{dust}(min), p

SED + scattered light + millimetre imaging + Si feature

Dust temperature and density structure, dust properties

Multi-isotopologue submillimetre interferometer observations [2, 3]
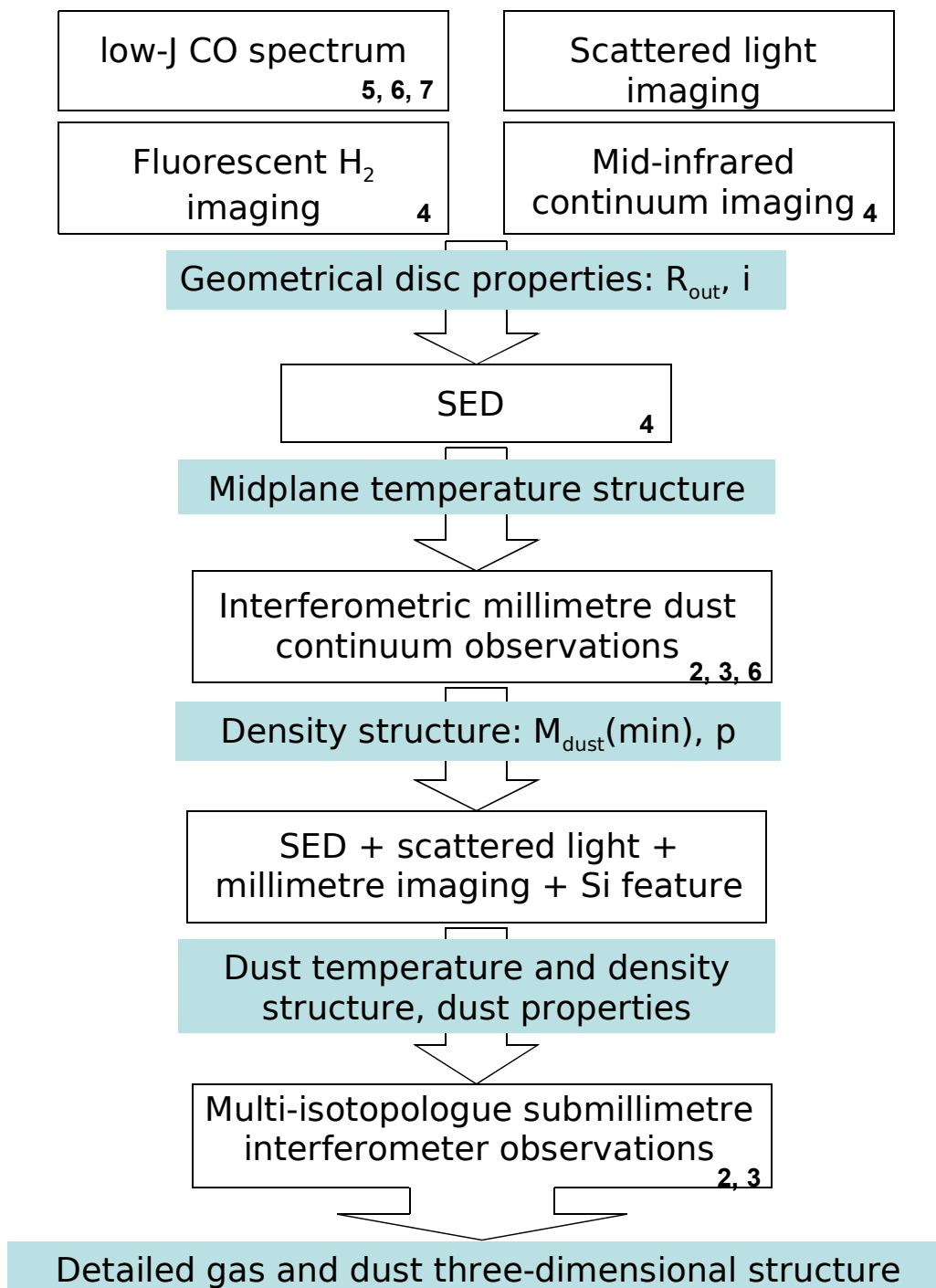
Detailed gas and dust three-dimensional structure

Figure 1.4: Recipe for disc modelling

the three-dimensional structure of the disc main mass component, the molecular gas can be investigated through spatially resolved observations of ^{12}CO and isotopologue line emission as shown in Chapters 2 and 3. This approach has allowed us to go a step further than commonly done: in Chapter 2 we constrain the disc gas mass, while in Chapter 3 we find a striking discontinuity in disc structure that would not have been possible to identify without comparison between the gas observations and dust emission-based model. These models represent the most reliable description of the structure of the objects studied, and are a necessary input for testing of the physical and chemical processes heavily dependent on the disc density and temperature structure and the relative distribution of gas and dust.

1.6.2   Chapter 2

We investigate the three-dimensional structure of a gas-rich disc around the young star HD 169142 by observing the CO isotopologue rotational transitions of different optical depth with the Submillimetre Array interferometer. Our observations confirm the vertical and radial structure proposed by the SED model. The stellar luminosity is sufficient to heat the disc above the freeze-out limit (20 K) out to 150 AU in the disc midplane, nearly the full extent of the disc, and we estimate that the CO freeze-out affects only ≈8% of the disc mass. Furthermore, photodissociation is negligible due to the sufficient dust mass and our result that the gas and dust are well mixed. This enables us to derive the disc gas mass of $(0.6\text{-}3.0)\times10^{-2}$ M$_\odot$ from our ^{13}CO and the optically thin C^{18}O J =2–1 line observations. The lower limit on the dust mass is 2×10^{-4} M$_\odot$, based on our 1.3 mm dust continuum data and the disc model. Our results, for standard dust opacities and molecular abundances, place the gas-to-dust mass ratio in this disc in the range 13-135. These unique constraints are facilitated by the small size of the disc around this A type star. We conclude that the small discs around Herbig AeBe stars are good potential targets for measuring the disc gas mass and in Chapter 5 we build on this result, concluding that the discs around Herbig AeBe stars are typically smaller than 200 AU. Chapter 5 also investigates whether the SED modelling produces a good base for modelling the low-J CO lines in discs in general.

1.6.3   Chapter 3

A similar approach as in Chapter 2 is used to study the structure of the disc around the low-mass young (T Tauri) star IM Lup. The SED model incorporates the constraints on the dust size and composition, dust settling, disc size and surface density distribution from a range of observations including the silicate feature, scattered light images and millimeter interferometry of the thermal dust continuum emission. Our ^{12}CO and ^{13}CO J =2–1 interferometric images show the 900 AU large disc in Keplerian rotation around the central star. Because of the sufficiently high inclination (i=50°), the stellar mass is well constrained by our observations to 1.2±0.2 M$_\odot$, and is relatively insensitive to the exact disc inclination. The disc model based entirely on the dust emission does not trace the full extent of the disc, but merely the disc structure up to 400 AU

from the star. We establish that there is a discontinuity in disc structure at 400 AU, with a notable drop in density of both gas and dust by a factor of 10-100. The region at 400-900 AU has a very low density (H_2 column density $10^{20} - 10^{21}$ cm^{-2}) and temperature (10 K due to interstellar radiation field), and is therefore traced only with our CO submillimetre observations. The derived physical conditions in the disc and the estimated age of the star indicate that the dust radial drift combined with photodissociation of the gas is a plausible scenario to explain the observed low-density outer region in the IM Lup disc. A radial variation in the efficiency of angular momentum transport, resulting in a steep density profile, may trigger the drift process in the low-density outermost disc regions wherethe largest particles in the interstellar medium-like dust size distribution have the optimal drift size and contain most of the dust mass. Our results encourage studying very large discs for observational signatures of radial drift - the process that is believed to ultimately lead to accumulation of solid material in the regions closer to the star, up to densities sufficient for planets to form.

1.6.4   Chapter 4

We trace the spatial distribution of the circumstellar material associated with the weak-lined T Tauri star DoAr 21 by using, for the first time, the spatially resolved observations of the H_2 2.12 μm line emission with the SINFONI integral field spectroscopy unit on the Very Large Telescope (VLT). The inner 70 AU from the star are devoid of detectable amounts of H_2, a region found to be depleted of dust as well. The line emission arises entirely from a partial arc around the star at distances 70-200 AU. Warm dust imaging at 18μm with the VISIR mid-infrared imager on VLT, and some recent observations by other authors, confirm that this is the true distribution of the material, and that the disc is highly asymmetric. We investigate different scenarios in which this asymmetry may arise. Besides the possibility that the disc at the late stages of evolution has been severely perturbed, the observed emission may also come from material that has been gravitationaly "captured" by the (diskless) star. Even illumination of unrelated cloud material is a plausible scenario. These results show that a young star with an SED indicative of a circumstellar disc with a large hole, must be imaged to confirm this hypothesis.

1.6.5   Chapter 5

As found in Chapter 2, the discs around Herbig Ae stars offer a possibility to constrain the gas mass when the disc is sufficiently small. Here, we study the spatially unresolved CO 3–2 line emission from a sample of Herbig AeBe stars from the literature, and the disc parameters probed by this emission: the disc radius, temperature and inclination. We use simple parametric disc models and find that the power law $T = 60 \times (R/100\,\mathrm{AU})^{-0.5}$ provides a good description of the surface layers where the ^{12}CO 3–2 line is emitted. At $i \leq 45°$ we can separate the contribution from the inclination and disc size to the line emission and profile, but for higher inclinations the two

parameters are degenerate. We find that 75% of the observed sources have low line intensity and radii $\leq$200 AU. Therefore, the discs around Herbig AeBe stars are typically small enough to have the bulk of the CO in the gas phase, and observations of isotopologues like ^{13}CO and C^{18}O in these objects are sensitive to the total gas mass, unlike in the discs around T Tauri stars. Measuring the gas mass in these discs by using optically thin CO transitions may improve our understanding of the evolution of the disc gas content. For sources where SED models are available, we compare the CO 3–2 spectra calculated based on the models with the observations. We find that the SED modeling alone often leads to an underestimate of the disc outer radius, also seen in Chapter 3, and an overestimate of the inclination (especially in sources with inner holes). Because of this, the SED models generally do not provide a good description of the low-J CO spectra. Conversely, the spectral line fits provide useful estimates of i and $R_{\rm out}$ and should be taken into account when modelling the SEDs.

1.6.6   Chapter 6

We study the spatially unresolved interferometric observations of ^{12}CO J=1-0, ^{13}CO J=1–0 and HCO$^+$ J=1–0, as well as the dust continuum at 2.7 mm towards a sample of six discs around T Tauri stars. Disc size and inclination are available from previous, spatially resolved, observations. Simple parametric models, with the midplane temperature given by the SED models and power-law density structure with density scaled to fit the dust continuum flux, roughly reproduce the molecular line emission and are a good starting point for spectral line modelling and further modelling of the disc structure, e.g. by fitting the SEDs. We derive minimum disc dust masses in the range of (0.7-4.5)$\times 10^{-4}$ M$_\odot$ and, in some sources, evidence of substantial CO freeze out and/or photoevaporation.

1.6.7   Chapter 7

We analyse and model both low-J and high-J ^{12}CO line emission towards the disc around a Herbig Ae star HD 100546, observed using the Atacama Pathfinder Experiment Telescope at the resolution of 7-14″. The dust emission from this source has been studied extensively over the past years and shows an intriguing disc structure, accompanied by an extended component. We identify the presence of significant amounts of warm gas associated with the disc at scales of 400 AU or smaller (half-size of the beam at 810 GHz). This is contrary to the late stages of evolution of the disc suggested by studies of its dust emission. The line profile is characteristic of a rotating disc of 400 AU in size seen at a 50° inclination. The observed asymmetry of the optically thick ^{12}CO lines may be due to asymmetry in the disc temperature, with one side of the disc colder than the other, possibly due to the obscuration of the outer disc surface by the warped inner disc suggested by previous work. We model the disc with a temperature asymmetry and obtain best fits for a 10-20 K temperature difference at 100 AU. A systematic mispointing by 1″9 in our different sets of observations can reproduce the line asymmetry, but is highly unlikely. Spatially resolved observations of this source,

especially with ALMA in the future, are essential to characterise this puzzling source, one of the brightest discs of the southern sky.

1.7   CONCLUSIONS AND FUTURE PROSPECTS

- A reliable estimate of the disc gas mass can be made based on the spatially resolved observations of optically thin rotational line emission of CO isotopologues in discs, when this emission is analysed in the framework of a well constrained disc structure model, and for discs where:

  - dust and gas are co-spatial radially and vertically, and

  - the midplane region between the radius where the temperature is 20 K and disc outer radius contains a minor fraction of the total disc mass.

- The discs around Herbig AeBe stars are typically small enough to have the bulk of their mass above 20 K, and thus freeze-out in these sources has a minor effect on the CO abundance (second condition of the previous conclusion).

- Molecular discs can extend beyond the disc regionsthat are optically thick in the near-infrared, and beyond the boundaries derived based on dust observations alone.

- Quiescent H_2 line emission at 2.12 μm can originate from circumstellar material located as far as 100-200 AU from the young star.

- Simplistic power-law disc models are a more efficient tool in the analysis of spatially unresolved submillimetre molecular line observations (spectra) than sophisticated models with a large number of free parameters.

- The modelling of the inner disc and the outer disc are interdependent. The "outside-in" disc modelling, starting from the spatially resolved submillimetre observations of gas and dust, is faster and more reliable than the SED modelling with or without additional constraints on disc large scale structure.

The future instrument of unprecedented sensitivity and spatial resolution in the submillimetre - the Atacama Large Millimetre Array will open new horizons for the studies of circumstellar discs. We will be able to discern smaller scale asymmetries, holes and gaps within the disc structure, that can be linked to planet-disc interaction. High spatial resolution will also allow to probe the radial distribution of the material better and in particular the dust emissivity. ALMA will be sensitive enough to image the submillimetre emission of low amounts of gas and dust in discs at later stages of evolution, a disc population that is just barely within reach of the current instruments but may provide an indication of the dissipation mechanism. Disc chemistry will be better constrained, through observations of molecular lines of a variety of species, many of which will be detected and resolved for the first time.

The recent launch of Herschel carries a promise of probing the far-infrared emission from discs, the region of the SED that has been lacking observational input. This wavelength regime is sensitive to disc geometry (flat or flared) and grain growth, and will allow us to probe them better. Last but not least, Herschel/HIFI will allow us to surmount the obstacle of water absorption by the atmosphere and search star-forming regions for water, the prerequisite for life.

REFERENCES

Alexander, R. D., Clarke, C. J., & Pringle, J. E. 2006a, MNRAS, 369, 216

Alexander, R. D., Clarke, C. J., & Pringle, J. E. 2006b, MNRAS, 369, 229

Alonso-Albi, T., Fuente, A., Bachiller, R., et al. 2009, A&A, 497, 117

Alves, J. 2004, Ap&SS, 289, 259

Alves, J. F., Lada, C. J., & Lada, E. A. 2001, Nature, 409, 159

Andrews, S. M. & Williams, J. P. 2007, ApJ, 659, 705

Beckwith, S., Sargent, A. I., Scoville, N. Z., et al. 1986, ApJ, 309, 755

Beckwith, S., Skrutskie, M. F., Zuckerman, B., & Dyck, H. M. 1984, ApJ, 287, 793

Beckwith, S. V. W., Sargent, A. I., Chini, R. S., & Guesten, R. 1990, AJ, 99, 924

Brauer, F., Dullemond, C. P., & Henning, T. 2008, A&A, 480, 859

Brown, J. M., Blake, G. A., Dullemond, C. P., et al. 2007, ApJ, 664, L107

Burrows, C. J., Stapelfeldt, K. R., Watson, A. M., et al. 1996, ApJ, 473, 437

Calvet, N., Hartmann, L., Wilner, D., Walsh, A., & Sitko, M. L. 2004, in Astronomical Society of the Pacific Conference Series, Vol. 324, Debris Disks and the Formation of Planets, ed. L. Caroff, L. J. Moon, D. Backman, & E. Praton, 205

Caselli, P., Walmsley, C. M., Zucconi, A., et al. 2002, ApJ, 565, 331

D'Alessio, P., Merín, B., Calvet, N., Hartmann, L., & Montesinos, B. 2005, Revista Mexicana de Astronomia y Astrofisica, 41, 61

Dent, W. R. F., Torrelles, J. M., Osorio, M., Calvet, N., & Anglada, G. 2006, MNRAS, 365, 1283

Dullemond, C. P. & Dominik, C. 2004a, A&A, 417, 159

Dullemond, C. P. & Dominik, C. 2004b, A&A, 421, 1075

Dullemond, C. P., Dominik, C., & Natta, A. 2001, ApJ, 560, 957

Evans, N. J., Dunham, M. M., Jørgensen, J. K., et al. 2009, ApJS, 181, 321

Grady, C. A., Woodgate, B., Bruhweiler, F. C., et al. 1999, ApJ, 523, L151

Guilloteau, S. & Dutrey, A. 1994, A&A, 291, L23

Hartmann, L., Calvet, N., Gullbring, E., & D'Alessio, P. 1998, ApJ, 495, 385

Herbig, G. H. 1960, ApJS, 4, 337

Hillenbrand, L. A. 2008, Physica Scripta Volume T, 130, 014024

Hogerheijde, M. R. & van der Tak, F. F. S. 2000, A&A, 362, 697

Hughes, A. M., Andrews, S. M., Espaillat, C., et al. 2009, ApJ, 698, 131

Isella, A., Testi, L., Natta, A., et al. 2007, A&A, 469, 213

Koerner, D. W. & Sargent, A. I. 1995, AJ, 109, 2138

Lada, C. J., Alves, J. F., & Lombardi, M. 2007, in Protostars and Planets V, ed. B. Reipurth, D. Jewitt, & K. Keil, 3–15

Lynden-Bell, D. & Pringle, J. E. 1974, MNRAS, 168, 603

Mac Low, M.-M. & Klessen, R. S. 2004, Reviews of Modern Physics, 76, 125

Mouschovias, T. C. & Ciolek, G. E. 1999, in NATO ASIC Proc. 540: The Origin of Stars and Planetary Systems, ed. C. J. Lada & N. D. Kylafis, 305

Padgett, D. L., Brandner, W., Stapelfeldt, K. R., et al. 1999, AJ, 117, 1490

Piétu, V., Guilloteau, S., & Dutrey, A. 2005, A&A, 443, 945

Pinte, C., Padgett, D. L., Ménard, F., et al. 2008, A&A, 489, 633

Qi, C., Kessler, J. E., Koerner, D. W., Sargent, A. I., & Blake, G. A. 2003, ApJ, 597, 986

Sargent, A. I. & Beckwith, S. 1987, ApJ, 323, 294

Shu, F. H. 1977, ApJ, 214, 488

Tafalla, M., Mardones, D., Myers, P. C., et al. 1998, ApJ, 504, 900

Udry, S. & Santos, N. C. 2007, ARA&A, 45, 397

Ungerechts, H. & Thaddeus, P. 1987, ApJS, 63, 645

Weidenschilling, S. J. 1977, MNRAS, 180, 57

Whipple, F. L. 1972, in From Plasma to Planet, ed. A. Elvius, 211

Wilner, D. J., Ho, P. T. P., Kastner, J. H., & Rodríguez, L. F. 2000, ApJ, 534, L101

CHAPTER 2

Gas and dust mass in the disc around the Herbig Ae star HD169142

O. Panić, M.R. Hogerheijde, D. Wilner and C. Qi

S PATIALLY resolved observations of circumstellar discs at millimetre wavelengths allow detailed comparisons with theoretical models for the radial and vertical distribution of the material. We investigate the physical structure of the gas component of the disc around the pre-main-sequence star HD169142 and test the disc model derived from the spectral energy distribution. The ^{13}CO and C^{18}O J=2–1 line emission was observed from the disc with $1\overset{''}{.}4$ resolution using the Submillimeter Array. We adopted the disc physical structure derived from a model that fits the spectral energy distribution of HD169142. We obtained the full three-dimensional information on the CO emission with the aid of a molecular excitation and radiative transfer code. This information was used for the analysis of our observations and previous ^{12}CO J=2–1 and 1.3 mm continuum data. The spatially resolved ^{13}CO and C^{18}O emission shows a Keplerian velocity pattern. The disc is seen at an inclination close to $13°$ from face-on. We conclude that the regions traced by different CO isotopologues are distinct in terms of their vertical location within the disc, their temperature, and their column densities. With the given disc structure, we find that freeze-out is not efficient enough to remove a significant amount of CO from the gas phase. Both observed lines match the model prediction both in flux and in the spatial structure of the emission. Therefore we use our data to derive the ^{13}CO and C^{18}O mass and consequently the ^{12}CO mass with standard isotopic ratios. We constrain the total disc gas mass to (0.6-3.0)$\times10^{-2}$ M$_\odot$. Adopting a maximum dust opacity of 2 cm^{2}g$_{dust}^{-1}$ we derive a minimum dust mass of 2.16×10^{-4} M$_\odot$ from the fit to the 1.3 mm data. Comparison of the derived gas and dust mass shows that the gas-to-dust mass ratio of 100 is only possible under the assumption of a dust opacity of 2 cm^{2}g^{-1} and ^{12}CO abundance of 10^{-4} with respect to H$_2$. However, our data are also compatible with a gas-to-dust ratio of 25, with a dust opacity of 1 cm^{2}g^{-1} and ^{12}CO abundance of 2×10^{-4}.
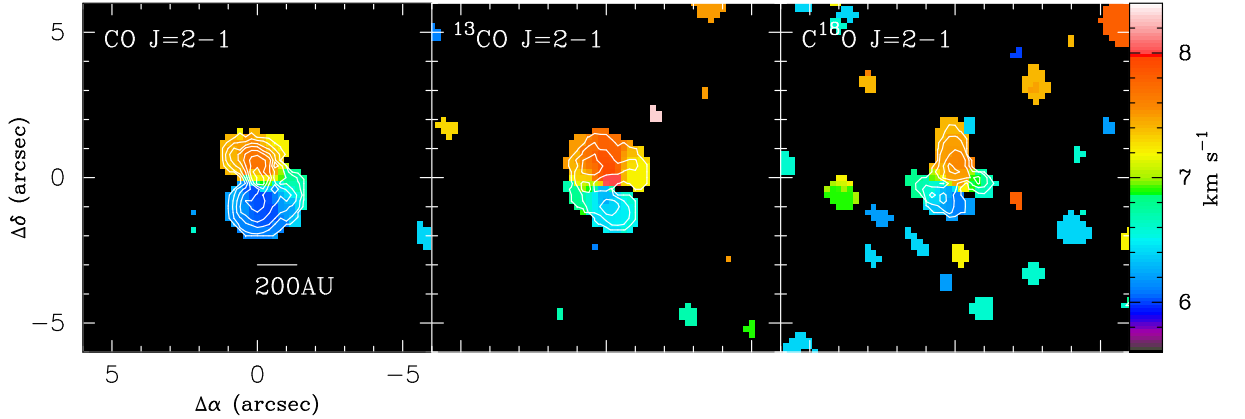
Figure 2.1: Integrated intensity (contours) and first moment maps (colour scale) of ^{12}CO J=2–1 (left panel, from Raman et al. (2006)), ^{13}CO J=2–1 (middle panel) and C^{18}O J=2–1 line (right panel). Contours are 1, 2, 3,...×200 mJy beam^{-1} km s^{-1} for ^{12}CO and ^{13}CO, and 1, 2, 3,...×100 mJy beam^{-1} km s^{-1} for C^{18}O. The integrated intensity and first moment maps are obtained over a velocity range of 5.6-8.4 km s^{-1}. The data were clipped at 0.7, 0.5, and 0.35 Jy beam^{-1} for ^{12}CO, ^{13}CO, and C^{18}O, respectively.

2.1 INTRODUCTION

Although the presence of molecular gas in discs around intermediate mass pre-main-sequence (Herbig Ae) stars was reported a decade ago (Mannings & Sargent 1997), the research in this field has focused more on their less massive counterparts (T Tauri stars). The discs around T Tauri stars have masses ranging from 0.001 to 0.1 M$_\odot$ (Beckwith et al. 1990), usually derived from millimetre continuum fluxes assuming a gas-to-dust mass ratio of 100, as in molecular clouds. Their outer radii are constrained by molecular line observations and are typically a few hundred AU (Simon et al. 2000; Thi et al. 2001, and references therein). Due to the low luminosity of the central star (0.5 to 1 L$_\odot$), these discs are relatively cold (less than 20 K beyond 100 AU from the star) causing a significant depletion of the CO in the midplane of the outer disc. On the other hand, the Herbig Ae stars are about ten times more luminous than T Tauri stars, and consequently their discs are warmer. This allows the CO, the easiest to detect and the most commonly used gas tracer, to remain in the gas phase even in the disc midplane. Observations of CO and its isotopologues toward Herbig Ae stars are therefore expected to be more powerful probes of the full disc structure. Only a few Herbig Ae discs have been studied thoroughly via spatially resolved observations of molecular line emission that includes the optically thin CO isotopologues: AB Aur (Piétu et al. 2005), MWC480 (Piétu et al. 2007), and HD163296 (Isella et al. 2007).

2.2 HD169142

The object of our study, HD169142, is a 2.0 M$_\odot$ Herbig Ae star of spectral type A5Ve surrounded by a gas-rich circumstellar disc located at 145 pc (Sylvester et al. 1996).
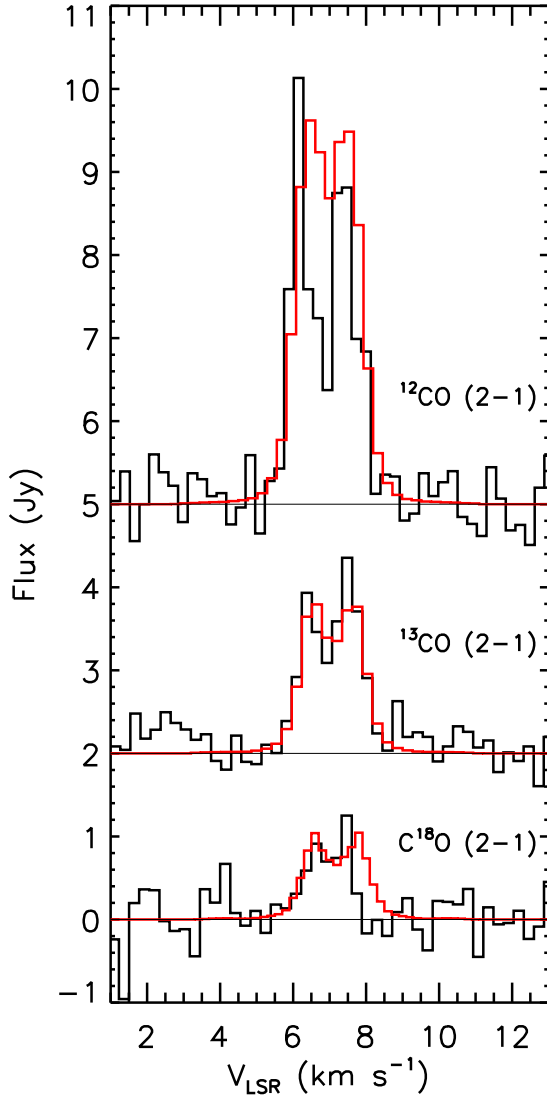
Figure 2.2: Spectra of C^{18}O J=2–1 (bottom), ^{13}CO J=2–1 (middle), and ^{12}CO J=2–1 line (top, from Raman et al. (2006)) summed over the central $4'' \times 4''$ toward HD169142. The ^{13}CO and ^{12}CO fluxes are shifted vertically by 2 and 5 Jy, respectively. Black lines show the observed spectra and the red lines show the model fit found in Section 4.3.1. For ^{12}CO, the model from Raman et al. (2006) was used.

With an age of 6^{+6}_{-3} Myr (Grady et al. 2007) and its spectral energy distribution marked by infrared excess and the lack of silicate features (Dent et al. 2006), HD169142 is an example of an advanced pre-main-sequence evolutionary stage. Unlike most of the Herbig Ae/Be stars, it shows no evidence of proximity to a cloud or extended molecular gas (Meeus et al. 2001). Observations of molecular gas in this disc are therefore easier to interpret. However, HD169142 is not completely isolated from other young stars; e.g., Grady et al. (2007) find three coeval pre-main-sequence stars within a projected separation of 1160 AU. The closest companion is located at 9$\overset{''}{.}$3 separation and may form a binary system with HD169142. Near-infrared polarisation images show that the dust in the disc extends to at least 217 AU (Kuhn et al. 2001). More recent submillimetre observations (Dent et al. 2005; Raman et al. 2006) show bright and narrow CO lines. Raman et al. (2006) spatially resolve the disc and find a fit to the CO J=2–1 line and 1.3 mm continuum observations by adopting a flared accretion disc model with a 235 AU radius and a 13° inclination from face on. Observations at optical, IR,

and (sub)millimetre wavelengths allowed modelling of the disc's spectral energy distribution (SED) (Malfait et al. 1998; Dominik et al. 2003; Dent et al. 2006). Malfait et al. (1998) fitted the near-infrared and far-infrared excess of HD169142 by two disc components: an inner disc extending from 0.5 AU to 1 AU with a density exponent of 2.0 and the outer disc from 28 AU with a flatter density distribution. Dominik et al. (2003) adopt a low inclination of 8°, outer radius of 100 AU, and surface density exponent p=2 to fit the SED, and therefore derive a disc mass of 0.1 M$_\odot$. A more detailed SED modelling is done by Dent et al. (2006) where both the SED and resolved 7 mm continuum emission were fitted using an accretion disc model (D'Alessio et al. 2005) corresponding to a 10 Myr old A2 spectral type star. They adopt an inclination of 30° and outer radius of 300 AU, and derive a disc mass of 4×10^{-2} M$_\odot$. Grady et al. (2007) fit the SED and NICMOS image at 1.1 μm with a model consisting of two distinct disc components - the inner disc from 0.15 to 5 AU radius and the outer disc extending from 44 to 230 AU. It is important to stress that all the above mass estimates of the disc around HD169142 are based solely on the observed dust emission, and not gas.

This paper presents resolved interferometric observations of the ^{13}CO and C^{18}O J=2–1 lines from HD169142. The observations and results are shown in Secs 3 and 4. Section 4 introduces the disc model we adopt (D'Alessio et al. 2005; Dent et al. 2006; Raman et al. 2006) and our fit to the 1.3 mm data providing a measure of the minimum dust mass of the disc. We fit the ^{13}CO and C^{18}O emission, thereby deriving the corresponding ^{13}CO and C^{18}O mass in the disc. We place constraints on the total gas mass of the disc. We discuss the implications for the gas-to-dust ratio and microturbulence in the disc. Section 5 summarises our findings.

2.3   OBSERVATIONS AND RESULTS

The observations of HD169142 were carried out with the Submillimeter Array[1] (SMA) on 2005 April 19, simultaneous with the observations of ^{12}CO J=2–1 line presented in Raman et al. (2006). A more detailed description of the observations and of the calibration procedure is given there. The correlator provided 2 GHz of bandwidth in each sideband and was configured to include the ^{13}CO J=2–1 line at 220.3986765 GHz and the C^{18}O J=2–1 line at 219.5603568 GHz in the lower sideband in a 104 MHz wide spectral band with channel spacing of 0.2 MHz ($\sim$0.26 km s^{-1}).

The data reduction and image analysis were done with the Miriad data reduction tools (Sault et al. 1995). The (u,v) data were Fourier transformed using natural weighting. The resulting synthesized beam size is $1\rlap{.}''4 \times 1\rlap{.}''0$ (PA=26°). The rms of the line images is 180 mJy beam^{-1} per channel or 4.6 K (4.8 K for ^{12}CO).

Emission of ^{13}CO and C^{18}O J=2–1 was detected from the HD169142 circumstellar disc. Figure 3.2 shows the intensity weighted velocity maps with overlaid integrated intensity contours for both lines as well as the previously published ^{12}CO J=2–1 line (Raman et al. 2006). The intensity integrated over the velocity range from 5.6 to

---

8.4 km s^{-1}, in which the line emission is fully contained, and over the central $4'' \times 4''$ region is 12.1, 6.5 and 2.7 Jy km s^{-1} for ^{12}CO, ^{13}CO and C^{18}O J=2–1 line, respectively. All three lines follow a similar velocity pattern, interpreted as a clear indication of Keplerian rotation around a 2 M$_\odot$ star of a disc seen at 13° inclination (Raman et al., 2006; this work). Figure 6.5 shows the ^{12}CO, ^{13}CO and C^{18}O J=2–1 line spectra summed over a $4'' \times 4''$ region centred on the HD169142 position. The profiles are relatively symmetric, double-peaked, and centered on 7.1$\pm$0.2 km s^{-1} and reflecting the underlying rotation pattern. The ^{12}CO and 1.3 mm results were presented by Raman et al. (2006). They report a 1.3 mm line flux of 169$\pm$5 mJy. In Fig. 2.3 the emission stucture is shown over a range of velocities corresponding to the ^{13}CO J=2–1 line (top panel). The emission extends to $2''$ (270 AU) from the star at a 2σ level and shows a Keplerian velocity pattern. Figure 2.4 presents the channel maps of the C^{18}O J=2–1 line (top panel) with a kinematic structure similar to that of the ^{13}CO J=2–1 line seen in Fig. 2.3. The 2σ level emission reaches $1''5$ (220 AU) from the star. At 7.4 km s^{-1} a localised emission peak of 0.94$\pm$0.35 Jy is seen $1''0$ north from the star.

2.4 DISCUSSION

Raman et al. (2006) show that the model that fits the SED of HD169142 can also be used to fit the structure and intensity of the resolved ^{12}CO emission. They note that some weak residual emission is still present after subtracting the model from the observational data, that may correspond to real substructure within the disc. We analysed the ^{13}CO and C^{18}O data, which are expected to probe different depths in the disc due to their lower opacities.

2.4.1   Adopted disc model

Dent et al. (2006) fit the spectral energy distribution (SED) of HD169142 using an accretion disc model from the D'Alessio et al. (2005) database with an accretion rate of 10^{-8} M$_\odot$yr^{-1}, an outer radius of 300 AU, and a 30° inclination. The age of the central star in this model is 10 Myr. They adopt an A2 spectral type for the central star because it provides a slightly better fit than the A6 spectral type model does to the SED in the range of 2-200 μm dominated by the warm dust emission. However, there is no significant difference between the SEDs corresponding to these two models. Beyond 44 AU from the star, the model is qualitatively similar to the model of the outer disc of HD169142 described in Grady et al. (2007). The detailed model structure, including plots of surface density distribution, temperature at different scale heights, and optical thickness of the disc, is provided in the online database of accretion disc models (D'Alessio et al. 2005)[2].

In order to match their resolved submillimetre observations of CO, Raman et al. (2006) modify the model used in Dent et al. (2006) to have a disc radius of 235 AU. Assuming the mass of the central star to be 2 M$_\odot$, they derive an inclination of 13$\pm$1°

---

[2]www.astrosmo.unam.mx/ dalessio/
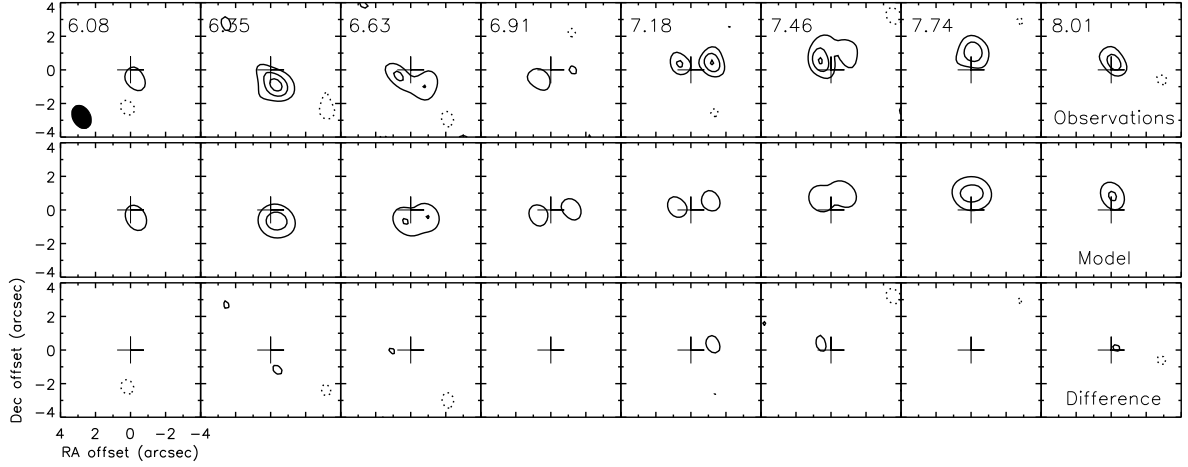
Figure 2.3: – *Top panel:* Channel maps of the observed ^{13}CO *J*=2–1 emission at a range of velocities over which the line is detected. The lower left corner of this panel shows the size and position angle of the synthesized beam. – *Middle panel:* ^{13}CO *J*=2–1 chanel maps from the best-fit disc model from Section 4.3.1. – *Lower panel:* Channel maps showing the residual emission after subtraction of the best-fit model from the data. The contour levels are -1,1,2,3,4×360 mJy beam^{-1} (2 sigma) in all panels.
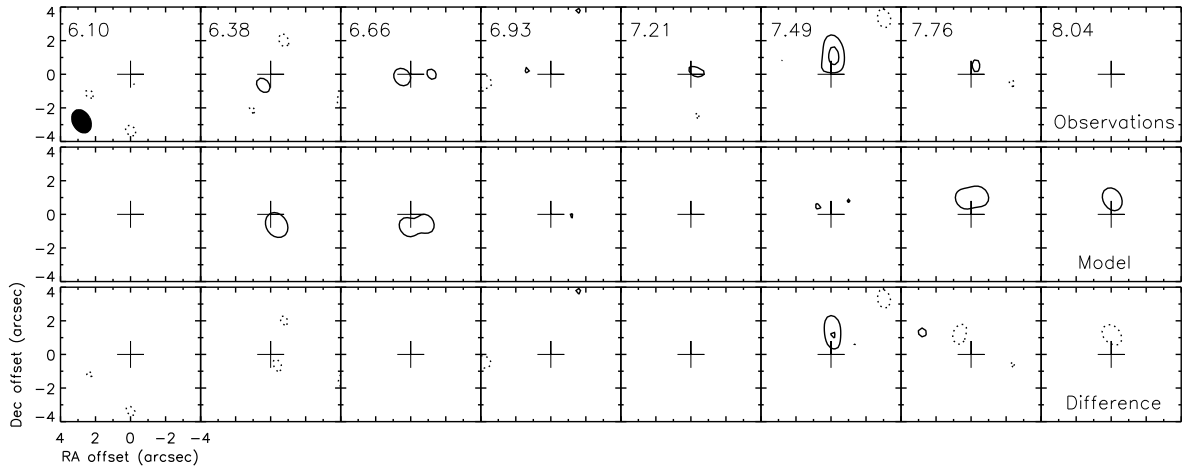
Figure 2.4: – *Top panel:* Channel maps of the observed C^{18}O *J*=2–1 emission at a range of velocities over which the line is detected. The lower left corner of this panel shows the size and position angle of the synthesized beam. – *Middle panel:* C^{18}O *J*=2–1 channel maps from the best-fit disc model from Section 4.3.1. – *Lower panel:* Channel maps showing the residual emission after subtraction of the best-fit model from the data. The contour levels are -1,1,2,3,4,5×360 mJy beam^{-1} (2 sigma) in all panels.

from face-on and use it in the model. These modifications are not expected to affect the quality of the SED fit since the SED of HD169142 alone does not constrain the outer radius and inclination of the disc well. They show that this SED model can be used to fit the structure and intensity of the resolved ^{12}CO emission. However, the SED does not provide reliable constraints of the disc dust mass, which in the model is set to 2×10^{-4} M$_\odot$. This parameter depends only on the optically thin thermal emission from the disc in the millimetre wavelength region.

The density in the model is a parameter that can be scaled by a factor of few, without significantly affecting the computed disc temperature structure. The resulting mass only affects the millimetre flux in the modelled SED, i.e., the 1.3 mm data point. In section 4.2 we re-analyse the 1.3 mm data from Raman et al. (2006) using a radiative transfer code to calculate the emission from the model and better constrain the dust mass of the disc.

In the analysis of our ^{13}CO and C^{18}O line emission (section 4.3) we use this improved disc model, which already encompasses a range of observational constraints. We assume that the gas follows the dust distribution prescribed by the model and that their temperatures are the same. The micro turbulent FWHM of the lines is set to 0.16 km s^{-1} throughout the disc. One conclusion that we can already draw from the disc model is the fraction of disc mass where freeze-out of CO is likely to be efficient, which is believed to happen at temperatures below 20 K. The mass weighted temperature in the model is 35 K, which indicates that the bulk of the disc material is at temperatures above 20 K. The temperature falls below 20 K only in the midplane region of the disc beyond 150 AU from the star and there the abundance of the gas phase CO and its isotopologues is expected to be heavily decreased due to freeze-out of these molecules onto dust grains. This region contains only 8% of disc mass and therefore any mass estimate based on ^{13}CO and C^{18}O emission may represent 92-100% of the true disc mass.

In all previously published work on HD169142, the disc gas mass was inferred indirectly from the derived disc dust mass, adopting a standard gas-to-dust ratio. In our analysis of the ^{13}CO and C^{18}O emission we argue that it is reasonable to assume a standard ^{12}CO abundance in the case of HD169142, because freeze-out affects less than 8% of the mass in this disc. Therefore we investigate the constraints that can be obtained from our molecular line data on the disc gas mass.

2.4.2   Dust continuum emission

From the observed 1.3 mm continuum flux of 169$\pm$5 mJy, Raman et al. (2006) derive a dust mass of 2×10^{-4} M$_\odot$ assuming an emissivity κ_ν^{dust}=2 cm^{2}g$_{dust}^{-1}$ and a single temperature of 30 K. We reanalyse the 1.3 mm emission using the disc temperature and density structure from the model described in section 4.1, where we vary the dust density (i.e., the dust mass) to fit the observations. A large uncertainty on the mass determination from the 1.3 mm continuum flux is due to the dust opacity, which is not well-determined in circumstellar discs. Ossenkopf & Henning (1994) study the effects of dust coagulation, and ice coverage of grains on their opacity in protostellar cores and

suggest 1.3 mm opacity of 1 $cm^2 g_{dust}^{-1}$ for very dense ($n > 10^7$ cm^{-3}) regions, and up to 5 times more if the grains are not covered in ice mantles. The latter is thus only valid for regions above water ice desorption temperature (80-100 K, Fraser et al. (2001)). In their study of the dust opacity in circumstellar discs Draine (2006) find that astrosilicate and pirolysed cellulose at 600 °C are materials representative of the dust properties which may be expected in circumstellar discs. They explore a wide range of grain size distributions and find that these materials have mm-wavelength opacities which are close to the observational constraints on dust opacity from extinction studies of the diffuse interstellar medium presented in Weingartner & Draine (2001). The resulting opacity could be anywhere between 0.1 and 2 $cm^2 g_{dust}^{-1}$ at the wavelength of 1.3 mm, depending on the adopted grain size. We use this information to calculate the minimum amount of dust needed to produce the observed flux by adopting the opacity (and emissivity) of 2 $cm^2 g_{dust}^{-1}$. The SED modelling of the disc emission at shorter wavelengths is not affected by our assumptions of dust opacity at 1.3 mm. The dust thermal emission is dominated by the cold disc midplane at large radii, likely to contain settled and/or grown dust particles whose optical properties may differ from those of the small dust at disc surface, responsible for the optically thick near-infrared and infrared emission of the disc.

We do the full modelling of the interferometric visibilities using the radiative transfer code of Hogerheijde & van der Tak (2000) (RATRAN). We perform a χ^2 minimisation to fit the 1.3 mm visibilities by varying the disc dust mass. The best match is shown in Fig. 3.8, top-left panel, resulting in an estimate of the dust mass of the disc, given by

$$M_{dust} = 2.16 \times 10^{-2} \frac{2 \ cm^2 g_{dust}^{-1}}{\kappa_{1.3 \ mm}} \times M_{\odot}. \qquad (2.1)$$

Assuming that the adopted dust opacity of 2 $cm^2 g_{dust}^{-1}$ is the maximum value, our estimate presents the lower limit on the dust mass in HD169142: $M_{dust} \geq 2.16 \times 10^{-4}$ $M_{\odot}$. A slightly higher maximum dust opacity of 7 $cm^2 g_{dust}^{-1}$ is obtained for pyrolised cellulose at 800 °C but this value exceeds greatly the observational contraints from Weingartner & Draine (2001) and although not impossible, is unlikely in discs (Draine 2006). However we cannot exclude the possibility that other dust properties like cristallinity, porosity and shape, which are not understood well, may enhance dust submillimetre opacity beyond 2 $cm^2 g_{dust}^{-1}$ by a factor of a few.

2.4.3   Molecular line emission

Due to their low abundance relative to ^{12}CO, the ^{13}CO and $C^{18}O$ molecules emit lines that are comparatively less optically thick. As a result of this, they saturate at different heights in the disc allowing us to use them as a probe of the physical conditions in different disc layers and investigate the disc vertical structure (Dartois et al. 2003). Furthermore, the $C^{18}O$ line emission is often optically thin in the outer disc region, where the bulk of disc mass is located, which makes it a valuable probe of the disc gas mass.

The commonly employed route for the analysis of the CO isotopologue and dust continuum emission from circumstellar discs is to convert the continuum flux to disc mass by adopting a certain dust opacity, usually 0.02 cm^{2}g$^{-1}_{gas}$ (Beckwith et al. 1990), under the assumption of the canonical gas-to-dust mass ratio of 100. In this way, the molecular line emission is fit for abundance, where any discrepancy with respect to the canonical abundances and isotopic ratios of observed molecules is explained by a depletion factor, indicating the fraction of the CO gas affected by the freeze-out onto dust grains or selective photodissociation. This approach is used in Raman et al. (2006) where the analysis of the ^{12}CO J=2–1 line emission and 1.3 mm continuum from HD169142 is done for a disc mass of 2×10^{-2} M$_\odot$ and ^{12}CO was found to be depleted by a factor four, having an abundance of 2.5×10^{-5}. This corresponds to 6×10^{-6} M$_\odot$ of ^{12}CO molecules present in gas phase in the disc. In the present work, we argue that the ^{12}CO abundance is not significantly affected by freeze-out or selective photodissociation and we chose to follow a different route, in which we derive a rough gas mass estimate from the molecular line observations taking into account all related uncertainties.

To interpret our ^{13}CO and C^{18}O observations, we adopt the disc model described in detail in section 4.1. We set the dust mass in the model to 2.16×10^{-4} M$_\odot$; the value derived as the minimum dust mass for HD169142 in section 4.2. We assume that the molecular gas follows the dust temperature and density structure and we vary the ^{13}CO and C^{18}O gas masses to fit the observations. We calculate the ^{13}CO and C^{18}O J=2–1 line emission from the model using the RATRAN molecular excitation and radiative transfer code. The model visibilities are generated with the miriad task uvmodel, and the comparison to the observed visibilities is done directly. We use assumptions about the molecular abundances of the ^{12}CO and isotopic ratios to make a conversion to the total gas mass ($1.2\times$M$_{H_2}$). We explore a range of values of the gas-to-dust mass ratio f$_{g/d}$.

Disk structure probed by ^{13}CO and C^{18}O

We find fits to the observed visibilities of ^{13}CO and C^{18}O line for M$_{^{13}CO}$=2.9×10^{-7} M$_\odot$ and M$_{C^{18}O}$=4.6×10^{-8} M$_\odot$, shown in the bottom panels of Fig. 3.8. For comparison, the visibilities of the ^{12}CO J=2–1 line are also shown in Fig. 3.8, top-right panel, with the best fit obtained by Raman et al. (2006) for M$_{^{12}CO}$=6×10^{-6} M$_\odot$ contained in the gas phase. In order to test our fit further, we invert and deconvolve the visibilities using the miriad reduction package and compare the observed (top panels) and modelled (middle panels) velocity channel maps in Figs. 2.3 and 2.4. The structure and intensity of the emission is found to be well-matched. Figures 2.3 and 2.4 (lower panels) show the residual emission resulting from subtraction of the modelled from the observed data. For ^{13}CO the residuals appear randomly distributed and do not exceed the noise level. Significant residuals are seen in C^{18}O at 7.4 km s^{-1} about $0''.5$ north from the star. The C^{18}O data (Fig. 2.4) have a marginally significant localised excess $1''.0$ north of the star seen at 3 σ level in the residual emission. This excess emission corresponds to the redshifted peak of the spectral line at v$_{LSR}$=7.4 km s^{-1}. It is marginally resolved at $1''.5 \times 2''.5$ and contains about 20% of C^{18}O line flux. Similar, but not spatially coincident
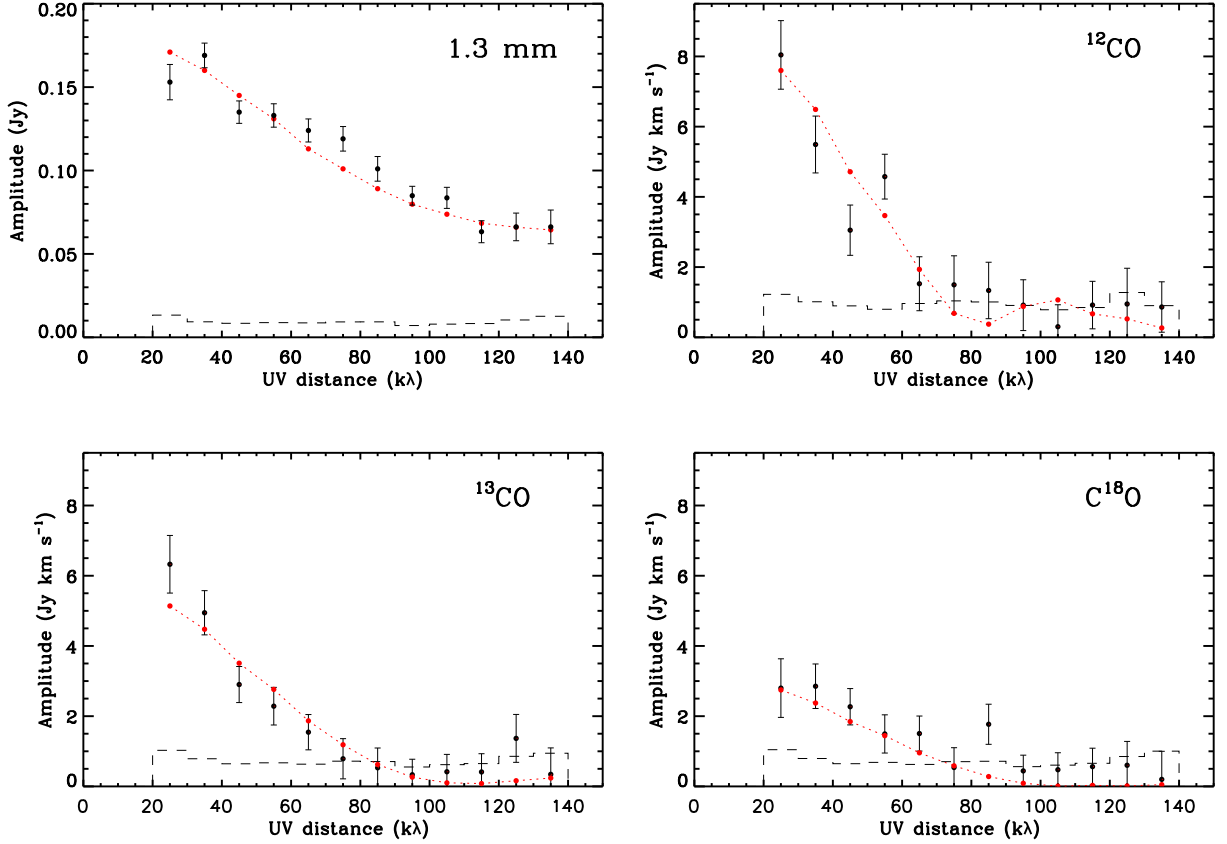
Figure 2.5: *Top-left:* Vector-averaged continuum flux as a function of projected baseline length (black dots). The error bars represent the variance within each annular average. The zero-signal expectation value is shown by the dashed histogram. The red dotted line shows the best-fit model for a dust emissivity of 2.0 $\mathrm{cm^2 g_{dust}^{-1}}$ with the disc mass of 2.16×10^{-4} $M_\odot$. *Top-right:* Same for the ^{12}CO emission from Raman et al. (2006), integrated over the width of ≈ 2.7 km s^{-1} (10 spectral channels) centred on each line. The red dotted line shows the model presented by Raman et al. (2006). *Bottom-left and bottom-right:* Same for our ^{13}CO and C^{18}O J=2–1 data, respectively. The red dotted lines show the best-fit model from Section 4.3.1.

residual emission is also seen in ^{13}CO (Figure 2.3, lower panel) near the noise levels, but not in ^{12}CO. A cause of this feature may lie in disc midplane asymmetry. Any connection with the reported companion at 9″.3 is unlikely, but a hypothesized body within the inner disc is an interesting prospect (Grady et al. 2007). Nevertheless, an instrumental or calibration artefact may have affected the 7.4 km s^{-1} channel resulting in a slight increase of flux in that channel in the lower sideband, only noticeable in the weak C^{18}O line.

In this section we will use our ^{13}CO and C^{18}O results to make an estimate of the total gas mass M$_{gas}$ in the disc, related to the ^{12}CO gas mass M$_{^{12}CO}$ through

$$\mathrm{M_{gas}} = 1.2 \times \frac{\mathrm{m_{H_2}}}{\mathrm{m_{^{12}CO}}} \times \frac{1}{[^{12}\mathrm{CO}]} \times \mathrm{M_{^{12}CO}}. \tag{2.2}$$
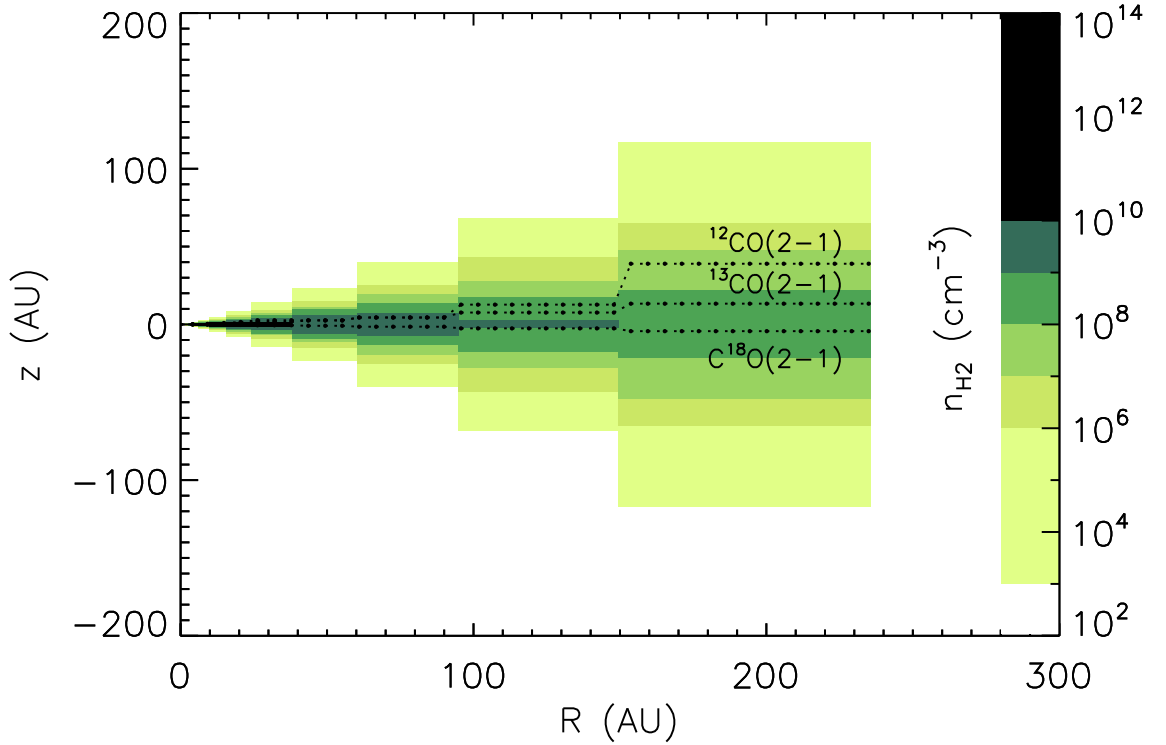
Figure 2.6: Density structure of the best-fit disc model shown as colour scale. The disc is viewed by us from almost straight above. The three dotted lines show the heights above which 90% of the integrated line emission of ^{12}CO, ^{13}CO and C^{18}O J=2–1 originates. For the C^{18}O emission this line lies below the disc midplane.

where m_{H_2} and $m_{^{12}CO}$ are the masses of the H$_2$ and ^{12}CO molecule, and [^{12}CO] is the abundance of ^{12}CO with respect to H$_2$. The factor of 1.2 accounts for one fifth of the gas contained in helium. We can use the derived masses of the ^{13}CO and C^{18}O gas to calculate the mass of the ^{12}CO gas. We adopt the isotopic ratios of ^{12}C/^{13}C=77±7 and ^{16}O/^{18}O=560±25 from Wilson & Rood (1994).

$$M_{^{12}CO} = \frac{m_{^{12}CO}}{m_{C^{18}O}} \times \frac{[^{16}O]}{[^{18}O]} \times M_{C^{18}O} = (2.4 \pm 1.0) \times 10^{-5} M_\odot \qquad (2.3)$$

$$M_{^{12}CO} = \frac{m_{^{12}CO}}{m_{^{13}CO}} \times \frac{[^{12}C]}{[^{13}C]} \times M_{^{13}CO} = (2.2 \pm 0.6) \times 10^{-5} M_\odot \qquad (2.4)$$

The values obtained here are given with errors which are dominated by the rms of our data and also include the errors on isotopic ratios. If we take into account that 8% of the ^{12}CO and its isotopologues in HD169142 may be depleted onto dust grains and therefore not contributing to the emission observed, then the full ^{12}CO mass range is (1.4-3.7)×10^{-5} M$_\odot$. The fact that both datasets roughly agree on the ^{12}CO mass provides an additional argument for the validity of the model. However, the fit to the

^{12}CO J=2–1 data done in Raman et al. (2006) corresponds to a mass of gas phase ^{12}CO of 6×10^{-6} M$_\odot$ (mentioned in section 4.3), two to six times lower than the range derived here. The ^{12}CO emission is optically thick and therefore it does not trace the entire disc but originates from a layer much higher in the disc than either the ^{13}CO or C^{18}O lines (Dartois et al. 2003). The discrepancy between the ^{12}CO result and that of the isotopologues indicates that the adopted disc model may not provide the best description in these high layers. We will discuss this in more detail in section 4.5 where the effects of temperature and turbulence on the line profile are discussed.

Our model calculations allow us to identify which regions of the disc contribute most to the observed lines. We followed the line-of-sight integration step by step from the observer into the disc and find the location where 90% of the integrated intensity is reached for a face-on orientation of the disc. We show these locations in Fig. 2.6 in a cross-section of the disc showing the underlying density structure. We chose to use the intensity integrated over a range of wavelengths in which the line is emitted, in order to better represent the region corresponding to the physical quantity that is observed, i.e., the line flux. The use of surfaces with equal opacity (often used τ=3) may be misleading, because the opacity at the line centre is not necessarily consistent with the opacity in the line wings, and the amount of flux still produced in the line wings beyond the τ=3 surface may contribute significantly to the line flux in some species more than in the others. The calculation was done for the ^{12}CO, ^{13}CO, and C^{18}O J=2–1 lines. The discontinuous shape of the surface above which 90% of the integrated intensity in these lines is emitted stems from the discrete cells in the grid of our model that were used to sample the density and temperature structure. As expected, the less optically thick species trace regions deeper in the disc with C^{18}O tracing the disc midplane, while ^{12}CO traces the disc surface layer. We analysed the physical properties of the emitting regions in the outer disc, beyond 100 AU from the star (scales resolved by our SMA observations). For the two outermost radial positions in our model grid, we calculated the column of ^{12}CO gas contained in the region where 90% of the emission is coming from, which is located above the vertical position shown in Fig. 2.6, for each molecular line. These values are shown in Table 2.1[3]. Also, the average temperature of these gas columns was calculated, taking the temperature weighted by the column density (i.e., mass) into account for each cell located above the vertical positions from Fig. 2.6. The C^{18}O J=2–1 line generally traces three times as much CO gas as traced by the ^{13}CO J=2–1 line in the outer disc, while the ^{12}CO J=2–1 line traces only a small fraction of the gas, a few percent of the column traced by C^{18}O. It is clearly seen that the C^{18}O traces deep into the disc, to the height of several AU at the far side of the midplane, showing that it is very sensitive to the total gas mass. The 90% of the C^{18}O J=2–1 line emission traces around 60% of the total gas column.

In section 4.1 we already concluded from the disc model that the CO freeze-out could only be efficient in the cold outer disc midplane region that contains 8% of the total disc mass. This very small fraction is due to the luminosity of the Herbig Ae star HD169142, which is higher than the typical luminosity of T Tauri stars. In the latter, the circumstellar discs are colder and the CO freeze-out presents a major obstacle to deter-

---

[3]The calculations for ^{12}CO J=2–1 are done for the model presented in Raman et al. (2006)

Molecular Line	z(AU) 100-149 AU	z(AU) 149-235 AU	N_{CO}(cm^{-2}) 100-149 AU	Fraction Of Total N_{CO}	N_{CO}(cm^{-2}) 149-235 AU	Fraction Of Total N_{CO}	T_{ave} (K) 100-149 AU	T_{ave} (K) 149-235 AU
^{12}CO J=2-1	12.7	39.0	6.5×10^{17}	7%	6.6×10^{16}	1%	33.3	38.6
^{13}CO J=2-1	7.6	13.0	4.2×10^{18}	17%	2.6×10^{18}	18%	29.1	25.6
C^{18}O J=2-1	-2.5	-4.3	1.5×10^{19}	62%	8.9×10^{18}	62%	25.7	21.8

Table 2.1: Column of ^{12}CO traced by 90% of the emission of each line, and the corresponding average temperature, at two radial intervals beyond 100 AU.

mining gas mass based on observations of CO or its isotopologues. As a caveat, we note that Piétu et al. (2006) find somewhat lower dust temperature in the disc around the Herbig Ae star MWC 480 (10-25 K at 100 AU). Since we have no indications to the contrary, we adopt the dust temperature that SED disc modelling suggests. If observed with a sufficiently high resolution and sensitivity, discs where CO freeze-out is efficient are expected to have smaller radii derived from CO isotopologues compared to the outer radius derived from the ^{12}CO and from the dust emission. Although our observations are limited by the beam size (1″.4≈200 AU) we have tested a range of different outer radii and found that, based on our molecular line data, the outer radius should not be very different from 200 AU for either of the observed lines. We also do not find any significant discrepancy between the molecular line data and dust continuum that could indicate different outer radii for gas and dust.

Another factor that can influence the ^{12}CO abundance is photodissociation. The effect of photodissociation via the stellar UV radiation on CO abundance in circumstellar discs is studied in van Zadelhoff (2002) and van Zadelhoff et al. (2003). They find that the CO abundance decrease due to photodissociation is significant only in the upper disc layers and that the CO column density is not much affected by it. Jonkheid et al. (2004) show that the stellar UV field is only able to heat 10% of the gas mass in the disc to considerably high temperatures, in the surface disc layer. The effect of photodissociation on the CO content of HD169142 is expected to be small, due to the significant dust mass of the disc. Since we adopt a maximum emissivity and therefore minimal dust mass, the conclusion that photoionization can be neglected is robust. In addition, the C^{18}O emission that we use to derive the gas mass, arises predominantly from the outer disc midplane region that contains the bulk of the disc mass and does not receive any direct UV illumination from the central star. This further minimises the effects of photodissociation on our results. Therefore, we find it appropriate to use the ^{12}CO mass derived from our best fit to the C^{18}O and ^{13}CO data to make an estimate of the total gas mass.

The abundance of ^{12}CO is a key factor in this conversion and the values found in the literature for the interstellar medium range from 9.5×10^{-4} (Frerking et al. 1982) to 2.0×10^{-4} (Lacy et al. 1994). If we adopt the ^{12}CO abundance of 10^{-4} with respect to H$_2$, we obtain M$_{gas} = 1.2 \times$ M$_{H_2} = (2.0^{+1.0}_{-0.8}) \times 10^{-2}M_\odot$. The error estimate includes the error due to the rms of our C^{18}O data (41%) and to the isotopic ratio of [^{16}O]/[^{18}O] (4%). The upper margin is extended to include the 8% uncertainty in the gas mass estimate due to freeze-out. The factor 1.2 takes the gas mass contained in helium into account. Adopting a ^{12}CO abundance of 2.0×10^{-4} with respect to H$_2$ results in M$_{gas}$ as low as 6×10^{-3} M$_\odot$. Therefore, due to the uncertainty largely dominated by the ^{12}CO abundance, we can only conclude that the gas mass of the disc around HD169142 falls in the range of $(0.6\text{-}3.0) \times 10^{-2}$ M$_\odot$.

2.4.4 Gas-to-dust ratio

To investigate the gas-to-dust ratio, we ran several models in which we assume that M$_{dust}$=2.16×10^{-4} M$_\odot$, [CO]=10^{-4}, ^{12}C/^{13}C=77, ^{16}O/^{18}O=560, and gas-to-dust mass ra-
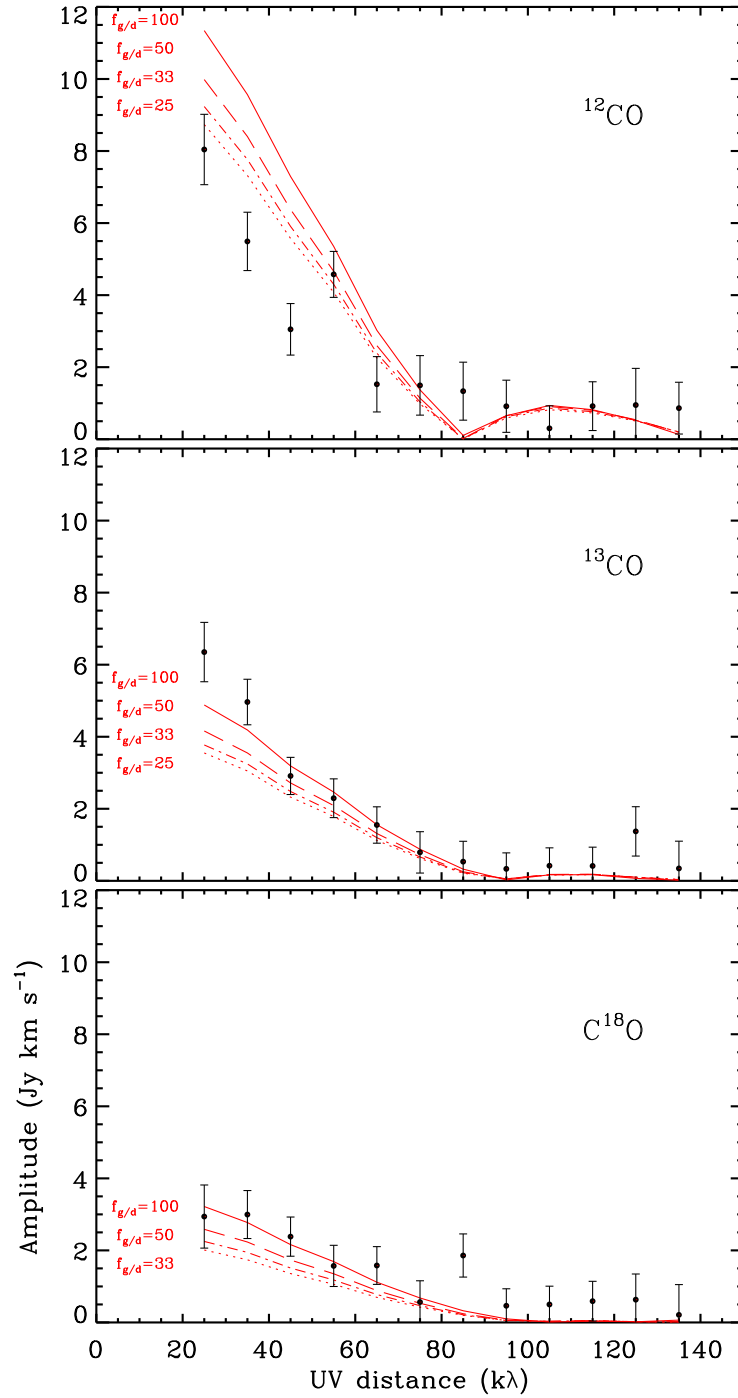
Figure 2.7: Comparison of the observed vector-averaged ^{12}CO (*top panel*), ^{13}CO (*middle panel*) and C^{18}O (*lower panel*) line fluxes (black) to four models with different gas-to-dust ratios (red lines). The error bars represent the variance within each annular average. The models assume the dust mass of 2.16×10^{-4} M$_\odot$ and gas-to-dust mass ratio $f_{g/d}$=100,50,33,25 marked respectively by the full, dashed, dashed-dotted and dotted red lines in each panel. The line fluxes are integrated over the width of ≈ 2.7 km s^{-1} (10 spectral channels) centred on each line.

tios of 100, 50, 33, and 25. From the comparison of the synthetic visibilities of these models with the observations (Fig. 2.7, middle and lower panel) we find that a good fit for ^{13}CO and C^{18}O data is obtained for $f_{g/d}$=100. Under the assumptions used above, lower values of $f_{g/d}$ fail to provide a fit to the data. The ^{12}CO data (Fig. 2.7, top panel) shows a discrepancy, already discussed in Sect. 4.3.1, with respect to the ^{13}CO and C^{18}O data in the sense that the model we use overestimates the ^{12}CO emission. This suggests that the model assumptions like the temperature, micro turbulence, and ^{12}CO abundance used for the upper disc layers where the ^{12}CO emission arises from should be reconsidered. From the gas and dust masses derived in Secs. 4.2 and 4.3, we see that a gas-to-dust mass ratio of 100:1 only holds for special circumstances considered here: a maximum dust emissivity of 2 cm^{2}g$^{-1}_{\rm dust}$ at 1.3 mm and a ^{12}CO abundance of 10^{-4} with respect to H$_2$, or lower. For equally likely values of 1 cm^{2}g$^{-1}_{\rm dust}$ for the dust emissivity and 2×10^{-4} for the ^{12}CO abundance, a gas-to-dust mass ratio of 25 would be inferred, suggesting that the disc has lost significant amounts of gas with respect to dust. In fact, gas loss is expected in circumstellar discs due to photoevaporation of gas by the stellar radiation. The typical timescale for this process of a few Myr (Hollenbach et al. 1994; Font et al. 2004) is similar to the estimated age of HD169142 of 6^{+6}_{-3} Myr (Grady et al. 2007).

2.4.5 Micro turbulence

As mentioned in the previous section, the overestimate of the ^{12}CO emission by the model that fits the ^{13}CO and C^{18}O J=2–1 line emission well may be due to model assumptions used for the upper disc layers, e.g., temperature, ^{12}CO relative abundance, turbulence.

In Sect. 4.1 we mention that a disc model with a less luminous A6 spectral type star also reproduces the SED of HD169142 well (Dent et al. 2006). However, the temperature in that model is less than 10% lower than the temperature used in our model. This is too low to provide a significant decrease in the ^{12}CO line flux.

A fit to all observed lines simultaneously by varying the isotopic ratios yields an unusually low value of both the ^{12}C/^{13}C and the ^{16}O/^{18}O isotopic ratios: 21 and 171, respectively. These values are far from the observationally derived ratios in the interstellar medium and this scenario would be highly unlikely. An overabundance of ^{13}CO was measured at large radial distances from the star (several hundreds of AU) in the discs DM Tau, MWC 480, and LkCa 15 (Piétu et al. 2007) In general, discs are often found to have ^{13}CO and C^{18}O abundances depleted by large factors, mainly in discs around T Tauri stars (Dutrey et al. 1994, 1996).

In the above analysis, the turbulent line FWHM was set to 0.16 km s^{-1} throughout the disc. In a more realistic scenario, the turbulence in the cold and dense midplane differs from the turbulence in the warmer and less dense surface layers. We investigate the effect of micro turbulence on the modelled line emission and find that a simultaneous match is possible in our model, as shown in Fig. 2.8. This fit is obtained for a gas-to-dust ratio of 33, i.e., a disc gas mass of 7×10^{-3} M$_\odot$, if a higher value of turbulence is assumed for the disc midplane (turbulent FWHM of 0.33 km s^{-1}) and no turbulence

for the upper disc layers traced by the ^{12}CO emission (0.00 km s^{-1}, only thermal broadening). For the ^{12}CO J=2–1 line, that is fully optically thick at all radii in our model, the turbulent line broadening is degenerate with temperature and density in its effect on the line flux and profile. This is because the turbulence additionally broadens the thermally broadened line profile and in this way the optical thickness decreases allowing for more gas column to be traced. On the other hand, by decreasing the turbulence, at a given temperature, the same ^{12}CO data can be fit with comparably more M_{CO}. The effect of the increase in turbulence on the ^{13}CO and C^{18}O lines is present but less pronounced, due to their lower optical thickness. In particular, the C^{18}O J=2–1 line emission is only marginally optically thick. The effect of turbulence on the modelled C^{18}O J=2–1 line emission is below the rms of our observations. It is not possible to obtain simultaneous fits to all data if the gas-to-dust ratio is higher than 33 (disc mass higher than 7×10^{-3} M$_\odot$). A lower gas-to-dust ratio (disc mass lower than 7×10^{-3} M$_\odot$) would require the turbulent FWHM of the lines to be more than 0.33 km s^{-1} in the disc midplane.

2.5   SUMMARY

The circumstellar disc around the Herbig Ae star HD169142 was imaged in ^{13}CO and C^{18}O J=2–1 line emission at 1$\farcs$4 resolution. The disc is resolved and the emission extends to 200-300 AU from the star at 2σ levels. We adopted an accretion disc model that matches the SED of HD169142 and we used a molecular excitation and radiative transfer code to analyse our data. We revisited existing 1.3 mm and ^{12}CO data and interpret it in view of our new results. The observed kinematic pattern and line profiles are consistent with a disc seen at 13° inclination from face on, in Keplerian rotation around a 2 M$_\odot$ star. The structure of the emission suggests a disc radius of roughly 200 AU for both gas and dust.

- We calculated the minimum disc dust mass of M_{dust}=2.16×10^{-4} M$_\odot$ through the fit to the 1.3 mm data using the maximum dust opacity theoretically predicted in circumstellar discs.

- The adopted disc model reproduces our molecular line observations with masses $M_{C^{18}O}$=4.6×10^{-8} M$_\odot$ and $M_{^{13}CO}$=2.9×10^{-7} M$_\odot$. The derived amount of C^{18}O implies a M_{CO}=(2.4±1.0)×10^{-5} M$_\odot$. The ^{13}CO amount is also in agreement with this value.

- We identify the regions of the disc that contribute most to the emission of ^{12}CO, ^{13}CO, and C^{18}O J=2–1 line and find, as expected due to different optical depth of these lines, that they are physically distinct. In particular, the C^{18}O J=2–1 line is marginally optically thin throughout the disc and traces the bulk of the mass contained in the disc's midplane.

- We find that the effect of freeze-out in the model is relatively small, allowing us to make an estimate of the gas mass based on our observations. For plausible CO abundances of (1-2)×10^{-4}, we can only derive a range of M_{gas}=(0.6-3.0)×10^{-2} M$_\odot$.
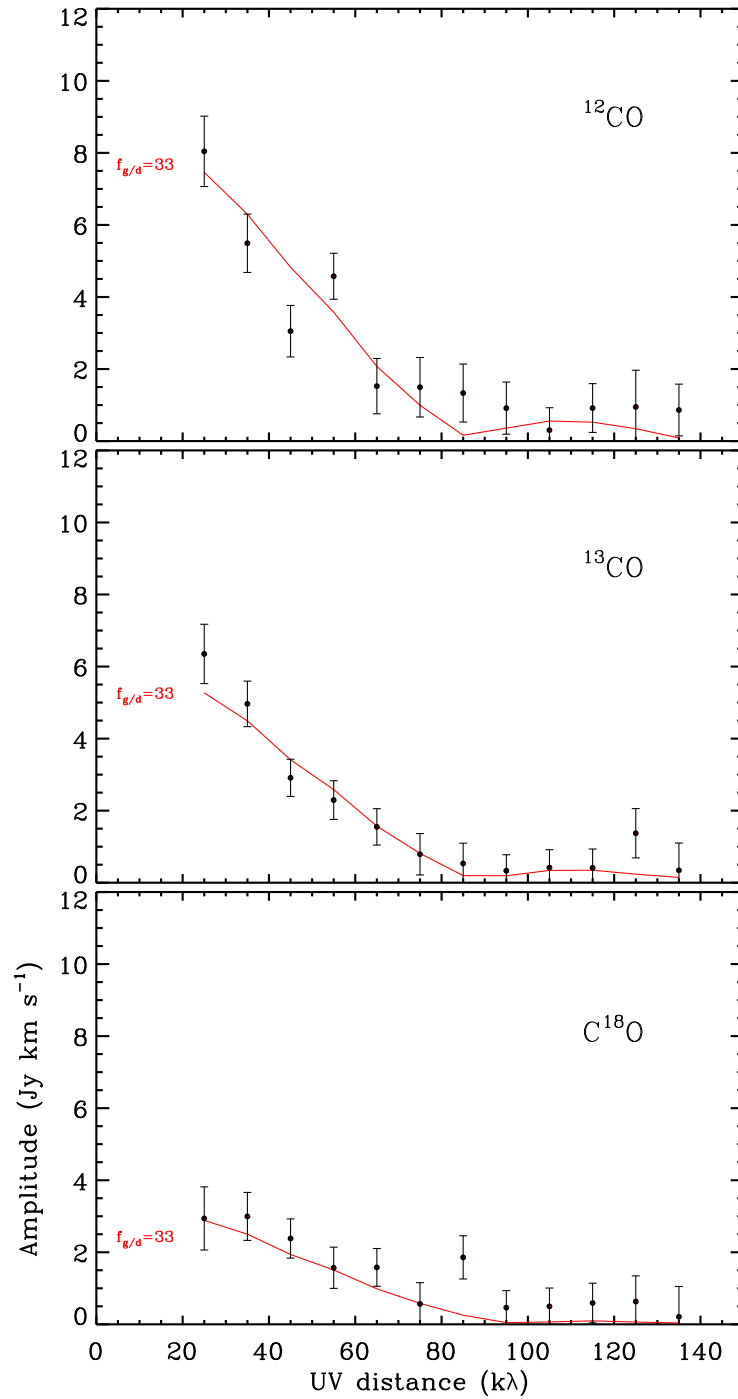
Figure 2.8: Comparison of the observed vector-averaged ^{12}CO (*top panel*), ^{13}CO (*middle panel*) and C^{18}O (*lower panel*) line fluxes (black) to a model which assumes the total disc mass of 7×10^{-3} M$_\odot$, gas-to-dust mass ratio $f_{g/d}$=33, no microturbulent line broadening in the upper disc layers from which the ^{12}CO emission originates (only thermal broadening), and a microturbulent broadening of 0.33 km s^{-1} FWHM in the layers from which the ^{13}CO and C^{18}O emission arises.

- The comparison of the derived gas and dust mass shows that the gas-to-dust mass ratio of 100 is only possible under the assumption of a high dust opacity of $2\ \mathrm{cm}^2\mathrm{g}_{dust}^{-1}$ and low $^{12}\mathrm{CO}$ abundance of 10^{-4} with respect to H_2. Otherwise, this ratio may be as low as 25.

- Existing observations of the optically thick $^{12}\mathrm{CO}$ line can be fit simultaneously to our $^{13}\mathrm{CO}$ and $\mathrm{C}^{18}\mathrm{O}$ data by the model adopted here, only if the micro turbulence in the disc midplane is higher than the micro turbulence in the upper disc layers that dominate the $^{12}\mathrm{CO}$ emission.

The discrepancy between the CO gas mass derived here and the one derived based on the $^{12}\mathrm{CO}$ line emission likely implies that the micro turbulence is much lower than $0.1\ \mathrm{km\ s}^{-1}$ in the upper disc layers where the $^{12}\mathrm{CO}$ emission originates. Better constraints of the $^{12}\mathrm{CO}$ abundance in discs are needed to enable us to measure gas mass more precisely in discs. Better knowledge of dust properties such as dust size distribution and composition is essential for a better estimate of dust opacity in discs. However, these properties vary from source to source and are not necessarily linked with other parameters, age or mass for example, and the studies need to focus on individual sources. Since the discs around Herbig Ae stars have the advantage that the gas mass estimate from $\mathrm{C}^{18}\mathrm{O}$ line emission is more reliable, it would be useful to investigate dust properties, i.e., emissivity in these sources in more detail, to be able to have a reliable estimate of dust mass as well. This would, for the first time, open a real opportunity to study the gas-to-dust mass ratio, the unknown property on which the theories of disc evolution and planet formation depend strongly.

REFERENCES

Beckwith, S. V. W., Sargent, A. I., Chini, R. S., & Guesten, R. 1990, AJ, 99, 924

D'Alessio, P., Merín, B., Calvet, N., Hartmann, L., & Montesinos, B. 2005, Revista Mexicana de Astronomia y Astrofisica, 41, 61

Dartois, E., Dutrey, A., & Guilloteau, S. 2003, A&A, 399, 773

Dent, W. R. F., Greaves, J. S., & Coulson, I. M. 2005, MNRAS, 359, 663

Dent, W. R. F., Torrelles, J. M., Osorio, M., Calvet, N., & Anglada, G. 2006, MNRAS, 365, 1283

Dominik, C., Dullemond, C. P., Waters, L. B. F. M., & Walch, S. 2003, A&A, 398, 607

Draine, B. T. 2006, ApJ, 636, 1114

Dutrey, A., Guilloteau, S., Duvert, G., et al. 1996, A&A, 309, 493

Dutrey, A., Guilloteau, S., & Simon, M. 1994, A&A, 286, 149

Font, A. S., McCarthy, I. G., Johnstone, D., & Ballantyne, D. R. 2004, ApJ, 607, 890

Fraser, H. J., Collings, M. P., McCoustra, M. R. S., & Williams, D. A. 2001, MNRAS, 327, 1165

Frerking, M. A., Langer, W. D., & Wilson, R. W. 1982, ApJ, 262, 590

Grady, C. A., Schneider, G., Hamaguchi, K., et al. 2007, ApJ, 665, 1391

Hogerheijde, M. R. & van der Tak, F. F. S. 2000, A&A, 362, 697

Hollenbach, D., Johnstone, D., Lizano, S., & Shu, F. 1994, ApJ, 428, 654

Isella, A., Testi, L., Natta, A., et al. 2007, A&A, 469, 213

Jonkheid, B., Faas, F. G. A., van Zadelhoff, G.-J., & van Dishoeck, E. F. 2004, A&A, 428, 511

Kuhn, J. R., Potter, D., & Parise, B. 2001, ApJ, 553, L189

Lacy, J. H., Knacke, R., Geballe, T. R., & Tokunaga, A. T. 1994, ApJ, 428, L69

Malfait, K., Bogaert, E., & Waelkens, C. 1998, A&A, 331, 211

Mannings, V. & Sargent, A. I. 1997, ApJ, 490, 792

Meeus, G., Waters, L. B. F. M., Bouwman, J., et al. 2001, A&A, 365, 476

Ossenkopf, V. & Henning, T. 1994, A&A, 291, 943

Piétu, V., Dutrey, A., & Guilloteau, S. 2007, A&A, 467, 163

Piétu, V., Dutrey, A., Guilloteau, S., Chapillon, E., & Pety, J. 2006, A&A, 460, L43

Piétu, V., Guilloteau, S., & Dutrey, A. 2005, A&A, 443, 945

Raman, A., Lisanti, M., Wilner, D. J., Qi, C., & Hogerheijde, M. 2006, AJ, 131, 2290

Sault, R. J., Teuben, P. J., & Wright, M. C. H. 1995, in Astronomical Society of the Pacific Conference Series, Vol. 77, Astronomical Data Analysis Software and Systems IV, ed. R. A. Shaw, H. E. Payne, & J. J. E. Hayes, 433–+

Simon, M., Dutrey, A., & Guilloteau, S. 2000, ApJ, 545, 1034

Sylvester, R. J., Skinner, C. J., Barlow, M. J., & Mannings, V. 1996, MNRAS, 279, 915

Thi, W. F., van Dishoeck, E. F., Blake, G. A., et al. 2001, ApJ, 561, 1074

van Zadelhoff, G.-J. 2002, PhD thesis, , Leiden University, May 2002.

van Zadelhoff, G.-J., Aikawa, Y., Hogerheijde, M. R., & van Dishoeck, E. F. 2003, A&A, 397, 789

Weingartner, J. C. & Draine, B. T. 2001, ApJ, 548, 296

Wilson, T. L. & Rood, R. 1994, ARA&A, 32, 191

A break in the gas and dust surface density of the disc around the T Tauri star IM Lup

O. Panić, M. R. Hogerheijde, D. Wilner and C. Qi

W E study the distribution and physical properties of molecular gas in the disc around the T Tauri star IM Lup on scales close to 200 AU. We investigate how well the gas and dust distributions compare and work towards a unified disc model that can explain both gas and dust emission. ^{12}CO, ^{13}CO, and C^{18}O J=2–1 line emission, as well as the dust continuum at 1.3 mm, is observed at 1″8 resolution towards IM Lup using the Submillimeter Array. A detailed disc model based on the dust emission is tested against these observations with the aid of a molecular excitation and radiative transfer code. Apparent discrepancies between the gas and dust distribution are investigated by adopting simple modifications to the existing model. The disc is seen at an inclination of 54° ±3° and is in Keplerian rotation around a 0.8–1.6 M$_\odot$ star. The outer disc radius traced by molecular gas emission is 900 AU, while the dust continuum emission and scattered light images limit the amount of dust present beyond 400 AU and are consistent with the existing model that assumes a 400 AU radius. Our observations require a drastic density decrease close to 400 AU with the vertical gas column density at 900 AU in the range of 5×10^{20}–10^{22} cm^{-2}. We derive a gas-to-dust mass ratio of 100 or higher in disc regions beyond 400 AU. Within 400 AU from the star our observations are consistent with a gas-to-dust ratio of 100 but other values are not ruled out.

3.1 INTRODUCTION

Low-mass star formation is commonly accompanied by the formation of a circumstellar disc. The disc inherits the angular momentum and composition of the star's parent cloud, and is shaped by the accretion and other physical processes within the disc during the evolution that may result in a planetary system. Over the past two decades observations of circumstellar discs at millimetre wavelengths have been established as powerful probes of the bulk of the cold molecular gas and dust. Spatially resolved observations of the molecular gas with (sub) millimetre interferometers constrain the disc size and inclination, the total amount of gas, its radial and vertical structure, and the gas kinematics (e.g., Guilloteau & Dutrey 1998; Dartois et al. 2003; Qi et al. 2004; Isella et al. 2007; Piétu et al. 2007) and Chapter 2 of this thesis. In parallel, continuum observations of the dust at near-infrared to millimetre wavelengths provide the disc spectral energy distribution (SED), that through modelling (e.g., Chiang & Goldreich 1997; Dullemond et al. 2001; D'Alessio et al. 2005) yields the disc's density and temperature structure from the disc inner radius to a few hundred AU from the star. Studies of the gas through spatially resolved molecular line observations using results from the SED modelling, as done in Chapter 2 of this thesis, offer the means of addressing the gas-to-dust ratio, differences between the radial and vertical distributions of the gas and the dust, and the thermal coupling between the gas and the dust in the upper disc layers exposed to the stellar radiation (e.g., Jonkheid et al. 2004). Recent papers have suggested different disc sizes for the dust and the gas (e.g., HD 163296, Isella et al. 2007), which may be explained by sensitivity effects in discs with tapered outer density profiles (Hughes et al. 2008). Here, we present the results of a combined study using spatially resolved molecular-line observations and SED modelling of the disc around the low-mass pre-main-sequence star IM Lup.

Most pre-main-sequence stars with discs studied so far in detail are located in the nearby star-forming region of Taurus-Aurigae, accessible for the millimetre facilities in the northern hemisphere. Much less is known about discs in other star-forming regions such as Lupus, Ophiuchus or Chamaeleon. It is important to compare discs between different regions, to investigate if and how different star-forming environments lead to differences in disc properties and the subsequent planetary systems that may result. IM Lup is a pre-main-sequence star located in the Lupus II cloud for which Wichmann et al. (1998) report a distance of 190±27 pc using Hipparcos parallaxes. From its M0 spectral type and estimated bolometric luminosity of 1.3±0.3 L$_\odot$, Hughes et al. (1994) derive a mass of 0.4 M$_\odot$ and an age of 0.6 Myr using evolutionary tracks from Swenson et al. (1994), or 0.3 M$_\odot$ and 0.1 Myr adopting the tracks of D'Antona & Mazzitelli (1994). In Pinte et al. (2008), a much higher value of 1 M$_\odot$ is derived using tracks of Baraffe et al. (1998).

IM Lup is surrounded by a disc detected in scattered light with the Hubble Space Telescope (Pinte et al. 2008) and in the CO J=3–2 line with the James Clerk Maxwell Telescope by van Kempen et al. (2007). Lommen et al. (2007) conclude that grain growth up to millimetre sizes has occured from continuum measurements at 1.4 and 3.3 mm. Recently, Pinte et al. (2008) present a detailed model for the disc around IM Lup based on the full SED, scattered light images at multiple wavelengths from the
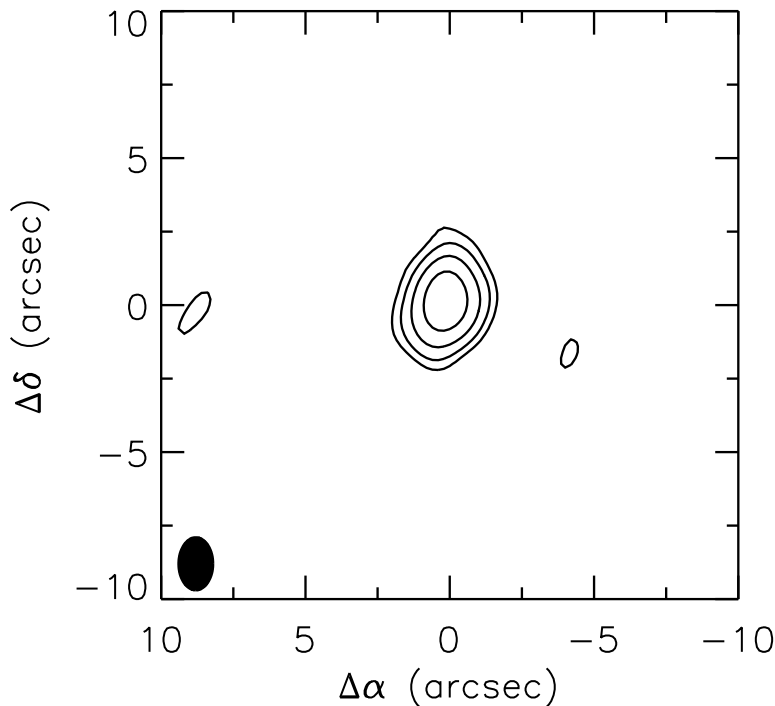
Figure 3.1: Dust continuum image at 1.3 mm. The contours are at (2, 4, 8, 16)×3.67 mJy beam^{-1} (2, 4, 8, 16 sigma) levels. The filled ellipse in the lower left corner shows the synthesized beam.

Hubble Space Telescope, near- and mid-infrared spectroscopy from the Spitzer Space Telescope, and continuum imaging at 1.3 mm with the Submillimeter Array. They conclude that the disc is relatively massive, $M \approx 0.1\,\mathrm{M}_\odot$ with an uncertainty by a factor of a few, has an outer dust radius not greater than $\approx$400 AU set by the dark lane and lower reflection lobe seen in the scattered light images, and has a surface density $\Sigma(R)$ proportional to R^{-1} constrained by the 1.3 mm data. Furthermore, they find evidence for vertical settling of larger grains by comparing the short-wavelength scattering properties to the grain-size constraints obtained at 1.4 and 3.3 mm by Lommen et al. (2007).

In this Chapter, we present (Sect. 3.2) spatially resolved observations of the disc around IM Lup in ^{12}CO, ^{13}CO and C^{18}O J=2–1 line emission, together with 1.3 mm dust continuum data, obtained with the Submillimeter Array[1] (SMA). The results of Sect. 6.3 show that the gas disc extends to a radius of 900 AU, more than twice the size inferred by Pinte et al. (2008). A detailed comparison (Sect. 3.4.1) to the model of Pinte et al. (2008) suggests a significant break in the surface density of both the gas and the dust around 400 AU, and we discuss possible explanations. We summarise our main conclusions in Sect. 3.5.

---

[1]The Submillimeter Array is a joint project between the Smithsonian Astrophysical Observatory and the Academia Sinica Institute of Astronomy and Astrophysics and is funded by the Smithsonian Institution and the Academia Sinica.

3.2   OBSERVATIONS

IM Lup was observed with the SMA on 2006 May 21 in a 8.6-hour track, with a 4.3 hours on-source integration time. The J2000 coordinates of the phase centre are RA= $15^h56^m09\overset{s}{.}17$ and Dec= $-37°56'06\overset{''}{.}40$. Eight antennas were included in an extended configuration providing a range of projected baselines of 7 to 140 meters. The primary beam half-power width is $55\overset{''}{.}0$. The SMA receivers operate in a double-sideband (DSB) mode with an intermediate frequency band of 4–6 GHz which is sent over fiber optic transmission lines to 24 "overlapping" digital correlator chunks covering a 2 GHz spectral window in each sideband. The DSB system temperatures ranged from 90 to 150 K. The correlator was configured to include the ^{12}CO J=2–1 line (230.538 GHz) in the upper sideband and the ^{13}CO 2–1 (220.399 GHz) and C^{18}O 2–1 line (219.560 GHz) in the lower sideband. Each of the three lines was recorded in a spectral band consisting of 512 channels with 0.2 MHz spacing ($\sim$0.26 km s^{-1}). Simultaneously to the line observations, the 1.3 mm dust continuum was recorded over a bandwidth of 1.8 GHz.

The data were calibrated and edited with the IDL-based `MIR` software package[2]. The bandpass response was determined from Jupiter, Callisto and 3C273. After the passband calibration, broadband continuum in each sideband was generated by averaging the central 82 MHz in all line-free chunks. Complex gain calibration was performed using the quasar J1626−298. The absolute flux scale was set using observations of Callisto. Subsequent data reduction and image analysis was carried out with the Miriad software package (Sault et al. 1995). The visibilities were Fourier transformed with natural weighting, resulting in a synthesized beam of $1\overset{''}{.}8 \times 1\overset{''}{.}2$ at a position angle of $0.2°$. 1 Jy/beam corresponds to 15.9 K. The r.m.s noise level is 125, 94 and 102 mJy beam^{-1} per channel respectively for the ^{12}CO, ^{13}CO and C^{18}O spectral line data and 4 mJy beam^{-1} for the continuum data.

3.3   RESULTS

3.3.1   Dust continuum

Figure 3.1 shows the 1.3 mm continuum emission observed toward IM Lup, previously reported in Pinte et al. (2008). The emission is centered on RA=$15^d56^m09\overset{s}{.}20$, Dec= $-37°56'06\overset{''}{.}5$ (J2000), offset by $+0\overset{''}{.}4$ in right ascension and by $-0\overset{''}{.}1$ in declination from the pointing center. We adopt the peak of the continuum emission as the position of IM Lup. The peak intensity of the continuum emission is 104 ± 4 mJy beam^{-1} and the total flux 176±4 mJy. The emission intensity is fit to the precision of one sigma by an elliptical Gaussian, yielding a source FWHM size of $1\overset{''}{.}52\pm0\overset{''}{.}15 \times 1\overset{''}{.}06\pm0\overset{''}{.}15$ and a position angle of $-35\overset{\circ}{.}5 \pm 4\overset{\circ}{.}0$ deconvolved with the synthesized beam. This position angle, and the inclination in the range of 33°–53° suggested by the deconvolved aspect ratio, agree well with the values obtained by Pinte et al. (2008) of, respectively, $-37°\pm5°$ and 45°–53° from scattered light imaging.

---

[2]http://www.cfa.harvard.edu/∼cqi/mircook.html
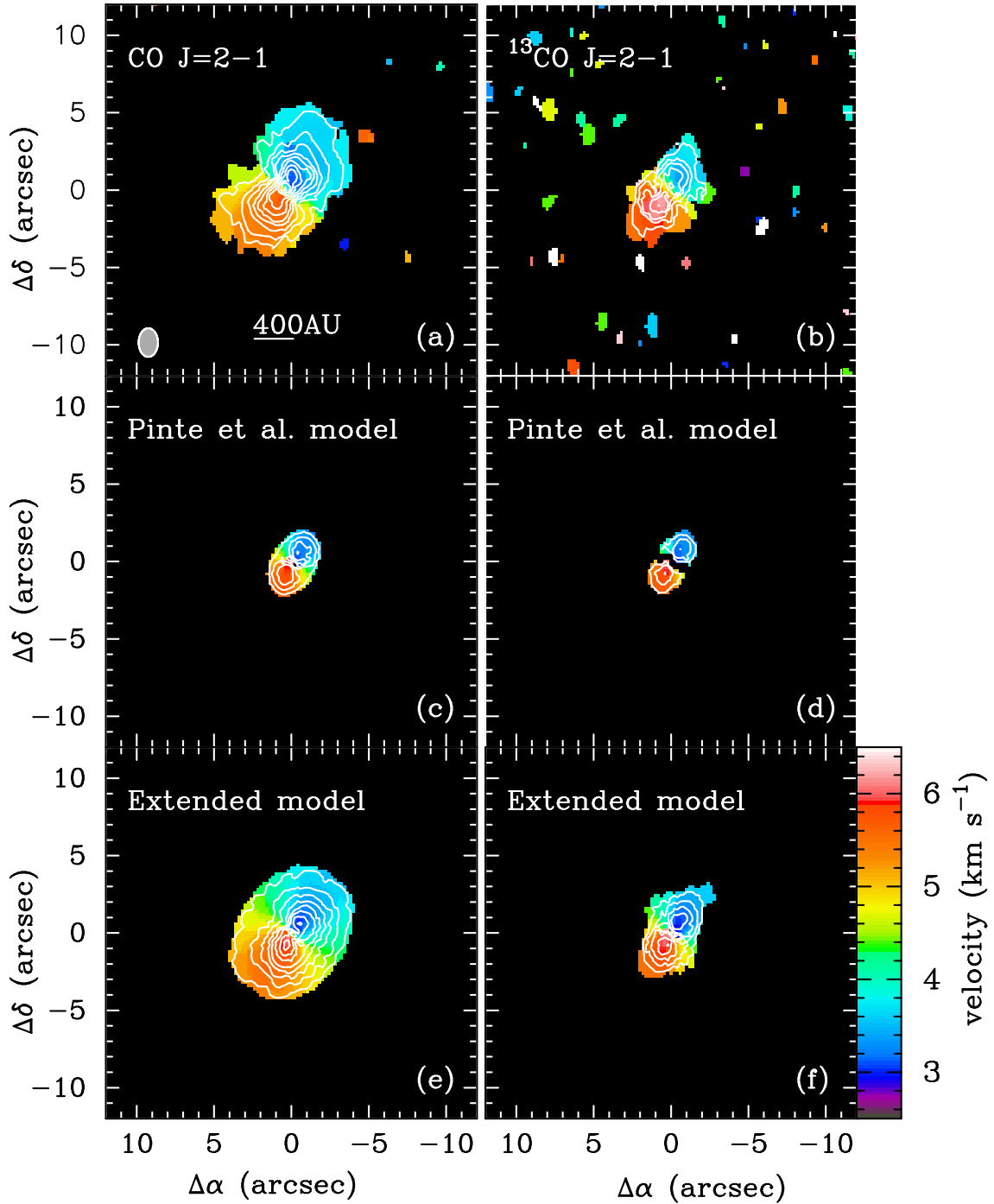
Figure 3.2: *(a),(b):* First moment maps in the ^{12}CO and ^{13}CO J=2–1 lines, from 1.9 kms^{-1} to 6.9 kms^{-1} observed towards IM Lup. These maps are created using the Miriad task 'moment' with clip levels of 0.5 and 0.3 Jy respectively. The integrated emission of ^{12}CO J=2–1 is shown in contours of 1, 2, 3, ...×500 mJy, and that of ^{13}CO J=2–1 with 1, 2, 3, ...×160 mJy contours. *(c), (d):* First moment and integrated emission maps calculated using Pinte et al. model and same clip level, velocity range and contour levels as in (a) and (b). *(e), (f):* First moment and integrated emission maps calculated using extended disc model (described in Sect. 3.4.2) with model parameters Σ_{400} =2×10^{21} cm^{-2} and p =1. The clip level, velocity range and contour levels are as in (a), (b), (c) and (d).

A fit to the 1.3 mm visibilities done in Pinte et al. (2008) provides a rough disc mass estimate of 0.1 $M_\odot$, with an uncertainty of a factor of few, dominated by the adopted dust emissivity and gas-to-dust mass ratio in the model.

3.3.2 Molecular lines

Emission of ^{12}CO and ^{13}CO J=2–1 was detected toward IM Lup, and an upper limit on C^{18}O 2–1 obtained. Figure 3.2[3] shows the zero moment (integrated emission, contours) and first moment (velocity centroid, greyscale) of the ^{12}CO and ^{13}CO emission from IM Lup. Significantly detected ^{12}CO emission extends to 5″ from the star (roughly 900 AU for IM Lup). This is more than double the size inferred from the dust continuum image, and Sect. 7.3 discusses if this is due to different sensitivity in these two tracers or if the gas disc indeed extends further than the dust disc. The aspect ratio (5/3), suggesting an inclination of $53° \pm 4°$, and orientation PA=$-36 \pm 5°$ of the CO disc agree with the continuum image (Sect. 3.3.1) and scattered light imaging results (Pinte et al. 2008).

The first moment images of Fig. 3.2 show velocity patterns indicative of a rotating disc inclined with respect to the line of sight. This is also seen in Fig. 6.5, which presents the ^{12}CO, ^{13}CO, and C^{18}O spectra averaged over 8″$\times$8″ boxes around IM Lup. The ^{12}CO and ^{13}CO lines are double-peaked and centered on v_{LSR} =4.4$\pm$0.3 km s^{-1}. Figures 3.4 and 3.5 show the channel maps of the ^{12}CO and ^{13}CO emission, respectively, revealing the same velocity pattern also seen from the first-moment maps and the spectra. The Keplerian nature of the velocity pattern is most clearly revealed by Fig. 3.6, which shows the position-velocity diagram of the ^{12}CO emission along the major axis of the disc. In Section 7.3, we derive a stellar mass of 1.2 $M_\odot$, and, as an illustration, the rotation curves for stellar masses of 0.8, 1.2, and 1.6 $M_\odot$ are plotted in Fig. 3.6.

Using single-dish ^{12}CO 3–2 observations, van Kempen et al. (2007) first identified molecular gas directly associated with IM Lup, but they also conclude that the v_{LSR}-range of 4 to 6 km s^{-1} is dominated by gas distributed over a larger ($> 30″$) scale. In our ^{12}CO 2–1 data this same v_{LSR}-range is also likely affected: where the single-dish ^{12}CO 3–2 spectrum from van Kempen et al. shows excess emission over v_{LSR} =4–6 km s^{-1}, the red peak of our ^{12}CO 2–1 spectrum, which lies in this v_{LSR}-range, is weaker than the blue peak at $+3.5$ km s^{-1}. We suspect that absorption by the same foreground layer identified by van Kempen et al. is resonsible for this decrement, while its emission is filtered out by the interferometer. The ^{13}CO 2–1 spectrum is symmetric, suggesting that the foreground layer is optically thin in this line.

The spatial extent of the line emission is further explored in Fig. 3.7 which plots the ^{12}CO and ^{13}CO J=2–1 vector-averaged line fluxes against projected baseline length. The ^{12}CO flux is integrated from 2.5 to 4.0 kms^{-1} to avoid the range where foreground absorption affects the line. The ^{13}CO flux does not suffer from absorption and is integrated over its full extent from 2.5 to 6.9 kms^{-1}. Comparing the curves of Fig. 3.7 to those of the continuum flux versus baseline lengths (Fig. 3.8) it is clear that the line flux is much more dominated by short spacings (<40 kλ). This profile may indicate the presence of a larger structural component (outer disc or envelope), combined with

---

[3]Panel (a) of this figure can be seen in colour on page 8 of this thesis, Fig. 1.2.
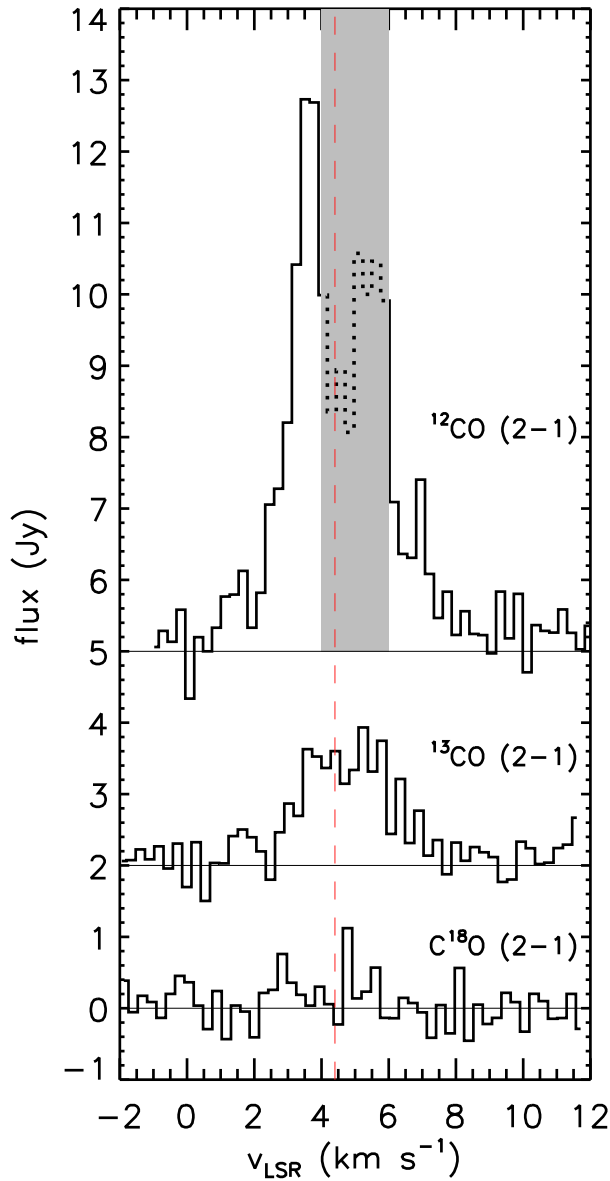
Figure 3.3: ^{12}CO, ^{13}CO, and C^{18}O J=2–1 line spectra summed over $8''\times 8''$ regions centered on the location of IM Lup. The ^{13}CO and ^{12}CO spectra are shifted upward by 2 and 5 Jy, respectively. The dashed red line shows the line centre at v_{LSR}=4.4 km s^{-1}. The grey zone indicates the range from 4 to 6 km s^{-1} where the ^{12}CO line is significantly affected by the foreground absorption; the corresponding part of the ^{12}CO spectrum is plotted with a dotted line.

the disc emission (See Jørgensen et al. 2005, Fig. 2). We explore disc structure beyond 400 AU in the following section.

3.4 DISCUSSION

The results of the previous section show that IM Lup is surrounded by a gaseous disc in (roughly) Keplerian rotation. The gas disc has a radius of 900 AU, and its surface density may have a break around a radius of 400 AU. In contrast, the size of the dust disc is constrained to a radius of 400 AU by our continuum data and the modelling of
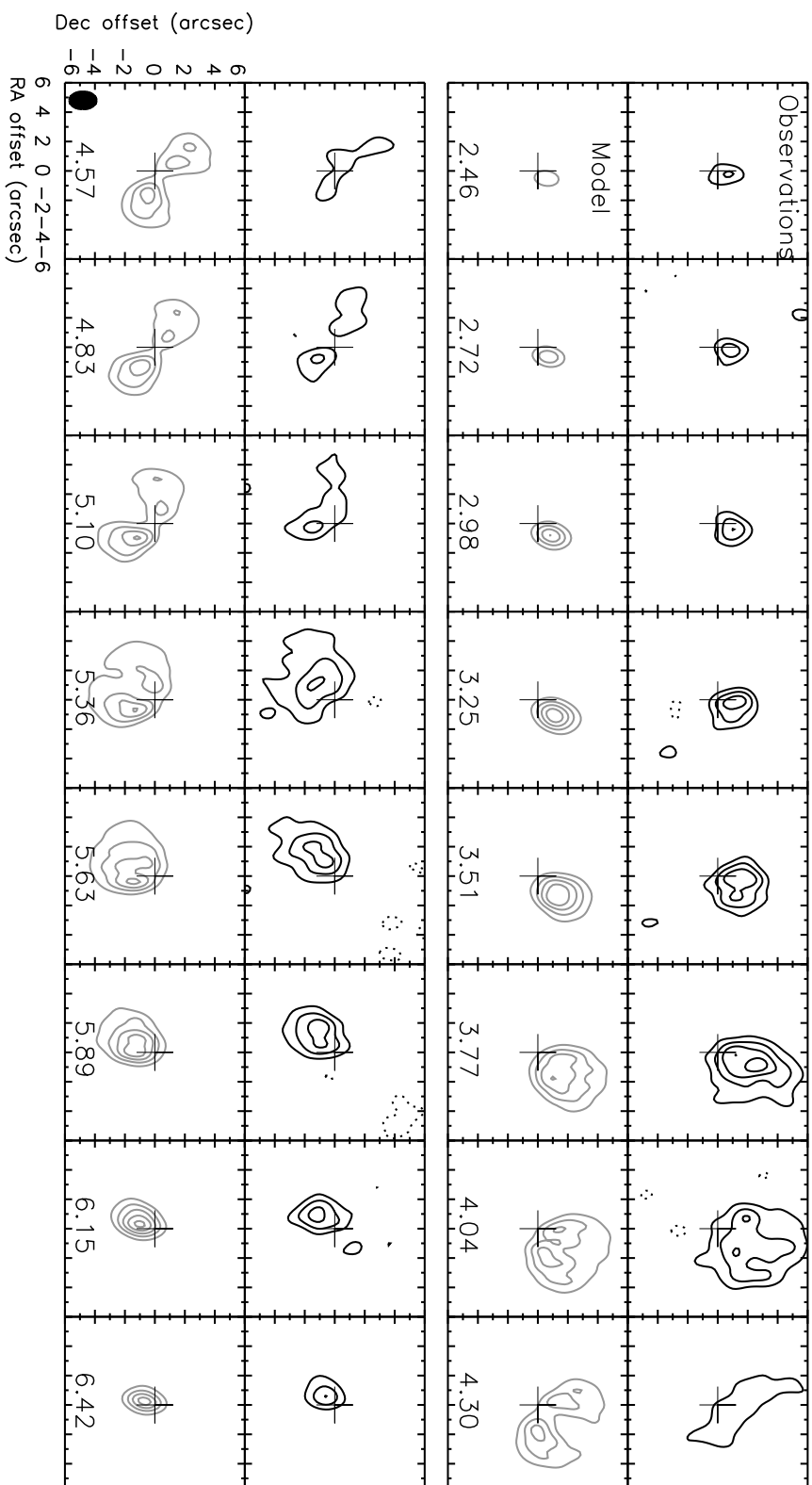
Figure 3.4: The black contours show the observed ^{12}CO J=2–1 emission in the velocity range from 2.46 to 6.42 km s^{-1}. Alongside the observations, the panels with grey contours show the calculated emission from the extended disc model described in Sect. 3.4.2, with parameters $\Sigma_{400} = 2 \times 10^{21} cm^{-2}$ and p =1. Labels indicate the velocity of each channel. The lower left corner of bottom-left panel shows the size and position angle of the synthesized beam. The contour levels are −1, 1, 2, 3, 4×400 mJy beam^{-1} (~3σ) in all panels.
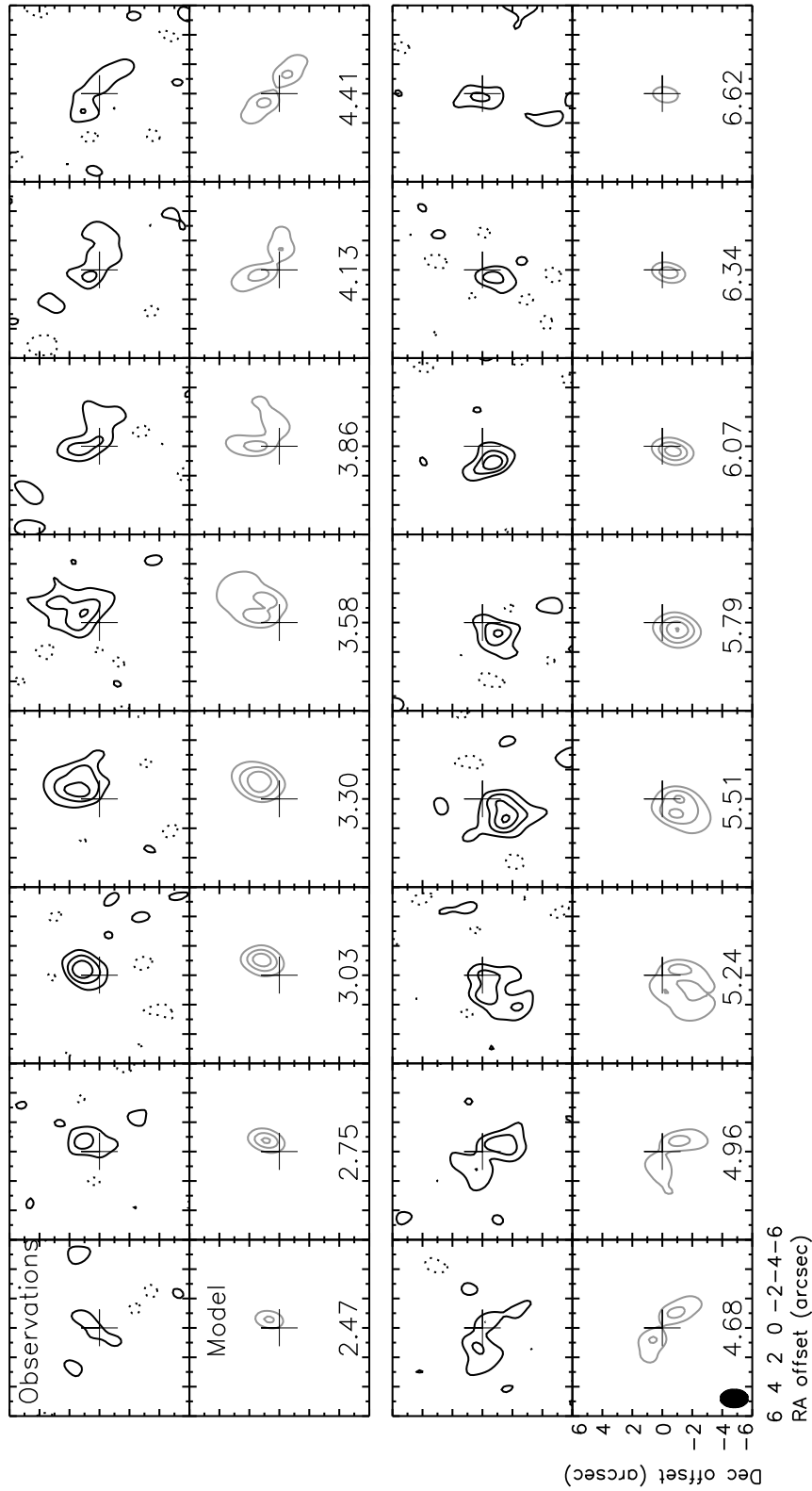
Figure 3.5: Channel maps of the observed ^{13}CO $J=2-1$ emission at the velocities where the line is detected are shown in black contours. For comparison, the line emission calculated from our extended disc model described in Sect. 3.4.2 is shown in grey contours. The model parameters are $\Sigma_{400} = 2 \times 10^{21}\,\mathrm{cm}^{-2}$ and $p = 1$. Labels indicate the velocity of each channel. The lower left corner of bottom-left panel shows the size and position angle of the synthesized beam. The contour levels are -1, 1, 2, 3, 4×200 mJy beam^{-1} ($\sim 2\sigma$) in all panels.
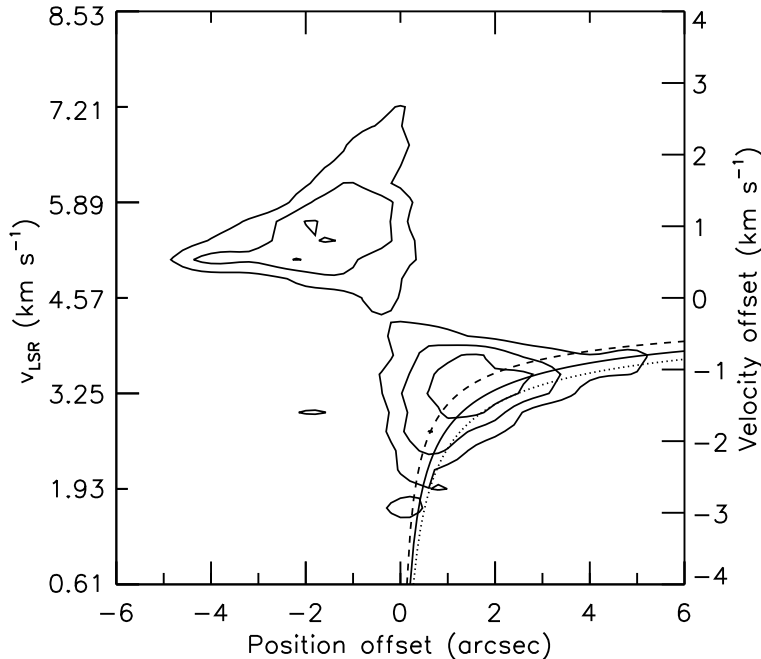
Figure 3.6: Position-velocity diagram of the ^{12}CO 2–1 line emission along the disc's major axis. Contour levels are (1, 2, 3, ...)×400 mJy ($\sim 3\sigma$). For comparison, the thick solid line corresponds to Keplerian rotation around a 1.2 M$_\odot$ star; dashed and dotted lines correspond to the stellar masses of 0.8 and of 1.6 M$_\odot$, respectively.

Pinte et al. (2008). This section explores if the gas and dust have the same spatial distribution (in which case different sensitivity levels need to explain the apparent difference in size) or if the gas and dust are differently distributed radially. First we investigate whether the model of Pinte et al. (2008) can explain the molecular line observations (Sect. 3.4.1). After we conclude that this is not the case, we construct new models for the gas disc (Sect. 3.4.2) describing their best-fit parameters, and compare them to the dust disc (Sect. 3.4.3).

3.4.1 Molecular-line emission from the dust-disc model

Recently, Pinte et al. (2008) present a detailed model for the disc around IM Lup based on the full SED, scattered light images at multiple wavelengths from the Hubble Space Telescope, near- and mid-infrared spectroscopy from the Spitzer Space Telescope, and continuum imaging at 1.3 mm with the Submillimeter Array.

Based on the two-dimensional density and temperature structure of the Pinte et al. model, with $M = 0.1$ M$_\odot$, $R_{out} = 400$ AU, and $i = 50°$, we calculate the resulting line intensity of the ^{12}CO and ^{13}CO J=2–1 lines. To generate the input model for the molecular excitation calculations, we adopt a gas-to-dust mass ratio of 100 and molecular abundances typical for the dense interstellar medium (Frerking et al. 1982; Wilson & Rood 1994): a ^{12}CO abundance with respect to H$_2$ of 10^{-4} and a ^{12}CO/^{13}CO abundance ratio of 77. No freeze-out or photodissociation of CO is included. The velocity of the material in the disc is described by Keplerian rotation around a 1.0 M$_\odot$ star plus a Gaussian microturbulent velocity field with a FWHM of 0.16 km s^{-1}; the exact value of the latter parameter has little effect on the results. Using the molecular excitation and
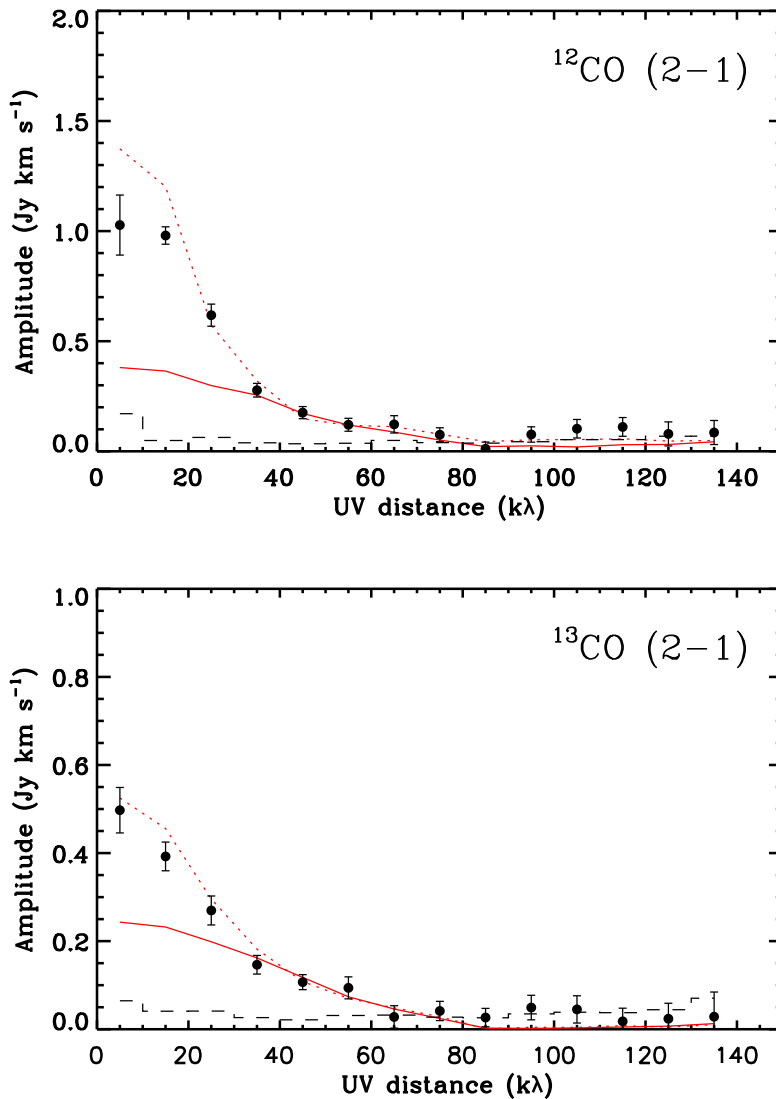
Figure 3.7: The left and the right panel show vector-averaged ^{12}CO and ^{13}CO line flux (black symbols), respectively. Dashed black lines represent the zero-signal expectation value of our line visibility data. The calculated visibilities based on Pinte et al. model (full line) and our extended disc model described in Sect. 3.4.2 (dotted line) are shown for comparison. Our model parameters are $\Sigma_{400} = 2 \times 10^{21}$ cm^{-2} and $p = 1$. The ^{12}CO flux is integrated over the 0.8-4.0 kms^{-1} range and ^{13}CO over 2.5-6.9 kms^{-1}, covering the full line width.

radiative transfer code RATRAN (Hogerheijde & van der Tak 2000) and CO-H_2 collision rates from the Leiden Atomic and Molecular Database (LAMBDA[4]; Schöier et al. 2005) we calculate the sky brightness distribution of the disc in the ^{12}CO and ^{13}CO J=2–1 lines for its distance of 190 pc. From the resulting image cube, synthetic visibilities corresponding to the actual (u, v) positions of our SMA data were produced using the MIRIAD package (Sault et al. 1995). Subsequent Fourier transforming, cleaning, and image restoration was performed with the same software.

Figure 3.2 compares the zeroth-moment (integrated intensity; contours) and first-moment (velocity-integrated intensity) maps of the resulting synthetic images to the observations. Clearly, the Pinte et al. model produces ^{12}CO and ^{13}CO 2–1 emission with spatial extents and intensities too small by a factor close to two. In Fig. 3.7 it is

---

[4]http://www.strw.leidenuniv.nl/~moldata/
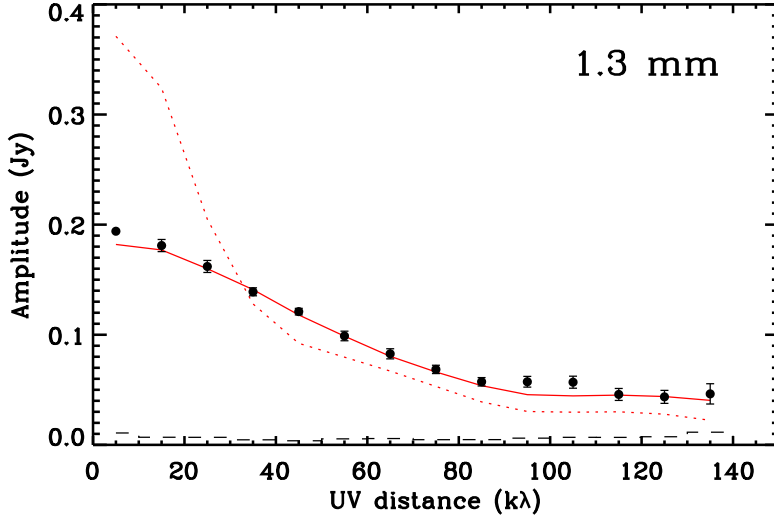
Figure 3.8: Vector-averaged continuum flux as a function of projected baseline length (black symbols). Error bars show the variance within each annular bin. The dashed histogram shows the zero-signal expectation value. The full line shows the continuum flux calculated from Pinte et al. model. The dotted line corresponds to the extended disc model with $\Sigma_{400} = 2 \times 10^{21}$ cm^{-2} and $p = 1$ (see Sect. 3.4.2 for model description).

clear that the Pinte et al. model fails to reproduce the ^{12}CO and ^{13}CO line fluxes at short projected baseline lengths, but is consistent with the observations longward of 40 kλ that correspond to spatial scales $\leq$500 AU. Our comparison with Pinte et al. model thus suggests that the gas extends much further than 400 AU from the star.

The observed 1.3 mm continuum emission traces the extent of larger dust particles (up to millimetre in size). Pinte et al. (2008) show that their 400 AU model reproduces these observations well. In Sect. 3.4.3 we explore to what level larger particles can be present outside 400 AU.

3.4.2   Extending the gas disc beyond 400 AU

As mentioned in Sect. 3.3.2, the CO line flux as function of projected baseline length suggests a possible break in the emission around 40 kλ (Fig. 3.7). Results of Sect. 3.4.1 show that the Pinte et al. model, while providing a good description of line fluxes at small spatial scales (baselines> 40kλ), requires a more extended component to match the observed line fluxes (baselines< 40kλ). In this section we extend the Pinte et al. model by simple radial power laws for the gas surface density and temperature, and place limits on the gas column densities in the region between 400 and 900 AU.

Table 3.1 lists the model parameters. For radii smaller than 400 AU, the radial and vertical density distribution of the material follows the Pinte et al. model. As in Sect. 3.4.1 we adopt 'standard' values of gas-to-dust mass ratio and molecular abundances, and a Gaussian microturbulent velocity field with equivalent line width of 0.16 km s^{-1}. Unlike the calculations of Sect. 3.4.1 we add as free parameters the stellar mass $M_\star$ and the gas kinetic temperature. For the latter, we follow the two-dimensional structure prescribed by Pinte et al., but scale the temperatures upward by a factor f

Table 3.1: Model parameters

Parameter	$R <400$ AU	$400\leq R \leq 800$ AU
Surface density	$\Sigma \propto R^{-1}$, see Pinte et al. (2008)	$\Sigma_{400} (R/400\ \mathrm{AU})^{-p}$ with $\Sigma_{400} \leq 0.9$ g cm^{-2} , $p \geq 0$
Gas-to-dust mass ratio	100	100
Gas temperature structure	$f\,T_{\mathrm{dust}}$ with $1 \leq f \leq 2$	$T_{400} (R/400\ \mathrm{AU})^{-q}$, $T_{400} = 30$ K, $q = 0.5$
Vertical structure	see Pinte et al. (2008)	$T(z) =$ constant, $\rho(z) =$ constant, $z_{max} = 100$ AU
[CO]/[H$_2$]	10^{-4}	10^{-4}
[^{12}CO]/[^{13}CO]	77	77
$M_\star$	1.2 M$_\odot$	1.2 M$_\odot$
Inclination	50°	50°
FWHM microtubulence	0.16 km s^{-1}	0.16 km s^{-1}

with $1 \leq f \leq 2$. This corresponds to a decoupling of the gas and dust temperatures, as may be expected at the significant height above the midplane where the ^{12}CO and ^{13}CO lines originate (see, e.g., Qi et al. 2006; Jonkheid et al. 2004). Because the highly red- and blue-shifted line emission (line wings) comes from regions closer to the star than 400 AU and is optically thick, factor f is determined by the observed fluxes in the line wings. The molecular excitation and synthetic line data are produced in the same way as described in Sect. 3.4.1.

Outside 400 AU we extend the disc to 900 AU, as suggested by the observed ^{12}CO image of Fig. 3.2, by simple radial power laws for the surface density and temperature, $\Sigma = \Sigma_{400} \, (R/400 \, \mathrm{AU})^{-p}$ and $T = T_{400} \, (R/400 \, \mathrm{AU})^{-q}$. At 400 AU, the surface density is Σ_{400} and the temperature is T_{400}; the parameter p is assumed to be ≥ 0. To limit the number of free parameters, we set $T_{400} = 30$ K and $q = 0.5$; we assume that the disc is vertically isothermal and that the ^{12}CO abundance is 10^{-4}, constant throughout the disc. At $R >$400 AU, the disc thickness is set to z_{max}=100 AU and the density $\rho(R, z) = \Sigma(R)/z_{\mathrm{max}}$ is vertically constant. For our free parameters Σ_{400} and p, we assume that $\Sigma_{400} \leq 0.9$ g cm^{-2} (vertical gas column density of 2×10^{23} cm^{-2}), the value at the outer radius of the Pinte et al. model. We have run a number of disc models, with the inner 400 AU described by the Pinte et al. model (with the gas kinetic temperature scaled as described in the previous paragraph) and the region from 400 to 900 AU described here by the disc extension. Figure 3.10 shows the surface density in the models that we have tested: within 400 AU it is the surface density as in Pinte et al. (blue line) and between 400 and 900 AU different combinations of Σ_{400} and p (black lines). The models are tested against the observed ^{12}CO and ^{13}CO uv-data, channel maps, spectra, and position-velocity plots. The comparison of modelled emission with uv-data for the line wings, $v_{\mathrm{LSR}} <$3.0 km s^{-1} for ^{12}CO and $v_{\mathrm{LSR}} <$3.5 km s^{-1}+$v_{\mathrm{LSR}} >$5.5 km s^{-1} for ^{13}CO is also examined.

Figure 3.10 shows the models that overproduce the observed emission with dashed black lines and those that underproduce it with dotted black lines. The full black lines correspond to the models that reproduce well our ^{12}CO and ^{13}CO data. The general area (beyond 400 AU) allowed by the models is shaded in Fig. 3.10 for guidance. It can be seen that the ^{12}CO and ^{13}CO observations constrain the column density of ^{12}CO at $R = 900$ AU to $N_{\mathrm{CO}} = (0.05 - 1.0) \times 10^{18}$ cm^{-2}, where the lower bound follows from the requirement that the ^{12}CO emission is sufficently extended and the upper bound from the requirement that the ^{12}CO and ^{13}CO peak intensity, and the extent of the ^{13}CO emission are not overestimated. The corresponding surface density at 900 AU is $\Sigma_{900} = (0.2 - 4.0) \times 10^{-2}$ g cm^{-2}, i.e., a vertical gas column density $(0.05$–$1.0) \times 10^{22}$ cm^{-2}. Our data do not constrain the parameters Σ_{400} and p, that determine how the surface density decreases from its value at the outer edge of the Pinte et al. model, to its value at 900 AU. This is either a marked change from the power-law slope of $p = 1$ found inside 400 AU to $p = 5$ beyond 400 AU, or a discontinuous drop by a factor $\sim$10-100 in surface density at 400 AU.

Figure 3.7 compares observations to synthetic ^{12}CO and ^{13}CO line visibilities for our model with $\Sigma_{400} = 2 \times 10^{21}$cm^{-2} and $p = 1$, plotted with dotted lines. There is a good match between the model and the data for both transitions. In particular, the model

reproduces well the change in the slope of visibilities, mentioned in Sect. 3.3.2. The match between the model (red lines) and observations is also seen in the line spectra, Fig. 3.9. Figures 3.4 and 3.5 show, respectively, the ^{12}CO and ^{13}CO channel maps (black contours) compared to our extended disc model (grey contours). It can therefore be seen that our model provides a good description not only of the line intensity at each channel (spectra), but also a very close match in the spatial extent of the emission in each spectral channel.

A good fit to the wings of the ^{12}CO and ^{13}CO spectra (Fig. 3.9, thick grey-white lines) and the spatial distribution of the respective line fluxes at highly blue- and red-shifted velocities (lower panels, Figs.3.4 and 3.5) is found for temperature scalings f of 1.7 for ^{12}CO and 1.4 for ^{13}CO. These values of f suggest that the gas is somewhat warmer than the dust at the heights above the disc where the ^{12}CO and ^{13}CO emission originates, and more so at the larger height probed by the ^{12}CO line compared to the ^{13}CO line.

At the adopted disc inclination of $50°$, the line peak separation provides a reliable contraint on the stellar mass. We find a best-fit of $M_\star = 1.2 \pm 0.4$ M$_\odot$, where the uncertainty is dominated by our limited spectral resolution. This value is consistent with the rough estimate of 1 M$_\odot$ from Pinte et al. (2008), but a few times higher than derived by Hughes et al. (1994).

We conclude that the surface density *traced through* ^{12}CO *and* ^{13}CO has a discontinuity around $R = 400$ AU either in $\Sigma_{\rm CO}(R)$ or in its derivative $d\Sigma_{\rm CO}/dR$, or both. This may, or may not be an indication of an overall discontinuity of the gas surface density. A break in the temperature $T(R)$ cannot explain the observations, since our model already adopts a low temperature at the margin of ^{12}CO freeze-out in the outer regions. An alternative explanation for the observations is a radical drop in the abundance of CO (with respect to H$_2$ and H) or its radial derivative. Freeze out onto dust grains or photodissociation can significantly reduce the gas-phase abundance of CO. In the next section we explore the limits that the dust emission can give us on the gas content outside 400 AU, and compare them to the ^{12}CO results.

3.4.3   Comparing gas and dust at radii beyond 400 AU

The previous section concluded that both the gas and the dust out to 400 AU in the disc around IM Lup is well described by the model of Pinte et al., with the exception of gas temperatures that exceed the dust temperature at some height above the disc midplane. It also found that the *gas* disc needs to be extended to an outer radius of 900 AU, albeit with a significant decrease in the surface density of CO, $\Sigma_{\rm CO}$, or in its first derivative, $d\Sigma_{\rm CO}/dR$ close to 400 AU.

Pinte et al. (2008) show that some dust is present outside 400 AU as well, visible as an extended nebulosity in their 0.8 μm scattered light images. At the same time, the visible *lower* scattering disc surface places a stringent limit on the surface density $\Sigma_{\rm dust}$ of small dust particles outside 400 AU. Requiring the optical depth $\tau = \Sigma_{dust}\,\kappa < 1$ and adopting an emissivity per gram of dust of κ=(8-10)$\times 10^3$ cm^{2}g^{-1} at 0.8 μm (See first row of Tab. 1, Ossenkopf & Henning 1994), we find $\Sigma_{dust} \leq (1.0 - 1.3) \times 10^{-4}$ g cm^{-2}.
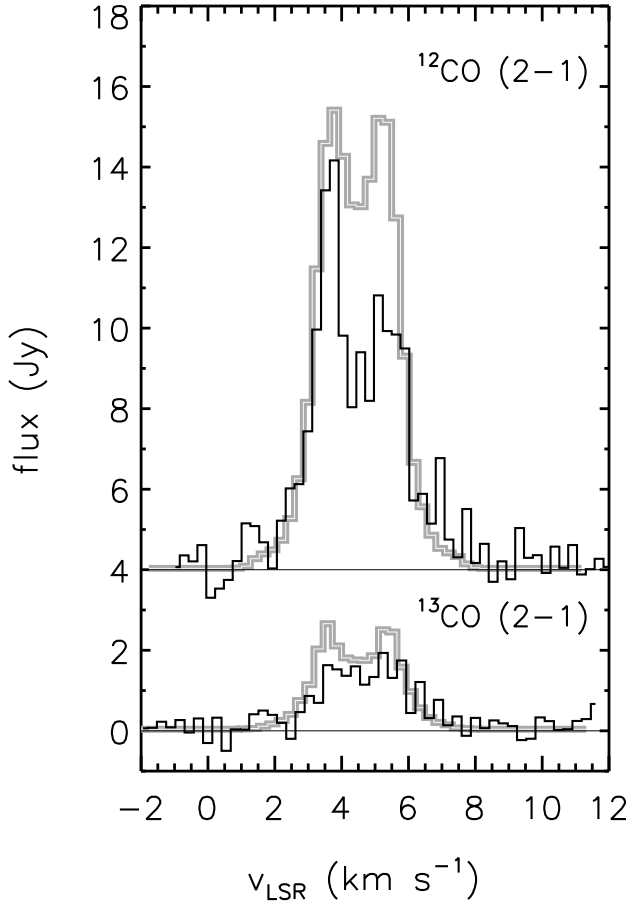
Figure 3.9: ^{12}CO and ^{13}CO J=2–1 line spectra averaged over a $8\overset{''}{.}0 \times 8\overset{''}{.}0$ region centered on IM Lup. The ^{12}CO spectrum is shifted up by 4 Jy for clarity. The grey-white lines show the emission predicted the extended disc model described in Sect. 3.4.2 with $\Sigma_{400} = 2 \times 10^{21}$cm^{-2} and $p = 1$.

If we adopt the gas-to-dust mass ratio of 100, this corresponds to $N_{H_2} \leq (2.5 - 3.1) \times 10^{21}$ cm^{-2}. Our limit differs from that given in Pinte et al. (2008) (0.2 g cm^{-2}) because we use dust opacities representative of small dust, while they assume considerable grain growth in disc midplane and thus use much lower dust opacities at 0.8 μm. The limit on surface density we derive is two orders of magnitude lower than the column density at the outer radius of 400 AU of the Pinte et al. model. This indicates that either the dust surface density drops sharply at 400 AU, or that efficient grain growth beyond 400 AU has caused a significant decrease in dust near-IR opacity. As can be seen in Fig. 3.10, the upper limit on surface density of $(2.5 - 3.1) \times 10^{21}$ cm^{-2} is consistent with the gas surface density range inferred in Sect. 3.4.2 from our CO data, using the canonical CO/H$_2$ abundance of 10^{-4}.

While 0.8 μm imaging traces the small dust, our observations of 1.3 mm dust continuum emission, on the other hand, trace the millimetre-sized dust particles. In Fig. 3.8 we can see that the Pinte et al. model (full line), with the radius of 400 AU, compares well to the observed continuum flux at all projected baseline lengths. On the other hand, the comparison of the 1.3 mm visibilities to our extended disc model with Σ_{400}=2×10^{21} cm^{-2} and p =1 shows that the model overestimates emission at short uv-distances (large spatial scales). A constant dust emissivity of 2.0 cm^2 g^{-1} (emissivity of mm-sized grains, as in Draine 2006) was used throughout the disc in the calculation
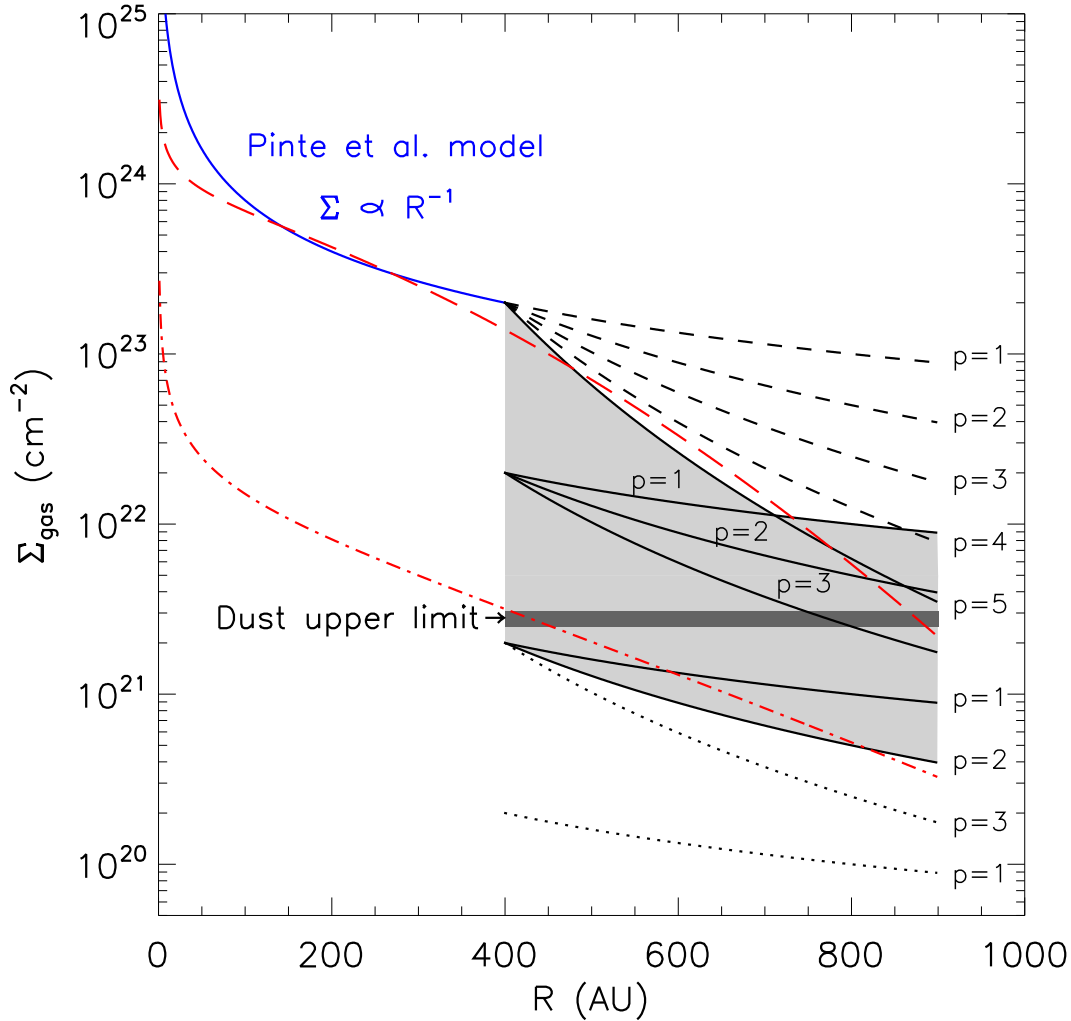
Figure 3.10: Gas surface density in our disc models is plotted as a function of radius. Within 400 AU, it is identical to the Pinte et al. model shown with the full line (0-400 AU). Outside 400 AU, we explore different power-law distributions, each plotted in black and marked with the corresponding slope p. The models which overestimate the observed ^{12}CO emission are plotted with dashed lines, while those that underpredict it are shown in dotted lines. The full black lines represent the models that fit well the ^{12}CO J=2–1 emission, and define the shaded region which shows our constraint on $\Sigma_{CO}/[CO]$ in the outer disc, where a CO abundance of [CO]=10^{-4} is used. The upper limit on $\Sigma_{dust}\, g/d$ placed by scattered light images is shown with a thick dark grey line, with a gas-to-dust mass ratio g/d=100. For comparison, the long-dashed and dash-dotted lines correspond to disc models with an exponential drop off as described in Hughes et al. (2008). The model shown with the long-dashed line has parameters γ =0.3, c_1=340 AU and $c_2 = 3.1 \times 10^{24}$ cm^{-2} and fits the gas constraints. The model with the dash-dotted line γ =0.6, c_1=340 AU and $c_2 = 1.8 \times 10^{23}$ cm^{-2} fits the scattered light constraints. No single model with a tapered outer edge can fit both these constraints and the constraints within 400 AU simultaneously.

of 1.3 mm fluxes. Our model indicates that any dust present in the outer disc regions must be poor in mm-sized grains, i.e., have low millimetre wavelength opacities, while dust within 400 AU has likely undergone grain growth as found by Pinte et al. (2008). This further supports our choice of κ at 0.8 μm when estimating the upper limit on dust column (see above). Therefore, a viable model for the disc of IM Lup consists of an 'inner' disc extending to 400 AU as described in Pinte et al. augmented with an 'outer disc' extending from 400 to 900 AU with a significantly reduced surface density (with negligible mass) but standard gas-to-dust mass ratio and CO-to-H_2 ratios. The SED of this new model should not differ significantly to that of Pinte et al. model, and is therefore expected to provide a good match to the observed SED of IM Lup.

Hughes et al. (2008) find that the apparent difference between the extent of sub-millimetre dust and gas emission in several circumstellar discs can be explained by an exponential drop off of surface density which naturally arises at the outer edge of a viscous disc. In Fig. 3.10 we show how, with a careful choice of parameters (γ =0.3, c_1=340 AU and $c_2 = 3.1 \times 10^{24}$ cm^{-2}), the model of Hughes et al. (2008) (red long-dashed line) can reproduce the surface density distribution of the models which describe well the ^{12}CO 2–1 line emission. This model, and the one discussed below, are only examples. A proper modelling of IM Lup in the context of viscous disc models would require a revision of the entire disc structure both in terms of temperature and density, which is outside of the scope of the current work. We notice that the Hughes et al. models cannot simultaneously comply with the gas and dust constraints in the outer disc and the surface density derived by Pinte et al. (2008) in the inner disc. This is illustrated by the Hughes et al. (2008) model with parameters γ =0.6, c_1=340 AU and $c_2 = 1.8 \times 10^{23}$ cm^{-2}, shown with the dash-dotted line in Fig. 3.10. The surface density of this model outside 400 AU is in agreement with observational constraints from gas and dust, but it is roughly two orders of magnitude lower than suface density from Pinte et al. (2008) within 400 AU.

In the standard theory of viscous discs (See Pringle 1981), irrespective of the initial density distribution, a radially smooth surface density distribution with a tapered outer edge is rapidly reached. If there is a significant change in the nature of the viscosity inside and outside of 400 AU, discontinuities in the equilibrium surface density may follow. Such changes could, for example, result from differences in the ionization structure of the disc or from a drop of the surface density below some critical level. Here we explore some scenarios that could explain this:

A young disc

An extreme example of such a configuration is a disc where the inner 400 AU follows the standard picture of a viscous accretion disc, but where the region outside 400 AU has not (yet) interacted viscously with the inner disc. This outer region may be the remnant of the flattened, rotating prestellar core that has not yet made it onto the viscous inner disc. This configuration, reminiscent of the material around the object L1489 IRS (Brinch et al. 2007), suggests that IM Lup would only recently have emerged from the embedded phase. L1489 IRS showed clear inward motion in its rotating envelope. Our observations limit any radial motions in the gas between 400 and 900 AU

to < 0.2 km s^{-1}, or 20% of the Keplerian orbital velocities at these radii. Furthermore, for the 900 AU structure to survive for the lifetime of IM Lup of 0.1–0.6 Myr, inward motions cannot exceed $\sim 10^{-2}$ km s^{-1}. Any mass inflow is therefore small, and the material between 400 and 900 AU is likely on Keplerian orbits.

A companion body.

Another explanation for the break in the disc density structure around 400 AU would be the presence of a companion near this radius. A companion of ~ 1 M$_{\mathrm{Jup}}$ at 400 AU could open a gap in the disc and affect the viscous disc spreading. No companions at this separation are visible in the HST images of (Pinte et al. 2008) or in K-band direct imaging (Ghez et al. 1997). Whether these observations exclude this scenario is unclear: it requires modelling of the orbital evolution of a companion in a viscously spreading disc and calculation of the observational mass limits at the age of IM Lup. This is beyond the scope of this Chapter.

Gas to dust ratio.

While our model is consistent with standard gas-to-dust and CO-to-H$_2$ ratios beyond 400 AU, this is not the only solution. Instead of adopting these standard ratios, which requires explaining the drop in Σ or $d\Sigma/dR$ around 400 AU, we can hypothesize that the gas (H$_2$ or H) surface density is continuous out to 900 AU and that both the CO-to-H$_2$ and dust-to-gas ratios show a break around 400 AU. This scenario requires a drop between 400 and 900 AU of the CO abundance by a factor between 10 and 200, and of the dust-to-gas mass ratio by a factor ≥ 90. These drops can be sudden, with a discontinuity at 400 AU, or more gradual, with a rapid decline of the two ratios from 400 to 900 AU. Since a low amount of dust emission outside 400 AU is observed both at wavelengths of ~ 1 mm (our data) and ~ 1 μm (Pinte et al. 2008), the overall dust-to-gas ratio is likely affected, and not just the individual populations of small and large grains.

Dust radial drift and photoevaporation.

If a large fraction of the dust is removed from the disc regions outside 400 AU, the increased penetration of ultraviolet radiation could explain the drop in ^{12}CO surface density through increased photodissociation (van Zadelhoff et al. 2003). Radial drift of dust particles due to the gas drag force (Whipple 1972; Weidenschilling 1977) is a possible scenario in circumstellar discs. The difference in velocity between the dust, in Keplerian rotation, and gas, sub-Keplerian because of the radial pressure gradient, can cause dust particles to lose angular momentum and drift inward. The optimal drift particle size depends on the gas density, Keplerian rotation frequency and hydrostatic sound speed. Most dust evolution models focus on the inner 100 AU of discs, relevant to planet formation. In these regions, the grains from 100 μm to about 0.1 m efficiently migrate inwards on a timescale shorter than 2 Myr. However, the optimal grain size for inward drift decreases with the gas density. Our modelling of the disc region from

400 AU to 900 AU, predicts surface densities of $\sim 10^{-3}$ g cm^{-2}, low enough even for sub-micron-sized particles to drift inward (to < 400 AU). For the estimated age of IM Lup of 0.1–0.6 Myr, all particles larger than 0.1–0.02 μm will have migrated inward. This process leaves the outer disc unshielded by dust against UV radiation. Infrared emission of PAHs may be used to trace the disc surface in this scenario. However, Geers et al. (2007) do not detect PAH emission at 3.3 μm in their VLT-ISAAC L-band observations of IM Lup. This may indicate that either there are not enough PAHs in the disc or that they are not exposed to a significant level of UV flux. The latter possibility allows the outer disc to remain molecular. Otherwise, the outer disc is exposed to photodissociating radiation, destroying much of the CO and likely also a significant fraction of the H$_2$ given the limit on the dust surface density of 10^{21} cm^{-2} corresponding to $A_V \approx 1^{\mathrm{mag}}$. In this scenario, the outer disc between 400 and 900 AU would be largely *atomic* and possibly detectable through 21 cm observations of H I, or line observations of C I at 609 and 370 μm or C II at 158 μm. If *photoevaporation* is efficient in this region it may remove the (atomic) gas and reduce the gas surface density further. Therefore, a combined effect of efficient drift, photodissociation and photoevaporation in the outermost disc regions may be a reason for the low gas and dust density observed. The efficiency of these processes decreases with density and perhaps the density at 400 AU is high enough so that material is no longer efficiently removed from the disc. Only the detailed simultaneous modelling of drift, photodissociation and photoevaporation could test this scenario.

3.5 CONCLUSIONS

We probe the kinematics and the distribution of the gas and dust in the disc around IM Lup through molecular gas and continuum dust emission. Our SMA observations resolve the disc structure down to scales of 200 AU, and allow us to probe the structure of the inner disc (< 400 AU) and the outer disc (400–900 AU). Our main conclusions can be summarized as follows.

- The ^{12}CO and ^{13}CO emission extends to 900 AU from IM Lup, much further than the outer radius of 400 AU inferred earlier from dust measurements.

- The H$_2$ gas surface density in the region between 400 and 900 AU lies in the range of 5×10^{20} to 10^{22} cm^{-2}, using the standard CO-to-H$_2$ ratio of 10^{-4}.

- The disc is in Keplerian rotation around a central mass of 1.2 ± 0.4 M$_\odot$. Infall motions, if present in the outer disc, are negligible at < 0.2 km s^{-1}.

- The molecular line emission from the inner disc, within 400 AU, is well described by the model of Pinte et al. (2008), except that the gas temperature in the layers dominating the line emission of ^{12}CO and ^{13}CO exceeds the dust temperature by factors 1.7 and 1.4, respectively.

- Outside 400 AU, the surface densities of the molecular gas, as traced through ^{12}CO and ^{13}CO, of small (~ 1 μm) dust grains, and of larger (~ 1 mm) dust grains

have a break in their radial dependence. At 400 AU, the dust surface density (in small grains) drops by a factor ~ 100, while the gas surface density shows a comparable drop of a factor 10–200 or steepens its radial power-law slope from $p = 1$ to $5 \leq p \leq 8$.

Our observations show that the disc around IM Lup consists of two regions. The inner 400 AU is well described by a 'standard' accretion disc; the region between 400 and 900 AU has a much lower surface density as traced through dust grains with sizes from $\sim 1\ \mu$m to 1 mm and through CO emission. Our observations do not tell us if this outer region consists of material from the original prestellar core that has not (yet) made it onto the viscous accretion disc, or of material that is part of the disc but has had a different evolution. Sensitive, spatially resolved observations at various (sub) millimetre wavelengths, as may be obtained with the Atacama Large Millimeter Array may help to assess whether significantly different grain populations exist inside and outside of 400 AU. With the same telescope, very high signal-to-noise observations of ^{12}CO lines at high spectral resolution may allow determination of any radial (inward or outward) motions in the > 400 AU gas. Spatially resolved mid-infrared imaging in several emission bands of PAHs, as could be obtained with the VISIR instrument on VLT, would shed light on the question if the 400–900 AU zone in the disc is largely photodissociated or -ionized. Detailed modelling of dust evolution in the outer disc may answer whether radial drift is responsible for the low column of dust beyond 400 AU in IM Lup disc.

REFERENCES

Baraffe, I., Chabrier, G., Allard, F., & Hauschildt, P. 1998, VizieR Online Data Catalog, 333, 70403

Brinch, C., Crapsi, A., Hogerheijde, M. R., & Jørgensen, J. K. 2007, A&A, 461, 1037

Chiang, E. I. & Goldreich, P. 1997, ApJ, 490, 368

D'Alessio, P., Merín, B., Calvet, N., Hartmann, L., & Montesinos, B. 2005, Revista Mexicana de Astronomia y Astrofisica, 41, 61

D'Antona, F. & Mazzitelli, I. 1994, ApJS, 90, 467

Dartois, E., Dutrey, A., & Guilloteau, S. 2003, A&A, 399, 773

Draine, B. T. 2006, ApJ, 636, 1114

Dullemond, C. P., Dominik, C., & Natta, A. 2001, ApJ, 560, 957

Frerking, M. A., Langer, W. D., & Wilson, R. W. 1982, ApJ, 262, 590

Geers, V. C., van Dishoeck, E. F., Visser, R., et al. 2007, A&A, 476, 279

Ghez, A. M., McCarthy, D. W., Patience, J. L., & Beck, T. L. 1997, ApJ, 481, 378

Guilloteau, S. & Dutrey, A. 1998, A&A, 339, 467

Hogerheijde, M. R. & van der Tak, F. F. S. 2000, A&A, 362, 697

Hughes, A. M., Wilner, D. J., Qi, C., & Hogerheijde, M. R. 2008, ApJ, 678, 1119

Hughes, J., Hartigan, P., Krautter, J., & Kelemen, J. 1994, AJ, 108, 1071

Isella, A., Testi, L., Natta, A., et al. 2007, A&A, 469, 213

Jonkheid, B., Faas, F. G. A., van Zadelhoff, G.-J., & van Dishoeck, E. F. 2004, A&A, 428, 511

Jørgensen, J. K., Bourke, T. L., Myers, P. C., et al. 2005, ApJ, 632, 973

Lommen, D., Wright, C. M., Maddison, S. T., et al. 2007, A&A, 462, 211

Ossenkopf, V. & Henning, T. 1994, A&A, 291, 943

Piétu, V., Dutrey, A., & Guilloteau, S. 2007, A&A, 467, 163

Pinte, C., Padgett, D. L., Menard, F., et al. 2008, ArXiv e-prints, 808

Pringle, J. E. 1981, ARA&A, 19, 137

Qi, C., Ho, P. T. P., Wilner, D. J., et al. 2004, ApJ, 616, L11

Qi, C., Wilner, D. J., Calvet, N., et al. 2006, ApJ, 636, L157

Sault, R. J., Teuben, P. J., & Wright, M. C. H. 1995, in Astronomical Society of the Pacific Conference Series, Vol. 77, Astronomical Data Analysis Software and Systems IV, ed. R. A. Shaw, H. E. Payne, & J. J. E. Hayes, 433–+

Schöier, F. L., van der Tak, F. F. S., van Dishoeck, E. F., & Black, J. H. 2005, A&A, 432, 369

Swenson, F. J., Faulkner, J., Rogers, F. J., & Iglesias, C. A. 1994, ApJ, 425, 286

van Kempen, T. A., van Dishoeck, E. F., Brinch, C., & Hogerheijde, M. R. 2007, A&A, 461, 983

van Zadelhoff, G.-J., Aikawa, Y., Hogerheijde, M. R., & van Dishoeck, E. F. 2003, A&A, 397, 789

Weidenschilling, S. J. 1977, MNRAS, 180, 57

Whipple, F. L. 1972, in From Plasma to Planet, ed. A. Elvius, 211

Wichmann, R., Bastian, U., Krautter, J., Jankovics, I., & Rucinski, S. M. 1998, MNRAS, 301, L39+

Wilson, T. L. & Rood, R. 1994, ARA&A, 32, 191

CHAPTER 4

An arc of gas and dust around the young star DoAr 21

M. R. Hogerheijde, O. Panić, H. Schouten and B. Merín

T HE dissipation of protoplanetary disks is currently thought to occur inside-out, either through photoevaporation or gap formation following giant-planet formation. So-called 'transitional' disks, with cleared-out inner regions, are characterized by nearly photospheric near-infrared fluxes and strong mid-infrared excess. We investigate the spatial distribution of circumstellar material around the ~0.3–1.0 Myr old, weak-line T Tauri star DoAr 21, which has a 'transitional' SED. We resolve the emission of the H_2 1–0 S(1) line at a resolution of ~250 mas using adaptive-optics assisted Integral Field Unit spectroscopic measurements from VLT/SINFONI. We also detect the H_2 1–0 S(0) line, but at insufficient signal-to-noise to spatial resolve the emission; and we obtain upper limits to several other H_2 lines. Diffraction limited VLT/VISIR imaging at λ =18.72 μm shows the emission from warm dust at a resolution of 0.''48. The H_2 line emission and the 18.72 μm dust continuum reveal a $230°$ arc of emission located on the northwest side of the star at 73–219 AU distances. The mass of the circumstellar material is estimated at $\gtrsim 1 \times 10^{-4}$ $M_\odot$ of gas and dust. The temperature of the dust traced at 18.72 μm is estimated at ~50–100 K, while the H_2 lines appear to be thermally excited in gas heated to 1000–2000 K, likely by stellar X-rays. We conclude that this arc may be caused by an unseen companion of no more than a few Jupiter masses interacting with disk material; perturbation of the disk by a stellar fly-by is considered unlikely. Alternatively, it may be the result of unrelated cloud material illuminated by the star. Our results illustrate that the presence of a cleared-out disk cannot be inferred from spatially unresolved observations alone. At the same time, they suggest that detectable ro-vibrational H_2 lines arise when X-rays are not confined to the immediate surroundings of the star.

4.1 Introduction

The disks that surround many newly formed stars have typical lifetimes of 2–3 Myr, although some disks disappear much earlier and others retain significant amounts of mass up to 10 Myr (e.g., Hillenbrand 2008; Meyer 2009). The presence of circumstellar disks is usually inferred from infrared and (sub) millimeter excess emission apparent in the object's Spectral Energy Distribution (SED), while their mass is obtained from continuum and/or molecular-line measurements at (sub) millimeter wavelengths (see, e.g., Isella et al. 2009, for a recent example). Recently, much attention has been given to so-called 'transitional' or 'cold' disks (e.g., Forrest et al. 2004; D'Alessio et al. 2005; D'Alessio 2009; Piétu et al. 2007; Hughes et al. 2007, 2009; Brown et al. 2007, 2008), which lack excess at near-infrared wavelengths but have mid-infrared fluxes comparable to those of 'classical' disks. The favored explanation is that the inner regions of these disks (one to tens of AU) are devoid of (small) dust, but that the outer regions ($\gtrsim$ tens of AU) still contain enough material to form a planetary system ($\gtrsim 10^{-4}$ M$_\odot$). Mechanisms responsible for the clearing of the inner disk can be photoevaporation of the gas and dust by the stellar radiation (Shu et al. 1993; Clarke et al. 2001; Matsuyama et al. 2003; Alexander et al. 2006) or dynamic interaction with a giant planet (Lin & Papaloizou 1993). The presence of (previously unknown) (sub)stellar companions may also explain a number of disks with cleared-out inner regions (e.g., Ireland & Kraus 2008). In some cases, residual amounts of gas remain in the inner disks that are otherwise free of dust (e.g., Goto et al. 2006; Pontoppidan et al. 2008; Salyk et al. 2009), hinting at the complex dynamics of the gas and dust in accretion disks.

In this Chapter we present spatially resolved observations of molecular gas and warm dust of DoAr 21, a young star with a 'transitional' SED, and show that such measurements are essential to interpret the spatial distribution of the circumstellar material. Sub-arcsecond resolution is required to spatially resolve the emission at the typical distances of young stars (50–200 pc). Common tracers that allow such resolution include (sub) millimeter continuum and molecular-line emission as studied in Chapters 2 and 3 of this thesis (e.g., Guilloteau & Dutrey 1998; Simon et al. 2000; Andrews & Williams 2005, 2007a,b; Piétu et al. 2007; Qi et al. 2004, 2006, 2008; Hughes et al. 2008; Isella et al. 2009), near-infrared scattered light imaging (e.g., Grady et al. 2000; Schneider et al. 2003; Roberge et al. 2005; Pinte et al. 2008), and mid-infrared imaging with 8-m class telescopes (e.g., Geers et al. 2007). In this Chapter we use this latter approach, presenting diffraction limited (0''.48) imaging at 18.72 μm with VISIR on the Very Large Telescope (VLT), and we explore a novel technique using Adaptive-Optics (AO) assisted spectroscopic imaging of ro-vibrational H$_2$ lines in the near-infrared K-band with the Integral Field Unit (IFU) SINFONI on VLT.

Ro-vibrational and pure-rotational emission of H$_2$ has been detected around numerous young stars (e.g., van Langevelde et al. 1994; Richter et al. 2002; Lahuis et al. 2007; Martin-Zaïdi et al. 2007, 2008, 2009; Beck et al. 2008). The pure-rotational lines are thermally excited in warm (~ 100 K) gas, but can generally only be observed with some difficulty at their mid-infrared wavelengths. Ro-vibrational lines at near-infrared wavelengths are much more easily accessible through, for example, long-slit spectroscopy, but require higher temperatures (> 1000 K) or non-thermal mechanisms

to be excited.

Around a dozen young stars spatially unresolved, narrow emission of H_2 1–0 S(1) at 2.1218 μm has been detected (including LkHα264, GG Tau A, V773 Tau, DM Tau, LkCa 15, GM Aur, CS Cha, DoAr 21, and TW Hya; Weintraub et al. 2000; Bary et al. 2002, 2003, 2008; Itoh et al. 2003; Ramsay Howat & Greaves 2007; Carmona et al. 2007). Because these lines are narrow and centered on the stellar velocity, these authors conclude that the emission originates in quiescent gas, presumably in their circumstellar disks, and not from gas that is heated by shocks (cf. Beck et al. 2008). Interestingly, about one-third (6/18) of the objects with detected quiescent ro-vibrational H_2 emission have 'transitional' SEDs suggesting cleared-out inner disk regions (Bary et al. 2008).

A viable mechanism to heat disk material to > 1000 K temperatures required to excite ro-vibrational H_2 lines, is offered by the secondary electrons produced by X-ray photoionization (e.g., Gredel & Dalgarno 1995; Maloney et al. 1996; Tiné et al. 1997; Glassgold et al. 1997; Igea & Glassgold 1999; Glassgold et al. 2004; Nomura et al. 2007; Gorti & Hollenbach 2008). Alternatively, a *non*-thermal process if offered by excitation of electronic states of H_2 by ultraviolet radiation, followed by a radiative cascade and fluorescent emission in the 1–0 S(1) and other ro-vibrational lines (Black & van Dishoeck 1987; Sternberg & Dalgarno 1989; Draine & Bertoldi 1996). Using intensity ratios of several ro-vibrational H_2 transitions, thermal processes can be distinguished from non-thermal fluorescence (e.g., Mouri 1994). In this way, Carmona et al. (2007) conclude that the ro-vibrational H_2 emission from LkHα 264 originates from ~ 1000 K gas heated by the stellar X-rays; a similar mechanism has been suggested for the other stars with detected H_2 1–0 S(1), based on their strong X-rays (e.g., DoAr 21; Bary et al. 2002).

The young star DoAr 21 (also known, among other names, as V2246 Oph, ROXR1 13, and ROX 8), $\alpha_{2000} = 16^h26^m03^s031$, $\delta_{2000} = -24°23'36''43$, (Dolidze & Arakelyan 1959) is a 2.2 $M_\odot$ K1 star (Luhman & Rieke 1999) located at $121.9^{+5.8}_{-5.3}$ pc (Loinard et al. 2008) in the Lynds 1688 star-forming cloud in Ophiuchus; it is located just outside the Oph A millimeter condensation (Loren & Wootten 1986; Motte et al. 1998), $6'$ (0.2 pc) west of the core's center. From the star's luminosity (15–30 $L_\odot$; Bouvier & Appenzeller 1992; Luhman & Rieke 1999; Bontemps et al. 2001) and effective temperature (5080 K), Luhman & Rieke (1999) estimate an age of $\sim$0.3 Myr using evolutionary tracks of D'Antona & Mazzitelli (1996). Its Hα equivalent width of -0.6 Å (Bouvier & Appenzeller 1992) classifies it as a weak-line T Tauri star. In a recent paper, Jensen et al. (2009) obtain a similar age and mass for the star when assumed single, and slightly lower masses and higer age of 1.0 Myr when assumed to be an equal-mass binary. They also show that the Hα emission is variable and has a complex line profile.

Mid-infrared observations of DoAr 21 by Barsony et al. (2005) and, more recently using measurements from the Spitzer Space Telescope, Jensen et al. (2005) and Cieza et al. (2007) reveal significant amounts of warm dust. DoAr 21 is not detected at 1.3 mm by André & Montmerle (1994) to an upper limit of 5 mJy; however, significant extended cloud emission is visible in archival JCMT/SCUBA data (Di Francesco et al. 2008) making is difficult to discern any possible continuum emission directly related to the star.

Similar extended emission is visible in Spitzer IRAC and MIPS images (Padgett et al. 2008). The object emits copious (L_X of a few times 10^{31} erg s^{-1}, or $L_X/L_{\rm bol} \sim 10^{-4}$) and hard (3–4 keV) X-rays (Koyama et al. 1994; Casanova et al. 1995; Grosso et al. 2000; Gagné et al. 2004; Imanishi et al. 2002), and appears to be in a continuously flared state. DoAr 21 has also long been known to be variable at radio wavelengths (Feigelson & Montmerle 1985; Stine et al. 1988). Recent VLBI measurements resolve the object into a 15 mas binary, supporting the hypothesis that DoAr 21 is directly comparable to the object V773 Tau (Feigelson & Montmerle 1985; Loinard et al. 2008). In V773 Tau (Massi et al. 2006, 2008), and in the similar system DQ Tau (Salter et al. 2008), the periodic overlap of the magnetospheres of the two stars on an eccentric binary orbit generate periodic radio flares, and a similar mechanism may operate for DoAr 21.

Quiescent H$_2$ emission from DoAr 21 was reported by Bary et al. (2002), who estimate 4.4×10^{-10} M$_\odot$ of emitting gas and extrapolate this to a total disk mass of 10^{-3}–1.0 M$_\odot$. From the (marginally) resolved line width, they infer that the emission originates between 5 and 30 AU from the star. Bitner et al. (2008) detect pure-rotational emission from DoAr 21 at 12.28 μm, finding a $\sim$5 times larger mass of warm ($\sim$100 K) gas, and conclude that the material is located outside 30 AU. Our spatially resolved observations directly address the question of the spatial distribution of the circumstellar material traced through the SED and the H$_2$ line emission.

Section 4.2 of this Chapter describes our observations[1] and Section 4.3 list the results. Instead of an axisymmetric circumstellar disk, we find that the emission originates from an arc of material circling the star at radii between 70 and 220 AU, and in Section 4.4 we explore various explanations for the observed characteristics. Section 4.5 summarizes our findings and addresses their relevance for the class of objects with 'transitional' SEDs and for the class of objects with quiescent H$_2$ emission.

When this thesis was completed, a manuscript by Jensen et al. (2009) appeared, presenting mid-infrared imaging, and optical and X-ray spectroscopy of DoAr 21. The results of their imaging are consistent with our 18.72 μm data, and they reach similar conclusions regarding the spatial extent of the circumstellar material. Their spectroscopy confirms the assumptions made by us about the energy input by the stellar radiation field. Our work presented in this Chapter strongly complements the work of Jensen et al. by presenting spatially resolved data of the H$_2$ line emission – directly confirming their suggestion that the warm dust and H$_2$ 2.12 μm line emission are co-spatial –, and by placing observational limits on the excitation mechanism of the H$_2$ lines. Our observations show that the H$_2$ lines arise in gas heated to 1000–2000 K by X-rays and that FUV fluorescence is likely collisionally quenched (Sect. 4.4).

---

[1]Collected at the European Organisation for Astronomical Research in the Southern Hemisphere, Chile, under proposal numbers 075.C-0378 and 081.C-0742.

4.2   OBSERVATIONS

4.2.1   SINFONI observations

Using the Spectrograph for Integral-Field Observations in the Near Infrared (SIN-FONI) on the European Southern Observatory's Very Large Telescope UT4 (Yepun), we observed the star DoAr 21 on 2005 July 1. The observing conditions were good with light cirrus and a visual seeing of $0\overset{''}{.}35$–$0\overset{''}{.}6$. The K-band grating was selected with a spectral resolving power of $R = 4000$. With its K-band magnitude of 6.16 (Barsony et al. 1997) and V-band magnitude of 13.9 (Bouvier & Appenzeller 1992), DoAr 21 was sufficiently bright to serve as a reference for the Adaptive Optics system. Strehl ratios of 0.43–0.48 were reached, and the full width at half maximum (FWHM) of the Point Spread Function (PSF) FWHM was 63 mas, consistent with diffraction-limited observations at K band. Using a plate scale of 250 mas pixel^{-1}, we obtained eight 1-second integrations. At this plate scale, the PSF is undersampled by the pixels, and only very short integrations were possible to avoid saturating the detector array. Using a plate scale of 25 mas pixel^{-1}, we obtained twenty 15-second integrations for a total of 300 second integration time. This plate scale resolves the PSF well.

In addition to DoAr 21, observations of DoAr 20 and DoAr 34 were also obtained to serve as PSF standards (six integrations of 20 seconds at a plate scale of 25 mas pixel^{-1}). Standard calibration observations were performed including darks and flats, using the stars HIP 93393 (HD 176871, $m_{\rm K} = 5.8$) and HIP 64075 (HD 113949, $m_{\rm K} = 8.7$) as standard stars. All observations were obtained while chopping with a $30''$ offset to subtract the sky background, and a jitter of 4 pixels, using the standard observing mode `SINFONI_ifs_obs_AutoJitterOffset`.

The data reduction and calibration was carried using the standard recipes provided by the ESOREX and GASGANO packages. Integrated light images were constructed summing over a 0.245 μm bin centered on 2.20 μm. A continuum-subtracted H_2 1–0 S(1) line emission image was obtained on a pixel-by-pixel basis by summing six channels with detected emission, and subtracting the contribution from the stellar continuum obtained from 16 channels on either side, selected to be free of spectral features (either stellar, atmospheric, or due to imperfect standard-star subtraction). This procedure resulted in a very accurate subtraction of the stellar continuum, with a dynamic range of ~ 100 at the core of the PSF increasing to 500–1000 outside the central $\sim 0\overset{''}{.}2$. For DoAr 20 and DoAr 34 (which do not show H_2 line emission), residual emission (both positive and negative) remains present within $0\overset{''}{.}1$ of the stellar images, due to imperfections of the continuum subtraction. For DoAr 21, negative emission fills the 25 mas plate-scale image, as well as the inner $0\overset{''}{.}7$ around the star in the 250 mas plate-scale image. If this were due to line-of-sight absorption by H_2, the required optical of $\tau \sim 0.01$ corresponds to unrealistically high values for the hydrogen column density of $\sim 6 \times 10^{23}$ cm^{-2} and the optical extinction A_V of 500. We therefore conclude that the negative residual is due to imperfect subtraction of the stellar radiation. However, this does not affect out results.

4.2.2 VISIR observations

Using the VLT spectrometer and imager for the mid–infrared (VISIR) on VLT UT3 (Melipal), we observed the star DoAr 21 on 2008 April 10. The Q2-filter was selected with a central wavelength of 18.72 μm and a width of 0.88 μm. At this wavelength the VLT is diffraction limited, and a FWHM of the PSF of $0\rlap{.}''48$ was measured. The plate scale of the detector is 75 mas pixel^{-1} resolving the PSF well. A total integration time of 1 s was reached in 38 observations of 25 ms each. The observations were obtained with a chop throw of $4\rlap{.}''8$ (half-array size) and the telescope was offset by one-quarter of the field-of-view in RA and Dec, so that both positive and negative images were recorded. Observations of the star HD 145897 (χ Sco, $m_V = 6.7$) were obtained for flux calibration; from its effective temperature of 5000 K (Bouvier & Appenzeller 1992; Luhman & Rieke 1999) we estimated a Q2-band flux of 2.02 Jy. Subsequent reduction and calibration was carried out with the standard pipeline recipes provided by the ESOREX package.

At these mid-infrared wavelengths the sky generates a highly variable background, and no flatfielding is usually performed. However, in our observations of the relatively weak and extended emission (see §4.3), a variable background is clearly discernible. A background of similar shape is seen in the observations of the standard star, and we have used these to 'flatfield' the exposures of the science target. We first subtracted a PSF-fit from the standard star image consisting of a diffraction-limited Airy pattern followed by a Gaussian convolution with a FWHM of $0\rlap{.}''217$. We then smoothed the residual to a resolution of $0\rlap{.}''75$ and normalized the image. And finally we subtracted the resulting flatfield from the science image. This generates better images with a flatter background; it does not affect our conclusions on emission extended over $\lesssim \frac{1}{4}$ of the field, but the flatfielding procedure (and the presence of the varying background) limits our possibility to detect emission extended over larger scales.

4.3 RESULTS

Figure 4.1[2] shows the images of DoAr 21: the integrated-light images in K-band from SINFONI showing the stellar continuum (both plate scales); the continuum-subtracted H_2-line images (both plate scales); and the 18.72 μm VISIR image.

The stellar photosphere is clearly detected at 2.20 and 18.72 μm; it completely dominates the emission at the shorter wavelength. At both wavelengths the stellar image is (nearly) diffraction limited with respective PSF cores of FWHM 73×69 mas (at 2.20 μm) and $0\rlap{.}''48$ (at 18.72 μm); at the 250 mas pixel^{-1} plate scale at 2.20 μm (Fig. 4.1b) the PSF is under-resolved and diffraction spikes are clearly visible. At 18.72 μm extended emission $\sim 1''$ NW of the star is also clearly detected, roughly forming an arc of 90° with a radius of $1\rlap{.}''2$ (146 AU) and a width of $0\rlap{.}''5$ (61 AU), i.e., close to the diffraction limit in the radial direction. The 18.72 μm image is very similar to the 18.3 μm results presented by Jensen et al. (2009).

---

[2]Panels (c) and (e) of this figure can be seen in colour on page 8 of this thesis, Fig. 1.2.
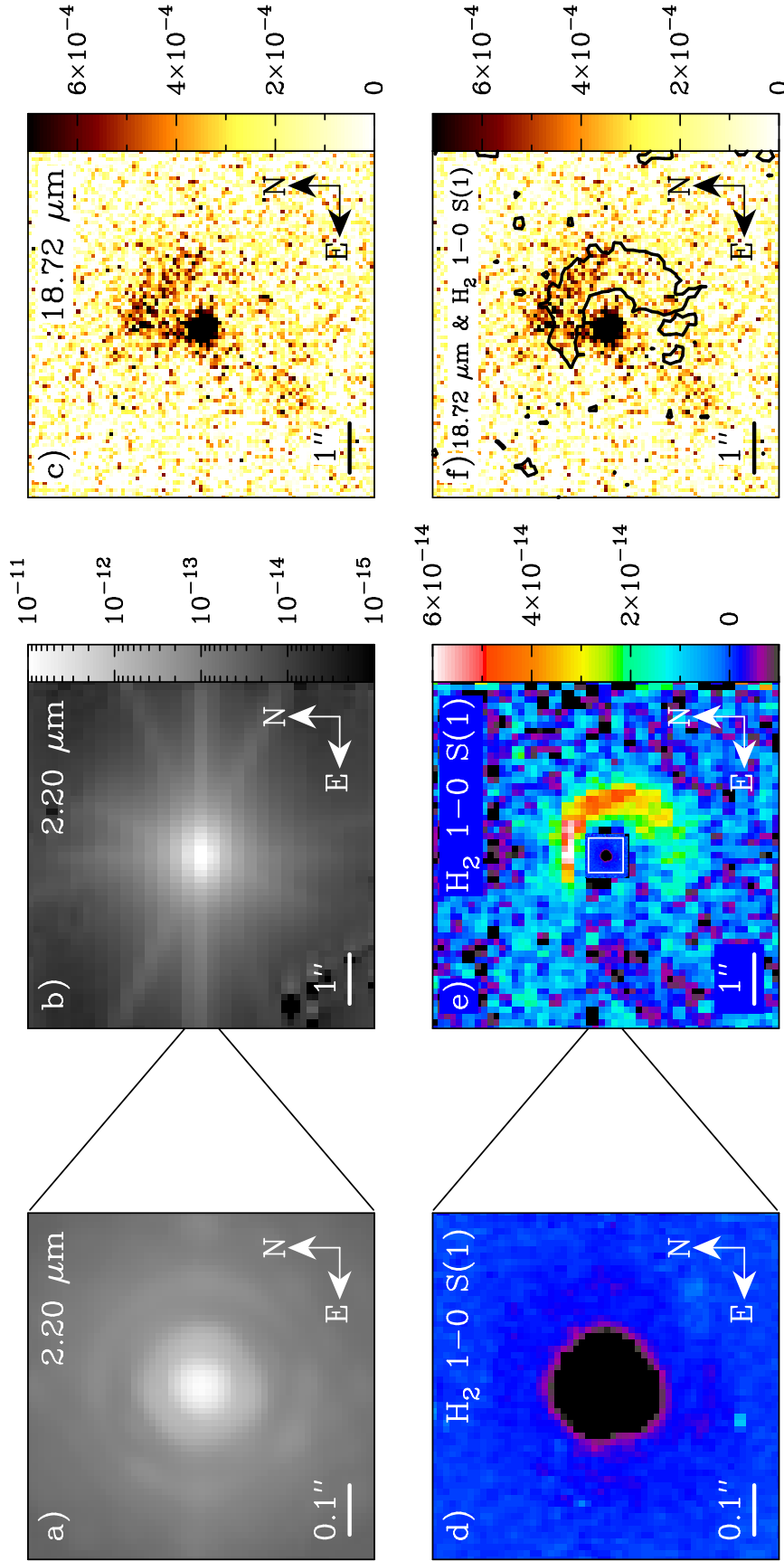
Figure 4.1: **(a)** Image of the 2.20 μm emission of DoAr 21 recorded on the 25 mas plate scale, averaged over a 0.245 μm width and plotted using a logarithmic stretch ranging from 10^{-15} to 10^{-11} erg s^{-1} cm^{-2} μm^{-1} pixel^{-1}. **(b)** Same as (a), recorded on the 250 mas plate scale, which under-resolves the PSF. **(c)** Image of the 18.72 μm emission, plotted on a linear stretch ranging from 0 to 0.7 mJy pixel^{-1}. **(d)** Continuum subtracted image of the six channels centered on 2.1218 μm, the wavelength of the H$_2$ 1–0 S(1) line, recorded on the 25 mas plate scale. The intensity is plotted with a linear stretch ranging from -1×10^{-14} to 4×10^{-14} erg s^{-1} cm^{-2} μm^{-1} pixel^{-1}. Note the negative residual of the stellar continuum subtraction due to imperfect subtraction of the stellarradiation. **(e)** Same as (d), recorded using the 250 mas plate scale. The 25 mas image of panel (d) is plotted as an inset at the center of the image. **(f)** Overlay of the H$_2$ 1–0 S(1) line emission (one contour at 1.5×10^{-14} erg s^{-1} cm^{-2} μm^{-1} pixel^{-1}) on the 18.72 μm continuum emission.

Table 4.1: Measured continuum and line fluxes of DoAr 21

Measurement	Value
DoAr 21: F_λ ($\lambda = 2.20$ μm)	2.3 ± 0.02 Jy
DoAr 21: F_λ ($\lambda = 18.72$ μm)	84 ± 2 mJy
Arc: F_λ ($\lambda = 18.72$ μm)	~ 159 mJy
Total: F_λ ($\lambda = 18.72$ μm)	~ 700 mJy
H$_2$ 1–0 S(1), 2.1218 μm: $\int F_\lambda d\lambda$	$8.0 \pm 0.5 \times 10^{-15}$ erg s^{-1} cm^{-2}
H$_2$ 1–0 S(0), 2.2235 μm: $\int F_\lambda d\lambda$	$2.2 \pm 0.3 \times 10^{-15}$ erg s^{-1} cm^{-2}

No H$_2$ line emission is detected in the 25 mas plate-scale image, down to a noise level of 5×10^{-15} erg s^{-1} cm^{-2} μm^{-1} pixel^{-1}. In the 250 mas plate-scale image, an arc of emission in the H$_2$ 1–0 S(1) line is detected extending from the north to the southwest of the star, where the emission is lost in the noise. This arc starts at a position angle of $-40°$ (as measured from north to west), where the H$_2$ emission ranges from $0\rlap{.}''6$ (73 AU) to $1\rlap{.}''0$ (122 AU) from the star, over $230°$ to a position angle of $+170°$, where the H$_2$ emission stretches from $1\rlap{.}''1$ (134 AU) to $1\rlap{.}''8$ (219 AU) from the star. Panel (f) of Fig. 4.1 shows an overlay of the 18.72 μm continuum and H$_2$ line emission, indicating that both trace the same region (with the H$_2$ emission apparently outlining the inner side from the 18.72 μm emission as seen from the star). The location of the H$_2$ emission is consistent with the conclusion of Bitner et al. (2008) that it originates outside 30 AU from the star.

Figure 4.2 shows the H$_2$ 1–0 S(1) line spectrum integrated over the region where the emission was detected above the noise in the 250 mas plate-scale image, roughly corresponding to the contour in Fig. 4.1f. In addition to the H$_2$ 1–0 S(1) line at 2.1218 μm, at least a dozen other H$_2$ ro-vibrational lines have wavelengths within the SINFONI spectrum; of these, only H$_2$ 1–0 S(1) is detected at sufficient signal-to-noise for imaging. The H$_2$ 1–0 S(0) line at 2.2235 μm is detected when integrating over the same area where the 1–0 S(1) was found to emit. No other lines H$_2$ were detected. For example, an upper limit of $\sim 1.5 \times 10^{-15}$ erg s^{-1} cm^{-2} is found for the H$_2$ 2–1 S(1) line at 2.2477 μm. Figure 4.2 also shows the detected 1–0 S(0) line and the location of the (undetected) 3–2 S(4) line. Other features in the spectra are residual lines resulting from the standard star subtraction, as verified by inspection of the similarly processed spectra of DoAr 20 and DoAr 34 that show the same artifacts but no H$_2$ lines.

Line strengths and continuum fluxes are listed in Table 4.1. The integrated line strength of the 1–0 S(1) line of $8.0 \pm 0.5 \times 10^{-15}$ erg s^{-1} cm^{-2} agrees within the noise with the value reported by Bary et al. (2002) of $15 \pm 9 \times 10^{-15}$ erg s^{-1} cm^{-2} (Bary et al. 2002). This indicates that we have recovered essentially all H$_2$ 1–0 S(1) line emission by summing over the observed arc. Likewise, the 18.72 μm flux of the star of 84 ± 2 mJy agrees well with the expected photospheric value of $\sim$59 mJy given that the flatfielding procedure described in Sect. 4.2.2 complicates the extraction of accurate fluxes. This uncertainty strongly affects estimates of the extended fluxes: we estimate that the flux of the arc amounts to 160 mJy and that the entire field contains ~ 700 mJy, but note that the latter values are uncertain by a factor of 2. However, the value of 700 mJy is
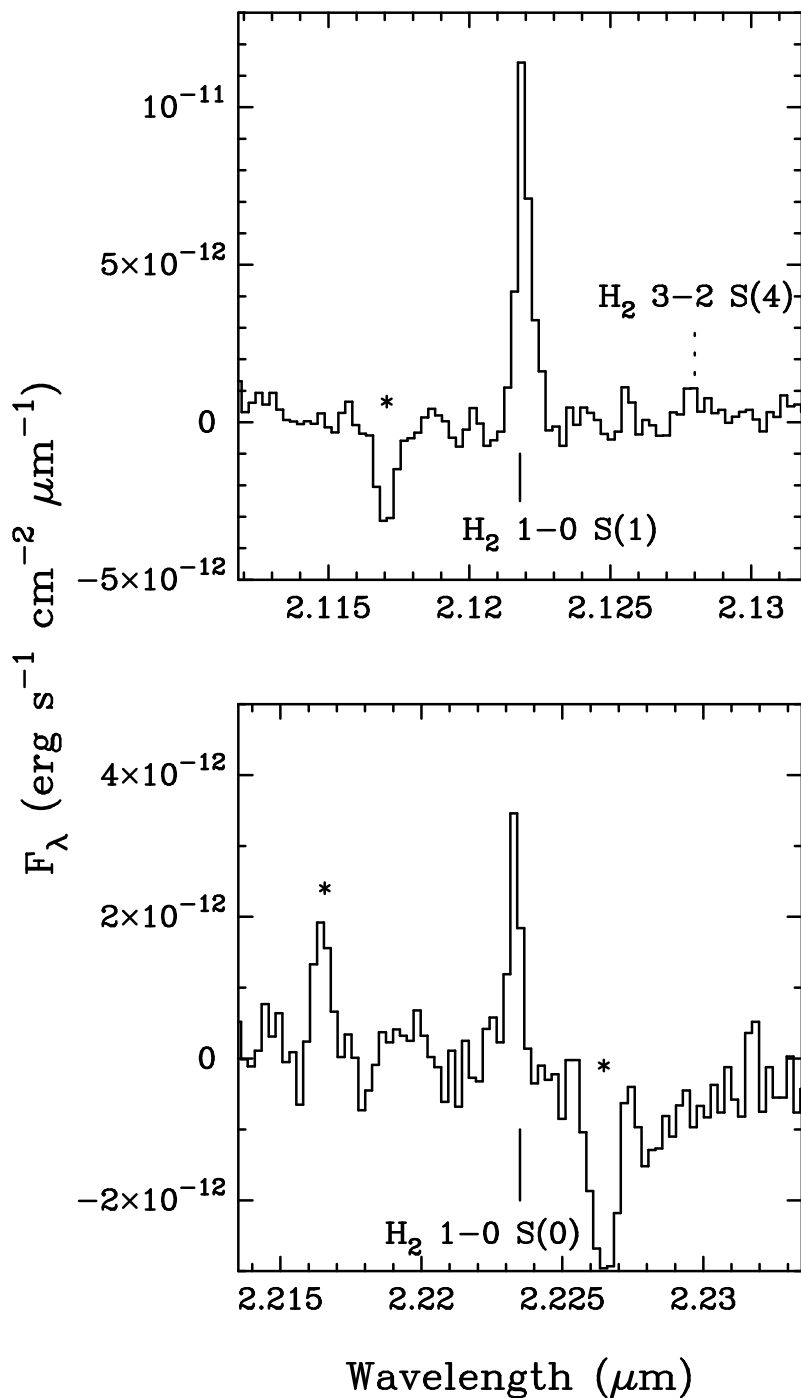
Figure 4.2: Spectrum of the H_2 1–0 S(1) (top) and H_2 1–0 S(0) (bottom) line emission, integrated over those areas of the 250 mas plate-scale image with 1–0 S(1) emission detected at $> 2\sigma$. Also indicated is the position of the 3–2 S(4) line, which is not detected. Other spectral features, marked with $*$, are residuals from the standard spectrum subtraction.

consistent with the mid-infrared SED as we will see in Sect. 4.4.1 (see also Fig. 4.3).

4.4 DISCUSSION

4.4.1 Location and mass of the emitting material

The previous Section and Fig. 4.1 convincingly show that the H_2 emission does not originate from radii of 5–30 AU in a circumstellar disk, as suggested before by the spatially unresolved observations of Bary et al. (2002), but instead from an arc on the northwest of DoAr 21 at distances of 73–219 AU. At least one-quarter of the excess emission at 18.72 μm emission originates from this same arc, comparing the measured flux of 160 mJy to the total flux of 700 mJy.

The SED of Fig. 4.3 clearly shows the presence of excess emission at mid- and far-infrared wavelengths. PAH bands contribute to the 7–12 μm flux (Hanner et al. 1995). We take two approaches to determine the amount of circumstellar material and its typical temperatures. In the first approach, we add a small number of components at different temperature to match the SED. Using emissivities from Ossenkopf & Henning (1994) for dust particles without ice mantles and a gas-to-dust mass ratio of 100, we find a reasonable match for a mass of 5×10^{-3} $M_\odot$, with the bulk of the material at 30 K, and 2% at 60 K, 0.02% at 90 K, and 1 part in 5×10^5 at 200 K.

In the second approach we use the grid of SED models and the fitting routines of Robitaille et al. (2006, 2007) to find a best fit. The best match is found for a stellar age of 5×10^5 yr, a rather low effective temperarture of 3872 K (compared to the 5080 K of DoAr 21), and disk mass of 6.7×10^{-5} $M_\odot$ and disk radius of 163 AU, and a surrounding envelope of 3.7×10^{-2} $M_\odot$ and 5000 AU radius (model # 3015448). Although this model fits very well, with a χ^2 value of 3.6, we caution that other models with very different parameters give fits that appear to the eye as nearly as good.

Both models described in the previous two paragraphs fit the SED equally well (Fig. 4.3). Clearly, without going into the full details of modeling the spatial extent of the emission, the SED alone does not provide sufficient constraints to provide a unique fit. A further complication may arise from the fact that the points in the SED are not contemporaneous. It appears that the flux around, e.g., 10 μm can vary by a factor of ~ 2. These variations may be caused by the different heating input from the stellar X-rays that are known to flare.

From our simple four-component model, we find that the 18.72 μm flux of the arc corresponds to $\sim 1 \times 10^{-4}$ $M_\odot$ at 60 K. We take this value as a conservative estimate of the total mass traced by the 18.72 μm emission. The amount of gas traced by the H_2 1–0 S(1) line was estimated by Bary et al. (2002). Scaling their value to our slightly lower intensity, we obtain a gas mass of $2.3 \pm 0.1 \times 10^{-10}$ $M_\odot$ emitting in the H_2 1–0 S(1) line. This is $\lesssim 10^{-6}$ times the mass inferred from the 18.72 μm dust emission of $\gtrsim 10^{-4}$ $M_\odot$, a similar small fraction as found toward other systems (Bary et al. 2003) and consistent with the notion that the ro-vibrational H_2 emission arises in a thin, hot surface layer heated by X-rays (e.g., Nomura et al. 2007) – but not necessarily that of a disk. The spatial correlation of the H_2 emission and 18.72 μm continuum emission (Fig.
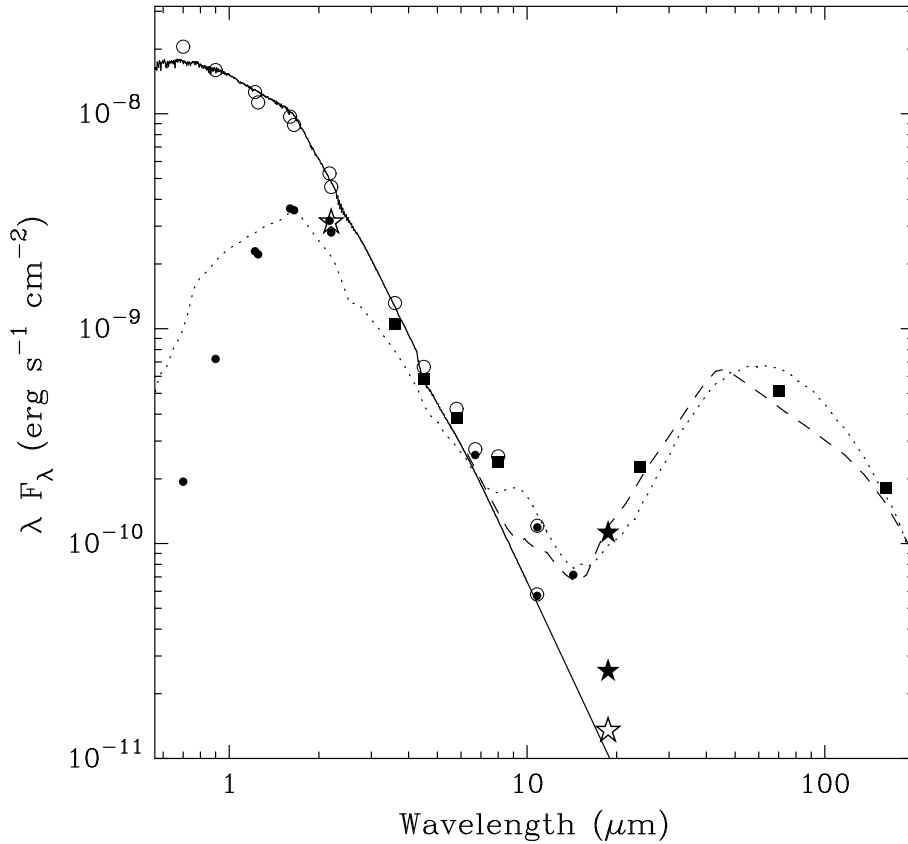
Figure 4.3: Spectral energy distribution of the star DoAr 21. Literature values are shown by filled circles. Open circles show dereddened values, assuming $A_V = 4.5$ mag. Filled squares are Spitzer measurements in apertures of $8''\!.4$ for the four IRAC bands, $17''\!.2$ for MIPS1, and $28''$ for MIPS2. The open stars are our measurements of the 2.20 μm and 18.72 μm of the stellar photosphere. The filled stars are our estimates of the flux at 18.72 μm from the star and the arc together (lower point) and the entire VISIR FOV (upper point). The solid line shows a Kurucz model for an effective temperature of 5000 K. The dashed line shows our four-component fit to the circumstellar material, and the dotted line the disk+envelope model (# 3015448) from the grid of calculations presented by Robitaille et al. (2006, 2007). Data points are taken from Lada & Wilking (1984); Bouvier & Appenzeller (1992); Barsony et al. (1997); Bontemps et al. (2001); Barsony et al. (2005) and the catalog of the 'Cores to Disks' Spitzer Legacy Survey (Evans et al. 2009).

4.1f) supports this model. A more accurate determination of the amounts of gas and dust traced by our observations would require a detailed modeling of the geometry, irradiation, and heating and cooling balance; this is beyond the scope of our analysis. Interferometric measurements at (sub) millimeter wavelengths are also essential for a proper assessment of the total amount of dust.

For a mass of $\sim 10^{-4}$ M$_\odot$ distributed over the area traced by the arc at 18.72 μm ($\sim$1.35$\times$10^4 AU^2), the dust is optically thin at 18.72 μm ($\tau \approx 1$) and moderately optically thick at 2.20 μm ($\tau \approx 2$–3). We can, therefore, be sure that we did not miss significant amounts of material due to opacity, and conclude that the circumstellar ma-

terial consists of at least 1×10^{-4} M$_\odot$ located in a $230°$ arc at 73–219 AU from DoAr 21, but may be as large as 3.7×10^{-2} M$_\odot$ with most mass at low temperatures ($\lesssim 30$ K) and undetected by our observations.

The temperature of the H$_2$ line emitting gas, and the excitation mechanism, can be constrained from the ratios of the detected lines, 1–0 S(1) and 1–0 S(0), and from the upper limit on the 2–1 S(1) line. We find 1–0 S(0) / 1–0 S(1)=0.28 ± 0.06 and 2–1 S(1) / 1-0 S(1)$\lesssim 0.2$. The various model results presented by Mouri (1994, their Fig. 3) indicate that these ratios are consistent with thermal excitation at a temperature of 1000–2000 K and strongly rule out ultraviolet fluorescence, for which a 2–1 S(1) / 1-0 S(1) ratio of ~ 0.55 is expected. This supports the assumptions made above and by Bary et al. (2002). Carmona et al. (2007) find similar conditions for the emission from LkHα 264, which favor a slightly lower temperature of ~ 1000 K.

Jensen et al. (2009) estimate that the FUV field of DoAr 21 is likely easily strong enough to excite the H$_2$ line through fluorescence. Our limit on the 2–1 S(1) line indicates that densities above $\sim 10^5$ cm^{-3} are present in the emitting gas that collisionally quench the fluorescently excited levels, leaving only the thermal emission from the 1–0 S(1) and 1–0 S(0) (cf. Sternberg & Dalgarno 1989). Such densities are expected for the estimated mass and size of the emitting volume: a mass of $\gtrsim 10^{-4}$ M$_\odot$ and a volume of (100 AU)^3 results in a density of $\gtrsim 10^7$ cm^{-3}.

4.4.2   Possible explanations for the observed arc of emission

This Section explores several scenarios for the observed asymmetric distribution of emission around DoAr 21. We start by stating that because the 18.72 μm emission is optically thin, we can rule out that the arc is a result from partial obscuration in a tilted ring, or even a PSF subtraction error. We therefore need to explain why the emitting material itself is distributed asymmetrically around the star, a distribution that is dynamically unstable. Our source is unique in the degree of asymmetry observed in the circumstellar material, with a contrast of a factor of > 6 between the region of maximum emission and the regions without detected emission. However, other sources with cleared-out inner disks (for example, HR4796A: Jayawardhana et al. 1998; Koerner et al. 1998; Telesco et al. 2000; AB Aur: Pantin et al. 2005; and LkHα 330: Brown et al. 2008) also show non-axisymmetric structure ('blobs').

Interaction of a disk with a passing star.

A close encounter with a passing star can disrupt a circumstellar disk. Because the observed arc is dynamically unstable, if orbiting DoAr 21, its lifetime is of the order of several orbital time scales, or roughly 10^4 yr. Again assuming a typical dispersion of stellar velocities of a few km s^{-1} we estimate that any such passing star must still lie with $\sim 1'$ from DoAr 21. Inspection of the Spitzer/IRAC images reveal a handful of point sources within this distance, but all are likely background sources. The closest young stellar object is located $1\rlap{.}'8$ south of DoAr 21, identified by the 'Cores to Disks' Spitzer Legacy survey with a typical sensitivity of 0.2 M$_\odot$ (cf. Merín et al. 2008). We

cannot exclude the passage of a substellar object, possibly as small as a few Jupiter masses; in the latter case, the distance of closest approach to the disk must have been very small, and we conclude that this scenario is unlikely.

Interaction with a substellar or planetary companion orbiting DoAr 21.

Planets or substellar companions can excite resonances in disk material (although these are usually symmetric, and not asymmetric as is the case here; Roques et al. 1994; Ozernoy et al. 2000; Kuchner & Holman 2003, e.g.), or the migration of a planet or companion to the 73–219 AU region could disrupt a previously stable outer disk. With the detection of giant planets at $\gtrsim 100$ AU distance from their star, such migration mechanisms are relevant (Kalas et al. 2008; Marois et al. 2008). No companion is visible in our data, to a limit of m_K=15 mag and 13 mag in the 250 and 25 mas fields, respectively, obtained after subtracting an azimuthally averaged image of the star from the images, leaving only non-axisymmetric residuals. Similarly, no object can be firmly detected in the 18.72 μm image, down to a flux limit of a few mJy. There is a tentative detection $\sim 1\rlap{.}''5$ south of the star, with a flux of 5.6 ± 0.8 mJy, but we estimate that this is too faint to constitute a firm detection[3]. Assuming an age of ~ 0.3 Myr for the system, we can limit the mass of any unseen companion to less than ~ 5 $M_{\rm Jupiter}$, using the tracks of Baraffe et al. (2003). However, an unseen body of a few $M_{\rm Jupiter}$ could still explain the observations.

Illumination of unrelated cloud material.

In this scenario, the emitting material belongs to the surrounding Ophiuchus cloud and is unrelated to the star. As mentioned before, JCMT/SCUBA and Spitzer/IRAC and MIPS images reveal extended emission within a few arcmin from DoAr 21. Clearly, significant cloud material is located (in projection) near DoAr 21. For a typical velocity dispersion of young stars in star-forming regions of a few km s^{-1} (Herbig 1977; Jones & Herbig 1979; Hartmann et al. 1986; Dubath et al. 1996), DoAr 21[4] traverses large distances (~ 1 pc) over its age of ~ 0.3 Myr. If it is currently moving through a denser region of the Ophiuchus cloud, its stellar radiation will heat up the dust and the star's X-rays will heat a gas layer at the surface to > 1000 K and excite the observed H_2 rovibrational emission. The arc-like appearances of the 18.72 μm and H_2 line emission are explained in this scenario by the combined results of the fact that only within ~ 100 AU from the star can dust and gas be sufficiently heated, and the shape of any material swept up by the stellar motion. Density variations in the surrounding material can explain the somewhat irregular shape of the arc. This scenario is somewhat similar to that proposed by Gáspár et al. (2008) for the infrared excess of the star δ Velorum.

---

[3]The 18 μm imaging by Jensen et al. (2009) does not show this source, and it is likely spurious.

[4]Jensen et al. (2009) quote a relative motion of DoAr 21 with respect to the surrounding gas of 9.5 ± 1.3 km s^{-1} to the west.

Capture of a cloud condensation and a brown-dwarf disk.

In a variation on the previous scenario, a sufficiently close passage of DoAr 21 to a small cloud condensation or a brown dwarf with a surrounding disk, may result in gravitational capture by the star (i.e., a passage at a velocity smaller than the escape velocity at the impact parameter, e.g., ~ 3 km s^{-1} at 100 AU). At the smallest and largest radius of the arc, 73 and 219 AU, the orbital time scales around a 2.2 M$_\odot$ star are 400 and 2300 yr, respectively. A spherical distribution of gas with a diameter of 146 AU ($=219 - 73$ AU) in an orbit around DoAr 21 would shear to an arc of $230°$ in approximately 330 yr. The likelihood of the close, low-velocity encounter between DoAr 21 and this putative cloud condensation is difficult to estimate.

Other explanations.

Finally we note that the distribution of the material may be caused by a collision between a Jupiter-mass (proto)planet and an other planetary object such as a 10 km sized asteroid as described by Grigorieva et al. (2007), resulting in a spray of material slowly spreading over several orbits. The distribution may also be the result of a global gravitational instability of a disk which has undergone progressive stages of disk clearing, dust coagulation, and gas loss (e.g., Klahr & Lin 2001, 2005). However, we regard both scenarios as speculative at this stage.

Future observations.

To decide which of these scenarios is correct follow-up observations of DoAr 21 are required in the H$_2$ line, at 18.72 μm, and/or at millimeter wavelengths. Our SED modeling suggests a flux of $\lesssim 1$ mJy at 1 mm, sufficient for high signal-to-noise imaging with ALMA at $< 1''$ resolution. If the material orbits around DoAr 21, in 10 year the arc is expected to rotate by $8°$ (80 mas) at its smallest radius of 73 AU and $1.6°$ (50 mas) at its largest radius of 219 AU. If DoAr 21 is travelling through the cloud, a proper motion of DoAr 21 of a few km s^{-1} corresponds to a positional shift of 10 AU or 100 mas in 10 yr. Either motion can be detected. In this context we recall that the mid-infrared flux of DoAr 21 appears to vary (Sect. 4.4.1; Barsony et al. 2005), which suggests that the position of DoAr 21 with respect to the emitting material may have changed or that the spatial distribution of the material has changed. We estimate that the reported flux variations could reflect a relative motion of DoAr 21 with respect to the illuminated material by ~ 5 AU; accurately calibrated follow-up observations are required to confirm this. However, as noted in Sect. 4.4.1, stellar flares as traced through the X-rays may also explain this mid-infrared variation.

4.5   CONCLUSIONS

We present spatially resolved observations of the 0.3–1.0 Myr old weak-line T Tauri star DoAr 21 at 2.20 μm and at 18.72 μm. The 2.20 μm AO-assisted IFU observations allow accurate continuum subtraction and subsequent imaging of the H$_2$ 1–0 S(1) line, while

the 18.72 μm diffraction limited imaging reveals the location of warm (50–100 K) dust. We detect the stellar photosphere at both wavelengths, and find an arc of emission in the H_2 line and in 18.72 μm emission located between 73 and 219 AU from the star and stretching over 230° along the northwest side of the star. We calculate that the circumstellar material contains $\gtrsim 1 \times 10^{-4}$ $M_\odot$. We conclude that the distribution of the extended emission reflects the true distribution of the emitting material and is not due to a radiative transfer / geometric effect. Since an asymmetric distribution of material at these radii cannot persist for more than a few orbital times scales ($\sim 10^4$ yr; in the absence of resonant motion with an unseen companion which we rule out to a mass limit of 5 $M_{Jupiter}$), we conclude that the observed distribution is the result of a recent event. We discuss the possibility of a recent stellar fly-by (unlikely because of the absence of a likely candidate) or internal instability which disrupted a (cleared-out) disk around DoAr 21. Other 'transitional' disks also show non-axisymmetric, 'blobby' structures, albeit at much lower contrast than seen toward DoAr 21 (Brown et al. 2008). An alternative explanation for the observed structure around DoAr 21 is, that the star is illuminating, and partially sweeping up unrelated material from the Ophiuchus cloud. Future epoch observations are required to rule out any of these scenarios.

Our observations show that not all young stars with 'transitional' SEDs are surrounded by disks with cleared-out inner regions. Spatially resolved observations are essential to firmly determine the nature of the circumstellar material. Deep mid-infrared imaging and aperture synthesis observations at (sub)millimeter wavelengths with, e.g., ALMA provide good tools to locate the warm and cold dust, respectively.

Conversely, our observations may provide a clue as to why objects with 'transitional' SEDs are overrepresented in the list of stars with detected quiescent ro-vibrational H_2 emission (Bary et al. 2008). First, excitation of these lines requires the presence of hot gas (> 1000 K), likely heated by stellar X-rays. These same X-rays may cause the inner disk regions to photoevaporate on a short timescale (e.g., Gorti & Hollenbach 2009). Second, and perhaps most important, once the region immediately around the star has been cleared of gas, the surface illuminated by the X-rays increases (provided there is dense material at these larger radii). As long as the X-ray luminosity is sufficiently high to heat this larger surface to > 1000 K, a larger H_2 line emitting area results, and therefore a higher line flux. At the same time, the dust in these regions will also be heated by the stellar radiation, generating the mid-infrared excess. In contrast, objects with a strong near-infrared excess have large amounts of gas and dust near the star, sufficient to block X-rays from penetrating to larger distances. In this picture, detectable quiescent ro-vibrational H_2 emission will arise when the distribution of circumstellar material allows the stellar X-rays to illuminate a sufficiently large area on the sky. In these cases, AO-assisted IFU observations of the H_2 in the K-band uniquely offer the possibility for high spatial-resolution imaging of the (illuminated) molecular gas.

REFERENCES

Alexander, R. D., Clarke, C. J., & Pringle, J. E. 2006, MNRAS, 369, 216

André, P., & Montmerle, T. 1994, ApJ, 420, 837

Andrews, S. M., & Williams, J. P. 2005, ApJ, 631, 1134

Andrews, S. M., & Williams, J. P. 2007, ApJ, 659, 705

Andrews, S. M., & Williams, J. P. 2007, ApJ, 671, 1800

Baraffe, I., Chabrier, G., Barman, T. S., Allard, F., & Hauschildt, P. H. 2003, A&A, 402, 701

Barsony, M., Kenyon, S. J., Lada, E. A., & Teuben, P. J. 1997, ApJS, 112, 109

Barsony, M., Ressler, M. E., & Marsh, K. A. 2005, ApJ, 630, 381

Bary, J. S., Weintraub, D. A., & Kastner, J. H. 2002, ApJ, 576, L73

Bary, J. S., Weintraub, D. A., & Kastner, J. H. 2003, ApJ, 586, 1136

Bary, J. S., Weintraub, D. A., Shukla, S. J., Leisenring, J. M., & Kastner, J. H. 2008, ApJ, 678, 1088

Beck, T. L., McGregor, P. J., Takami, M., & Pyo, T.-S. 2008, ApJ, 676, 472

Bitner, M. A., et al. 2008, ApJ, 688, 1326

Black, J. H., & van Dishoeck, E. F. 1987, ApJ, 322, 412

Bontemps, S., et al. 2001, A&A, 372, 173

Bouvier, J., & Appenzeller, I. 1992, A&AS, 92, 481

Brown, J. M., et al. 2007, ApJ, 664, L107

Brown, J. M., Blake, G. A., Qi, C., Dullemond, C. P., & Wilner, D. J. 2008, ApJ, 675, L109

Carmona, A., van den Ancker, M. E., Henning, T., Goto, M., Fedele, D., & Stecklum, B. 2007, A&A, 476, 853

Casanova, S., Montmerle, T., Feigelson, E. D., & Andre, P. 1995, ApJ, 439, 752

Chiang, E. I., & Goldreich, P. 1997, ApJ, 490, 368

Cieza, L., et al. 2007, ApJ, 667, 308

Clarke, C.J., Gendrin, A. & Sotomayor, M. 2001, MNRAS, 328, 485

D'Alessio, P., et al. 2005, ApJ, 621, 461

D'Alessio, P. 2009, Revista Mexicana de Astronomia y Astrofisica Conference Series, 35, 33

D'Antona, F., & Mazzitelli, I. 1996, ApJ, 456, 329

Di Francesco, J., Johnstone, D., Kirk, H., MacKenzie, T., & Ledwosinska, E. 2008, ApJS, 175, 277

Dolidze, M. V., & Arakelyan, M. A. 1959, AZh, 36, 444

Draine, B. T., & Bertoldi, F. 1996, ApJ, 468, 269

Dubath, P., Reipurth, B., & Mayor, M. 1996, A&A, 308, 107

Dullemond, C. P., Dominik, C., & Natta, A. 2001, ApJ, 560, 957

Evans, N. J., et al. 2009, ApJS, 181, 321

Feigelson, E. D., & Montmerle, T. 1985, ApJ, 289, L19

Forrest, W. J., et al. 2004, ApJS, 154, 443

Gagné, M., Skinner, S. L., & Daniel, K. J. 2004, ApJ, 613, 393

Gáspár, A., Su, K. Y. L., Rieke, G. H., Balog, Z., Kamp, I., Martínez-Galarza, J. R., & Stapelfeldt, K. 2008, ApJ, 672, 974

Geers, V. C., Pontoppidan, K. M., van Dishoeck, E. F., Dullemond, C. P., Augereau, J.-C., Merín, B., Oliveira, I., & Pel, J. W. 2007, A&A, 469, L35

Glassgold, A. E., Najita, J., & Igea, J. 1997, ApJ, 480, 344

Glassgold, A. E., Najita, J., & Igea, J. 2004, ApJ, 615, 972

Goto, M., Usuda, T., Dullemond, C. P., Henning, T., Linz, H., Stecklum, B., & Suto, H. 2006, ApJ, 652, 758

Gorti, U., & Hollenbach, D. 2008, ApJ, 683, 287

Gorti, U., & Hollenbach, D. 2009, ApJ, 690, 1539

Grady, C. A., et al. 2000, ApJ, 544, 895

Gredel, R., & Dalgarno, A. 1995, ApJ, 446, 852

Grigorieva, A., Artymowicz, P., & Thébault, P. 2007, A&A, 461, 537

Grosso, N., Montmerle, T., Bontemps, S., André, P., & Feigelson, E. D. 2000, A&A, 359, 113

Guilloteau, S., & Dutrey, A. 1998, A&A, 339, 467

Hanner, M. S., Brooke, T. Y., & Tokunaga, A. T. 1995, ApJ, 438, 250

Hartmann, L., Hewett, R., Stahler, S., & Mathieu, R. D. 1986, ApJ, 309, 275

Herbig, G. H. 1977, ApJ, 214, 747

Hillenbrand, L. A. 2008, Physica Scripta Volume T, 130, 014024

Hughes, A. M., Wilner, D. J., Calvet, N., D'Alessio, P., Claussen, M. J., & Hogerheijde, M. R. 2007, ApJ, 664, 536

Hughes, A. M., Wilner, D. J., Kamp, I., & Hogerheijde, M. R. 2008, ApJ, 681, 626

Hughes, A. M., et al. 2009, ApJ, 698, 131

Igea, J., & Glassgold, A. E. 1999, ApJ, 518, 848

Imanishi, K., Tsujimoto, M., & Koyama, K. 2002, ApJ, 572, 300

Ireland, M. J., & Kraus, A. L. 2008, ApJ, 678, L59

Isella, A., Carpenter, J. M., & Sargent, A. I. 2009, arXiv:0906.2227

Itoh, Y., Sugitani, K., Ogura, K., & Tamura, M. 2003, PASJ, 55, L77

Jayawardhana, R., Fisher, S., Hartmann, L., Telesco, C., Pina, R., & Fazio, G. 1998, ApJ, 503, L79

Jensen, E. L. N., Cohen, D. H., Swisher, V., & Gagné, M. 2005, Bulletin of the American Astronomical Society, 37, 1223

Jensen, E. L. N., Cohen, D. H., & Gagné, M. 2009, arXiv:0907.4980

Jones, B. F., & Herbig, G. H. 1979, AJ, 84, 1872

Kalas, P., et al. 2008, Science, 322, 1345

Klahr, H. H., & Lin, D. N. C. 2001, ApJ, 554, 1095

Klahr, H., & Lin, D. N. C. 2005, ApJ, 632, 1113

Koerner, D. W., Ressler, M. E., Werner, M. W., & Backman, D. E. 1998, ApJ, 503, L83

Koyama, K., Maeda, Y., Ozaki, M., Ueno, S., Kamata, Y., Tawara, Y., Skinner, S., & Yamauchi, S. 1994, PASJ, 46, L125

Kuchner, M. J., & Holman, M. J. 2003, ApJ, 588, 1110

Lada, C. J., & Wilking, B. A. 1984, ApJ, 287, 610

Lahuis, F., van Dishoeck, E. F., Blake, G. A., Evans, N. J., II, Kessler-Silacci, J. E., & Pontoppidan, K. M. 2007, ApJ, 665, 492

Lin, D. N. C., & Papaloizou, J. C. B. 1993, Protostars and Planets III, 749

Loinard, L., Torres, R. M., Mioduszewski, A. J., & Rodríguez, L. F. 2008, ApJ, 675, L29

Loren, R. B., & Wootten, A. 1986, ApJ, 306, 142

Luhman, K. L., & Rieke, G. H. 1999, ApJ, 525, 440

Maloney, P. R., Hollenbach, D. J., & Tielens, A. G. G. M. 1996, ApJ, 466, 561

Martin-Zaïdi, C., Lagage, P.-O., Pantin, E., & Habart, E. 2007, ApJ, 666, L117

Martin-Zaïdi, C., van Dishoeck, E. F., Augereau, J.-C., Lagage, P.-O., & Pantin, E. 2008, A&A, 489, 601

Martin-Zaïdi, C., Habart, E., Augereau, J.-C., Ménard, F., Lagage, P.-. O., Pantin, E., & Olofsson, J. 2009, ApJ, 695, 1302

Marois, C., Macintosh, B., Barman, T., Zuckerman, B., Song, I., Patience, J., Lafrenière, D., & Doyon, R. 2008, Science, 322, 1348

Massi, M., Forbrich, J., Menten, K. M., Torricelli-Ciamponi, G., Neidhöfer, J., Leurini, S., & Bertoldi, F. 2006, A&A, 453, 959

Massi, M., et al. 2008, A&A, 480, 489

Matsuyama, I., Johnstone, D. & Hartmann, L. 2003, ApJ, 582, 893

Merín, B., et al. 2008, ApJS, 177, 551

Meyer, M. R. 2009, IAU Symposium, 258, 111

Motte, F., Andre, P., & Neri, R. 1998, A&A, 336, 150

Mouri, H. 1994, ApJ, 427, 777

Nomura, H., Aikawa, Y., Tsujimoto, M., Nakagawa, Y., & Millar, T. J. 2007, ApJ, 661, 334

Ossenkopf, V., & Henning, T. 1994, A&A, 291, 943

Ozernoy, L. M., Gorkavyi, N. N., Mather, J. C., & Taidakova, T. A. 2000, ApJ, 537, L147

Padgett, D. L., et al. 2008, ApJ, 672, 1013

Pantin, E., Bouwman, J., & Lagage, P. O. 2005, A&A, 437, 525

Piétu, V., Dutrey, A., & Guilloteau, S. 2007, A&A, 467, 163

Pinte, C., et al. 2008, A&A, 489, 633

Pontoppidan, K. M., Blake, G. A., van Dishoeck, E. F., Smette, A., Ireland, M. J., & Brown, J. 2008, ApJ, 684, 1323

Qi, C., et al. 2004, ApJ, 616, L11

Qi, C., Wilner, D. J., Calvet, N., Bourke, T. L., Blake, G. A., Hogerheijde, M. R., Ho, P. T. P., & Bergin, E. 2006, ApJ, 636, L157

Qi, C., Wilner, D. J., Aikawa, Y., Blake, G. A., & Hogerheijde, M. R. 2008, ApJ, 681, 1396

Ramsay Howat, S. K., & Greaves, J. S. 2007, MNRAS, 379, 1658

Richter, M. J., Jaffe, D. T., Blake, G. A., & Lacy, J. H. 2002, ApJ, 572, L161

Roberge, A., Weinberger, A. J., & Malumuth, E. M. 2005, ApJ, 622, 1171

Robitaille, T. P., Whitney, B. A., Indebetouw, R., Wood, K., & Denzmore, P. 2006, ApJS, 167, 256

Robitaille, T. P., Whitney, B. A., Indebetouw, R., & Wood, K. 2007, ApJS, 169, 328

Roques, F., Scholl, H., Sicardy, B., & Smith, B. A. 1994, Icarus, 108, 37

Salter, D. M., Hogerheijde, M. R., & Blake, G. A. 2008, A&A, 492, L21

Salyk, C., Blake, G. A., Boogert, A. C. A., & Brown, J. M. 2009, ApJ, 699, 330

Schneider, G., Wood, K., Silverstone, M. D., Hines, D. C., Koerner, D. W., Whitney, B. A., Bjorkman, J. E., & Lowrance, P. J. 2003, AJ, 125, 1467

Siess, L., Dufour, E., & Forestini, M. 2000, A&A, 358, 593

Simon, M., Dutrey, A., & Guilloteau, S. 2000, ApJ, 545, 1034

Shu, F.H., Johnstone, D. & Hollenbach, D. 1993, Icarus, 106, 92

Sternberg, A., & Dalgarno, A. 1989, ApJ, 338, 197

Stine, P. C., Feigelson, E. D., Andre, P., & Montmerle, T. 1988, AJ, 96, 1394

Telesco, C. M., et al. 2000, ApJ, 530, 329

Tin e, S., Lepp, S., Gredel, R., & Dalgarno, A. 1997, ApJ, 481, 282

Thi, W. F., et al. 2001, ApJ, 561, 1074

Thi, W. F., et al. 2001, Nature, 409, 60

van Langevelde, H. J., van Dishoeck, E. F., van der Werf, P. P., & Blake, G. A. 1994, A&A, 287, L25

Weintraub, D. A., Kastner, J. H., & Bary, J. S. 2000, ApJ, 541, 767

CHAPTER 5

Characterising discs around Herbig Ae/Be stars through modelling of low-J ^{12}CO lines

O. Panić and M. R. Hogerheijde

W HILE there has been extensive investigation of the dust emission in discs around young intermediate-mass or Herbig Ae/Be stars at a range of wavelengths, their gas content has been systematically studied mainly via spatially unresolved (sub)millimetre observations of the rotational lines of ^{12}CO. We are interested in how the available low-J ^{12}CO spectra compare to the disc properties inferred from the dust emission, and to what extent the gas- and dust-emission approaches to disc modelling are complementary to each other. First, we use the disc structure derived from the spectral energy distribution (SED) modelling to produce the synthetic ^{12}CO J=3–2 spectra for a discrete sample of sources. We then compare these synthetic spectra to observations, to test the existing disc models for each source. In our second approach, we study the dependence of the ^{12}CO J=3–2 spectrum on disc size, inclination and temperature, for discs around Herbig Ae/Be stars in general. We calculate the spectral line profiles for a grid of parametric disc models. The calculated spectra are compared to the spectra observed towards a large sample of sources. Both methods use a molecular excitation and radiative transfer code for the calculation of the ^{12}CO line emission. SED models are insensitive to the parameters that dominate the low-J ^{12}CO emission, i.e., the disc size and orientation. To minimise some of the important parameter degeneracies, it is necessary to model a disc's SED with prior knowledge of the disc size and inclination. We show how the spectral profile of low-J ^{12}CO lines can be used to constrain these parameters, and to obtain disc models that are good starting points for the *outside-in* SED modelling of discs from long to shorter wavelengths. For a disc gas mass of the order of 0.01 M$_{\odot}$, the optically thick J=3–2 ^{12}CO line intensity shows that the majority of discs around Herbig Ae/Be stars are smaller than 200 AU, and that the largest and brightest sources thoroughly studied with submillimetre

interferometry are not representative of the sample.

5.1   INTRODUCTION

The physical processes that shape circumstellar discs during their evolution ultimately determine the amount of material available for, and the timescale of the planet formation. The dust grain growth and settling to the disc midplane are probed by mid-infrared spectroscopy (Bouwman et al. 2001; van Boekel et al. 2003) and the spectral energy distribution (SED) from the near-infrared to millimetre wavelengths (Dullemond & Dominik 2004, 2005). Disc modelling based on both SED and the mid-infrared spectrum has thus developed, and this approach has been combined with near-infrared and millimetre imaging and/or interferometry (Pinte et al. 2008; Tannirkulam et al. 2008). However, the dust presents only a small percentage of the disc mass contained in molecular gas. Furthermore, the SED only probes the inner disc regions, up to about 100 AU and are insensitive to the entire extent of the disc as already noted in the early work of Adams et al. (1988). Accretion, photoevaporation and photodissociation disperse the gas reservoir, and limit the timescale for gaseous planets to form. Due to these mechanisms, the mass ratio between the gas and the dust is expected to decrease with time, as the disc structure dominated by the gas pressure gradients and rotation becomes flatter and gas and dust decoupled. The bulk of the disc gas is best traced via submillimeter emission lines of abundant molecular species like ^{12}CO and its isotopologues (^{13}CO, C^{17}O, C^{18}O) (Guilloteau & Dutrey 1994; Mannings & Sargent 1997; Thi et al. 2001; Dent et al. 2005). However, the main problem in determining the gas mass is the uncertainty in the gas phase abundance of ^{12}CO, as this molecule is efficiently frozen onto dust grains at the low temperatures. Temperatures lower than 20 K are common in the dense midplane of discs around pre-main-sequence stars of spectral type M and K, and stellar mass <1 M$_\odot$ (T Tauri stars). The intermediate-mass pre-main-sequence stars, referred to as Herbig Ae/Be stars, are surrounded by discs of gas and dust observationally similar to those around T Tauri stars (Mannings & Sargent 1997, 2000; Natta et al. 2000). Due to the spectral type F to B of their central stars, these discs are warmer and provide an opportunity to overcome the uncertainty in the CO gas phase abundance, rendering CO a more reliable tracer of the entire disc. Motivated by our estimate of the gas-to-dust mass ratio in a 200 AU disc around an A type star HD 169142 unaffected by freeze-out (Chapter 2 of this thesis), we further explore the known gas-rich discs around Herbig Ae/Be stars. We aim to identify other sufficiently small and warm discs 'immune' to CO freeze-out, and establish whether these are statistically representative of the sample of known gas-rich discs around Herbig Ae/Be stars.

Our comparative study of the gas and dust content of discs focuses on a sample of nine Herbig Ae/Be stars, listed in Table 5.1, towards which the ^{12}CO J=3–2 line is firmly detected and associated with a circumstellar disc (Dent et al. 2005; Thi et al. 2001, 2004). The sources range from those with relatively weak ^{12}CO J=3–2 line emission, to some of the brightest and known sources like HD 163296 and AB Aur (Isella et al. 2007; Piétu et al. 2005; Schreyer et al. 2008). The spectral type spans from late F to late

B. Our choice of these sources was guided by the availability of SED models of the
disc physical stucture from Dominik et al. (2003). In our study of the ^{12}CO J=3–2 line
emission from discs around Herbig Ae/Be stars in general, we use our observations
of HD 100546 and the data for 21 sources from Dent et al. (2005) in which this line
was detected ($>2\sigma$). Dent et al. (2005) carried out the largest search for gas in discs
around young Herbig Ae/Be stars so far. Their full target list of 59 young stars includes
the Malfait et al. (1998) sample of isolated Herbig Ae/Be stars with IR excess due to
circumstellar dust. The 21 sources we use here are a subset biased towards the sources
with stronger ^{12}CO emission. Any discs with low amounts of gas that may have been
missed in this way do not affect the conclusions of our study.

We investigate the physical disc properties, primarily the size and temperature,
that can be constrained by the ^{12}CO low-J spectral line profiles, as well as the disc in-
clination, as an important parameter in disc modelling. Single dish observations of the
^{12}CO J=3–2 line from the literature are complemented with our JCMT ^{12}CO J=2–1 line
observations presented in Sect. 7.2. The ^{12}CO J=3–2 observations are used in Sect. 5.3
to test the structure proposed by the existing SED-based disc models for nine Herbig
Ae/Be stars. A molecular excitation and radiative transfer code was used to calculate
the emission from the disc model structure, which is then compared to the observa-
tions. We find that the SED modelling without a prior knowledge of disc size and
inclination tends to produce models that are incompatible with the observed submil-
limetre line emission, often underestimating the disc size. In Sect. 5.4 we calculate the
^{12}CO J=3–2 emission using a grid of simple parametric disc models, with disc size and
inclination as free parameters. We find that our model results predict the observed
spread in integrated intensity and line-width, as well as the lack of strong and wide
lines in a larger sample of Herbig Ae/Be discs. Although the number of known discs
with weak low-J ^{12}CO lines is limited by sensitivity the of the instruments, the small
discs ($<$200 AU) are clearly more frequent than the large ones. We discuss the implica-
tions of our parametric models for the particular sources in our sample, and find that
the results of our simple models compare well to the size and inclination measured
by the interferometric submillimeter, near-infrared and/or mid-infrared observations
already available for some of these sources. Section 5.5 summarises our results and
conclusions and outlines the future prospects.

5.2   OBSERVATIONS AND RESULTS

We observed the ^{12}CO J=2–1 line toward the sources HD 135344, HD 179218, HD
142666, HD 139614 and V892 Tau using the James Clerk Maxwell Telescope (JCMT)
and the ^{12}CO J=3–2 line toward HD 100546 using the Atacama Pathfinder Experiment
(APEX) telescope.

The observations of the ^{12}CO J=2–1 line, at the rest frequency of 230.538 GHz, were
carried out using the heterodyne receiver RxA3 on the JCMT. The JCMT beam size at
230 GHz is 21″ and beam efficiency 0.9. The integration times were approximately 20-
30 minutes on-source. The data were obtained in 2008 September under good weather
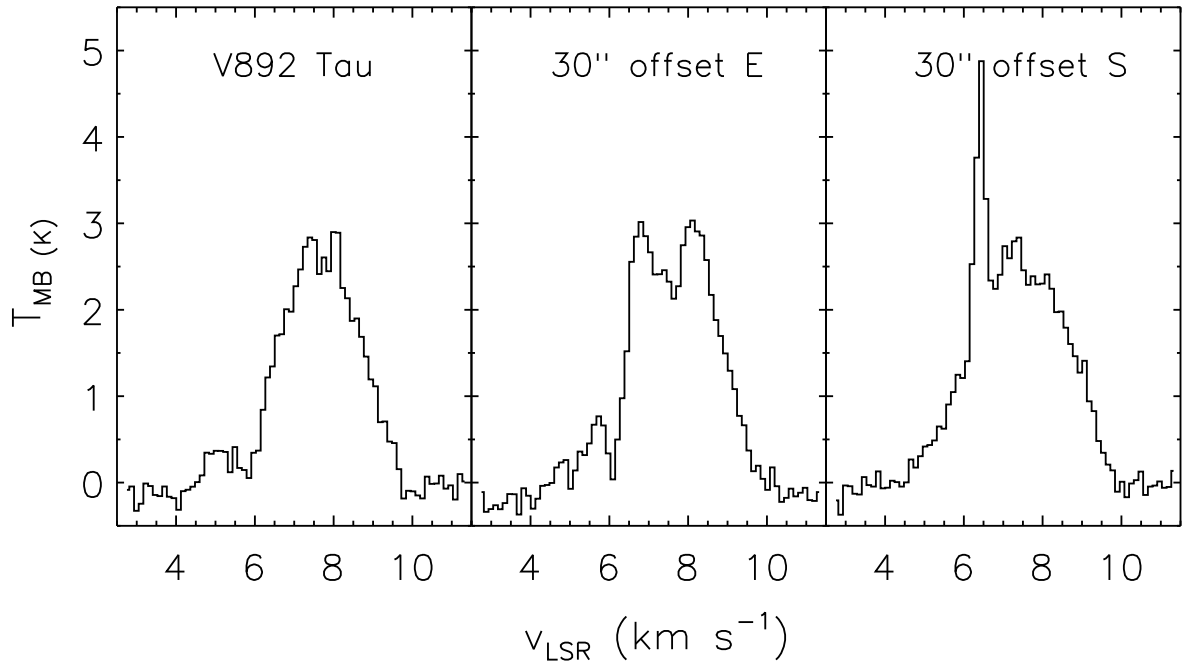conditions, with the atmospheric opacity τ_{230GHz} $\approx$0.2. Figure 5.2 shows the JCMT ob-

Figure 5.1: Spectrum of the ^{12}CO J=2–1 line observed towards V892 Tau and the two offset positions.

servations towards the remaining four sources. The rms level of the ^{12}CO J=2–1 line spectra is 50-70 mK for V892 Tau and HD 142666, 90-100 mK for HD 135344, HD 139614 and HD 179218 in 31 kHz channels (0.027 km s^{-1}). All sources, except V892 Tau, have been previously identified as isolated stars with no proximity to extended cloud material. We took two 30″ offset measurements, one to the East and the other to the South of V892 Tau and find that the line is dominated by extended cloud emission (See also Thi 2002). Figure 5.1 shows the spectra taken in the direction of the source and the offset positions. As a follow-up, the environment of V892 Tau is studied using HARP mapping towards V892 Tau (see Appendix for details).

The observations of the ^{12}CO J=3–2 line at 345.796 GHz towards HD 100546 were carried out using APEX on 2005 July 27, with the integration time of 15 minutes and the atmospheric opacity $\tau_{230\,\mathrm{GHz}}$=0.2. The rms level obtained is 120 mK in 61 kHz channels (0.053 km s^{-1}). The APEX beam efficiency at 345 GHz is 0.73.

In this paper, we extensively use the ^{12}CO J=3–2 observations taken previously with the JCMT, and presented in Dent et al. (2005).

5.2.1　Gas and dust submillimetre emision towards the source sample

Table 5.1 lists our sources and their interferometric 1.3 mm fluxes from the literature. Considering the fact that the distance to the sources ranges from 84 pc for HD 135344 to 240 pc for HD 179218, the continuum measurements do not differ greatly from one source to another. Using the continuum fluxes we obtain dust mass estimates for the
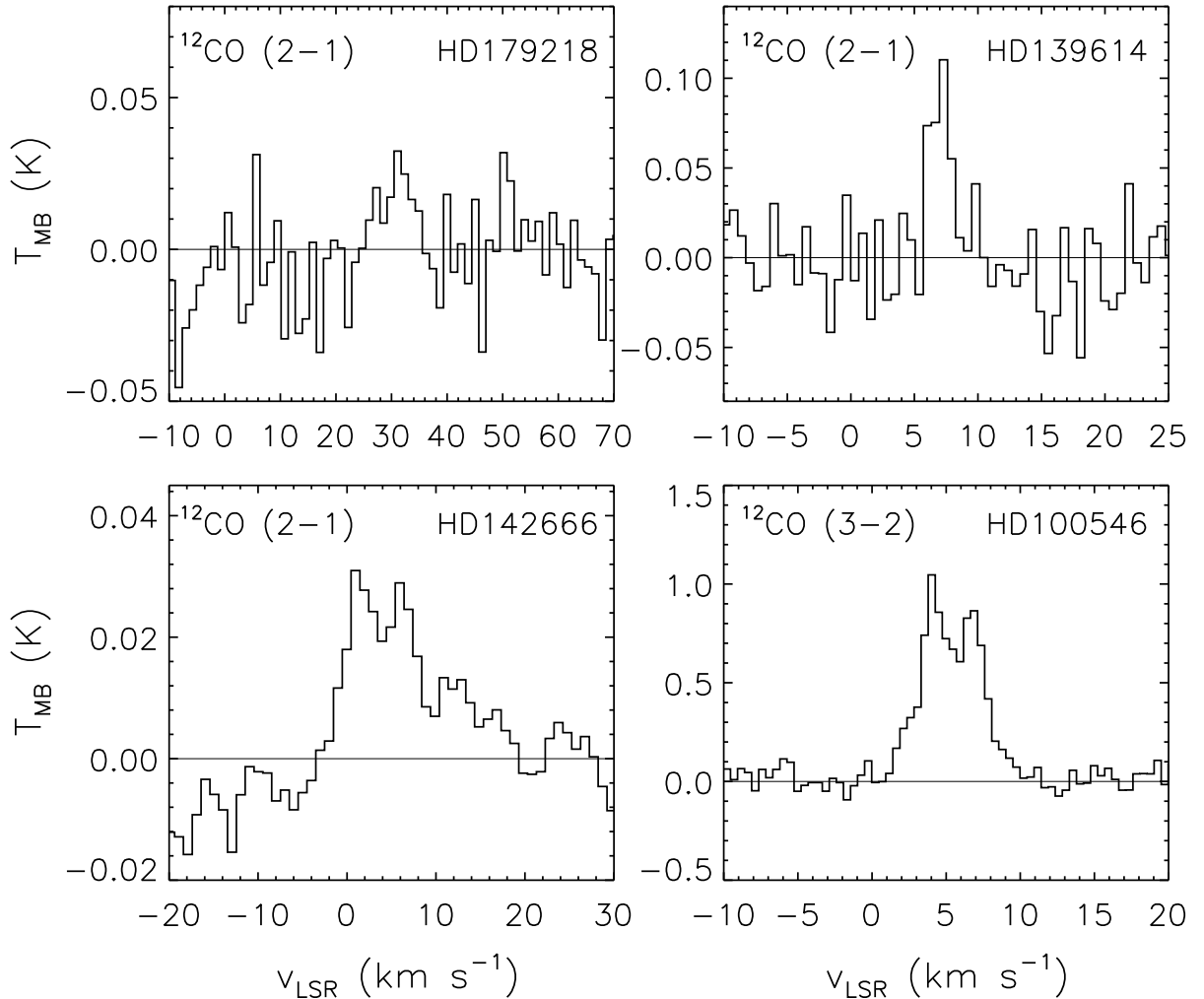
Figure 5.2: Spectra of ^{12}CO J=2–1 line observed towards HD 179218, HD 139614, and
HD 142666 and ^{12}CO J=3–2 line observed towards HD 100546.

discs in our sample, valid under assumption that the 1.3 mm emission is optically thin.
To calculate the disc masses we assume the temperature of the discs to be in the range
30-40 K, as in the disc midplane for Herbig AeBe stars in the irradiated accretion disc
models of D'Alessio et al. (2005) at 100-200 AU from the star. While the assumption of a
single temperature introduces an error of 20-50% in our dust mass estimates, they are
dominated by the highly uncertain dust millimetre emissivity in circumstellar discs.
We adopt the dust emissivity at 1.3 mm of 2 cm^{2}g^{-1} (emissivity is expressed per gram
of dust throughout the paper). The emissivity we adopt is at the high end of the range
suggested by Draine (2006) and can be as low as 0.1 cm^{2}g^{-1}, depending on the dust
size and composition. Thus the estimates we provide can be considered as rough lower
limits on dust mass.

The resulting dust masses are in the range of 0.4-6.9$\times10^{-4}$ M$_\odot$, as listed in Ta-
ble 5.1. Adopting a gas-to-dust mass ratio $f_{g/d}$ =100 this translates to total disc masses

$M_{disc}=M_{dust}\, f_{g/d}$ of roughly 10^{-3}-10^{-1} $M_{\odot}$, similar to the results of Beckwith et al. (1990) for discs around T Tauri stars.

The integrated intensities of the ^{12}CO lines we observed are shown in boldface in Table 7.1 alongside the values taken from the literature (Dent et al. 2005; Raman et al. 2006; Isella et al. 2007; Piétu et al. 2005) and from Chapter 2 of this thesis. We detect the ^{12}CO J=2–1 line from HD 142666, HD 139614, and V892 Tau, and the ^{12}CO J=3–2 line from HD 100546, but obtain only upper limits from ^{12}CO J=2–1 observations of HD 179218. Our observations towards HD 135344 are excluded from the analysis due to errors in data acquisition. The ^{12}CO J=3–2 integrated line intensities range from several to tenths of K km s^{-1} as seen in Table 7.1 (except for HD 100546, values are taken from Dent et al. 2005). The strong sources HD 100546 and HD 163296 are also at the high end of estimated disc masses, while the weak sources HD 135344 and HD 142666 correspond to discs with masses close to 1×10^{-2} $M_{\odot}$. The disc around AB Aur, in spite of the modest mass estimated from the dust continuum shows the strongest ^{12}CO J=3–2 line of 13.67 K km s^{-1} (calculated from Thi et al. (2001)). Some of this emission is arising from the surrounding envelope (Nakajima & Golimowski 1995; Thi et al. 2001; Schreyer et al. 2008; Semenov et al. 2005).

For the J=3–2 and J=2–1 lines arising from the range of temperatures and densities typically found in discs we expect similar intrinsic intensities (calculations done using RADEX online tool van der Tak et al. 2007). The ratio between the ^{12}CO J=3–2 and J=2–1 integrated line intensities as observed with the JCMT is expected to be close to two. This ratio is dominated by the beam dilution, which scales with the square of the beam size. The observed integrated intensities of both lines are listed in Table 7.1, and their ratio shows that five of the sources are consistent with the expected ratio of two. One of the exceptions is V892 Tau, which shows excess ^{12}CO J=2–1 line flux. This is due to the surrounding cloud material heavily contributing to the ^{12}CO line emission in spatially unresolved single dish observations. The strong ambient emission around V892 Tau is confirmed in observations of the offset positions and mapping of the region with HARP (see Appendix for details). For this reason we exclude V892 Tau from the further analysis. The source HD 179218 has an upper limit on the ^{12}CO J=2-1 line flux several times lower than the fluxes expected based on the J=3–2 line flux. This results in large line ratio of 6, indicating that the ^{12}CO J=3–2 emission toward this source is likely dominated by optically thin molecular gas at a higher temperature regime than found in discs (several hundreds of Kelvin).

5.3   COMPARISON TO THE SED-BASED DISC MODELS

The SEDs of our sources were fitted by Dominik et al. (2003) using a disc structure based on the flaring passive disc model of Chiang & Goldreich (1997). Modifications to the original Chiang & Goldreich (1997) models and the detailed disc parameters used in the fit can be found in Dominik et al. (2003) (see their Table 3) while our Table 7.2 lists the model parameters of direct relevance for the ^{12}CO lines. The disc masses span from 0.01 to 0.1 $M_{\odot}$ and outer radii from 10 AU to 800 AU.

With the help of the molecular excitation and radiative transfer code RATRAN

Table 5.1: Stellar properties[a] and the derived dust mass of the discs.

#	Source	Distance (pc)	Spectral type	Luminosity ($L_\odot$)	M_{star} ($M_\odot$)	$F_{1.3\ mm}$[c] (mJy)	T_{avg} (K)	M_{dust} ($10^{-4}\ M_\odot$)
(1)	HD 100546	103	B9	36	2.5	470	30-40	2.1-2.9
(2)	HD 179218	240	B9	80	2.7	71	30-40	1.7-2.4
(3)	V892 Tau[b]	–	B8 V	400	5.5	230	–	–
(4)	AB Aur	144	A0	47	2.5	100	30-40	0.9-1.2
(5)	HD 163296	122	A1-A3	30	2.4	780	30-40	4.9-6.9
(6)	HD 169142	145	A5	32	2.5	169[d]	30-40	1.5-2.1
(7)	HD 139614	157	A7	12	1.8	240	30-40	2.5-3.5
(8)	HD 142666	116	A7-A8	11	1.8	127	30-40	0.7-1.0
(9)	HD 135344	84	F4-F8	3	1.3	140	30-40	0.4-0.6

[a] See Tab. 3 of Dominik et al. (2003), and references therein.

[b] Binary system with two B8 V stars with total mass of 5.5 $M_\odot$ (Smith et al. 2005; Palla & Stahler 1993; Monnier et al. 2008).

[c] Mannings & Sargent (1997), unless noted otherwise.

[d] Raman et al. (2006).

Table 5.2: Observed ^{12}CO J=3–2 and J=2–1 line integrated intensities and full width at half-maximum. Calculated values for the J=3–2 line based on the SED-fitting disc model.

Source	$\int I_{CO(3-2)}dV$ (K km s^{-1})	$\int I_{CO(3-2)}^{\rm calc}$ (K km s^{-1})	FWHM$_{CO(3-2)}$ (km s^{-1})	FWHM$_{CO(3-2)}^{\rm calc}$ (km s^{-1})	$\int I_{CO(2-1)}dV$ (K km s^{-1})	$(\int I_{CO(3-2)})/(\int I_{CO(2-1)})$
HD 100546	**5.96±0.64**	9.40	**4.3**	5.0	–	–
HD 179218	0.60±0.12	0.03	7.0	9.7	**<0.11**	>6
V892 Tau	**7.12±0.20**	–	**1.6**	–	**8.23±1.08**	0.9
AB Aur	13.67±1.6	4.73	1.4	5.7	–	–
HD 163296	4.30±0.10	0.33	4.0	16.2	2.94	1.5
HD 169142	1.70±0.13	0.31	1.6	2.3	0.91	1.9
HD 139614	0.47±0.11	0.12	2.0	6.3	**0.30±0.09**	1.7
HD 142666	0.72±0.14	0.004	2.0	22.4	**0.29±0.06**	2.4
HD 135344	0.97±0.04	9.84	1.8	4.4	–	–

Table 5.3: Disc outer radius and inclination (i=0 corresponds to the face-on orientation) as used in the SED fitting, from our parametric models, and direct observations.

Source	SED modelling[a]			Parametric models (p=1)		Observed values	
	$R_{\rm out}$	i	p	$R_{\rm out}$	i	$R_{\rm out}$	i
HD 100546	400	51	0.0	300	35	350-380[b], 200[c]	51±3[b], 50±5[c]
HD 179218	30	20	-0.8	200	60-75	–	–
AB Aur	400	65	2.0	>800	10-20	1050[d]	33±1[d]
HD 163296	50	65	0.2	350	35-40	540[e]	46±4[e]
HD 169142	100	8	2.0	200	5	235[f,g]	13±1[f,g]
HD 139614	60	20	0.1	75-100	5	–	–
HD 142666	10	55	-0.5	75	5	–	–
HD 135344	800	60	0.8	50	0	210[h], ≥150[j]	46±5[h], 14±4°[i], $\leq$20°[j]

a Dominik et al. (2003) (note that they use p as $\Sigma \propto R^p$).

b Augereau et al. (2001), spatially resolved near-infrared coronographic scattered light observations.

c Pantin et al. (2000), spatially resolved J and K band near-infrared observations.

d Piétu et al. (2005), spatially resolved ^{12}CO J=2–1 line observations.

e Isella et al. (2007), spatially resolved ^{12}CO J=2–1 and J=3–2, and ^{13}CO J=1–0 line observations.

f Raman et al. (2006), spatially resolved ^{12}CO J=2–1 line observations.

g Chapter 2 of this thesis, spatially resolved ^{12}CO, ^{13}CO and C^{18}O J=2–1 line observations.

h Doucet et al. (2006), mid-infrared interferometry

i Pontoppidan et al. (2008)

j Grady et al. (2009)

(Hogerheijde & van der Tak 2000), we calculate the ^{12}CO J=2–1 and J=3–2 line emission from the SED disc models, assuming a standard gas-to-dust mass ratio of 100:1. In our calculations we neglect the contribution of the hot disc surface layer because of the low density at the disc surface and efficient ^{12}CO photodissociation. Therefore the disc is vertically isothermal and the temperature corresponds to the disc *midplane* temperature as used in Dominik et al. (2003). The disc temperature is well above the CO freeze-out temperature of 20 K in all the models except for the HD 135344 disc model beyond 400 AU from the star. For simplicity, we neglect any possible effect of freeze out on the ^{12}CO abundance in our analysis, and adopt a constant ^{12}CO abundance of 10^{-4} with respect to H$_2$. The effect of microturbulence is included with the equivalent line-width of 0.16 km s^{-1}. Each calculated spectrum is convolved with the JCMT beam of the corresponding size, using the Miriad software package (Sault et al. 1995).

Columns 2 and 5 in Table 7.1 show the resulting integrated intensity and full width at half-maximum (FWHM) of the ^{12}CO J=3–2 line. In comparison with the observed spectra, the modelled spectra of most sources underestimate the observed integrated intensities. This is especially pronounced for the discs with assumed outer radii of 10-50 AU, as HD 142666, HD 179218 and HD 163296. The width of the modelled lines for HD 142666 and HD 163296 significantly exceeds the observations, supporting the argument for a larger outer radius than assumed in the SED modelling. The reason is that in a small disc, the material dominating the line emission rotates at relatively large velocities, and thus produces very wide spectral profiles, with FWHM roughly 10-20 km s^{-1}, while a large disc has significant contribution from the slowly rotating material at large distances from the star. As mentioned, the SED is most sensitive to the region of a few tens of AU from the star. While the SED fitting is a valuable method to derive disc structure and temperature, when it is done without including the constraints on the disc size and inclination, the regions beyond 50 AU may not be accurately decribed. Some sources are modelled with a radially *increasing* surface density in Dominik et al. (2003). This was done to reproduce the slope of the mid-infrared emission at 10-30 μm wavelength, originating in the very inner disc regions, and is therefore not necessarily a good representation of the disc structure at larger scales as traced by the rotational ^{12}CO lines. Recent work of Meijer et al. (2008) shows that the SED is almost insensitive to the disc outer radius, and this explains the almost systematic underestimate of disc outer radii in Dominik et al. (2003).

In the sources HD 135344 and HD 100546, with assumed radii of 800 and 400 AU respectively, the line emission is overestimated. A disc model with an outer radius closer to the observed 210 AU (Doucet et al. 2006) may provide a better fit to the ^{12}CO J=3–2 line from HD 135344. In the model of HD 100546 surface density exponent steeper than the assumed p=0, may provide a better fit to the observed ^{12}CO line spectrum.

In the case of AB Aur, the relatively large assumed inclination of 65° is used to account for the relatively low near-infrared excess emission (Dominik et al. 2003). This choice of inclination is reflected in the larger FWHM of the modelled ^{12}CO line than observed. However, the millimeter interferometry observations (Piétu et al. 2005) indicate the inclination of 33°, an outer radius of 1050 AU and an inner radius close to 50 AU. In sources like AB Aur, exhibiting a low near-infrared excess, it is thus essen-

tial to establish whether the apparent lack of near-infrared emission is due to a lack of material in the innermost disc regions (presence of an inner hole) or due to the large disc inclination. As seen in this example, the ^{12}CO spectral line profile, as a diagnostic of disc inclination, provides a way to discern between these two scenarios, even in case of spatially unresolved, single dish observations. Meijer et al. (2008) (their Fig. 2) show the strong dependence of the overall shape of the disc SED on the inclination, that stresses the necessity for reliable estimates of inclination.

5.4 MODELLING AND ANALYSIS OF THE ^{12}CO J=3–2 SPECTRA

In the previous section we have shown that the disc models based on the SED emission alone fail to simultaneously reproduce the observed spectral lines of CO. It is very useful to design a simple way to estimate the disc size and inclination from the observed ^{12}CO spectra, providing valuable input for the SED modelling from the observational data already available for most gas-rich discs. In the current literature, the estimates of size and inclination are done predominantly through spectral line fitting with a large number of free model parameters. Here, we take a simpler approach.

The low-J ^{12}CO line emission is expected and often found to be optically thick in circumstellar discs. Therefore it traces a warm layer of gas above the disc midplane (van Zadelhoff et al. 2001; Dartois et al. 2003) and is relatively insensitive to the total disc mass. The emission is dominated by the disc material at scales of 100 AU from the star. For a known stellar mass, the shape of the line is sensitive to both disc size and inclination. In our approach, we focus on the parameters to which the presumably optically thick ^{12}CO J=3–2 line is most sensitive, disc size, inclination and temperature, and make simple assumptions about the remaining parameters like the disc mass, inner radius, surface density exponent, and disc vertical temperature and density structure.

5.4.1 Power-law disc models

We develop a grid of simple parametric disc models to interpret the observed ^{12}CO J=3–2 line profiles. Our models use a power-law surface density and temperature distribution: $\Sigma = \Sigma_{100}(R/100\,\mathrm{AU})^{-p}$ and $T = T_{100}(R/100\,\mathrm{AU})^{-q}$, and are comparable in the assumptions to those of Chiang & Goldreich (1997). The ^{12}CO J=3–2 line is optically thick, with the optical depth $\tau \geq 10$ in our models. The line spectrum alone does not provide any insight into the vertical temperature structure of the disc. Thus we use a vertically isothermal disc structure and describe the line flux by an 'effective' temperature representing a cummulative effect of the disc temperature structure on the line emission at the given radius. This simplification is used in the analysis of the submillimetre ^{12}CO emission in discs around T Tauri and Herbig Ae stars throughout the literature (Dutrey et al. 1994; Guilloteau & Dutrey 1998; Piétu et al. 2007, 2005; Isella et al. 2007). The vertical density structure is given by $n(z) = n_0 \exp\left(-z^2/2h^2\right)$ where
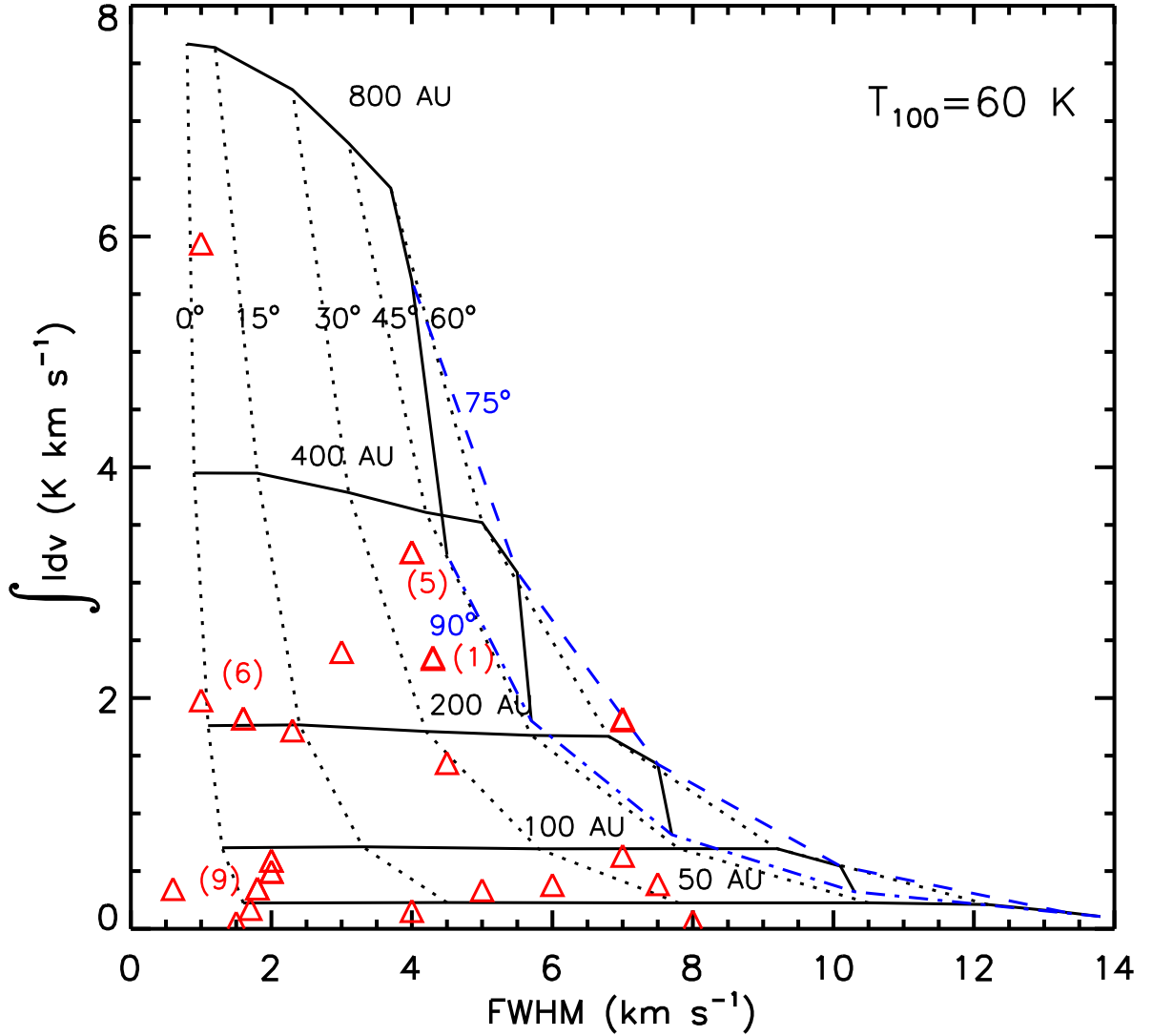
Figure 5.3: Integrated intensity of the modelled ^{12}CO J=3–2 line emission, plotted versus the FWHM, for M_{star}=2.0 $M_\odot$ and M_{disc}=0.01 $M_\odot$. The figure shows the results of the parametric disc models with T_{100}=60 K. The full black lines connect the results of models at a constant disc outer radius, the value of which is labeled. The dotted and the dashed lines connect the results for a constant inclination, also labeled. The triangles are the observed values, from Dent et al. (2005) and this work, with the observed integrated line intensities scaled as $\int IdV \times (d/140\,\mathrm{pc})^2$. Some of the sources from Table 5.1 are labeled by number.

$n_0 = \Sigma/\sqrt{\pi h}$ is the midplane density, and $h = h_{100}(R/100\,\mathrm{AU})$ is the scale height. The model parameters are listed in Table 5.4 along with the corresponding values.

We explore a wide range of *disc sizes*, with R_{out} from 50 to 800 AU, and the full range of *inclinations* with respect to the line of sight (0° corresponding to face-on orientation). These are the two parameters in the focus of our analysis. The parameters determining disc density structure (p, M_{disc}) are held fixed, with values close to those observationaly derived in the literature for discs in general (Beckwith et al. 1990; Mannings & Sargent

Table 5.4: Model parameters

| Parameter	Symbol	Type	Value(s)
Inclination	i	variable	0, 15, 30, 45, 60, 75, 90°
Outer radius	R_{out}	variable	50, 10, 200, 400, 800 AU
Inner radius	R_{in}	fixed	0.4 AU
Disc mass (gas+dust)	M_{disc}	fixed	0.01 M$_\odot$ (test calculations also done, up to 0.07)
Surface density at 100 AU	Σ_{100}	variable	calculated based on choice of R$_{\mathrm{out}}$
Surface density exponent	p	fixed	1
Temperature at 100 AU	T_{100}	fixed	30, 60 K
Temperature exponent	q	fixed	0.5
Scale height at 100 AU	h_{100}	fixed	10^{12} m
Scale height exponent	y	fixed	-1
Turbulent equivalent line width	dV	fixed	0.16 km s^{-1}
Stellar mass	M_{star}	fixed	2.0 M$_\odot$
Dust opacity	κ	fixed	2 cm^2 g^{-1}
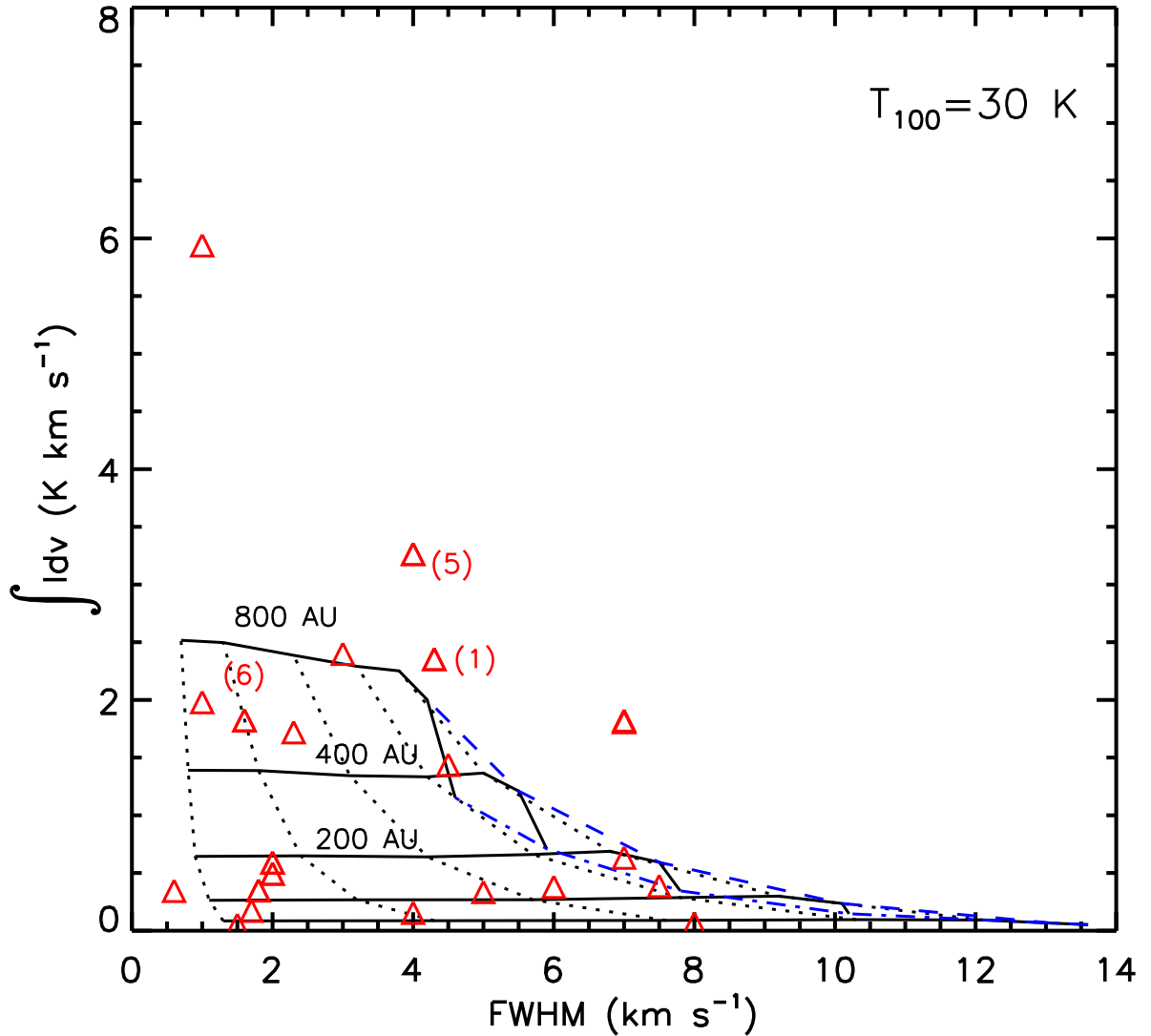
Figure 5.4: Same as in Fig. 5.3, but for the parametric disc models with T_{100}=30 K.

1997). The disc mass is set to 0.01 $M_\odot$. While the optically thick low-J ^{12}CO lines are not very sensitive to the radial density distribution, their fluxes depend stongly on the temperature. We have two sets of calculations, one setting the temperature at 100 AU to T_{100}=30 K and the other for T_{100}=60 K. We adopt the slope q=0.5 for the temperature radial dependence, as found to describe the ^{12}CO emission well in a number of sources (Thi et al. 2001; Piétu et al. 2007). In a more realistic modelling, T_{100} could be anywhere in this approximate range, depending on the exact spectral type, disc geometry, dust settling and other properties of each source. Below we argue that T_{100}=60 K, close to the values derived in the parametric modelling of the interferometric observations of the ^{12}CO J=2–1 line in AB Aur and MWC 480 (Piétu et al. 2007, 2005), provides a better fit to the disc size for several objects where we have independent measurements of the outer radius, and describes the observed line spectra from Dent et al. (2005) well.

The velocity field is given by Keplerian rotation around a central star with a mass
of M_{star} =2.0 $M_{\odot}$. The line width depends on $\sqrt{M_{\text{star}}}$, therefore the adopted value de-
scribes well our sample of sources (Table 5.1) given the spectral resolution of the data.
Turbulent line broadening is included, with the equivalent line width of 0.16 km s^{-1}.
Its influence on the results of our simple analysis is negligible. The calculations of the
synthetic spectra are done using RATRAN. The ^{12}CO abundance is set to a constant
value of 10^{-4} throughout the disc. Dust is included in the radiative transfer calcula-
tion of the ^{12}CO J=3–2 line, adopting a gas-to-dust mass ratio of 100:1 and with a dust
submillimetre emissivity of 2 cm^{2}g^{-1}. All calculations were done with an adopted
distance of 140 pc. We will later scale the observations to the same distance. The cal-
culated spectra were convolved with the 14″ beam of the JCMT and the contribution
of the dust continuum to the integrated line intensity was subtracted. We compare the
calculated FWHM and $\int IdV$ with the observed FWHM and $\int IdV \times (d/140\,\text{pc})^2$, where
d is the actual distance of the source.

5.4.2   Model results

The results from our grid of models with $T_{100} = 60$ K are presented in Fig. 5.3, where
the line integrated intensity is plotted against the FWHM. The full lines connect vary-
ing inclinations at constant radius, while the dotted and dashed lines connect model
results at varying radii for a fixed inclination. The two parameters, disc size and incli-
nation, are non-degenerate at inclinations 0°-45°. In this range, the FWHM grows with
the inclination, and the integrated line intensity with the size of the disc. For a fixed
R_{out}, at inclinations larger than 60° the line integrated intensity drops sharply, at an
almost constant FWHM in larger discs towards the results corresponding to a smaller
disc with a slightly lower inclination. At very high inclinations, the emission in the
line wings is relatively unaffected by the exact value of the inclination. However, the
line emission between the two peaks in the spectrum that dominates the line intensity
at i<45° decreases as the inclination increases beyond this value. This is because the
contribution from the warm disc layers is gradually absorbed by the superposed out-
ermost disc regions of low temperature that begin to dominate the line emission as the
inclination increases from 45° to 90°. Therefore, at high inclinations the parameters i
and R_{out} become degenerate, and the spectra cannot be fitted by a single model in the
region to the right of the i=45° curve in Fig. 5.3.

For comparison, the observed FWHM and $\int IdV \times (d/140\,\text{pc})^2$ values are plotted in
Figs. 5.3 and 5.4 (triangles) for 21 Herbig Ae/Be discs from Dent et al. (2005) and our
source HD 100546. The integrated intensities are scaled to the 140 pc distance using the
distances given in the same paper (except for HD 34282, where we adopt 160 pc as in
van den Ancker et al. (1998).All sources fall within the span of our model results, while
several very weak sources appear to require a radius smaller than our smallest size of
50 AU. Our model results are roughly consistent with some of the known disc radii
and inclinations (AB Aur, HD 169142, HD 163296), determined through millimetre
interferometry. Table 7.2 lists the disc outer radii and inclinations derived from the
SED modelling alongside the values we find from our parametric disc models. For

some of the sources, sizes and inclinations measured directly via near-infrared and/or submillimetre imaging are also listed, for comparison. In the following section we discuss the implications of the model fit for each of our sources in detail.

Close to 75% of the sources, or 17 out of the 22 sources, from Dent et al. (2005) have integrated line intensity lower than 2 K km s^{-1}, when scaled to 140 pc distance. In terms of our modelling this translates to sizes smaller than 200 AU, a result consistent to the disc size estimates in Dent et al. (2005, their Table 2). The disc size is very sensitive to the assumed T_{100}. However, while the optimal value of T_{100} may vary from one source to another depending on the exact spectral type of the star and disc geometry, T_{100}=60 K appears to represent our sample of the discs aroud Herbig AeBe stars well. In the light of this result, the sources with large outer radii like AB Aur, MWC480 and HD 163296, studied extensively with the sub-millimetre interferometers, have disc structures that are not necessarily a good representation of the entire sample of discs around intermediate mass stars. The smaller discs, although observationally more challenging, may hold the clues to the processes that shape discs in the course of their evolution. Furthermore their small size, coupled with the illumination by an A-type star, provides a fair chance that the CO depletion is not significant, leading to a better gas mass estimate than can be done in discs around T Tauri stars. The structure of some of these discs, close to 200 AU in size, has already been studied, e.g., in Chapillon et al. (2008) and in Chapter 2 of this thesis. Spatially resolved observations of more sources would also provide an answer to how many of these *weaker* sources are indeed small versus those that are perhaps larger but have lost a significant mass fraction of their gas or have cleared a large inner hole.

Figure 5.4 shows the results for models with $T_{100} = 30$ K. In comparison with the set of models with a higher temperature it is clear that the line strength, i.e., $\int IdV$ decreases with temperature. In this sense, R_{out} and T_{100} are degenerate parameters. The models with $T_{100} = 30$ K fail to describe the observed integrated line intensity and FWHM of a number of sources, mainly the ones with $\int IdV \times (d/140\,\mathrm{pc})^2 >$2 K km s^{-1} and FWHM>4 km s^{-1}. The only way for this group of models to reproduce all observations would be to adopt very large disc sizes, e.g., $R_{out} \approx$600 AU for HD 169142, and higher stellar masses, e.g., $M_{star} \approx$5 M$_\odot$ for HD 179218, both significantly larger than the values observed in some of our sources. Therefore, a higher temperature of $T_{100} \approx$60 K appears to be a good choice for the sample.

Our parametric disc models are designed to reproduce the low-J ^{12}CO line emission, and therefore they provide a description of the disc structure at large scales, where most of this emission arises. These regions dominate the dust thermal continuum emission at long wavelengths (> 300 μm), but the large uncertainties in the dust (sub)millimetre emissivity that heavily affects the continuum flux do not allow to test the disc structure we derive against the observed SEDs. For an opportune choice of the dust emissivity within the wide range expected in discs (Draine 2006), our disc models provide submillimetre SED slopes consistent with those observed.

5.4.3 Individual sources

Our model calculations with T_{100}=60 K yield size and inclination estimates for the 22 sources indicated by triangles in Fig. 5.3. Table 5.5 summarises these estimates and shows the results of a similar analysis done in Dent et al. (2005) but with more free parameters. Although their results differ from ours, they are relatively close, considering the simplicity of our uniform approach to line modeling in comparison with the more detailed modelling based on the individual sources and their stellar properties in Dent et al. (2005). Our finding that roughly 25% of the sources with detected ^{12}CO emission have radii smaller than 200 AU is consistent with the modelling results in the work by these authors, as can be seen in Table 5.5.

We compare the results of our model with T_{100}=60 K to the SED modelling results and results from spatially resolved observations, where available. The comparison among the derived disc sizes and inclinations is shown in Table 7.2. The precise estimate of these two parameters requires spatially resolved observations, therefore the estimates from single dish observations must be considered as very rough qualitative estimates rather than measurements. Indicative errors on our size and inclination values are at most 40%.

HD 100546

The ^{12}CO 3–2 emission is well described by our model with R_{out}=300 AU, not too different from the 400 AU used in the SED model. The difference in size can account for the factor of two overestimate of the observed line emission by the SED model. Our inclination of 35° is somewhat lower than the 51±3° observed with NICMOS scattered light imaging (Augereau et al. 2001) and used by Dominik et al. (2003) in their modelling, but consistent with these values. Within the uncertainties involved in our model, our estimate of 300 AU is close to the 350-380 AU reported by Augereau et al. (2001). Spatially resolved J and K band near-infrared observations using ADONIS instrument indicate an inclination of 50±5° and a somewhat smaller size of 200 AU (Pantin et al. 2000), that can be considered as a lower limit on the actual disc radius.

HD 179218

There are no direct measurements of the disc size and inclination in the literature. In Sect. 5.2.1 we mention that the ^{12}CO J=3–2 line perhaps does not arise from the disc but is dominated by optically thin gas at a very high temperature. If we assume that the emission does arise from the disc, we derive the disc radius of 200 AU and the inclination of 60-75°. A larger disc size, up to 400 AU with an inclination of 75° is also possible. Therefore we conclude that the disc extends much further than the radius of 30 AU used in the SED modelling.

AB Aur

Our estimate of R_{out} >800 AU and i=10-20° for AB Aur disc is reasonably close to the 1050±10 AU and 33±1° derived by Piétu et al. (2005) from the spatially resolved

Table 5.5: List of the complete source sample, used in Fig. 5.3 and 5.4, and the corresponding disc parameters, according to our model with T_{100}=60 K (Fig. 5.3). Values derived in (Dent et al. 2005) are shown for comparison.

Source	Distance	R_{out} (Dent et al. 2005)	i (Dent et al. 2005)	R_{out} (this work)	i (this work)
HD4881	168	35	≤5	50	0
HD9672	61	17±5	16±3	<50	<30
AB Aur	144	600±50	12±2	>800	10-20
MWC480	131	245±30	28±2	300	20
HD34282	160[a]	380±20	50±5	175	30
HD34700	125	80±10	25±2	50	30
HD36112	204	170±30	≤10	200	15
CQ Tau	99	30±5	14	<50	10
HD38120	420	300≤50	<8	600	5
HD100546	103	–	–	300	35
HD135344	84	75±5	11±2	50	0
HD139614	157	110±3	≤10	75-100	5
HD141569	99	250±4	52	50-75	25
HD142666	116	45±10	18±5	75	5
HD143006	82	35±5	≤3	<50	0
HD144432	200	60±20	48±10	100	35
HD145718	130	60±30	32±10	50-75	30
HD163296	122	245±20	30±2	350	35-40
HD169142	145	130±10	≤5	200	5
HD179218	243	120±20	40±10	200	60-75
UX Ori	430	95	<8	200	0
TW Hya[b]	56	160±10	5±2	–	–

[a] Dent et al. (2005) adopt a distance of 400 pc for this star.

[b] K type star from the Dent et al. (2005) sample, considered to be T Tauri. Located near the origin of the axes in Figs. 5.3 and 5.4.

observations of ^{12}CO 2–1 line in this disc. The overestimate of the inclination in the SED
fit would be avoided if the inner hole, estimated by Piétu et al. (2005) to be 45±3 AU
large in this disc, is included.

HD 163296

We obtain a size of 350 AU, roughly consistent to the observationally derived 540 AU in
Isella et al. (2007), via spatially resolved sub-millimetre observations. Our inclination
of 35-40° is consistent with the 46±4° derived therein. The disc size of 50 AU used in
the SED modelling is much smaller.

HD 169142

The disc size and inclination from SED modelling, our parametric models, and spa-
tially resolved observations are all roughly close. In Raman et al. (2006) the disc around
HD 169142 was studied with spatially resolved ^{12}CO 2–1 line emission, indicating a
disc radius of 235 AU and inclination of 13°. In Chapter 2 of this thesis we find that
an SED model described in Dent et al. (2006) and Raman et al. (2006) provides a good
descripton to the ^{12}CO and isotopologue line emission. Dominik et al. (2003) use a
somewhat smaller disc size of 100 AU, while an extension of their model to 200 AU
and perhaps with a less steep density exponent p would probably be sufficient to re-
produce the ^{12}CO line emission.

HD 139614

The SED modelling produces a weak and broad line, while a nearly face-on orientation
is required to reproduce the observed narrow 3–2 line of ^{12}CO towards HD 139614
(Dent et al. 2005). Our model fit results in R_{out}=75-100 AU and i=5°, consistent with
110 AU and <10° found by Dent et al. (2005), while the SED model has a slightly
smaller disc size of 50 AU. Although there are no direct imaging measurements of the
size of the disc around HD 139614, the weak ^{12}CO lines would be very difficult to
reproduce by a disc much larger than 100 AU unless the disc is colder, or has a very
low gas (or CO) mass. The continuum flux of this source (Table 5.1) does not seem to
indicate a very low disc mass (0.035 M$_\odot$), however.

HD 142666

To reproduce the observed narrow ^{12}CO line, an outer radius much larger than the
10 AU assumed in the SED modelling is needed, as well as a much lower disc inclina-
tion. We obtain a 75 AU radius and a 5° inclination for this disc. There are no direct
measurements of these parameters for HD 142666 in the literature, however.

HD 135344

Our derived disc size of 50 AU and a face-on orientation are close to the 14±4° derived
from spectroastrometric imaging with CRIRES (Pontoppidan et al. 2008), but in con-

tradiction with the 210 AU outer radius and $46\pm5°$ inclination observed using MIDI instrument (Doucet et al. 2006). The 1.3 mm continuum flux leads to a disc mass estimate of 0.01 $M_\odot$ (Sect. 5.2.1). A model with this disc mass, a 210 AU radius and 46° inclination would have a roughly three times stronger and wider ^{12}CO 3–2 line than observed. At 8 ± 4 Myr, it is possible that this disc has lost significant amounts of its gas, but this does not explain the narrow line width. A presence of a considerably large inner hole, as indicated by the disc SED Brown et al. (2007), would remove the contribution of rapidly rotating material from the inner disc regions in the line profile and allow a narrow ^{12}CO line to arise from a disc at $46\pm5°$ inclination. If the process which caused the inner hole also helped to remove or dissociate most of CO gas in the outer disc regions while not affecting the dust (e.g., photoevaporation), we may have a weak and narrow ^{12}CO line profile from the disc described by 210 AU size and 46° inclination as observed with MIDI.

5.5 CONCLUSIONS

In this paper, we analyse the low-J ^{12}CO spectral lines and the dependence of their profiles on disc parameters, in particular the size and inclination. We present simple parametric disc models and find that the low-J ^{12}CO spectral line profiles are a valuable indicator of disc inclination and size, even in spatially unresolved observations.

  We place our analysis in the context of the disc structure derived based on the SED modelling. We conclude that the "outside-in" disc modelling, i.e., starting from sub-millimetre ^{12}CO spectral line observations or direct imaging of the dust thermal or scattered light emission, followed by the overall SED fitting, is more straight-forward and provides more reliable results than the standard "inside-out" disc modelling where SED is fitted with no prior knowledge of disc size and inclination and subsequently the outer disc emission interpreted in the context of the SED fitting results. The "outside-in" modelling of the disc structure helps remove degeneracies between disc inner radius and inclination, and provides a better estimate of the disc mass. For this purpose, we have developed a simple tool to get a rough indication of disc size and inclination for discs around Herbig Ae/Be stars from the observed J=3–2 ^{12}CO spectral line profiles.

  We find that the great majority (75%) of observed discs around Herbig Ae/Be stars have sizes smaller than 200 AU, while discs much larger than 200 AU (e.g., AB Aur) are rare and not representative of the whole sample. We stress the importance of studying the gas content of the small discs, facilitated by the fact that they are typically warmer and allow us to minimise or even overcome the problem of CO depletion. Some of the weaker sources may be large and gas-poor discs, and it would be particularly interesting to spatially resolve these discs through millimetre continuum observations. If the weak sources are mainly the large and gas-poor discs this would strengthen the conclusions about disc structure already derived from observations of bright sources. If, on the other hand, the vast majority of the weak sources are confirmed to be gas-rich discs small in size in spatially resolved observations, these will present themselves as perfect targets for measuring gas masses and ultimately the gas-to-dust mass ratio.

Due to the sufficiently strong millimetre fluxes, the existing submillimetre interferometers can be used to derive disc sizes and measure gas mass of 200 AU large gas-rich discs. The high sensitivity and spatial resolution that ALMA will provide in the coming years will enable us to explore the weaker sources and the detailed structure of small discs.

REFERENCES

Adams, F. C., Shu, F. H., & Lada, C. J. 1988, ApJ, 326, 865

Augereau, J. C., Lagrange, A. M., Mouillet, D., & Ménard, F. 2001, A&A, 365, 78

Beckwith, S. V. W., Sargent, A. I., Chini, R. S., & Guesten, R. 1990, AJ, 99, 924

Bouwman, J., Meeus, G., de Koter, A., et al. 2001, A&A, 375, 950

Brown, J. M., Blake, G. A., Dullemond, C. P., et al. 2007, ApJ, 664, L107

Chapillon, E., Guilloteau, S., Dutrey, A., & Piétu, V. 2008, A&A, 488, 565

Chiang, E. I. & Goldreich, P. 1997, ApJ, 490, 368

D'Alessio, P., Merín, B., Calvet, N., Hartmann, L., & Montesinos, B. 2005, Revista Mexicana de Astronomia y Astrofisica, 41, 61

Dartois, E., Dutrey, A., & Guilloteau, S. 2003, A&A, 399, 773

Dent, W. R. F., Greaves, J. S., & Coulson, I. M. 2005, MNRAS, 359, 663

Dent, W. R. F., Torrelles, J. M., Osorio, M., Calvet, N., & Anglada, G. 2006, MNRAS, 365, 1283

Dominik, C., Dullemond, C. P., Waters, L. B. F. M., & Walch, S. 2003, A&A, 398, 607

Doucet, C., Pantin, E., Lagage, P. O., & Dullemond, C. P. 2006, A&A, 460, 117

Draine, B. T. 2006, ApJ, 636, 1114

Dullemond, C. P. & Dominik, C. 2004, A&A, 417, 159

Dullemond, C. P. & Dominik, C. 2005, A&A, 434, 971

Dutrey, A., Guilloteau, S., & Simon, M. 1994, A&A, 286, 149

Grady, C. A., Schneider, G., Sitko, M. L., et al. 2009, ApJ, 699, 1822

Guilloteau, S. & Dutrey, A. 1994, A&A, 291, L23

Guilloteau, S. & Dutrey, A. 1998, A&A, 339, 467

Hogerheijde, M. R. & van der Tak, F. F. S. 2000, A&A, 362, 697

Isella, A., Testi, L., Natta, A., et al. 2007, A&A, 469, 213

Malfait, K., Bogaert, E., & Waelkens, C. 1998, A&A, 331, 211

Mannings, V. & Sargent, A. I. 1997, ApJ, 490, 792

Mannings, V. & Sargent, A. I. 2000, ApJ, 529, 391

Meijer, J., Dominik, C., de Koter, A., et al. 2008, A&A, 492, 451

Monnier, J. D., Tannirkulam, A., Tuthill, P. G., et al. 2008, ApJ, 681, L97

Nakajima, T. & Golimowski, D. A. 1995, AJ, 109, 1181

Natta, A., Grinin, V., & Mannings, V. 2000, Protostars and Planets IV, 559

Palla, F. & Stahler, S. W. 1993, ApJ, 418, 414

Pantin, E., Waelkens, C., & Lagage, P. O. 2000, A&A, 361, L9

Piétu, V., Dutrey, A., & Guilloteau, S. 2007, A&A, 467, 163

Piétu, V., Guilloteau, S., & Dutrey, A. 2005, A&A, 443, 945

Pinte, C., Padgett, D. L., Ménard, F., et al. 2008, A&A, 489, 633

Pontoppidan, K. M., Blake, G. A., van Dishoeck, E. F., et al. 2008, ApJ, 684, 1323

Raman, A., Lisanti, M., Wilner, D. J., Qi, C., & Hogerheijde, M. 2006, AJ, 131, 2290

Sault, R. J., Teuben, P. J., & Wright, M. C. H. 1995, in Astronomical Society of the Pacific Conference Series, Vol. 77, Astronomical Data Analysis Software and Systems IV, ed. R. A. Shaw, H. E. Payne, & J. J. E. Hayes, 433–+

Schreyer, K., Guilloteau, S., Semenov, D., et al. 2008, A&A, 491, 821

Semenov, D., Pavlyuchenkov, Y., Schreyer, K., et al. 2005, ApJ, 621, 853

Smith, K. W., Balega, Y. Y., Duschl, W. J., et al. 2005, A&A, 431, 307

Tannirkulam, A., Monnier, J. D., Harries, T. J., et al. 2008, ApJ, 689, 513

Thi, W.-F. 2002, PhD thesis, , Leiden University, February 2002.

Thi, W. F., van Dishoeck, E. F., Blake, G. A., et al. 2001, ApJ, 561, 1074

Thi, W.-F., van Zadelhoff, G.-J., & van Dishoeck, E. F. 2004, A&A, 425, 955

van Boekel, R., Waters, L. B. F. M., Dominik, C., et al. 2003, A&A, 400, L21

van den Ancker, M. E., de Winter, D., & Tjin A Djie, H. R. E. 1998, A&A, 330, 145

van der Tak, F. F. S., Black, J. H., Schöier, F. L., Jansen, D. J., & van Dishoeck, E. F. 2007, A&A, 468, 627

van Zadelhoff, G.-J., van Dishoeck, E. F., Thi, W.-F., & Blake, G. A. 2001, A&A, 377, 566

5.6   APPENDIX: HARP MAPPING OF THE V892 TAU RE-GION

Following the detection of ^{12}CO J=2–1 line emission at the offset positions from V892 Tau, we mapped this region using the 16-pixel heterodyne array receiver HARP-B on the JCMT. The observations were carried out on 2008 September 10. The line observed was ^{12}CO J=3–2 at 345.796 GHz, with the beam size of 14″ and beam efficiency of 0.85. The rms obtained is 0.13 K per channel, at the spectral resolution of 0.026 km s^{-1}. The receiver array provided 11 spectra taken on a 4 × 4 raster, with the separation of 30″. The resulting spectra are shown in Fig. 5.5. The spectrum taken at the (2,2) position corresponds to the source V892 Tau. The integrated line emission is 7.12±0.20 K km s^{-1} and FWHM=1.6 km s^{-1}. These data show that V892 Tau is located in a region where the low-J ^{12}CO lines are dominated by the extended cloud material.
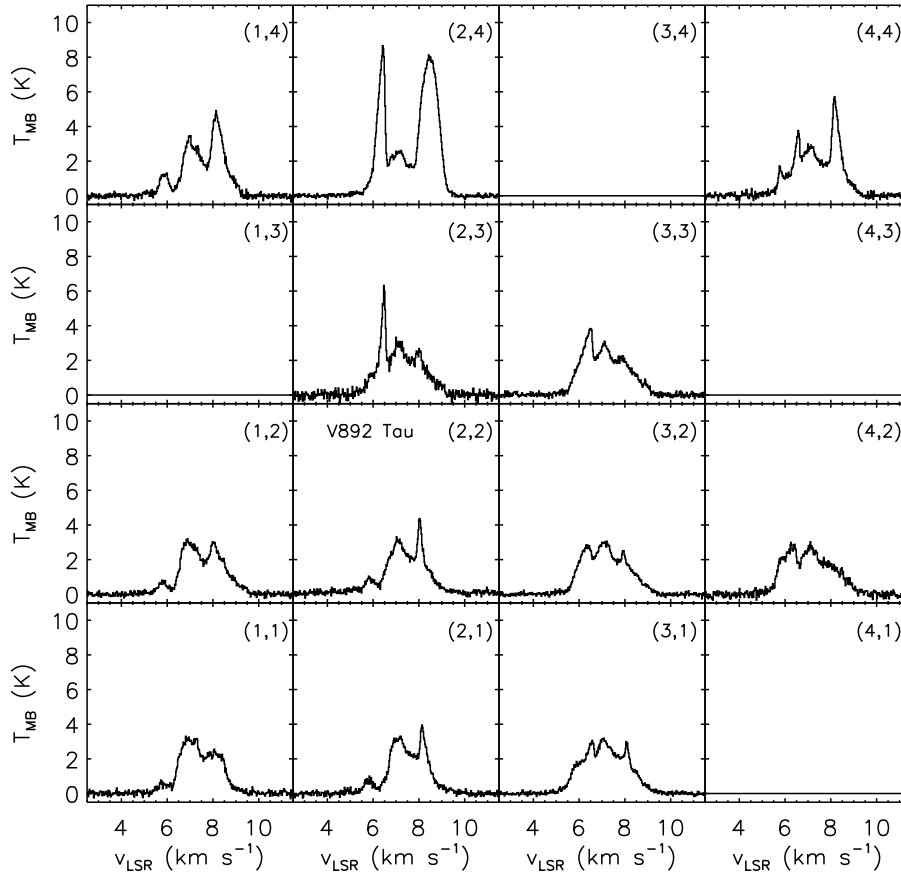

Figure 5.5: HARP mapping of the V892 Tau region. The spectrum toward V892 Tau is labeled.

CHAPTER 6

Comparing molecular gas and dust in discs around T Tauri stars

O. Panić, M. R. Hogerheijde and G. A. Blake

As protoplanetary discs evolve, their gas content is expected to decrease and the dust particles settle to the midplane. Observational constraints on the gas-to-dust mass ratio (g/d) in discs around T Tauri stars are essential to follow this process. We investigate the relative amounts of gas and dust in the discs around a sample of six T Tauri stars. Using the Combined Array for Research in Millimeter Astronomy and archival data from the Owens Valley Radio Observatory, we study the J=1–0 line of ^{12}CO, ^{13}CO and HCO$^+$, as well as the dust continuum at 2.7 mm towards a sample of six discs around T Tauri stars at a spatial resolution of 5″-10″. We use simple disc models and a molecular excitation and radiative transfer code to model the line and continuum emission. We test our best-fit dust continuum models against the observed line emission. Our 2.7 mm data combined with 1.3 mm data from the literature indicate dust emissivity spectral slopes of β=0.7−1.8 in our sources. Using a maximum dust emissivity we derive lower limits on the disc dust masses of 0.7–4.5×10^{-4} M$_\odot$ or total masses of 0.7–4.5×10^{-2}M$_\odot$ assuming a standard value $g/d = 100$. With prior knowledge of the disc radius and inclination, the models that fit the dust continuum also reproduce the ^{12}CO and ^{13}CO spectra within a factor two in intensity.To obtain exact fits to the line data, ^{12}CO depletion factors 10–100 are required in DM Tau and CQ Tau, likely due to efficient freeze-out and/or photodissociation. Sources AA Tau and Haro 6-5 B have optically thick lines, and require the emission to originate from layers warmer by factors close to two compared to the disc midplane. The spectral profiles towards DL Tau and RY Tau are not well defined, but the line intensity is consistent with $g/d = 100$ and no ^{12}CO depletion.

6.1   INTRODUCTION

The gas and dust content of discs around young stars has been studied in great detail over the last decade, in particular using submillimetre interferometers that enable us to disentangle the emission of the disc from that of the surrounding cloud material. The Taurus-Auriga cloud complex is our closest test-ground for star formation and the brightest discs around young low-mass stars (T Tauri stars) like DM Tau, LkCa 15 and GM Aur have been spatially resolved in both gas and dust millimetre emission (Piétu et al. 2007; Qi et al. 2003; Dutrey et al. 2008; Hughes et al. 2009). These studies have allowed to understand the radial and vertical structure of these discs better. The most commonly used gas tracer in submillimetre regime is ^{12}CO, with the strongest line emission, followed by the gas tracers HCO$^+$, CN and HCN (Dutrey et al. 1997; van Zadelhoff et al. 2001; van Dishoeck et al. 2003; Thi et al. 2001; Greaves 2004; Chapillon et al. 2008). The estimates of the main disc property - its mass - have relied almost exclusively on the dust thermal continuum emission yielding disc masses in the range from 0.001 to 0.1 M$_\odot$ (e.g., Beckwith et al. 1990; Osterloh & Beckwith 1995; Mannings & Sargent 1997; Andrews & Williams 2005, 2007). The conversion from the estimated dust mass to the total (gas and dust) disc mass is done assuming the gas-to-dust mass ratio g/d=100, poorly constrained in discs. Most observations done so far have been biased towards the brightest sources, which are often those with the largest discs.

We study six T Tauri stars located in Taurus star-forming region and known to posses discs. Our source sample and some of the basic stellar properties are listed in Table 6.1. Besides including some of the well-known bright sources like DM Tau and CQ Tau, we include less well studied sources DL Tau, RY Tau, AA Tau and Haro 6-5 B. The presence of the circumstellar material around these sources is seen in Hubble Space Telescope images (Padgett et al. 1999; Grady 2004) and molecular gas observations at millimetre wavelengths (DM Tau: Guilloteau & Dutrey (1994); Handa et al. (1995); Saito et al. (1995); Guilloteau & Dutrey (1998); Thi et al. (2001); Dartois et al. (2003); Piétu et al. (2007), DL Tau: Koerner & Sargent (1995); Simon et al. (2000), RY Tau: Thi et al. (2001); Koerner & Sargent (1995), CQ Tau: Thi et al. (2001); Mannings & Sargent (1997); Chapillon et al. (2008), Haro 6-5 B: Dutrey et al. (1996); Yokogawa et al. (2002)). The masses of our stars range from 0.25 to 1.8 M$_\odot$ and their spectral types range from late A to early M. All sources have the class II spectral energy distribution (SED) characteristic of a circumstellar disc (Kenyon & Hartmann 1995; Chiang et al. 2001; Doucet et al. 2006), but Haro 6-5 B lacks the near- and mid-infrared SED information for proper classification (Kenyon & Hartmann 1995). Evidence of grain growth is found in discs around RY Tau and CQ Tau (Isella et al. 2009; Testi et al. 2003). The most massive star in our sample, CQ Tau, has properties at the border between T Tauri and Herbig Ae stars and is sometimes reffered to as an Herbig Ae star. This is also the oldest star in our sample, with estimated age close to 10 Myr (see Chiang et al. 2001; Testi et al. 2003, and references therein) and low far-infrared excess indicative of a relatively flat disc structure (Doucet et al. 2006, and references therein). We investigate to what extent the molecular line emission differs from one source to another, considering that all our sources appear similar in their thermal dust emission (i.e., dust mass). Both low-J molecular line emission and the thermal dust emission at the millimetre wavelengths

probe the bulk of the disc material, located up to several hundreds of AU from the central star, and are particularly well suited to address the global differences between the gas and dust contents of the discs.

To investigate the discs around our young T Tauri stars we use interferometric observations of ^{12}CO, ^{13}CO and HCO$^+$ line emission, and dust continuum obsevations, and draw a comparison between the disc gas and dust content. In Sect. 2 we describe our observations of the molecular lines and dust continuum, while the results are shown in Sect. 3. In Sect. 4 we analyse the observed continuum and line emission using simple parametric models. Section 5 gives a brief summary of our conclusions regarding the maximum amount of ^{12}CO gas and minimum dust mass, and the minimum temperature at which the observed line emission arises.

6.2 OBSERVATIONS

^{12}CO and HCO$^+$ J=1–0 line emission, at 115.271204 GHZ and 89.188518 GHz respectively, was observed using the Owens Valley Radio Observatory (OVRO) [1] between September 2002 and January 2003. The velocity resolution of the observations is 127 kHz (0.33 km s^{-1}) for ^{12}CO and 125 kHz (0.42 km s^{-1}) for HCO$^+$ and the spatial resolution of 5″-10″ (Table 6.1). The sources were observed in pairs, sharing 8-hour tracks, with approximately three hours on-source time for each individual source. The bandpass was calibrated using a boxcar fit to an internal noise source modified by a second order polynomial fit to the observations of the quasars 3C84, 3C454.3, 3C345, 3C279 and 3C273. The flux density scale was established with observations of the same quasars using fluxes bootstrapped with measurements of Neptune and Uranus. Bandpass, phase, and flux calibration were applied to the data with the MMA software package (Scoville et al. 1993). Further data reduction and image analysis was done using the MIRIAD data reduction software (Sault et al. 1995). We re-reduce and analyse the OVRO data, previously presented in Kessler-Silacci (2004). Kessler-Silacci (2004) also presents the observations of ^{12}CO and HCO$^+$ J=1–0 towards Haro 6-5 B, and HCO$^+$ J=1–0 from CQ Tau. However, calibrated data for these observations are no longer available and are omitted from our analysis.

The dust continuum at 2.7 mm was observed in May 2007 using Combined Array for Millimetre Astronomy (CARMA) [2]. The interferometer was in compact configuration providing spatial resolutions 4″-6″. The shared track duration was 7 hours for DM Tau and DL Tau with on-source integration times of 2.2 and 2.4 hours, respectively. RY Tau and CQ Tau shared a 5.6-hour track, with on-source integration times of 2.2 hours per source. AA Tau and Haro 6-5 B were observed in a 4-hour track, and

their on-source integration times are 1.6 and 1.4 hours, respectively. Flux and band-pass calibration were done using the 0530+135 calibrator, adopting a flux of 4.6 Jy for this source, and the MIRIAD software was used for all data processing. Simultaneous to the dust continuum at 2.7 mm, the ^{13}CO and C^{18}O J=1–0 lines were observed, at 110.201354 GHz and 109.782173 GHz respectively, with a spectral resolution of 122 kHz (0.33 km s^{-1}). Tables 6.1 and 6.2 list the synthesized beam sizes, noise levels and results of the observations.

6.3   RESULTS

We detect 2.7 mm continuum emission towards all our sources (Table 6.1). Only the dust emission from the disc around DL Tau is spatially resolved with the synthesized beam size of 4$''$68×3$''$79 (corresponding to approximately 600 AU resolution at 140 pc distance). Figure 6.1 shows the correlated flux as a function of the uv-distance for each source, averaged in concentric annuli in the uv-plane. The maps of the con-tinuum emission are shown in Fig. 6.2. The sensitivity of the continuum images is 1 mJy beam^{-1}, with detections exceeding 6 σ level and centered on the the locations of our sources. The total integrated flux at 2.7 mm, listed in Table 6.1, is measured by fitting the clean map of the emission with a point source, except in case of DL Tau where a gaussian distribution provides a better fit. The deconvolved aspect ratio of the gaussian of 2$''$4/2$''$7 is consistent with the inclination the 35$°$ inclination inferred for the DL Tau disc (Simon et al. 2000). Table 6.1 lists the pointing coordinates of our observations.

Based on the 2.7 mm continuum fluxes and the 1.3 mm fluxes from the literature (also listed in Table 6.1) we calculate the wavelength dependence of the millimetre flux, α=log[(2.7 $F_{1.3}$)/(1.3 $F_{2.7}$))]/log(2.7/1.3). Values range from 3.7 to 4.8 (Table 6.1). The slope of the millimetre dust emissivity β is obtained assuming optically thin emission. Following (Beckwith et al. 1990) we adopt $\beta = \alpha - 3$, yielding values that range from 1.8±0.9 to 0.7±0.9. While the former value suggests very small, ISM-type dust (AA Tau and Haro 6-5 B) the latter corresponds to dust that has undergone grain growth (see Draine 2006, their Fig. 3). However, due to the large errors in our estimates of β, we can not constrain the type of dust nor the emissivity in our sample. Our derived β slopes are consistent with more precise estimates of Rodmann et al. (2006), within the errors. In the Section 6.4.1 we use the millimetre continuum fluxes to estimate the minimum mass of the dust in the discs.

The ^{12}CO J=1–0 line emission is firmly detected in DM Tau and AA Tau (corre-sponding to 12σ and 4σ respectively in the maps of the velocity integrated emission), and marginally towards RY Tau and CQ Tau (3σ). Table 6.2 summarises the observed line intensities and upper limits. The spectra of the observed ^{12}CO lines are shown in Figure 6.5 (black line) integrated over a region centered on the source position. The ^{12}CO emission is observed at the V_{LSR}=4-8 km s^{-1} typical of the sources in the Taurus star-forming region, and is spatially coincident with the continuum detection. Fig-ure 6.3 shows the integrated intensity images of the molecular line emission for our unresolved sources. Only the ^{12}CO J=1–0 line emission from DM Tau is resolved spa-

Table 6.1: Source sample and dust continuum observations.

Source	RA (J2000)	Dec (J2000)	Sp. type [a]	$M_\star$ [b] ($M_\odot$)	Synthesized beam ($'' \times ''$)	$F_{2.7}$ [c] (mJy)	$F_{1.3}$ [d] (mJy)	α
DM Tau	4:33:48.77	18:10:09.78	M1	0.6	4.70×3.86	13.6±1.4	109±13	3.8±0.8
DL Tau	4:33:39.07	25:20:38.14	K7	0.6	4.68×3.79	29.7±2.8	230±14	3.8±0.6
RY Tau	4:21:57.42	28:26:35.66	F8-K1	1.7	5.67×4.13	33.1±3.8	229±17	3.7±0.9
CQ Tau	5:35:58.50	24:44:54.32	A8-F2	1.8	5.35×4.08	23.5±2.5	162±2	3.7±1.0
AA Tau	4:34:55.43	24:28:53.11	K7-M0	0.7	5.86×4.33	6±1	88±9	4.7±0.7
Haro 6–5 B [e]	4:22:00.70	26:57:32.67	–	0.25	5.85×4.37	8.5±1.0	134±6	4.8±0.9

[a] Simon et al. (2000), Mora et al. (2001), Akeson et al. (2005), Beckwith et al. (1990) and references therein.

[b] Beckwith et al. (1990), Chapillon et al. (2008), Yokogawa et al. (2002)

[d] Point source fit results, except for DL Tau where the resolved flux was fit with a Gaussian of $2''.7 \times 2''.4$ and peak intensity of 21.6±1.6 mJy beam^{-1}, offset by δRA=0.5 and δDec=-0.2 from the pointing position.

[d] Beckwith et al. (1990), Koerner & Sargent (1995), Chapillon et al. (2008), Osterloh & Beckwith (1995).
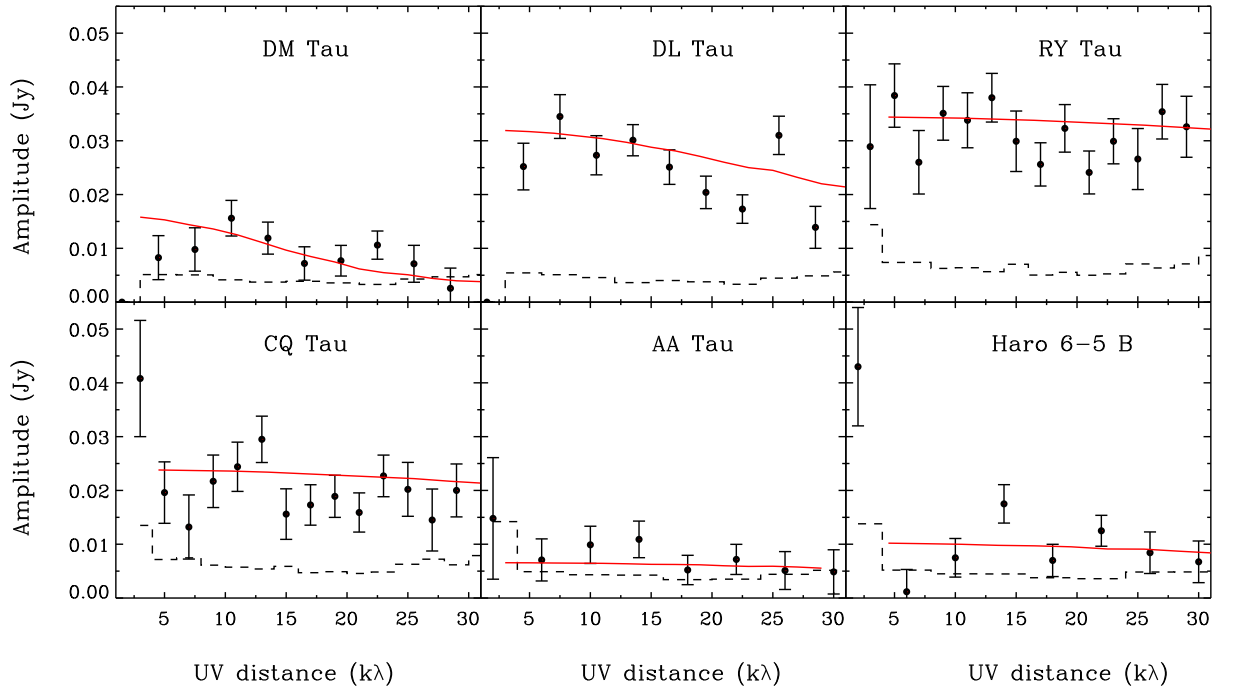
[d] Also known as FS Tau B.

Figure 6.1: Correlated 2.7 mm continuum flux as a function of *uv*-distance (black dots with the error bars corresponding to the variance in the annular averaging in the *uv*-plane). The zero-signal expectation value is plotted with the dashed black line. Our best fit models described in Section 6.4.1 are shown with the full lines.

tially, as can be seen in the visibility data shown in Fig. 6.6. The strongest ^{12}CO J=1–0 source, DM Tau, is also the largest disc in our sample, with the outer radius of 890 AU (Piétu et al. 2007). The extent of the emission can be seen in Fig. 6.4 where the integrated intensity and intensity-weighted velocity map characteristic of disc rotation are shown. At 2σ, the ^{12}CO extends to 8″ or 1100 AU from the star. RY Tau, CQ Tau and AA Tau are unresolved in ^{12}CO, limiting the size of these discs to $\leq$840 AU (the synthesized beam size of approximately 6″ at 140 pc distance).

Interestingly, one of the sources with the largest continuum flux, DL Tau, is not detected in the ^{12}CO line. As will be discussed in Sect. 6.4.3, this is likely due to the absorption by the foreground cloud (noted by Simon et al. 2000).

As shown in Figs. 6.3 and 6.5, we detect the ^{13}CO J=1–0 line emission from DM Tau and Haro 6-5 B, at V_{LSR}=5-7 km s^{-1}. These detections are at 8σ and 4σ, respectively, in the integrated emission maps. The emission is unresolved and arises from the source positions (see Fig. 6.3). We detect HCO$^+$ towards DM Tau at a 12σ level at V_{LSR} $\approx$5-7 km s^{-1}. The measured line intensities are shown in Table 6.2. The HCO$^+$ emission is marginally spatially resolved, and coincident with the source position (see Fig. 6.3). None of our sources is detected in C^{18}O J=1–0 line with an rms of 0.2-0.3 Jy beam^{-1}. In Table 6.2 we report upper limits on the line intensity.

Table 6.2: Molecular line results.

Source	Synthesized beam ($'' \times ''$)	I^a (Jy/beam)	$\int I dv$ (Jy/beam km/s)
		^{12}CO (1–0)	OVRO
DM Tau	6.59×6.07	2.09±0.17	3.63±0.16 [b]
DL Tau	11.02×7.74	<0.46	–
RY Tau	6.20×6.25	0.36±0.10	0.40±0.14
CQ Tau	9.20×6.25	0.86±0.25	0.80±0.25
AA Tau	5.64×4.21	0.43±0.13	0.58±0.15
		^{13}CO (1–0)	CARMA
DM Tau	4.44×3.97	0.39±0.12	0.77±0.11
DL Tau	4.48×3.90	<0.24	–
RY Tau	4.88×3.90	<0.28	–
CQ Tau	4.82×4.05	<0.26	–
AA Tau	4.97×3.88	<0.26	–
Haro 6-5 B	4.97×3.88	0.76±0.12	0.95±0.21
		C^{18}O (1–0)	CARMA
DM Tau	4.64×4.16	<0.26	–
DL Tau	4.68×4.07	<0.24	–
RY Tau	5.13×4.10	<0.26	–
CQ Tau	5.06×4.25	<0.26	–
AA Tau	5.17×4.01	<0.32	–
Haro 6-5 B	5.20×4.04	<0.32	–
		HCO$^+$ (1–0)	OVRO
DM Tau	5.02×3.67	0.30±0.08	1.12±0.10 [b]
DL Tau	5.30×3.99	<0.10	–
RY Tau	4.87×4.06	<0.10	–
AA Tau	13.27×7.08	<0.24	–

[a] Upper limits are given by 2σ.

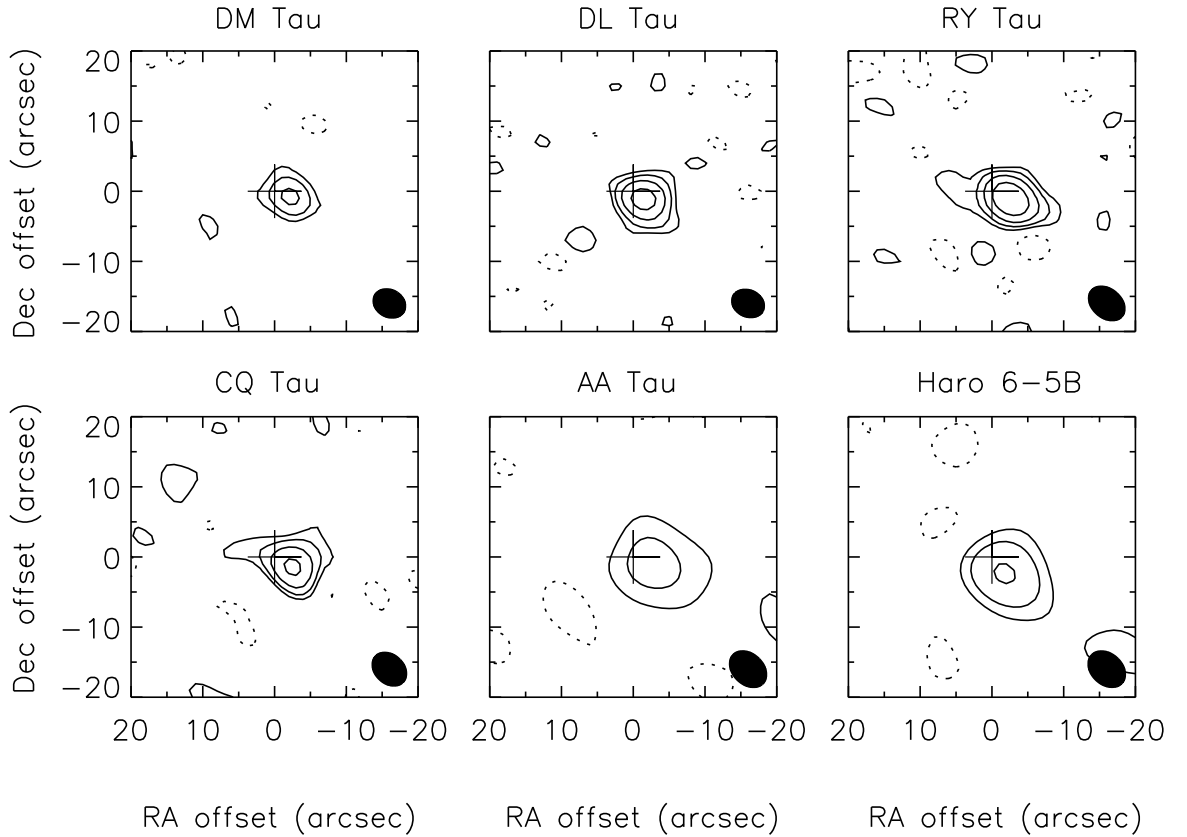[b] Integrated flux measured using a gaussian fit for DM Tau.

Figure 6.2: 2.7 mm continuum maps. The rms level of the maps is 1 mJy beam^{-1} and the contour levels are $-2, 2, 4, 8, 16, 32$ mJy beam^{-1} in all panels.

6.4 DISCUSSION

6.4.1 Modelling the millimetre continuum emission

The dust thermal continuum emission in the millimetre wavelength range is optically thin in discs of dust masses close to 10^{-4} M$_\odot$ and sizes of several hundred AU, as is the case for the sources in our sample. It is dominated by the dust located in the cold and dense disc midplane, which contains almost all of the disc dust mass. Throughout the literature, the millimetre flux is used to make disc mass estimates (e.g., Beckwith et al. 1990; Osterloh & Beckwith 1995; Mannings & Sargent 1997; Andrews & Williams 2005, 2007). The estimates are, however, heavily affected by the uncertainty in the millimetre dust emissivity that varies from roughly 0.1 to 2 cm^2 g^{-1} in circumstellar discs (see Draine 2006, for a detailed discussion). A frequent assumption of a single temperature for the entire disc, neglecting the disc temperature and density structure, introduces a further uncertainty in the mass estimates. In our analysis we make simple assumptions of the disc radial structure, relying on the results from the literature, and use a radiative transfer code to calculate the observed millimetre fluxes. We adopt the
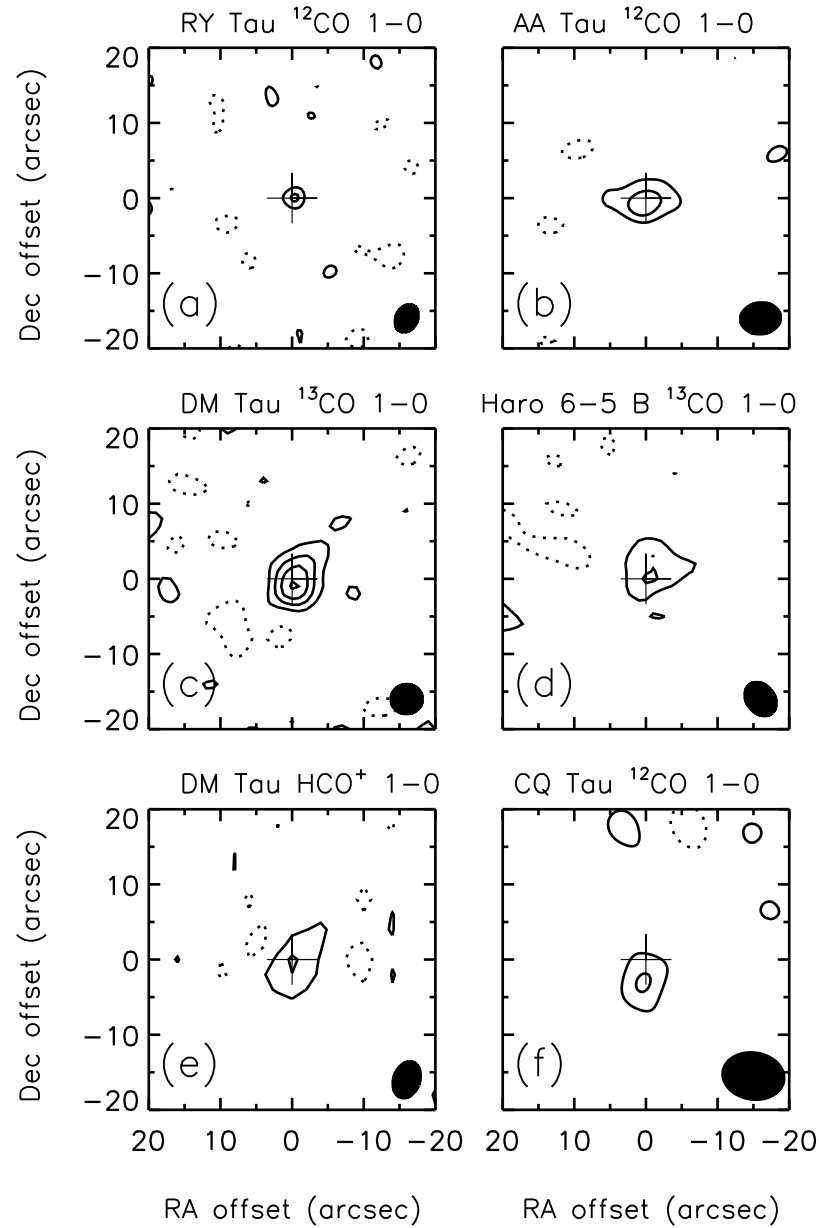
Figure 6.3: Integrated intensity images of the spatially unresolved molecular line emission from sources with detections or marginal detections. *(a):* RY Tau, ^{12}CO J=1–0 line integrated over 5.1-6.7 km/s velocity range. Contour levels -2,2,3×172 mJy beam^{-1} km s^{-1} (0.172 mJy beam^{-1} km s^{-1}=1 σ). *(b):* AA Tau, ^{12}CO J=1–0 line integrated over 4.9-9.1 km/s velocity range. Contour levels -2,2,4,6×200 mJy beam^{-1} km s^{-1} (200 mJy beam^{-1} km s^{-1}=1 σ). *(c):* DM Tau, ^{13}CO J=1–0 line integrated over 5.1-7.1 km/s velocity range. Contour levels -2,2,4,6,8×84 mJy beam^{-1} km s^{-1} (84 mJy beam^{-1} km s^{-1}=1 σ). *(d):* Haro 6-5B, ^{13}CO J=1–0 line integrated over 5.3-6.6 km/s velocity range. Contour levels -2,2,4×157 mJy beam^{-1} km s^{-1} (157 mJy beam^{-1} km s^{-1}=1 σ). *(e):* DM Tau, HCO$^+$ J=1–0 line integrated over 5.4-7.1 km/s velocity range. Contour levels -2,2,4×71 mJy beam^{-1} km s^{-1} (71 mJy beam^{-1} km s^{-1}=1 σ). *(f):* CQ Tau, ^{12}CO J=1–0 line integrated over 4.4-6.1 km/s velocity range. Contour levels -2,2,3×250 mJy beam^{-1} km s^{-1} (250 mJy beam^{-1} km s^{-1}=1 σ).
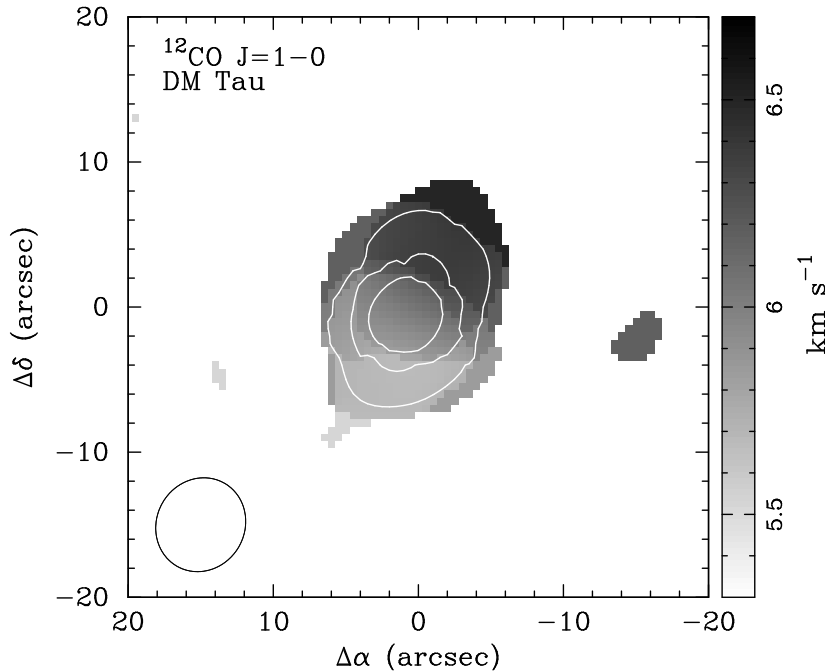
Figure 6.4: First moment map of the ^{12}CO J=1–0 emission towards DM Tau. Integrated intensity is shown with 500 mJy beam^{-1} contours (white). The synthesized beam size and orientation are indicated with the black ellipse.

highest millimetre dust emissivity expected in discs, corresponding to grain growth to millimetre sizes, and thus provide an estimate of a minimum amount of dust present in these discs. We obtain best fit models of our interferometric 2.7 mm data and the 1.3 mm flux from the literature, simultaneously.

Disc temperature structure. Our disc models are vertically isothermal and the expression for the temperature $T = T_{100} \left(R/100 \, \text{AU} \right)^{-q}$ is based on the midplane temperature in disc models of D'Alessio et al. (2005b), for the spectral types of our sources and an age of 1 Myr. The models for 10 Myr old sources may provide somewhat different temperatures but we do not use these, considering that that our sources are all estimated to be younger. The assumption of a vertically isothermal disc structure is appropriate for the optically thin thermal millimetre emission that is heavily dominated by the cold disc midplane, as the density decreases exponentially with height while the temperature increase is roughly linear. The values of T_{100} and q are listed in Table 6.3 for each source. In some cases a single power law does not provide a good mathematical description of the midplane temperature given by the D'Alessio et al. (2005b) models, and we use different power laws for the inner and the outer disc regions to reproduce their temperature values (see Table 6.3). For DM Tau, DL Tau, AA Tau and Haro 6-5 B we use the midplane temperature given by the models of D'Alessio et al. (2005b) for a disc around a K7 star, which is approximately $T = 16 \left(R/100 \, \text{AU} \right)^{-0.35}$ K in the inner few hundred AU but levels to 10 K in the outermost disc regions where the interstellar radiation field dominates the midplane temperature. This power-law description is valid irrespective of the size of grains assumed in the D'Alessio et al. models (1 μm$-$1 mm). For RY Tau we use a K1 star with a disc temperature of $T = 28 \left(R/100 \, \text{AU} \right)^{-0.45}$ K within 70 AU from the star, and $T = 26 \left(R/100 \, \text{AU} \right)^{-0.4}$ K beyond that radius. This description corresponds to micron-sized grains, while the disc model with millimetre-

sized grains has a 10% lower temperature and would yield up to 10% higher mass estimate. For CQ Tau, we use a temperature of $T = 50\,(R/100\,\mathrm{AU})^{-0.5}$ K corresponding to the midplane temperature of a disc around an F1 star. As in the case of RY Tau, this description corresponds to micron-sized grains. A 15% higher mass estimate may be obtained if millimetre-sized grains are assumed. As grains grow to millimetre sizes the amount of small grains decreases and thus less incident radiation is captured by the disc, since the small grains are the most effective absorbers at short wavelengths (D'Alessio et al. 2005a). However, the temperature decrease in the models we use is $\leq$15%, fraction not significant in terms of the mass estimate. We focus our dust emission analysis on deriving the lower limits on the dust mass and therefore use only the models with micron-sized grains.

Disc surface density distribution. The disc dust mass M_{dust} is our free fit parameter and the surface density $\Sigma \propto R^{-p}$ is distributed with a radial slope p=1. This slope, representative of a steady state viscous disc (Hartmann et al. 1998; D'Alessio et al. 1998, 1999; Calvet et al. 2002) is consistent with the observationally constrained values in some well-studied discs (Wilner et al. 2000; Pinte et al. 2008). Andrews & Williams (2007) report a median value of p=0.5 based on the SEDs and submillimetre continuum observations of a sample of 24 discs, but stress that this estimate is closely related to the assumptions of the disc temperature structure, and that a steeper median slope of p=1 is more reasonable. In their recent study of the dust distribution in T Tauri discs using high-resolution millimetre data, Isella et al. (2009) show that a power-law disc surface density distribution modified by an exponential taper is a good description of disc structure, also proposed by Hughes et al. (2008). However, our assumption of a single power-law is a good approximation for the overall disc structure at scales of several hundred AU, especially considering the limited spatial resolution of our data.

We use the vertical density distribution of a disc in hydrostatic equilibrium, calculated for the assumed temperature and surface density at a given radius. The inner radius of the disc is irrelevant for the disc millimetre emission, and its value is set to an arbitrary value of 0.6 AU. We adopt values for the outer radius and the disc inclination as determined through spatially resolved submillimetre interferometric observations of our sources in the literature, listed in Table 6.3. A good determination of R_{out} is essential for the interpretation of the spatially unresolved continuum and line emission in the submillimetre, dominated by the outer disc regions. We use the radiative transfer code RATRAN (Hogerheijde & van der Tak 2000) to calculate the 1.3 and 2.7 mm continuum flux, adopting the dust emissivity $\kappa = \kappa_{1.3\,\mathrm{mm}}\,(\lambda/1.3\,\mathrm{mm})^{\beta}$. We use β as derived in Sect. 6.3 (see Table 6.1), and a dust emissivity of $\kappa_{1.3\,\mathrm{mm}}$ =2 cm^{2}g^{-1}. These emissivities are not necessarily the same as those used in the SED modelling to derive the disc temperature structure (see above). The millimetre contiunuum emission is dominated by the properties and emissivity of the grains in disc midplane regions where the density is the highest and grain growth is most efficient. Conversely, the SED modelling is sensitive to the small dust population in the disc (Meijer et al. 2008), and to the disc layers at some height above the midplane due to optical thickness of the infrared emission. Vertical stratification of grain sizes (and thus emissivity) caused by grain growth and settling was found in some sources (e.g., T Tauri star IM Lup, Pinte

et al. 2008). Therefore, there is no inconsistency in our assumption of different dust emissivities for the upper and midplane layers.

We fit the 1.3 and 2.7 mm continuum flux simultaneously, and derive the minimum dust masses of $(0.7\text{-}4.5)\times10^{-4}$ $M_\odot$, shown in Table 6.3. Figure 6.1 shows the synthetic visibilities from our best fit models compared to the 2.7 mm visibilities observed with CARMA. In a recent study of spatially resolved submillimetre continuum emission in discs, Andrews & Williams (2007) use similar parametrisations for disc structure and simultaneously fit to the SED and submillimetre emission for a number of discs. Their results are consistent with our lower limits in Table 6.3 for AA Tau, DL Tau and RY Tau. However, for DM Tau they derive a dust mass of $1.4^{+0.3}_{-0.2}\times10^{-4}$ $M_\odot$, lower than our minimum dust mass of 2.5×10^{-4} $M_\odot$, probably due to their assumption of a disc radius of 150^{+250}_{-100}, much smaller than the outer disc radius derived from other spatially resolved observations of this source ranging from 650 AU to 890 AU (Simon et al. 2000; Dartois et al. 2003; Piétu et al. 2007). In a smaller disc, the bulk of the disc mass located in the outermost disc regions is at a comparably higher temperature than in a larger disc. This means that the submillimetre flux measurement (dominated by the outer regions) yields a lower mass estimate in a smaller disc. This is valid for optically thin submillimetre emission. Our minimum dust mass estimates correspond to the total disc mass of $(0.7\text{-}4.5)\times10^{-2}$ $M_\odot$ when a gas-to-dust mass ratio of g/d=100 is assumed.

6.4.2   Modelling the ^{12}CO and ^{13}CO J=1–0 emission

Comparison with the dust disc models

We use the disc models described in Sect. 6.4.1 (*dust disc models* hereafter), with the derived minimum dust masses and a gas-to-dust mass ratio of g/d=100, to analyse the ^{12}CO and ^{13}CO J=1–0 emission. We adopt a ^{12}CO gas phase abundance [^{12}CO]=10^{-4} with respect to H$_2$ (Frerking et al. 1982; Lacy et al. 1994) and a [^{12}C]/[^{13}C] isotopic ratio of 77 (Wilson & Rood 1994), constant throughout the disc. A more realistic disc model requires including the freeze-out of ^{12}CO and its isotopologues onto dust grains, through a decreased ^{12}CO abundance in the cold midplane regions. For the purpose of a simple comparison of gas and dust emission we neglect this process. In Sect. 6.4.3, we fit the line spectra and derive molecular abundances, providing estimates of ^{12}CO depletion factors. We calculate the molecular line emission using the molecular excitation and radiative transfer code RATRAN. The velocity field is given by Keplerian rotation (see Table 6.1 for stellar masses used). We sample the synthetic line emission in the *uv*-plane according to our obtained interferometric data and derive synthetic images and spectra using the MIRIAD data reduction package.

The comparison between the modelled and observed spectra is shown in Fig. 6.5, where the line intensity is summed over a several arcseconds wide region centered at the position of the source. An important first conclusion is that, without adjusting any parameters, the modelled line intensity differs by at most a factor of two to three from the observed line intensity. In the sources where we firmly detect the ^{12}CO and/or ^{13}CO J=1–0 line (DM Tau, AA Tau and Haro 6-5 B), the modelled line shape matches

Table 6.3: Adopted model parameters and derived minimum dust mass.

Source	R_{out} [a] (AU)	i [a] (°)	T_{100} (K)	q	$M_{\mathrm{dust}}(min)$ [b] (10^{-4} $M_\odot$)
DM Tau	890	32	16	0.35 (if T<11 then T=11)	2.5
DL Tau	400	35	16	0.35 (if T<10 then T=10)	4.5
RY Tau	150	25	28 (26 beyond 70 AU)	0.45 (0.4 beyond 70 AU)	1.9
CQ Tau	200	29	50	0.5	0.65
AA Tau	300	70	16	0.35	2.0
Haro 6−5 B	300	75	16	0.35	3.7

[a] Disc size and inclination from interferometric imaging (Piétu et al. 2007; Simon et al. 2000; Koerner & Sargent 1995; Chapillon et al. 2008; Pinte & Ménard 2005) or assumed relying on near-infrared imaging (Grady 2004; Padgett et al. 1999)

[b] Calculated using κ_{230}=2 cm^2 g$_{\mathrm{dust}}^{-1}$ and α given in Table 6.1.
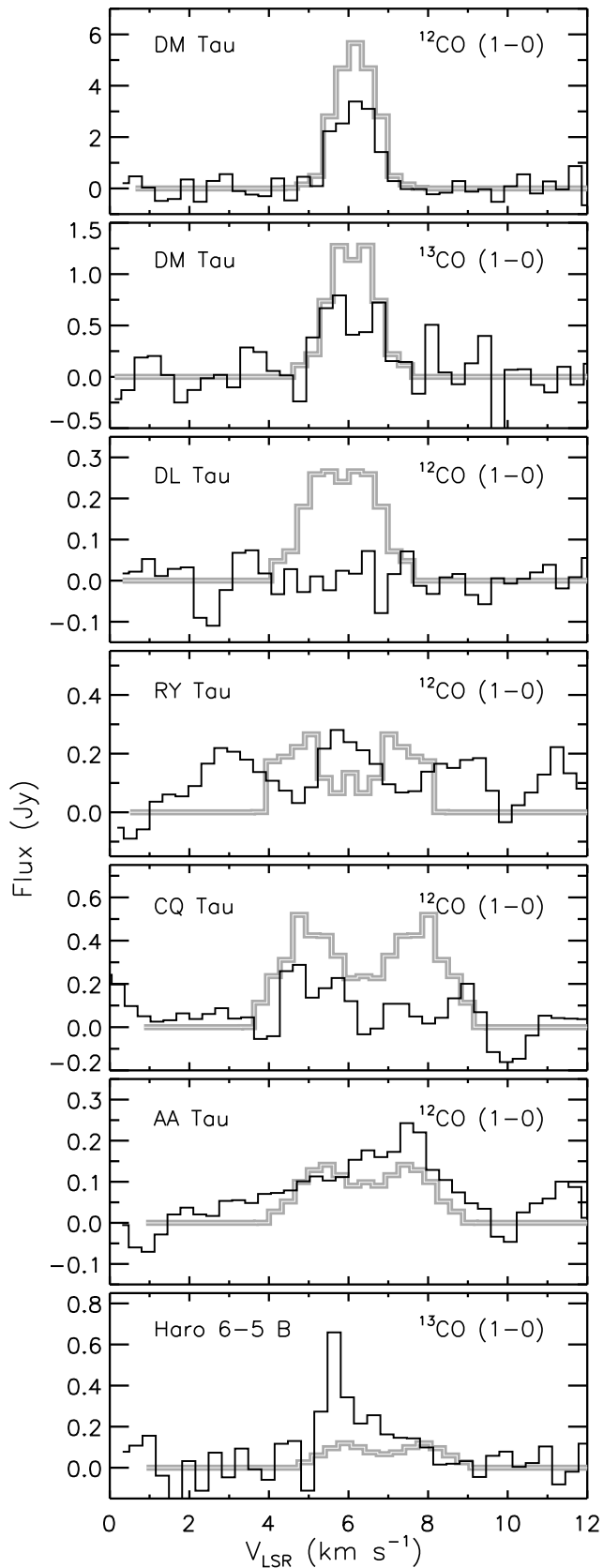
Figure 6.5: The observed ^{12}CO and ^{13}CO J=1–0 line spectra (black lines) compared to the synthetic line spectra (thick grey-white lines) from the disc models that fit the dust continuum emission, calculated without any adaptation of the model parameters. The spectra are integrated over a region centered on the source position, of the following sizes: for DM Tau $20'' \times 20''$, for CQ Tau $8'' \times 8''$, and for the remaining sources: $4'' \times 4''$.
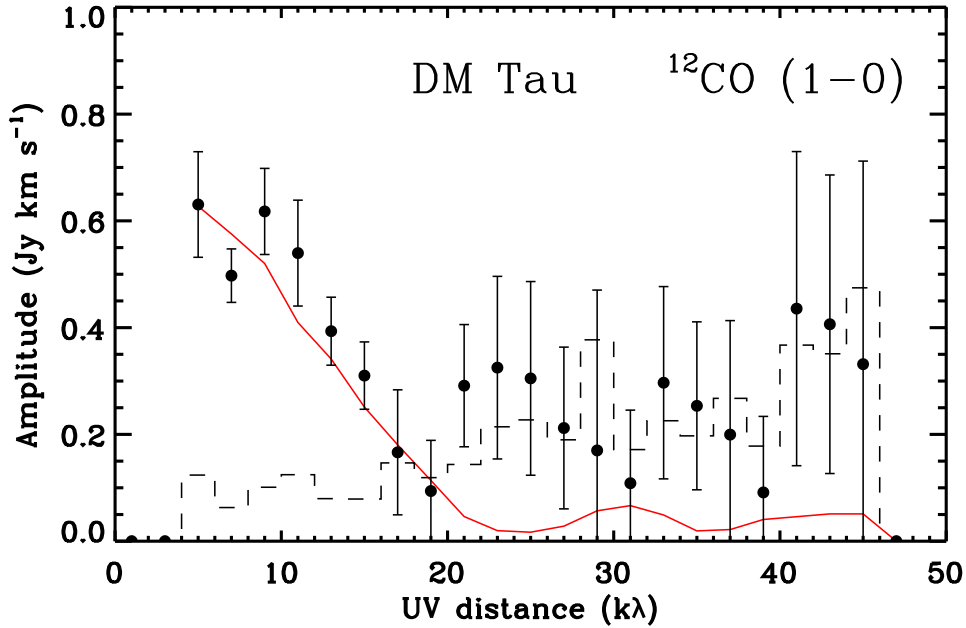
Figure 6.6: The vector-averaged ^{12}CO J=1–0 line flux from DM Tau (black symbols) integrated over the velocity range of 5.8-7.5 km s^{-1}, plotted versus the *uv*-distance. Dashed black lines represent the zero-signal expectation value of our line visibility data. The visibilities of our best-fit model are shown with the full line. The model corresponds to a ^{12}CO depletion factor of f_d=10 within 750 AU and of f_d=100 between 750 AU and the disc outer radius of 890 AU. The wavy shape of the model visibilities beyond 25 kλ is due to the adopted sharp outer edge of the disc and step function of f_d.

the observations well. In sources with a weak detection of the ^{12}CO J=1–0 line, RY Tau and CQ Tau, the observed spectral profiles are not well defined because of the low signal-to-noise ratio, and cannot be compared well to the models. The dust disc model of DL Tau predicts a ^{12}CO J=1–0 line with a peak intensity of 0.25 Jy integrated over $4'' \times 4''$ centered on the source (0.66 Jy beam^{-1}) detectable at 3σ in our observations. However, there is no detected ^{12}CO J=1–0 line emission in our observations. The reason for this is confusion of the ^{12}CO emission from DL Tau with the foreground cloud material in the interferometric observations, in the velocity range 5.0-6.6 km s^{-1} as discussed in Simon et al. (2000) where the ^{12}CO J=2–1 line observations are presented. We conclude that all ^{12}CO J=1–0 emission above the noise level of our observations is likely absorbed by the foreground cloud. Using data from Simon et al. (2000) we find that the emission from the dust disc model is consistent with the observed ^{12}CO J=2–1 emission at the velocities higher than 6.6 km s^{-1}, where the emission from the disc is unaffected by the cloud, see Fig. 6.7.

The differences between the models and observations are not large, considering the simplistic approach to the disc structure and the molecular abundances applied here. The fact that the intensities of the synthetic spectra are roughly consistent with the
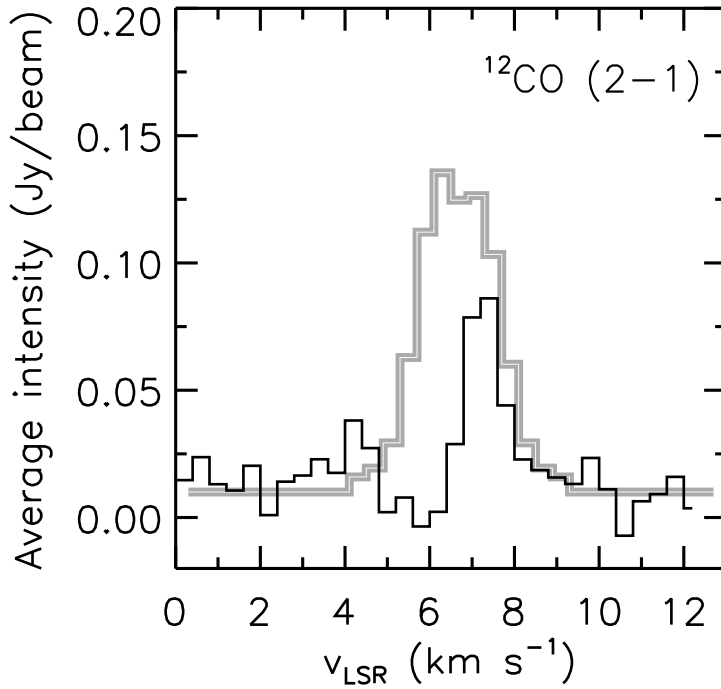
Figure 6.7: ^{12}CO J=2–1 spectrum of DL Tau (Simon et al. 2000) shown in black, compared to our dust disc model of this source (thick grey-white line). The spectral region where the emission is confused with the foreground cloud is 5.0-6.6 km s^{-1}.

observations in all our sources shows that the parametric models of dust emission at millimetre wavelengths are good starting points for the detailed modelling of molecular lines in discs around T Tauri stars. This is consistent with our finding for the intermediate-mass young stars (Herbig AeBe stars) that similar parametric models can be used to reproduce the low-J ^{12}CO line spectra while models derived based on SED alone do not (Chapter 5 of this thesis). It is important to stress that the knowledge of R_{out} is crucial in this approach, as the submillimetre line and continuum emission are very sensitive to the outer disc regions.

6.4.3   Optimising the model parameters

In this section we take a step further in the modelling of the molecular lines and explore to what extent the observed emission probes the molecular abundances, the temperature in the line emitting layer, and the overall gas-to-dust mass ratio. Starting from the disc models obtained in the previous section, which are entirely based on the observed millimetre fluxes and theoretical calculations of the disc midplane temperature for the young stars of the given spectral type, and using a gas-to-dust mass ratio of 100, we vary the basic disc parameters to fit the observed spectral line profiles.

In those sources where the emission from the dust disc model exceeds the observed line intensity, DM Tau and CQ Tau, the fit to the spectral profile is obtained with the ^{12}CO abundance as a free parameter. We assume that the gas temperature is the temperature of the disc midplane, the coldest disc region. This assumption is appropriate for optically thin line emission, while for the optically thick lines warmer layers above
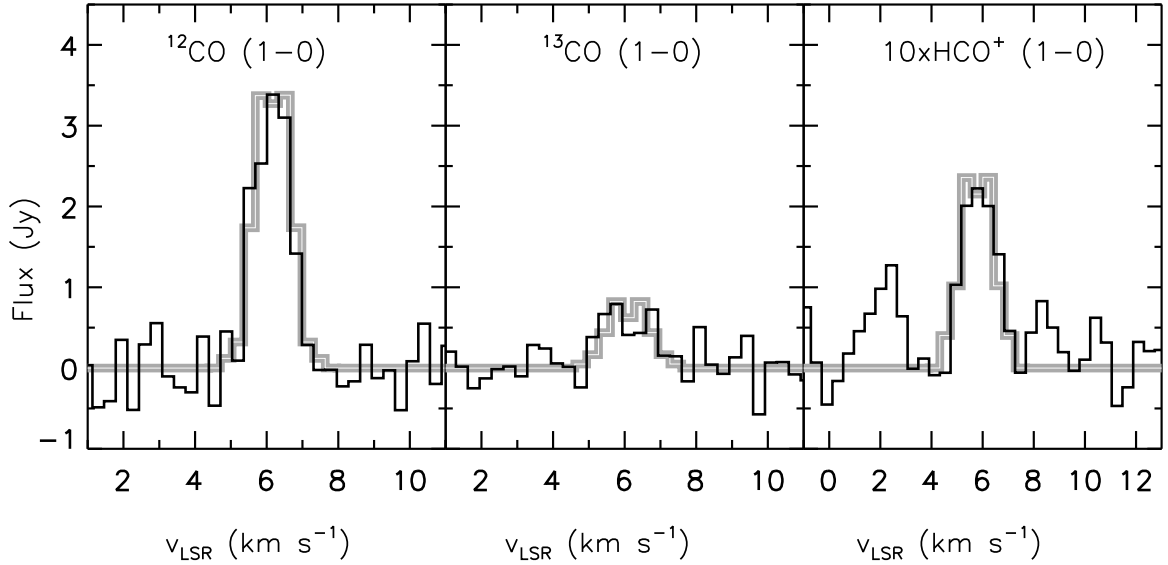
Figure 6.8: The observed ^{12}CO, ^{13}CO and HCO$^+$ J=1–0 line spectra (black) compared to our best fit model for dust and gas in DM Tau (thick grey-white line). The flux is integrated over a $20'' \times 20''$ region centered on the DM Tau position.

the midplane dominate the line emission. Our assumption of a relatively low gas temperature results in an upper limit on the amount of gas phase ^{12}CO. In these two discs, we find that ^{12}CO is depleted by factors 10-100 by freeze-out and/or an overall gas dispersal.

In the sources where the dust disc model underestimates the observed line intensity, CQ Tau, AA Tau and Haro 6-5 B, the spectra are fitted by increasing the gas temperature. In this scenario, the disc is emitting optically thick ^{12}CO and ^{13}CO lines, relatively insensitive to the amount of gas-phase ^{12}CO. The fits provide lower limits of the temperature of the disc layer where the lines are emitted.

DM Tau. To fit the ^{12}CO J=1–0 spectrum of DM Tau, overestimated by the dust disc model by a factor ≈ 2, we decrease the ^{12}CO gas phase abundance $[^{12}CO] = 10^{-4}/f_{\rm d}$, where $f_{\rm d}$ is the ^{12}CO depletion factor. Moderate depletion of ^{12}CO is reported in previous molecular line observations of this disc (Dutrey et al. 1997; Dartois et al. 2003). The assumed midplane temperature is the minimum temperature for the ^{12}CO emitting layer and cannot be decreased further, therefore it is necessary to decrease the molecular abundance. The same reasoning is applied when fitting the ^{13}CO J=1–0 spectrum, overestimated by the dust disc model that assumes the isotopic ratio $[^{12}CO]/[^{13}CO]$=77 and the ^{12}CO gas phase abundance of 10^{-4}. We find that it is not possible to fit both the ^{12}CO and ^{13}CO J=1–0 spectra with a single value of $f_{\rm d}$ throughout the disc. The fit to the ^{13}CO J=1–0 results in f_d =10, while the fit to the ^{12}CO J=1–0 results in f_d =100. This apparent discrepancy cannot be explained by an anomalous isotopic ratio, because the isotopic fractionation, e.g., when ^{13}CO is photodissociated in layers where the more abundant ^{12}CO is self-shielding, causes an increase of $[^{12}CO]/[^{13}CO]$, and not a decrease. However, a radially increasing depletion factor, perhaps due to an enhanced

penetration of the interstellar radiation field in the outer disc regions of DM Tau can reproduce both lines. We assume f_d as a radial step function, with a break at 750 AU, the radius where ^{13}CO emission in our synthetic images becomes negligible with respect to the ^{12}CO emission. In this way we obtain a fit to the observed spectra with f_d =10 within 750 AU and f_d =100 beyond this distance from the star. Our fit to the spectra is shown in Fig. 6.8. Our result is consistent with that of Piétu et al. (2007) where the radially increasing depletion factor $f_d \propto R^{-p_m}$ is derived, with p_m in the range from 3 to 5 for a set of ^{12}CO and ^{13}CO low-J rotational transitions. Our best fit model yields a mass of the gas phase ^{12}CO $M_{^{12}CO}$=3×10^{-6} M$_\odot$ and of ^{13}CO $M_{^{13}CO}$=4×10^{-8} M$_\odot$. These values represent upper limits, as the ^{12}CO mass may be lower if a higher gas temperature is assumed.

The HCO$^+$ J=1–0 line observed towards DM Tau is fitted by using our dust disc model and HCO$^+$ abundance [HCO$^+$]=3×10^{-10} with respect to H$_2$, constant throughout the disc. The fit to the spectral line is shown in Fig. 6.8. However, this model overestimates the HCO$^+$ J=4–3 emission observed by Greaves (2004) by a factor ≈10. This suggests that the HCO$^+$ emission does not arise in the disc midplane but, as predicted by the work of van Zadelhoff et al. (2001) and Semenov et al. (2008), in a lower density layer of intermediate height. If the density of the emitting gas is $\leq 10^{-6}$ cm^{-3}, the J=4–3 line is less efficiently excited than in the dense midplane.

DL Tau. As mentioned above, the ^{12}CO J=1–0 line emission from DL Tau is heavily affected by confusion with the foreground cloud and our non-detection provides no information regarding the disc's gas content. However, the dust disc model is consistent with the detected ^{12}CO J=2–1 emission (data from Simon et al. 2000) at high velocities, see Fig. 6.7, and suggests a ^{12}CO gas mass of $M_{^{12}CO}$=6×10^{-5} M$_\odot$, obtained from our dust model assuming g/d=100 and no depletion.

RY Tau. The ^{12}CO J=1–0 line intensity from the dust disc model matches the observed line intensity, while the line shape is poorly defined in the marginal detection of the line emission, see Fig. 6.5. The model uses a mass of the gas-phase ^{12}CO of $M_{^{12}CO}$=3×10^{-5} M$_\odot$, corresponding to g/d=100 and no depletion.

CQ Tau. The dust disc model for CQ Tau overestimates the observed ^{12}CO J=1–0 line emission. Following the approach used for DM Tau, we use a ^{12}CO depletion factor f_d to fit the observations and derive upper limit on the mass of gas-phase ^{12}CO in this disc. The fit to the observed spectrum can be seen in Fig. 6.9. A constant of f_d=100 reproduces the observations well, with $M_{^{12}CO}$=9×10^{-8} M$_\odot$. Because this value is obtained using the disc midplane temperature, i.e., the lowest possible gas temperature in the disc, it represents an upper limit on the mass of the gas-phase ^{12}CO in the disc.

AA Tau. Opposite to the cases of DM Tau and CQ Tau, for AA Tau the dust disc model underestimates the observed line emission. Our line calculations for the AA Tau dust disc model show that its ^{12}CO J=1–0 line emission is optically thick, and insensitive to the disc mass (M_{disc}=2×10^{-4} M$_\odot$). Therefore we increase the gas temperature in the disc to fit the observed line flux. By increasing the disc temperature from $T = 16 \, (R/100 \, \mathrm{AU})^{-0.35}$ to $T = 24 \, (R/100 \, \mathrm{AU})^{-0.35}$ we reproduce the observed ^{12}CO J=1–0 spectrum. Our fit is shown in Fig. 6.9. However, even higher temperatures are possible if lower values for [^{12}CO] or g/d are allowed. Therefore we conclude that the
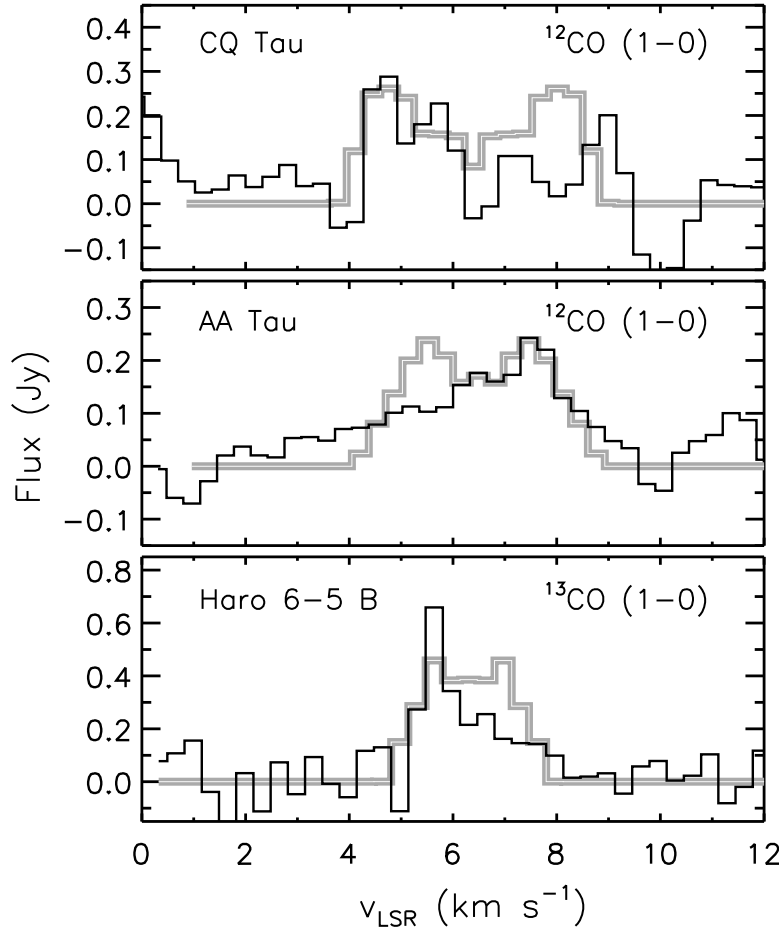
Figure 6.9: The observed ^{12}CO J=1–0 emission of CQ Tau and AA Tau, and the ^{13}CO J=1–0 emission of Haro 6-5 B (black), compared to the best fit models for dust and gas (thick grey-white line). The flux is integrated over a $4'' \times 4''$ region centered on the position of each source.

^{12}CO emission arises in a warm layer above the midplane, but cannot derive information about $f_{\rm d}$ or g/d. We note that the asymmetry in the spectral profile may be due to the large scale asymmetry in the disc around AA Tau, suggested by the quasi-periodic eclipses of the stellar photosphere by the circumstellar material (Bouvier et al. 1999; Pinte et al. 2008). Another possible explanation for the line asymmetry may be confusion with the foreground cloud, as in the case of DL Tau.

Haro 6-5 B. The ^{13}CO J=1–0 line observed towards Haro 6-5 B is stronger than the dust disc model predicts. We find that the line is optically thick and cannot be fitted by increasing the gas mass or molecular abundance. We use the same approach as for AA Tau, i.e., we scale the temperature in the model linearly to fit the line. The best fit is obtained for a temperature of $T = 32\,(R/100\,{\rm AU})^{-0.35}$, two times larger than the disc midplane temperature. The observed narrow line width is fitted by adopting a disc inclination of 30° (Fig. 6.9), lower than the 70° obtained from the scattered light images of this source and used in the dust disc model. In Dutrey et al. (1996) the ^{13}CO emission from this source was found to be well described by a qualitatively similar parametric disc model with $R_{\rm out}$=150 AU and i=0, while Yokogawa et al. (2002) derive a much larger disc size of $R_{\rm out}$=1300 AU and find the line emission consistent with

i=70°. Clearly, the inclination is very sensitive to the adopted outer radius, and submillimetric observations at a sufficiently high spatial resolution are necessary to constrain the disc size better. So far, the ^{13}CO J=1–0 line emission indicates that the scattered light imaging (Padgett et al. 1999) likely does not trace the full extent of the disc, and that the disc is larger than their derived size of 300 AU. Our fit suggests that the ^{13}CO J=1–0 line emission is dominated by a disc layer roughly two times warmer than the disc midplane. As for AA Tau, we cannot derive information about the amount of gas in the disc, or ^{13}CO abundance.

6.5   SUMMARY AND CONCLUSIONS

We report observations of the molecular lines ^{12}CO, ^{13}CO and HCO$^+$ J=1–0, as well as the 2.7 mm dust continuum emission towards a sample of discs around T Tauri stars.

The 2.7 mm continuum fluxes, combined with reported fluxes at 1.3 mm, yield minimum disc dust masses of approximately 10^{-4} M$_\odot$. We obtain very rough estimates of the dust millimetre emissivity slopes, but we cannot draw conclusions about the type of dust present in these discs. The dust mass estimates are comparable to the values found for discs around T Tauri stars in the literature (Beckwith et al. 1990).

The molecular line detections are roughly consistent with the observed millimetre fluxes, in the framework of simple parametric disc models. The ^{12}CO and HCO$^+$ J=1–0 line intensity is the highest in our largest disc, DM Tau with an outer radius of 890 AU.

We can divide the sources in our sample in two groups. In the first group are the sources where a ^{12}CO depletion factor must be invoked to account for the low line fluxes even when the molecular line emission is assumed to arise from very low temperatures as found in the disc midplane. In these sources, substantial amounts of the ^{12}CO and isotopologues are efficiently removed from the gas-phase, either through freeze-out and/or photo-dissociation resulting in [^{12}CO]$<10^{-4}$, or in a significant overall gas loss with g/d <100. The discs around DM Tau and CQ Tau fall in this category. In these sources we derive the maximum gas masses of ^{12}CO. Through the comparison with the minimum dust masses that we derive in these discs, the following constraint can be placed on the depletion factor and the gas-to-dust mass ratio:

$$\frac{M_{\mathrm{CO}}(\mathrm{max})}{M_{\mathrm{dust}}(\mathrm{min})} \geq 10^{-4} \frac{m_{\mathrm{CO}}}{m_{\mathrm{H_2}}} \frac{g/d}{f_d}. \tag{6.1}$$

For DM Tau we obtain $g/d\, f_d^{-1} \leq 9$, and CQ Tau $g/d\, f_d^{-1} \leq 1$. We speculate that the low amount of CO gas with respect to dust in DM Tau is due to freeze-out, a process expected to be efficient in the outer regions of discs around T Tauri stars where the temperature is below 20 K. Because of the large outer radius, DM Tau has most of its mass located in these cold regions. CQ Tau, on the other hand, is warm and small. The lack of CO gas suggested by our results is likely due to the stronger stellar radiation field and age close to 10 Myr. The evidence of grain growth and dust settling reported for this disc point to a scenario of an overall gas loss. In the second group of discs are AA Tau and Haro 6-5 B, and their observed ^{12}CO and ^{13}CO line emission is optically thick. Therefore no information can be obtained regarding the amount of the molecular

gas from the observed lines. In these discs we find that the line emission comes from disc layers warmer than the disc midplane, by factors 1.5-2.0, and thus located at some height above the disc midplane. CO observations at a higher spatial resolution ($\approx 1''$) would be useful to determine the outer radius of these two discs better, and thus test our finding.

We conclude that, while the disc structure models based on the millimetre continuum modelling (i.e., Andrews & Williams 2007; Isella et al. 2009, and this work) are good starting points for modelling the rotational emission from cold molecular gas, discs apparently similar in their cold dust emission may vary drastically in their ^{12}CO gas mass content, due to freeze-out, photodissociation and/or gas dispersal. Therefore, molecular line observations are necessary to asses the disc gas content. Instead using detailed three-dimensional disc structure models with a number of free parameters to interpret the millimetre dust and ^{12}CO line fluxes, valuable constraints on M_{dust} and $g/d\,f_d^{-1}$ can be obtained if the parameter uncertainties are minimised. In this paper, we show how this can be done by assuming extreme conditions (maximum emissivity, minimum temperature) in combination with a most simplistic disc model. A prior knowledge of disc outer radius and inclination is essential in deriving these information from spatially unresolved observations.

REFERENCES

Akeson, R. L., Walker, C. H., Wood, K., et al. 2005, ApJ, 622, 440

Andrews, S. M. & Williams, J. P. 2005, ApJ, 631, 1134

Andrews, S. M. & Williams, J. P. 2007, ApJ, 659, 705

Beckwith, S. V. W., Sargent, A. I., Chini, R. S., & Guesten, R. 1990, AJ, 99, 924

Bouvier, J., Chelli, A., Allain, S., et al. 1999, A&A, 349, 619

Calvet, N., D'Alessio, P., Hartmann, L., et al. 2002, ApJ, 568, 1008

Chapillon, E., Guilloteau, S., Dutrey, A., & Piétu, V. 2008, A&A, 488, 565

Chiang, E. I., Joung, M. K., Creech-Eakman, M. J., et al. 2001, ApJ, 547, 1077

D'Alessio, P., Calvet, N., Hartmann, L., Lizano, S., & Cantó, J. 1999, ApJ, 527, 893

D'Alessio, P., Calvet, N., & Woolum, D. S. 2005a, in Astronomical Society of the Pacific Conference Series, Vol. 341, Chondrites and the Protoplanetary Disk, ed. A. N. Krot, E. R. D. Scott, & B. Reipurth, 353

D'Alessio, P., Canto, J., Calvet, N., & Lizano, S. 1998, ApJ, 500, 411

D'Alessio, P., Merín, B., Calvet, N., Hartmann, L., & Montesinos, B. 2005b, Revista Mexicana de Astronomia y Astrofisica, 41, 61

Dartois, E., Dutrey, A., & Guilloteau, S. 2003, A&A, 399, 773

Doucet, C., Pantin, E., Lagage, P. O., & Dullemond, C. P. 2006, A&A, 460, 117

Draine, B. T. 2006, ApJ, 636, 1114

Dutrey, A., Guilloteau, S., Duvert, G., et al. 1996, A&A, 309, 493

Dutrey, A., Guilloteau, S., & Guelin, M. 1997, A&A, 317, L55

Dutrey, A., Guilloteau, S., Piétu, V., et al. 2008, A&A, 490, L15

Frerking, M. A., Langer, W. D., & Wilson, R. W. 1982, ApJ, 262, 590

Grady, C. A. 2004, in Astronomical Society of the Pacific Conference Series, Vol. 321, Extrasolar
    Planets: Today and Tomorrow, ed. J. Beaulieu, A. Lecavelier Des Etangs, & C. Terquem, 244

Greaves, J. S. 2004, MNRAS, 351, L99

Guilloteau, S. & Dutrey, A. 1994, A&A, 291, L23

Guilloteau, S. & Dutrey, A. 1998, A&A, 339, 467

Handa, T., Miyama, S. M., Yamashita, T., et al. 1995, ApJ, 449, 894

Hartmann, L., Calvet, N., Gullbring, E., & D'Alessio, P. 1998, ApJ, 495, 385

Hogerheijde, M. R. & van der Tak, F. F. S. 2000, A&A, 362, 697

Hughes, A. M., Andrews, S. M., Espaillat, C., et al. 2009, ApJ, 698, 131

Hughes, A. M., Wilner, D. J., Qi, C., & Hogerheijde, M. R. 2008, ApJ, 678, 1119

Isella, A., Carpenter, J. M., & Sargent, A. I. 2009, ArXiv e-prints

Kenyon, S. J. & Hartmann, L. 1995, ApJS, 101, 117

Kessler-Silacci, J. 2004, PhD thesis, AA(California Institute of Technology)

Koerner, D. W. & Sargent, A. I. 1995, AJ, 109, 2138

Lacy, J. H., Knacke, R., Geballe, T. R., & Tokunaga, A. T. 1994, ApJ, 428, L69

Mannings, V. & Sargent, A. I. 1997, ApJ, 490, 792

Meijer, J., Dominik, C., de Koter, A., et al. 2008, A&A, 492, 451

Mora, A., Merín, B., Solano, E., et al. 2001, A&A, 378, 116

Osterloh, M. & Beckwith, S. V. W. 1995, ApJ, 439, 288

Padgett, D. L., Brandner, W., Stapelfeldt, K. R., et al. 1999, AJ, 117, 1490

Piétu, V., Dutrey, A., & Guilloteau, S. 2007, A&A, 467, 163

Pinte, C. & Ménard, F. 2005, in Astronomical Society of the Pacific Conference Series, Vol. 343,
    Astronomical Polarimetry: Current Status and Future Directions, ed. A. Adamson, C. As-
    pin, C. Davis, & T. Fujiyoshi, 201

Pinte, C., Padgett, D. L., Menard, F., et al. 2008, ArXiv e-prints, 808

Qi, C., Kessler, J. E., Koerner, D. W., Sargent, A. I., & Blake, G. A. 2003, ApJ, 597, 986

Rodmann, J., Henning, T., Chandler, C. J., Mundy, L. G., & Wilner, D. J. 2006, A&A, 446, 211

Saito, M., Kawabe, R., Ishiguro, M., et al. 1995, ApJ, 453, 384

Sault, R. J., Teuben, P. J., & Wright, M. C. H. 1995, in Astronomical Society of the Pacific Confer-
    ence Series, Vol. 77, Astronomical Data Analysis Software and Systems IV, ed. R. A. Shaw,
    H. E. Payne, & J. J. E. Hayes, 433

Scoville, N. Z., Carlstrom, J. E., Chandler, C. J., et al. 1993, PASP, 105, 1482

Semenov, D., Pavlyuchenkov, Y., Henning, T., Wolf, S., & Launhardt, R. 2008, ApJ, 673, L195

Simon, M., Dutrey, A., & Guilloteau, S. 2000, ApJ, 545, 1034

Testi, L., Natta, A., Shepherd, D. S., & Wilner, D. J. 2003, A&A, 403, 323

Thi, W. F., van Dishoeck, E. F., Blake, G. A., et al. 2001, ApJ, 561, 1074

van Dishoeck, E. F., Thi, W.-F., & van Zadelhoff, G.-J. 2003, A&A, 400, L1

van Zadelhoff, G.-J., van Dishoeck, E. F., Thi, W.-F., & Blake, G. A. 2001, A&A, 377, 566

Wilner, D. J., Ho, P. T. P., Kastner, J. H., & Rodríguez, L. F. 2000, ApJ, 534, L101

Wilson, T. L. & Rood, R. 1994, ARA&A, 32, 191

Yokogawa, S., Kitamura, Y., Momose, M., & Kawabe, R. 2002, in 8th Asian-Pacific Regional Meeting, Volume II, ed. S. Ikeuchi, J. Hearnshaw, & T. Hanawa, 239–240

CHAPTER 7

Abundant warm molecular gas in the disc around HD 100546

O. Panić, E.F. van Dishoeck, M.R. Hogerheijde, W. Boland, A. Baryshev, A. Belloche, R. Güsten

THE disc around Ae star HD 100546 is one of the most extensively studied discs in the southern sky. Although there is a wealth of information about its dust content and composition, not much is known about its gas and large scale kinematics. Many recent results have stressed the importance of studying both the gas and dust in discs. ^{12}CO is an excellent gas tracer in the submillimetre, and the ratio between the lines of low and high rotational levels probes the gas temperature. Emerging submillimetre facilities in the Southern hemisphere allow us to characterise the gas and dust content in objects like HD 100546 better. We observe the molecular gas toward HD 100546 using the Atacama Pathfinder Experiment telescope. The lines ^{12}CO J=7–6, J=6–5, J=3–2, ^{13}CO J=3–2 and [C I] ^{3}P$_2$–^{3}P$_1$ are observed, diagnostic of the warm disc surface layers, disc size, chemistry, and kinematics. We use parametric disc models that reproduce the low-J ^{12}CO emission from Herbig Ae stars well. With the help of a molecular excitation and radiative transfer code we fit the observed spectral line profiles. We find that ≈0.01 M$_\odot$ of molecular gas is present within 400 AU from the star, based on the observed optically thick ^{12}CO lines, consistent with the dust continuum fluxes in the literature. The lines arise from gas at 20-60 K. The puzzling non-detection of the [C I] line indicates excess UV emission above that of the stellar photosphere. Asymmetry in the ^{12}CO line emission suggests that one side of the disc is slightly colder than the other. A plausible scenario is an asymmetry in the structure of the inner 200 AU of the disc, affecting the heating of the outer disc. We also consider pointing offsets and asymmetry in the disc extent as possible, but unlikely scenarios. We exclude foreground or extended emission as a cause of line asymmetry.

7.1 INTRODUCTION

Over the past decade our understanding of the structural and physical properties of discs around young stars has increased from basic theoretical modeling of the spectral energy distributions (SEDs) constrained by observations with no spatial information, to modelling based on not only the SEDs, but also spatially resolved dust observations, like scattered light images and interferometry (Pinte et al. 2008; Tannirkulam et al. 2008, and Chapter 3 of this thesis). Two decades ago, the first submillimetre interferometer observations resolved the molecular gas emission spatially and this allowed major progress in understanding the disc kinematics, structure and chemistry (see Beckwith & Sargent 1987; Koerner et al. 1993; Dutrey et al. 1994, and later work by those authors). (Sub)millimetre gas and dust emission is the ideal probe of the global disc properties, like size, mass and radial distribution of disc material, because the bulk of the disc mass is located beyond 100 AU from the star and at temperatures of only 10-50 K that dominate this part of the spectrum. Recently, disc modelling including constraints of both dust and molecular gas observations has stressed the importance of analysing the gas and dust components simultaneously, in the context each other (e.g. Wilner et al. 2003), as done in Chapters 2 and 3 of this thesis.

Until recently, observations of rotational transitions of molecules in the submillimetre regime were focused primarily on low-J emission from ^{12}CO, up to the J=3-2 line (Greaves et al. 2000; Thi et al. 2001; Qi et al. 2004; Thi et al. 2004; Dent et al. 2005a). In two of the brightest and most studies sources, TW Hya and LkCa 15, the observations of higher-J transitions of ^{12}CO were compared to the low-J lines, providing indications of the gas temperature in the intermediate-height molecular layer (van Zadelhoff et al. 2001). The physical conditions in this layer are crucial ingredients for chemical modeling of discs. van Zadelhoff et al. (2001) fit the single-dish line spectra with simplistic disc models and derive a temperature of 20-40 K in the ^{12}CO line-emitting layers of LkCa 15, and more than 40 K in TW Hya. Qi et al. (2006) analysed submillimetric interferometer observations of TW Hya in the context of a disc structure based on the accretion disc model of Calvet et al. (2002) and showed that X-ray heating of the gas is efficient in this source, in addition to the stellar radiation field. Such diagnostics of gas heating and ionisation improve our understanding of how the gas content evolves in discs.

The emerging millimetre facilities in the Southern hemisphere like the Australia Telescope Compact Array (ATCA) and the Atacama Pathfinder EXperiment (APEX) are opening the window towards the star-forming regions of the Southern sky and are well suited to study the circumstellar discs in these regions. These instruments also pave the path for future observations with the Atacama Large Millimeter / Submillimeter Array (ALMA), which will drastically improve our knowledge of disc structure and evolution. We use the APEX receivers APEX-2a and CHAMP^{+1} to observe the ^{12}CO J=7–6, J=6–5, J=3–2, ^{13}CO J=3–2 and [C I] ^{3}P$_2$–^{3}P$_1$ line emission towards the disc around the young intermediate-mass star HD 100546. A wealth of observations of dust in this bright disc (Waelkens et al. 1996; Malfait et al. 1998; Grady et al.

---

[1]CHAMP+ was constructed with funds from NWO grant 600.063.310.10.

2001; Augereau et al. 2001; Bouwman et al. 2003; Acke & van den Ancker 2006; Ardila et al. 2007) has motivated us to probe its molecular gas content and kinematics. The chosen transitions are particularly sensitive to the gas in the warm upper layers and kinematics of the outer disc. Our millimetre line observations probe the outer radius and inclination. The existing observational constraints on these parameters in the disc around HD 100546 provide an excellent basis for the analysis of our data.

HD 100546 is a young B9V type, 2.5 $M_\odot$ star, classified as a Herbig Be star due to its isolation, infrared excess and silicate emission (The et al. 1994; Malfait et al. 1998). With a distance of 103±6 pc, measured by Hipparcos, this is one of the nearest Herbig Ae/Be stars. In van den Ancker et al. (1998) the age of the star greater than 10 Myr is estimated. This makes the presence of circumstellar material intriguing, considering that the disc is expected to dissipate within 10 Myr in most young stars (e.g. Hollenbach et al. 2000; Hernández et al. 2007). Based on SED modeling, Bouwman et al. (2003) postulate the presence of an inner hole in the disk of 10 AU radius, likely caused by a ~Jupiter-sized planet (see also Acke & van den Ancker 2006). Direct evidence of cold disc material at larger radii is provided by Australia Telescope Compact Array observations of Wilner et al. (2003) at 89 GHz (3.4 mm) and 2″ resolution, with a flux of 36±3 mJy, values consistent with the 1.3 mm observations of Henning et al. (1998). They do not detect HCO^+ J=1–0 line emission and speculate that photodissociation of CO in the upper disc layers or an overall gas depletion may be the reason for this. In the recent spectroastrometric observations of rovibrational ^{12}CO transitions, van der Plas et al. (2009) suggest that ^{12}CO is depleted from the inner disc regions (up to 30 AU from the star).

Scattered light imaging of HD 100546 reveals the disc extending up to 4″ from the star viewed at an inclination of 50°, and an interesting disc structure resembling spiral arms (Pantin et al. 2000; Augereau et al. 2001; Grady et al. 2001). This structure was interpreted as due to disc perturbation by a companion (Quillen et al. 2005) and by a warped disc structure (Quillen 2006). Coronographic imaging by Augereau et al. (2001) finds steep surface brightness profiles in the environment of HD 100546 indicative of optically thin emission in the near-infrared, suggesting surface densities as low as 10^{-3} g cm^{-2}. Their images trace the emission of small dust ($< 5\,\mu$m), extending out to 800 AU from the star. The authors suggest the presence of an optically thick disc and an optically thin flattened halo or envelope.

In Sect. 7.2 we present our observations of the ^{12}CO, ^{13}CO, and [C I] lines. All ^{12}CO and ^{13}CO lines are detected while the [C I] remains undetected, and we model the lines in Sect. 7.3 deriving disc gas temperatures.

7.2   OBSERVATIONS AND RESULTS

The observations of ^{12}CO J=6–5 at 691.472 GHz and [C I] ^{3}P$_2$–^{3}P$_1$ ([C I] J=2–1 from here on) at 809.344 GHz towards HD 100546 at $11^h33^m25^s\!.4$ and Dec= $-70°11'41''$ (J2000) were obtained simultaneously with the CHAMP$^+$ heterodyne array receiver (Güsten et al. 2008) on APEX on 2008 November 11. The 7 pixels in each wavelength band are arranged in a hexagon of 6 pixels around one central pixel pointed towards the source,

Line	I	$FWHM$
	(K km s^{-1})	(km s^{-1})
^{12}CO J=7–6	12.2±1.9	4.2
^{12}CO J=6–5	10.5±0.9	4.2
^{12}CO J=3–2	4.0±0.6	4.0
^{13}CO J=3–2	1.3±0.6	–
[C I] J=2–1	<1.5	–

Table 7.1: Observed ^{12}CO J =6–5 and J =3–2 line integrated line intensities, $I = \int T_{mb} \, dv$, and line widths $FWHM$. The upper limit on the [C I] line is a 2σ value.

with beam sizes of 9″ at 690 GHz and 7.7″ at 810 GHz. The data were obtained in a staring mode with a chop of 120″. The backend consisting of Fast Fourier Transform Spectrometer units on all pixels was used, providing a spectral resolution of 0.12 MHz or 0.05 km s^{-1} at these frequencies. Main beam efficiencies are 0.56 at 690 GHz and 0.43 at 810 GHz. The calibration is uncertain by ≈30% at both frequencies. Pointing was performed directly prior to the observations providing an accuracy better than 3″. The CO J=6–5 line was also obsered on 2008 November 10 in jiggle mode and its intensity and spectral profile were found to be the same within 20%. During this observation, the high band was tuned to ^{12}CO J=7–6 at 806.665 GHz. The ^{12}CO J=6–5 data taken on 2008 November 11 are used in the further analysis.

The ^{12}CO and ^{13}CO J=3–2 lines at 345.796 GHz and 330.588 GHz, respectively, were observed on 2005 July 27 and 28 with the APEX-2a receiver using a single pointing. The spectral resolution of these data is 61 kHz or 0.05 km s^{-1}. The beam size and efficiency of APEX at 346 GHz are 14″ and 0.73, respectively. Our ^{12}CO J=3–2 line data was presented in Chapter 5 of this thesis.

We have detected all the observed molecular line transitions, but not the [C I] J=2–1 line. Figure 7.1 shows the observed spectra, baseline subtracted, corrected for the beam efficiency and re-binned to a lower spectral resolution. The ^{12}CO J=3–2 and J=6–5 lines are detected at the highest signal to noise ratio, and show a double peaked profile characteristic of disc rotation. The intensities integrated over the velocity range 0–10 km s^{-1}, over which line emission is detected, are listed in Table 7.1 together with the full width at half-maximum of the lines with sufficiently well defined profiles.

In addition to the observations towards the source, the CHAMP$^+$ array provides measurements at nearby offsets. This setup provides an excellent way to discern the emission from the disc, with an estimated size of 400 AU in radius (Augereau et al. 2001), from the surrounding material known to be present further away from the star. The central pixel of our CHAMP$^+$ data probes the ^{12}CO J=6–5 line emission from the region of 9″ centered on the position of the star (450 AU radius), while the surrounding pixels probe the more distant regions (roughly 1000–2000 AU). Similarly, at the frequency of the ^{12}CO J=7–6 line a smaller region around the star of 7.7″ is probed with the central pixel (390 AU radius), and regions roughly 1000–2000 AU with the surrounding pixels. Table 7.2 provides an overview of the pixel positions and the corresponding fluxes integrated from a velocity range from 0 to 10 km s^{-1}, over which the

	^{12}CO J=6–5	9″ beam		^{12}CO J=7–6	7.7″ beam
RA offset	Dec offset	$I_{CO(6-5)}$	RA offset	Dec offset	$I_{CO(7-6)}$
(″)	(″)	(K km s^{-1})	(″)	(″)	(K km s^{-1})
-9.8	-17.0	0.4 ± 0.2	+10.2	-17.0	< 2.0
+8.8	-18.0	0.5 ± 0.2	+20.2	-1.4	< 2.0
-18.9	-0.2	< 0.2	-9.0	-16.5	< 2.0
+19.4	-1.2	< 0.2	+11.0	+16.2	< 2.0
-9.3	+16.6	< 0.2	-18.8	+0.2	< 2.0
+10.0	+16.6	< 0.2	-9.1	+16.9	< 2.0

Table 7.2: Observed ^{12}CO J =6–5 and J =7–6 intensities integrated over avelocity range of 0–10 km s^{-1}, for each pixel of the CHAMP$^+$ heterodyne array.

^{12}CO lines are firmly detected in the central pixel. Compared to the on-source fluxes, these measurements clearly show that the ^{12}CO emission from the surrounding material is about 20 times weaker than from the region within 400 AU from the star.

The ^{12}CO J=3–2 line was observed with a single pointing of the beam of 14″, large enough to include any emission from regions beyond 400 AU. However, the strong resemblance in the line profile suggests that both low-J and high-J lines arise from the disc and that any contribution to the line emission by an extended low-temperature and low-velocity component is negligible. An extended envelope around HD 100546 extending to radii of 800 AU has been suggested based on optical imaging by Grady et al. (2001). However, considering the low dust density in the envelope, photodissociation of the molecular gas is expected to be efficient, resulting in largely atomic gas that does not contribute significantly to the ^{12}CO line flux. Concidering this, it is puzzling that [C I] line emission is not detected in any of the CHAMP$^+$ beams.

Our data clearly show presence of warm molecular gas in the region extending up to several hundred AU from the star (450 AU for the 6–5 line and 700 AU for the 3–2 line). We obtain the following integrated intensity ratios, corrected for beam dilution: ^{12}CO lines (6–5)/(3–2)=1.0±0.2 and (^{12}CO 3–2)/(^{13}CO 3–2)=2.8±0.5.

There is a clear asymmetry in the profile of the ^{12}CO lines, observed at a high signal-to-noise ratio. In some sources, asymmetries like this are explained through confusion with cloud emission, as seen in ^{12}CO lines towards IM Lup (van Kempen et al. 2007) and DL Tau (Simon et al. 2000). Also, such asymmetry is seen in ^{12}CO lines from sources with a pronounced disc asymmetry, like HD 141569 (Dent et al. 2005b). Another possibility is a pointing offset along the disc major axis. In the following section we investigate these and other possible causes of the observed line asymmetry.
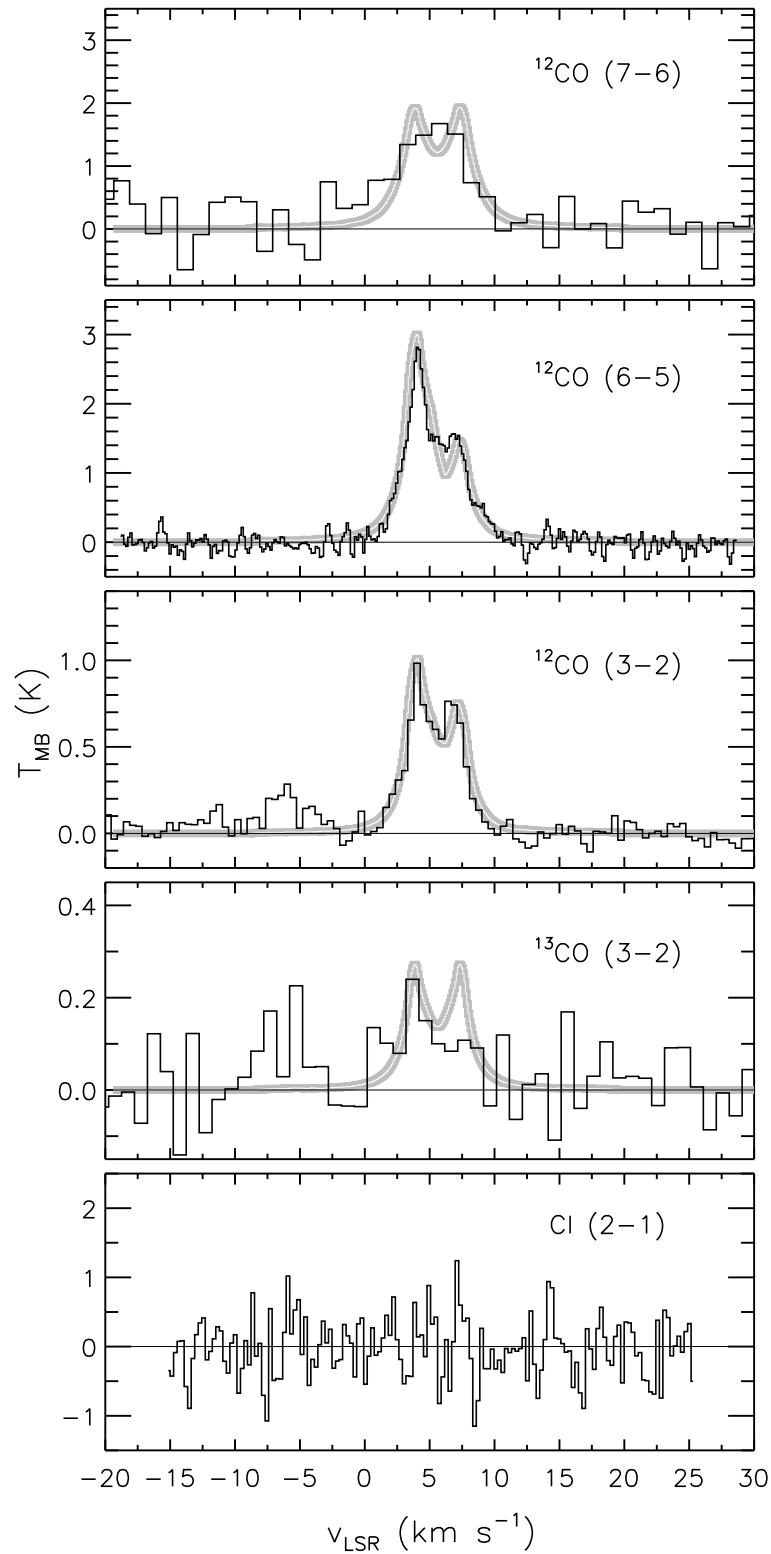
Figure 7.1: Spectra of the ^{12}CO and ^{13}CO submillimetre lines observed towards HD 100546, compared to our best fit models.

7.3 DISCUSSION

7.3.1 CO line emission

The ^{12}CO J=3–2 and J=6–5 line emission from circumstellar discs is generally optically thick and arises from warm upper disc layers. These lines are particularly sensitive to the temperature of these layers, and therefore to the stellar and external illumination of disc surface. The line ratio of (^{12}CO 3–2)/(^{13}CO 3–2)=2.8±0.5 indicates that the ^{12}CO line emission is optically thick and thus that substantial amounts of molecular gas are present in the disc around HD 100546. Assuming a temperature of 20 K, densities of 10^6-10^8 cm^{-3}, and a CO/H$_2$ abundance of 10^{-4}, a column density of H$_2$ of roughly 10^{22} cm^{-2} reproduces the observed line ratio (calculation done with the RADEX online tool[2]). This column density is typical of outer regions of gas-rich discs. The low ^{13}CO line flux may be in part due to freeze-out and/or selective photodissociation. Detailed modelling and spatially resolved submillimetre line observations of ^{12}CO and isotopologues would allow to constrain the disc structure better, and evaluate the effect of these processes (See Chapter 2 of this thesis).

The line emission of ^{13}CO J=3–2 is less optically thick than ^{12}CO, tracing deeper into the colder disc layers. A deeper integration of this line resulting in a higher signal-to-noise ratio would provide a better defined spectral profile. Comparison to the ^{12}CO line profile would allow us to draw conclusions on the relative spatial extent of the emission region of the two molecules and enable a more detailed modelling, including a disc vertical temperature structure and simple processes like freeze-out in the cold outer regions below disc surface layers (cf. Dartois et al. 2003).

Submillimetre ^{12}CO line emission is analysed using two different modelling approaches in the literature. Disc physical models, like the irradiated accretion disc models of D'Alessio et al. (2005), are especially well suited when the emission is spatially resolved and the three-dimensional structure of the disc can be investigated, for example when transitions of different optical depths are observed (Chapter 2 of this thesis). For spatially unresolved observations, like those presented here, simplistic models with a limited number of free parameters are more appropriate to derive some basic constraints on disc properties based on the line spectrum (Dutrey et al. 1994; Guilloteau & Dutrey 1998).

7.3.2 Disc parametric model and best-fit parameters

In Chapter 5 of this thesis, we show that simple power-law disc models, with a disc mass $M = 0.01 \, \mathrm{M}_\odot$, surface density $\Sigma \propto R^{-1}$ and temperature $T = 60 \, \mathrm{K} \, (R/100 \, \mathrm{AU})^{-0.5}$, are useful tools to analyse low-J ^{12}CO transitions from gas-rich discs around Herbig Ae stars. We use these models to fit the ^{12}CO spectra. We fix the outer radius and inclination to the observationally constrained values of 400 AU and 50° (Augereau et al. 2001). The size estimate is based on the scattered light observations and is a reliable guidance

---

[2]http://www.strw.leidenuniv.nl/~moldata/radex.html

for molecular line modeling. Without sufficient amounts of gas the dust settles to the midplane, and the disc becomes self-shadowed. As the scattered light only probes the illuminated disc surface at some height above the midplane, it provides a lower limit to the actual size of the disc. The inner radius is assumed to be 0.6 AU, close to the dust sublimation radius. Although an inner hole of 13 AU is found in HD 100546, its presence does not affect our results because the molecular lines observed are dominated by the outer disc regions, far beyond inner tens of AU. The surface density is given by a powerlaw $\Sigma \propto R^{-1}$, and the temperature $T = T_{100} \left(R/100\,\mathrm{AU}\right)^{0.5}$, where T_{100} is a free parameter. The disc models are vertically isothermal, and the vertical density structure is calculated assuming hydrostatic equilibrium. The ^{12}CO abundance with respect to H_2 is assumed to be 10^{-4}, constant throughout the disc. Because the observed ^{12}CO lines trace warm molecular material and are insensitive to the colder regions deeper in the disc, it is reasonable to neglect freeze-out in these calculations.

For the estimated disc mass and observed ^{12}CO/^{13}CO line ratio, the observed ^{12}CO lines are optically thick, with a H_2 surface density of 10^{22} cm^{-2}. The evident line asymmetry mentioned in Sect. 7.2 cannot be fit by assuming different densities at the two sides of the disc, because the optically thick ^{12}CO lines are insensitive to the column density.

For the optically thick ^{12}CO lines, the temperature and the outer radius determine the line intensity, and any asymmetry in either of these two parameters affects the emerging line profile. We consider these two possibilities separately.

^{12}CO J=6–5 and J=3–2 line profile fit

Temperature asymmetry. In this scenario we consider that the observed line asymmetry is caused by a temperature asymmetry in the disc, with one side of the disc colder than the other. We use different T_{100} parameters for the two sides of the discs, separated by the minor axis. These two sides contribute almost exclusively to the two respective sides of the spectral line (with respect to the line centre at 5.6 km s^{-1}). The radial density structure is determined by our assumed disc mass, outer radius and surface density power-law. Some difference in the disc vertical thickness may be present as a result of different temperatures at the two sides, but this difference is negligible and the resulting spectra are insensitive to it.

We use the molecular excitation and radiative transfer code RATRAN (Hogerheijde & van der Tak 2000) to calculate the line emission from the model. In these calculations, Keplerian rotation of the disc around a 2.5 $M_\odot$ star and a disc inclination of 50° (0° corresponding to face-on) are assumed. Dust continuum emission, although negligible for the molecular line transfer, is included in the calculation and subtracted from the final image cubes. The calculated emission is convolved with the corresponding beam size, and the spectra toward the image centre extracted.

We obtain the best fit to the ^{12}CO J=6–5 spectrum by assuming values of T_{100} of 40 and 60 K for the two disc sides, respectively. The ^{12}CO J=3–2 spectrum is fitted assuming 40 and 50 K, where the difference in temperature contrast may be explained by (part of) the ^{12}CO 3–2 emission originating from deeper layers in the disc. The corresponding synthetic spectra are compared to the observations in Fig. 7.1. The tem-
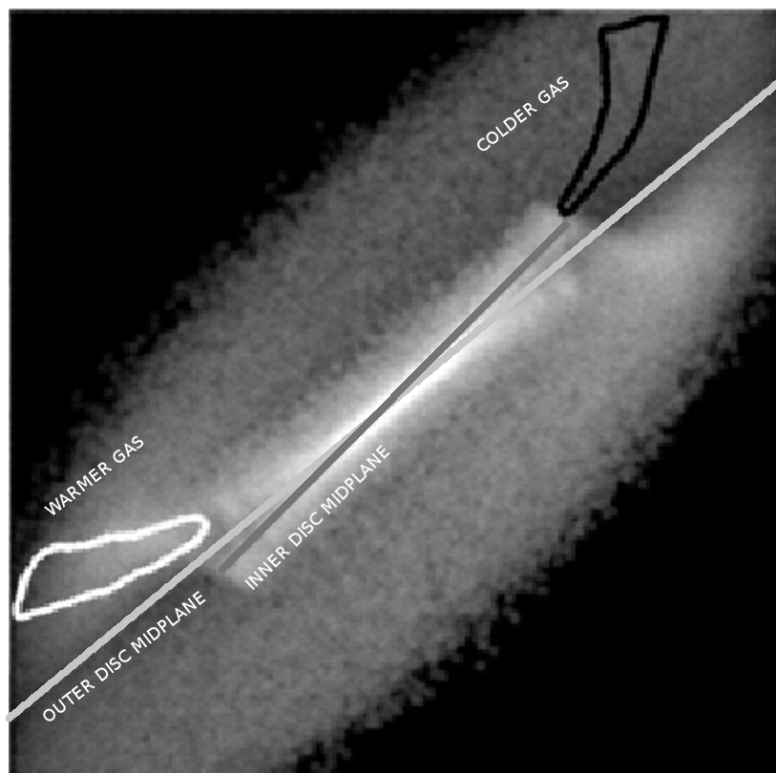
Figure 7.2: Illustration of a warped disc structure, in an edge-on projection. Straight light and dark grey lines show the plane of the disc and of the inner warped disc component, respectively. The white curve shows the surface region with a higher temperature, heated well by the star, and the black curve shows the cooler region partly obscured by the warp. The image of the disc with a 400 AU radius is adapted from Quillen (2006), where a detailed warped disc model is presented.

peratures of 40–60 K compare well to the theoretical predictions of the temperature in the regions where these lines saturate in discs (see Fig. 6 in van Zadelhoff et al. 2001). The difference in temperature between the two sides of the disc may be explained by a warped inner disc, as illustrated in Fig. 7.2, with the elevated side of the inner disc intercepting a fraction of stellar light that would otherwise reach the outer disc, while the opposite side is slightly more illuminated, with the inner part of the disc shifted downwards. The possibility of an inner warp is suggested by Quillen (2006) for HD 100546, with an inner component extending up to 200 AU inclined by $\approx 15°$ with respect to the outer component extending beyond that radius.

The temperature asymmetry is possible also if the disc has a different thickness at the two sides. This may happen in a disc with dust settling underway, or if a planet or another body embedded in the disc stirs up the dust. In this case the 'stirred up' part of the disc intercepts more stellar light and becomes somewhat warmer. A companion body in HD 100546 is suggested in the literature, to explain the observed inner hole, gas kinematics, and spiral arms (Bouwman et al. 2003; Acke & van den Ancker 2006; Quillen et al. 2005).

Asymmetry in the disc spatial distribution. If one side of the disc extends slightly further out than the other (e.g., on the SE side), the increase in disc surface at that side will contribute to the line flux at one side of the spectral line causing line asymmetry. This may be a plausible explanation for the 3–2 line, but not the observed 6–5 line with a 9″ beam size, unless the asymmetry is within 450 AU. Such an asymmetry may affect

the scattered light images of HD 100546, with the disc extending further to the SW than to the NE of the star. However this is not seen in the observations of Augereau et al. (2001). Furthermore, the additional emission from this region would dominate the frequencies closer to the line centre, and not the redshifted peak.

Disc density asymmetry. A different density on the two sides of the disc, with one side significantly denser than the other, may cause asymmetry in the molecular line emission. This scenario only applies if the observed line emission is at least marginally optically thin and thus sensitive to the disc midplane density. This seems unlikely, given the ratio between ^{12}CO and ^{13}CO J=3–2 lines, unless the isotopic fractionation is pronounced in this disc. If we decrease the disc mass to allow the ^{12}CO line emission in our models to be sensitive to the density variations in the midplane, we would have to assume a lower temperature in the calculations, close to the temperature in the disc midplane (10–30 K in the outer disc). While the asymmetry in the line profile could be reproduced in this way, the observed line intensity would be underestimated.

Pointing offset A systematic pointing offset of APEX towards the SE of δRA=1$\farcs$1 and δDec=$-$1$\farcs$6, well within the measured pointing accuracy of 3$''$, may cause a line asymmetry as observed in the ^{12}CO J=3–2 and J=6–5 lines. Figure 7.3 shows the comparison between the observed spectra of the two lines and the spectra extracted from axially symmetric models using the abovementioned offset. The T_{100} parameter in these models is 50 K for the ^{12}CO J=3–2 and 60 K for the J=6–5 line. To explain the observations, the 1$\farcs$9 pointing offset would need to be present in both our 2005 and 2008 data, thus consistent over a three year period. Given that the pointing model of the APEX telescope has been significantly improved over the period between the two observations, a consistent, systematic pointing error is unlikely. The stellar coordinates are also known to better than the required offset. Finally, in our APEX jiggle map obtained on 2008 November 10, the asymmetric profile corresponds to the pixel with the largest integrated intensity. We therefore conclude that a pointing offset is an unlikely explantion for the observed asymmetry, but cannot entirely rule out the possibility. Only future interferometric observations of this source can answer whether the apparent asymmetry is real or due to a pointing offset.

^{13}CO J=3–2 and ^{12}CO J=7–6 line fit

The ^{13}CO J=3–2 spectrum is suggestive of asymmetry, but the difference between the line intensity at the expected location of the two peaks is within the noise level. This line arises from denser and colder disc layers, distinct to those traced by the high-J transitions. A temperature asymmetry in the upper layers is unlikely to have a detectable effect on the temperature deeper in the disc, and it is likely that any future, high-sensitivity observations of optically thin CO isotopologue emission, C^{18}O for example, will reveal symmetric line profiles.

As in the calculations of Sect. 7.3.2, we use the RATRAN code, including Keplerian rotation and a disc inclination as above. No freeze-out is included. We adopt a constant ^{13}CO abundance, assuming an isotopic ratio [^{12}C]/[^{13}C]=77 (Wilson & Rood 1994). We fit the ^{13}CO J=3–2 spectrum assuming an axially symmetric temperature structure, with T_{100}=25 K. The comparison of the synthetic spectrum from our best-fit model to
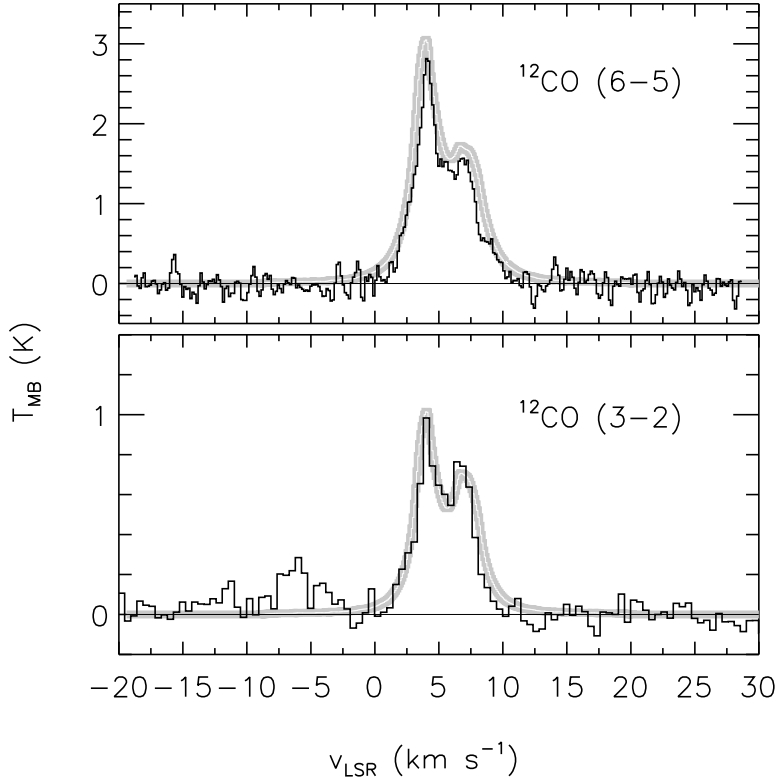
Figure 7.3: Spectra of the ^{12}CO J=3–2 and J=6–5 lines observed towards HD 100546, compared to the spectra from symmetric models with a pointing offset of δRA=1.″1 and δDec=-1.″6.

the observed one is shown in Fig. 7.1.

The ^{12}CO J=7–6 is fit with T_{100}=50 K, close to the temperatures used to fit the J=6–5 lines. These two transitions are energetically close and our data are consistent with the expectation that they should trace the same disc layers. The ^{12}CO J=7–6 line profile is therefore likely asymmetric, but this asymmetry is hiden in the noise of our observations.

7.3.3 ^{12}CO line ratios

As discussed in Sect. 7.2, the observed CO 6–5/3–2 integrated intensity ratio is 1.0 $\pm$ 0.2 when the observations are scaled to the same beam. This is a factor of 2 higher that the ratios of $\sim$0.5 found for the discs around the T Tauri stars LkCa 15 and TW Hya by van Zadelhoff et al. (2001) and Qi et al. (2006). The TW Hya 6–5/3–2 ratio has been interpreted as proof that the gas temperature is higher than that of the dust in the surface layers where gas and dust are not thermally coupled. Both UV radiation and X-rays have been invoked to provide the additional gas heating (Jonkheid et al. 2004; Kamp & Dullemond 2004; Glassgold et al. 2004; Nomura & Millar 2005; Gorti & Hollenbach 2008).

The higher ratio found for HD 100546 implies higher gas temperatures than for the T Tauri disks. This is expected based on models where most of the gas heating comes from UV radiation from the central star, since the cooler stars simply have less

UV radiation (e.g. Woitke et al. 2009). The gas temperature is also strongly affected by the PAH abundance in the disc. PAH features are seen prominently in the HD 100546 mid-infrared spectrum (e.g. Malfait et al. 1998), and have been shown to be spatially extended across the disk (Geers et al. 2007). In contrast, neither of the two T Tauri disks show PAH emission, implying typical PAH abundances a factor of 10–100 lower (Geers et al. 2006).

For the specific case of Herbig Ae disks, Jonkheid et al. (2007) have computed the gas heating and chemistry as well as the resulting CO 6–5 and 3–2 line emission starting from a set of dust disk models developed by Dullemond & Dominik (2005). Models with decreasing disk mass from 10^{-1} to 10^{-4} M$_\odot$ and and decreasing dust/gas ratios from 10^{-2} to 10^{-6} (simulating grain growth and settling) were investigated. For Herbig stars, X-rays can be neglected (Kamp et al. 2008), so all the heating is through UV radiation. The UV radiation field was taken to be that of a B9.5 star, very close to that expected for HD 100546. An accurate treatment of the shape of the UV field at short wavelengths, < 1100 Å, is very important for a correct calculation of the CO photodissociation and atomic carbon photoionization rates, since the UV intensity of a B9 star is orders of magnitude weaker in this wavelength range than the (scaled) standard interstellar radiation field. The PAH abundance is taken to follow the dust/gas ratio, with an abundance of 10^{-7} for a normal dust/gas ratio=100.

The resulting ^{12}CO J =6–5/3–2 integrated intensity ratios computed by Jonkheid et al. (2007) summed over the entire model disk are remarkably close to unity for the entire range of disk parameters investigated. The absolute ^{12}CO and ^{13}CO intensities for model B2 – a disk with a mass of 0.01 M$_\odot$ with a standard gas/dust ratio of 100, appropriate for HD 100546 – are also within 40% of the observed values when scaled to the same source distance and beam size, indicating a good agreement between models and observations.

7.3.4   Implications of the [C I] J=2–1 non-detection

Figure 1 includes the high-quality spectrum around the [C I] J=2–1 line at 809.344 GHz. No significant feature is detected down to 0.3 K rms in a 0.27 km s^{-1} velocity bin, implying a limit on the integrated intensity of ≈ 1.5 K km s^{-1} over the range 0-10 $km\ s^{-1}$ (same width as for the detected ^{12}CO lines). Model B2 of Jonkheid et al. (2007) predicts integrated [C I] intensities, scaled to the distance of HD 100546, around 15–20 K km s^{-1}. whereas the model intensities are even larger in disks with significant grain growth and settling (BL model series). Thus, while the CO data appear entirely consistent with their sophisticated UV-heated disk atmosphere models, the [C I] data are clearly discrepant by an order of magnitude.

One possible solution could be that the radiation field contains more carbon ionizing photons than assumed here, shifting the chemical balance from neutral to ionized atomic carbon. Indeed, the predicted [C II] line intensities for the model disks of Jonkheid et al. (2007) are very low, < 0.1 K km s^{-1}, whereas they are more than an order of magnitude higher for disks around T Tauri stars with excess UV emission (Jonkheid et al. 2004). Such excess of UV emission could come from the disk-star accre-

tion boundary layer. Indeed, HD 100546 is observed to undergo significant accretion, in spite of the known (dust) gap in the inner disk (Vieira et al. 1999). Searches for the [C II] line with the HIFI instrument on the Herschel Space Observatory can test this scenario. In this case, the [C I] line intensity and the [C II]/[C I] line ratio could be a diagnostic of the presence of excess UV emission over that of the stellar photosphere.

7.3.5   Implications for the dust continuum emission

Our assumed gas mass of 0.01 M$_\odot$ corresponds to 10^{-4} M$_\odot$ of dust adopting a gas-to-dust mass ratio of 100. To calculate continuum fluxes, we assume that the dust emission is optically thin and arises at temperatures close to 25 K, the 100 AU temperature found to fit the ^{13}CO line emission well. With these parameters, the dust continuum flux at 3.4 mm of 36 mJy reported in the observations of Wilner et al. (2003) at 2″ resolution and the flux at 1.3 mm of 690 mJy reported by Henning et al. (1998) at 23″ resolution can both be fitted with a dust emissivity $\kappa_{1.3\,\mathrm{mm}} = 0.1 \times (1.3\,\mathrm{mm}/\lambda\,(\mathrm{mm}))^{0.9}$, representative of grain growth to sizes of 100 cm in discs (Draine 2006). A shallow slope of the emissivity of $\beta \approx 1.0$ is also suggested by Wilner et al. (2003).

7.4   CONCLUSIONS

We summarise our conclusions as follows:

- We present evidence for abundant warm molecular gas associated with the disc around HD 100546, in regions within 400 AU from the star, successfuly separated from more extended material in our CHAMP$^+$ observations;

- The gas kinematics are consistent with Keplerian rotation around an 2.5 M$_\odot$ star in a disc with a 400 AU radius, viewed at an inclination of 50° from face-on;

- The ^{12}CO (6–5)/(3–2) line ratio of 1.0±0.2 is a factor of two higher than measured towards discs around T Tauri stars;

- Line asymmetry seen in the ^{12}CO J=6–5 and J=3–2 lines can be explained by a temperature asymmetry, with one side of the disc slightly colder than the other, possibly due to a partial obscuration of one side by a warped inner disc or a high disc rim, but a systematic pointing offset of the telescope is also possible;

- Our data are consistent with a total disc mass of 0.01 M$_\odot$. We exclude the possibility of a low-density disc and optically thin ^{12}CO emission, as the disc midplane temperature is insufficient to reproduce the observed line intensities. Furthermore, efficient freeze out would limit the emission to a much smaller radius, altering the line profile.

- The puzzling non-detection of [C I] J=2–1 line may indicate efficient photoionisation.

Future observations with ALMA will be crucial to characterise the disc around HD 100546, spatially resolve its kinematics and structure. In particular, such observations will allow a detailed comparison between the spatial distribution of the gas traced by rotational transitions of ^{12}CO and its isotopologues, and the dust traced by millimetre continuum emission.

REFERENCES

Acke, B. & van den Ancker, M. E. 2006, A&A, 457, 171

Ardila, D. R., Golimowski, D. A., Krist, J. E., et al. 2007, ApJ, 665, 512

Augereau, J. C., Lagrange, A. M., Mouillet, D., & Ménard, F. 2001, A&A, 365, 78

Beckwith, S. & Sargent, A. 1987, in IAU Symposium, Vol. 122, Circumstellar Matter, ed. I. Appenzeller & C. Jordan, 81–83

Bouwman, J., de Koter, A., Dominik, C., & Waters, L. B. F. M. 2003, A&A, 401, 577

Calvet, N., D'Alessio, P., Hartmann, L., et al. 2002, ApJ, 568, 1008

D'Alessio, P., Merín, B., Calvet, N., Hartmann, L., & Montesinos, B. 2005, Revista Mexicana de Astronomia y Astrofisica, 41, 61

Dartois, E., Dutrey, A., & Guilloteau, S. 2003, A&A, 399, 773

Dent, W. R. F., Greaves, J. S., & Coulson, I. M. 2005a, MNRAS, 359, 663

Dent, W. R. F., Greaves, J. S., & Coulson, I. M. 2005b, MNRAS, 359, 663

Draine, B. T. 2006, ApJ, 636, 1114

Dullemond, C. P. & Dominik, C. 2005, A&A, 434, 971

Dutrey, A., Guilloteau, S., & Simon, M. 1994, A&A, 286, 149

Geers, V. C., Augereau, J.-C., Pontoppidan, K. M., et al. 2006, A&A, 459, 545

Geers, V. C., van Dishoeck, E. F., Visser, R., et al. 2007, A&A, 476, 279

Glassgold, A. E., Najita, J., & Igea, J. 2004, ApJ, 615, 972

Gorti, U. & Hollenbach, D. 2008, ApJ, 683, 287

Grady, C. A., Polomski, E. F., Henning, T., et al. 2001, AJ, 122, 3396

Greaves, J. S., Mannings, V., & Holland, W. S. 2000, Icarus, 143, 155

Guilloteau, S. & Dutrey, A. 1998, A&A, 339, 467

Güsten, R., Baryshev, A., Bell, A., et al. 2008, in Presented at the Society of Photo-Optical Instrumentation Engineers (SPIE) Conference, Vol. 7020, Society of Photo-Optical Instrumentation Engineers (SPIE) Conference Series

Henning, T., Burkert, A., Launhardt, R., Leinert, C., & Stecklum, B. 1998, A&A, 336, 565

Hernández, J., Calvet, N., Briceño, C., et al. 2007, ApJ, 671, 1784

Hogerheijde, M. R. & van der Tak, F. F. S. 2000, A&A, 362, 697

Hollenbach, D. J., Yorke, H. W., & Johnstone, D. 2000, Protostars and Planets IV, 401

Jonkheid, B., Dullemond, C. P., Hogerheijde, M. R., & van Dishoeck, E. F. 2007, A&A, 463, 203

Jonkheid, B., Faas, F. G. A., van Zadelhoff, G.-J., & van Dishoeck, E. F. 2004, A&A, 428, 511

Kamp, I. & Dullemond, C. P. 2004, ApJ, 615, 991

Kamp, I., Freudling, W., Robberto, M., Chengalur, J., & Keto, E. 2008, Physica Scripta Volume T, 130, 014013

Koerner, D. W., Sargent, A. I., & Beckwith, S. V. W. 1993, Icarus, 106, 2

Malfait, K., Waelkens, C., Waters, L. B. F. M., et al. 1998, A&A, 332, L25

Nomura, H. & Millar, T. J. 2005, A&A, 438, 923

Pantin, E., Waelkens, C., & Lagage, P. O. 2000, A&A, 361, L9

Pinte, C., Padgett, D. L., Ménard, F., et al. 2008, A&A, 489, 633

Qi, C., Ho, P. T. P., Wilner, D. J., et al. 2004, ApJ, 616, L11

Qi, C., Wilner, D. J., Calvet, N., et al. 2006, ApJ, 636, L157

Quillen, A. C. 2006, ApJ, 640, 1078

Quillen, A. C., Varnière, P., Minchev, I., & Frank, A. 2005, AJ, 129, 2481

Simon, M., Dutrey, A., & Guilloteau, S. 2000, ApJ, 545, 1034

Tannirkulam, A., Monnier, J. D., Harries, T. J., et al. 2008, ApJ, 689, 513

The, P. S., de Winter, D., & Perez, M. R. 1994, A&AS, 104, 315

Thi, W. F., van Dishoeck, E. F., Blake, G. A., et al. 2001, ApJ, 561, 1074

Thi, W.-F., van Zadelhoff, G.-J., & van Dishoeck, E. F. 2004, A&A, 425, 955

van den Ancker, M. E., de Winter, D., & Tjin A Djie, H. R. E. 1998, A&A, 330, 145

van der Plas, G., van den Ancker, M. E., Acke, B., et al. 2009, A&A, 500, 1137

van Kempen, T. A., van Dishoeck, E. F., Brinch, C., & Hogerheijde, M. R. 2007, A&A, 461, 983

van Zadelhoff, G.-J., van Dishoeck, E. F., Thi, W.-F., & Blake, G. A. 2001, A&A, 377, 566

Vieira, S. L. A., Pogodin, M. A., & Franco, G. A. P. 1999, A&A, 345, 559

Waelkens, C., Waters, L. B. F. M., de Graauw, M. S., et al. 1996, A&A, 315, L245

Wilner, D. J., Bourke, T. L., Wright, C. M., et al. 2003, ApJ, 596, 597

Wilson, T. L. & Rood, R. 1994, ARA&A, 32, 191

Woitke, P., Kamp, I., & Thi, W.-F. 2009, A&A, 501, 383

Nederlandse Samenvatting

I N de afgelopen 15 jaar zijn door astronomen veel planeten ontdekt rond sterren. Het aantal groeit nog steeds, tot inmiddels circa 300 planeten. Dit zijn meestal grote planeten, zoals Jupiter, omdat een grotere planeet makkelijker te detecteren is. Maar er zijn redenen om aan te nemen dat kleine planeten, zoals de Aarde of Mars, niet zeldzaam zijn. Een van de laatste sensationele ontdekkingen is de planeet genaamd Fomalhaut b, in beeld gebracht in zijn baan binnen de schijf rond de ster Fomalhaut (Fig. 8.1).

Planeten worden gevormd in een gigantische schijf van gas en kleine stofdeeltjes die draait rond een jonge ster, honderden keren groter dan de afstand zon–aarde[1]. Hoe dit process precies werkt en waarom niet alle sterren schijven of planeten hebben, is een van de grootste motivaties om naar jonge sterren te kijken met heel geavanceerde instrumenten: telescopen werkzaam van optische golflengtes tot het radio gebied. Figuur 8.2 laat een artistieke interpretatie van zo'n schijf van gas zien, met stofbrokken en planeten die rond de ster draaien. Op de kaft van dit proefschrift staat een schilderij van de Spaanse kunstenaar Miquel Barceló geïnspireerd door de sterrenkunde en genoemd 'Konstelatie'. Dit schilderij zie ik echt als een protoplanetaire schijf: stofdeeltjes, stenen en proto-planeten draaien rond de ster in een schijf van gas. Het oppervlak van de schijf wordt belicht door de ster (gele kleur) en is niet perfect symmetrisch. Kouder materiaal binnen de schijf is geschilderd met een donkere, grijze kleur. Insekten die samen met proto-planeten rond de ster draaien, representeren de mogelijkheid voor leven: het is niet duidelijk dat deze insekten zullen overleven, net zoals het ook niet duidelijk is of leven echt kan ontstaan in de planetenstelsels die wij rond andere sterren ontdekt hebben. De vorming van planeten waar leven mogelijk is, en het ontstaan van het leven zijn delicate en complexe processen die de wetenschap niet nog volledig kan begrijpen. Met het onderzoek aan protoplanetaire schijven komen wij een klein stap verder naar het begrip van het ontstaan van de aarde en het leven.

Enerzijds wordt er veel theoretisch onderzoek gedaan om, met de kennis over stervorming die we nu hebben, te bepalen welke 'ingredienten' nodig zijn om planeten te vormen en wat de consequenties daarvan zijn voor de waargenomen schijfstructuur.

Aan de andere kant kijken astronomen met steeds meer raffineerde en precieze telescopen naar jonge sterren, schijven en planeten om te proberen te begrijpen wat voor soort ster en omgeving er nodig zijn om een zware schijf te vormen en welk soort schijf er nodig is om planeten te vormen. Helaas is het niet voldoende om naar slechts

---

[1]Eén astronomische eenheid (AE), circa 150 miljoen km
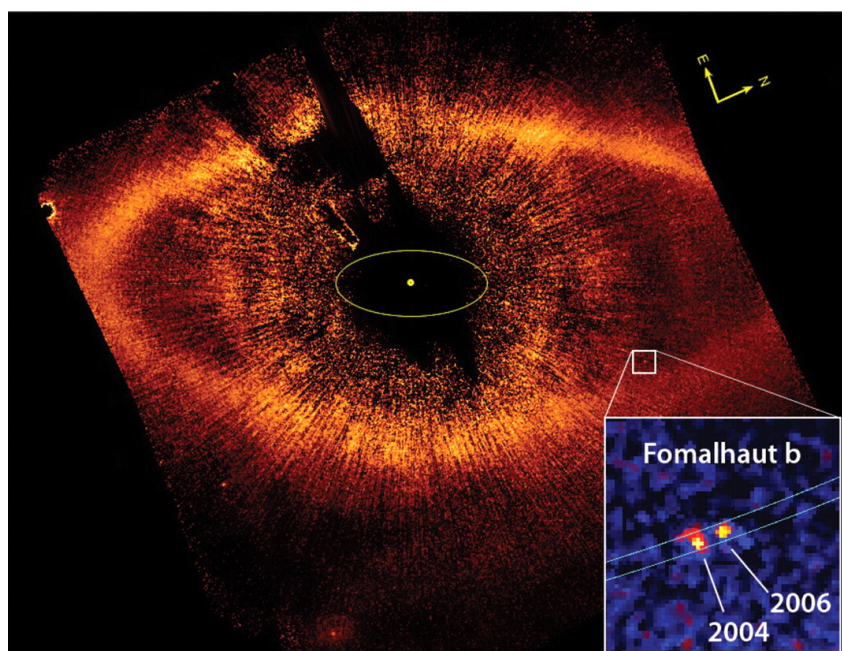
Figuur 8.1: Een voorbeeld van een planeet in een baan rond een jonge ster, Fomalhaut, op 25 lichtjaar van de aarde (Kalas et al., Science, 2008). De planeet, Fomalhaut b, is aangegeven met het witte kader. De beweging van de planeet is te zien in de inzet, waar de verschillende posities van de planeet in waarnemimgen uit 2004 en 2006 te zien is. Directe opnames zoals deze zijn een recente techniek – de meeste planeten zijn tot nu toe ontdekt via indirecte waarnemingen, door het effect van hun baanbeweging op de beweging van de ster en sterlicht.

een aantal sterren te kijken en zo de schijfevolutie te begrijpen. Er zijn jonge sterren met lichte, geëvolueerde schijven, en er zijn soms oudere sterren met nog steeds gas-rijke, primitieve schijven. Dit laat zien dat het schijfevolutie een complexe proces is, niet alleen bepaald door de ster maar ook door andere factoren zoals de stellaire omgeving, eventuele begeleiders van de ster, de initiële rotatie en magnetische velden.

    Het onderzoek in dit veld richt zich vooral op jonge sterren van lage massa, bijna zo zwaar als de zon tot enkele malen de massa van de zon[2], omdat deze ons een momentopname laten zien van de zon en het zonnestelsel toen deze nog erg jong waren.

VORMING VAN STERREN EN PLANETEN

[3] Sterren en planeten worden geboren in de ijle volken die zich overal tussen de sterren in onze Melkweg bevinden. De interstellaire volken bestaan uit gas (99% qua massa, meest waterstof en helium) en kleine stofdeeltjes (1% qua massa, vooral silicaten en koolstofachtige verbindingen) van ongeveer een tienduizendste millimeter grootte, ruim duizend keer kleiner dan een zandkorreltje op het strand. De wolken van gas en

---

[2]De massa van de zon is 1.99×10^{33} g

[3]Deze paragraaf is voornamelijk gebaseerd op de lezing van Prof.dr. E. F. van Dishoeck tijdens de 434^e dies natalis van de Universiteit Leiden, 2009.
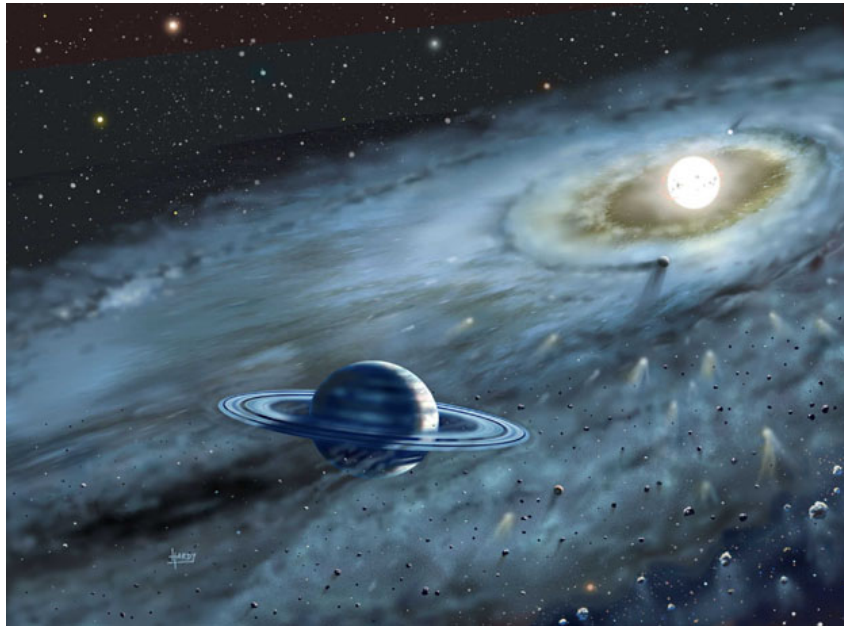
Figuur 8.2: Artistieke interpretatie van de schijf rond Fomalhaut met de planeet Fomalhaut b. Bron: D. A. Hardy, ROE, ATC, NSF, NASA.

stof tussen de sterren kunnen zichzelf maar zo'n 10 miljoen jaar in fragiel evenwicht houden, en storten op een gegeven moment onder hun eigen gewicht ineen. Hierbij ontstaat een protoster in het centrum van de wolk. In de eerste honderdduizendjaar blijft nog materiaal uit de wolk op de jonge ster regenen, waardoor deze blijft groeien. Op een gegeven moment stopt de inval omdat de wolk door de wind van de jonge ster uiteen is gedreven.

Omdat de wolk altijd wel een klein beetje hoekmoment ('draaing') heeft, kan het materiaal niet van alle kanten recht op de ster blijven vallen, maar komt het merendeel in een roterende platte schijf rond de ster terecht. Het bestaan van zulke circumstellaire schijven was al bedacht door o.a. Emmanuel Kant in 1755 omdat alle planeten in ons zonnestelsel in één vlak liggen en dezelfde kant opdraaien. Heel lang kwam men niet verder dan dit beeld van onze Oernevel. Pas zo'n 40 jaar geleden zijn meer gedetailleerde theorieën over planeetvorming ontwikkeld. In het meest gangbare scenario klitten de stofdeeltjes in de schijf aaneen tot steeds grotere rotsblokken, die uiteindelijk planeten worden. Hoe dit process gebeurt is overigens nog een raadsel: twee bakstenen blijven niet zomaar aan elkaar plakken. De meest zware protoplaneten trekken het gas aan, en vormen gasrijke planeten als Jupiter.

De schijven rond jonge sterren waarin planeten worden gevormd zijn pas zo'n 15 jaar geleden voor het eerst in beeld gebracht, ongeveer op hetzelfde moment dat de eerste exoplaneten werden ontdekt. Het heeft zo lang geduurd omdat deze schijven veel kleiner en zwakker zijn dan de wolken waaruit de sterren gevormd worden, en door het sterlicht makkelijk overstraald worden. Inmiddels is het detecteren van schijven een routineklus geworden en weten we dat vrijwel alle sterren in onze Melkweg met zo'n schijf geboren worden. Meestal bevatten ze voldoende materiaal om een zon-

nestelsel te vormen, waarvoor ongeveer 10 keer de massa van Jupiter nodig is. Voor planeetvorming, is het ook belangrijk te weten hoe de massa in de schijf gedistribueerd is, en wat de stuctuur van de schijf is. Het in kaart brengen van de structuur van de schijven is echter veel moeilijker. In dit proefschrift presenteer ik verschillende manieren om dit te doen met de beste telescopen dat ons nu ter beschikking staan. De nieuwe generatie telescopen, die ik later zal beschijven, zal onze kennis van de schijfstructuur veel verbeteren.

DIT PROEFSCHRIFT

Dit proefschrift gaat over protoplanetaire schijven die rond jonge sterren van lage massa gevonden worden.

In hoofdstuk 2 analyseren wij waarnemingen van de schijf rond de ster HD169142, die zijn gedaan met een submillimeter interferometer. De hoge ruimtelijke resolutie van deze data en de drie verschillende isotopen van CO die zijn waargenomen, zijn een krachtig middel om de drie-dimensionale structuur van de schijf te onderzoeken. Met deze methode testen wij de structuur van het schijfmodel dat gebaseerd is op straling van het stof alleen (zonder het gas). We vinden een goede overeenkomst tussen de gas- en stofstructuur van de schijf. De schijf is klein; alle massa bevindt zich vlakbij de ster en wordt daardoor verwarmd door de straling van de ster. Omdat de temperatuur hoog genoeg is, bevinden zich de meeste CO moleculen in de gasfase [4], en daarom zijn CO waarnemingen een goede maat voor de totale massa van het moleculaire gas (99% van de totale massa van de schijf). Nooit eerder was de gasmassa van een schijf zo precies bepaald. Geïnspireerd door de mogelijkheid om de gasmassa te meten, bestuderen we meer schijven rond jonge sterren van middelgrote massa zoals HD169142, in hoofdstuk 5.

In hoofdstuk 3 wordt de schijf rond de jonge, lage-massa ster IM Lup geanalyseerd middels vergelijkbare submillimeter waarnemingen als beschreven in hoofdstuk 2. In deze schijf bevinden veel CO moleculen zich voornamelijk op het oppervlak van de stofdeeltjes, zodat wij de gasmassa in deze schijf niet kunnen bepalen. Onze waarnemingen van het CO gas laten zien dat de schijfstructuur erg bijzonder is. Het is een van de grootste schijven die ooit in beeld zijn gebracht (1800 AE in diameter) en vertoont een groot verschil in dichtheid tussen de buitenste en de binnenste helft. De schijfstructuur verandert dus drastisch op een afstand van 400 AE van de ster, waarna het verder een heel lage dichtheid heeft. De ontdekking van deze unieke structuur geeft belangrijk inzicht in het vormingsproces van schijven. Zo'n dergelijke structuur zou nooit met waarnemingen van alleen stofstraling ontdekt kunnen zijn.

DoAr 21 is een erg jonge ster met een middelgrote massa, en is omringd door gas en stof die de resten zouden kunnen zijn van een geëvolueerde schijf. Het is te zwak voor submillimeter waarnemingen, zoals gedaan in de andere hoofdstukken van dit proefschrift. Wij gebruiken daarom een nieuwe waarnemingstechniek om moleculair

---

[4]In koude gebieden daarentegen vindt adsorptie van CO op het stof plaats en 'verdwijnt' de submillimeter emissielijn

Figuur 8.3: Een van de ALMA prototype antennes op locatie van de Antenna Testing Facilty in Socorro, New Mexico. Opname genomen in juli 2004. Bron: European Southern Observatory.

waterstof (H_2) te kunnen detecteren. Waterstof heeft echter geen overgangen op submillimeter golflengtes, zoals CO. Onze waarnemingen zijn daarom gedaan op meer energetische golflengtes, het infrarood. Voor het eerst is een schijf met waterstofwaarnemingen in kaart gebracht. Omdat de waarnemingen een erg asymmetrische structuur laten zien (emissie van alleen één kant van de schijf), vermoeden wij dat hier wellicht sprake is van een tweede object (een bruine dwerg met een eigen schijf), die langzaam wordt vernietigd door de zwaartekracht van DoAr 21. Schijf of geen schijf, uit onze waarnemingen blijkt dat het mogelijk is om de structuur van sommige schijven van lage massa te bepalen middels waterstofovergangen in het infrarood, iets dat niet mogelijk is in het submillimeter.

In hoofdstuk 5 bestuderen we schijven rond sterren van middelgrote massa, zoals gedaan hoofdstuk 1. Deze keer maken wij geen afbeeldingen van schijven, maar meten wij hun spectrum: de totale emissie in een klein gebied van sub-millimeter golflengtes waarop CO straalt. Ondanks dat het spectrum geen ruimtelijke dimensie heeft, kun-

nen we toch informatie over de ruimtelijke structuur verkrijgen door gebruik te maken van de rotatie van de schijf: aan de ene kant verwijdert het gas zich van ons (en domineren rode golflengtes van het spectrum door roodverschuiving) en aan de andere kant komt het gas naar ons toe (en domineren blauwe golflengtes). Met een eenvoudig model voor schijven bepalen wij hun grootte en orientatie en concluderen dat de meeste schijven (75%) klein en warm zijn, zoals HD169142 (hoofdstuk 2). Met deze informatie en vervolgwaarnemingen kunnen wij ook de schijfmassa bepalen.

In hoofdstuk 6 bestuderen wij schijven rond sterren met massa's zo laag als onze zon, en maken we een vergelijking tussen de stof- en de gasemissie in het submillimeter. Onze waarnemingen zijn niet nauwkeurig genoeg om de schijfstructuur in detail te kunnen analyseren, maar we kunnen wel de schijfemissie onderscheiden van de emissie van de gaswolk rondom de schijf, wat vaak een probleem is bij spectrale waarnemingen met een lage ruimtelijke resolutie. Met behulp van onze modellen van deze schijven concluderen wij dat deze objecten een vergelijkbare stofemissie en stofmassa hebben, maar dat de CO emissie soms heel zwak en soms juist heel sterk is. Hieruit concluderen wij dat de totale massa afgeleid uit stofemissie alléén niet voldoende is om te weten hoeveel (CO) gas er zich in de schijf bevindt, en dat waarnemingen van CO en/of andere moleculen nodig zijn.

In het laatste hoofdstuk gebruiken wij een nieuw instrument op het zuidelijke halfrond: de submillimeter emissielijn 'camera' CHAMP$^+$ op de APEX (Atacama Pathfinder EXperiment). Deze telescoop in Chili is een eerste test voor toekomstige ALMA waarnemingen (zie sectie: Toekomst met ALMA). De schijven aan de zuidelijke hemel waren tot nu toe nog niet veel bestudeerd, omdat de meeste submillimeter telescopen zich in het noordelijke halfrond bevinden. Wij kijken naar een van de helderste schijven, HD100546, en detecteren CO spectra op meerdere golflengtes in het submillimeter. Zoals genoemd in de beschrijving van hoofdstuk 5 geven deze spectra informatie over de twee kanten van de schijf. Om de asymmetrie in de gedetecteerde lijn te verklaren, denken wij dat één kant van de schijf kouder is dan de andere kant. Dit kan duiden op een asymmetrische belichting door de ster: de kant van de schijf die minder sterlicht krijgt, wordt minder warm. Toekomstige waarnemingen met ALMA zijn vereist om dit fenomeen in HD100546 verder te onderzoeken.

TOEKOMST MET ALMA

Over een paar jaren bevinden we ons in de toekomst: de langverwachte interferometer Atacama Large Millimeter/Submillimeter Array (ALMA) zal het onderzoek in het veld van ster- en planeetvorming in sneller vaarwater brengen. Wij hebben al veel ontdekt over schijven met bestaande telescopen. In dit proefschrift maken wij gebruik van nu bestaande submillimetrische interferometers - een soort mini-ALMA's met 8 tot 15 individuele antennes. ALMA zal 66 grote antennes hebben (een van die antennes is te zien in Fig. 8.3) en wordt gebouwd op een van de hoogste en droogste plekken ter aarde, precies wat dit soort instrumenten nodig heeft om de beperkende effecten van de atmosfeer op de straling zo veel mogelijk te verwijderen.

Het onderzoek aan protoplanetaire schijven is een van de velden waar onze kennis

het meest zal groeien met ALMA. Wij zullen de schijfstructuur van moleculair gas en stof in zoveel detail zien, dat het mogelijk zal zijn de effecten van planeten op de structuur, zoals gaten, direct in beeld te brengen. De grote gevoeligheid van ALMA zal het ons ook mogelijk maken de oudere schijven met weinig gas, zogenaamde 'transitionele schijven', te detecteren om zo een link te kunnen leggen tussen gas-rijke jonge schijven zoals bestudeerd in dit proefschrift, en de laatste fase van schijfevolutie: schijven zonder gas, bestaande uit grote stof-brokken, stenen en soms planetenstelsels. Een mogelijk exemplaar van een transitioneel schijf is wellicht het materiaal rond DoAr 21 dat, met andere technieken, wordt bestudeerd in hoofdstuk 4 van dit proefschrift. Met zijn grote gevoeligheid zal ALMA geschikt zijn veel nieuwe moleculen te detecteren en ons meer te leren over de chemische samenstelling van de schijven. Sommige moleculen zoals CN zijn erg afhankelijk van de straling van de ster en de effecten die straling heeft op het gas in de schijf. De hoeveelheid van deze moleculen is een belangrijke indicator voor het deel van de straling die op het schijfoppervlak valt en voor de natuurkunde die zich in de schijf afspeelt.

Curriculum Vitae

MY interest in nature and science grew with me, as my father often told me about the ways nature works, about agriculture, geology, meteorology and helped me search the sky for constellations from an astronomical atlas, one of very few publications related to astronomy in ex-Yugoslavia in the eighties. Until I was about 14 it wasn't really clear what my special gifts were as I was interested in practically everything, until my physics teacher, impressed by my explanation on why the dust sticks to the back of buses, declared I decisively had the talent for physics. I cherished the idea, and dreamed of following the path of Nikola Tesla leading to great discoveries that may change the world.

I was attending high-school in Bosnia while raging war was penetrating every aspect of the life of each person, soldier or child. The way I saw it, education was one thing that no one could deprive me of, and my way of rebelling to what was happening around me. By the time I graduated at top of the class, in 1996, my dreams and ambitions had outgrown the boundaries of the reality around me. For a few years I settled for what was possible, began undergraduate studies in Economics and worked in the OSCE[5] diplomatic mission, on the implementation of election results in the region of Eastern Bosnia. The first made it clear to me that I had to go and study abroad while through the latter I earned enough money to do so, or at least for a year. Becoming an astronomer was not on my mind, I had never heard of anyone becoming an astronomer and it was a possibility so exotic and outside-the-box that even I couldn't think of it. But as I saw Astronomy in the alphabetical list of studies at the University of Bologna (IT), I felt it was "the one" so much that I never even looked further beyond letter A.

In 2000, following a long battle to obtain an entry visa, I enrolled in the Astronomy joint BSc and MSc programme in Bologna. As soon as I had my first academic results, I discovered the magical words 'e lode' sometimes awarded with the maximum grade of an exam. Consequently, I won scholarships and fee-exemptions each year. I was dazzled by the intersection between physics, astronomy and chemistry and set to follow that line of research. In 2004 I did a small research project on "Mapping the cosmic evolution of metals in the Universe" in the University of Durham (UK). In 2005 I chose to do the MSc research project more connected to astro-chemistry, on the "Physical and chemical evolution of pre-stellar cores" at Arcetri Astrophysical Observatory in Florence (IT).

---

[5]Organisation for Security and Cooperation in Europe

I graduated cum laude the same year and not even a month later I was in the Netherlands, and begun my PhD project in Leiden. I was aspiring to work in the famous astro-chemistry group and learn from the best, but I got that and so much more. In the 4 years of my PhD I participated in 20 schools, workshops and international conferences in 9 countries. I carried out observations at the facilities of SMA and JCMT in Hawaii and CARMA in California (USA). A part of my PhD was funded through the Marie-Curie FP6 programme of the EU, and I was a member of the Molecular Universe Network bringing together experts and students in molecular astrophysics from different European countries.

I have been awarded a Fellowship of the European Southern Observatory in Garching (DE). There, I intend to pursue my protoplanetary discs' research further, and work specifically on the preparations for the great new future instrument: the Atacama Large Millimeter/Submillimeter Array (ALMA).

Acknowledgements

IN the first place, it is my family that has made me the way I am and has always given me their full support, even when it was difficult to fully grasp my unusual choices.

Mama i tata, vaša mi je podrška uvijek bila vjetar u jedrima, a sve što sam od vas naučila kormilo u rukama. Svakim danom vas sve više prepoznajem u sebi, i svaka moja pobjeda je zapravo velikim dijelom vaša.

Luis, pronto nos iremos a vivir a un tercer país que no es el tuyo. Sé lo que significa para ti estar lejos de tu ambiente y de tus familiares, y adaptarte cada vez a un sitio nuevo. Sin tu apoyo, amor y paciencia, habría sido difícil llegar hasta aquí. Pero contigo a mi lado todo lo puedo y por eso soy feliz.

Besides the co-authors' efforts, many people have helped to get the most out of the data presented in this thesis, through sharing their views, models, codes, or own data-sets and through their assistance during data-reduction. I am grateful to Christophe Pinte, Carsten Dominik, Kees Dullemond, Atilla Juhasz, Lars Kristensen, Demerese Salter, Wing-Fai Thi, Anders Johansen, Richard Alexander, Markus Hartung, Dieter Neuhäuser, Mario van den Ancker, Liesbeth Vermaas, Chris Wright, Stephane Guilloteau, Floris van der Tak, Anne Dutrey, Michel Simon, Christian Brinch, Roy van Boekel, Jeroen Bouwman, Gerrit van der Plas, Hideko Nomura, Andrea Isella and Joanna Brown.

I have enjoyed the classes and learned a lot from our Oort lecturers Prof. dr. S. Tremaine and Prof. dr. B. Draine during their stay in Leiden.

My research would't have been the same if it weren't for my current and past Leiden colleagues and our disc group meetings. It was great to work with you!

Sommige vrienden en collega's hebben door hun hulp mijn laatste werkdagen minder stressvol gemaakt, en dit betekent zoveel! Chris, Ruud, Dave en Sijme-Jan, van harte bedankt!

For their support during observing runs and hospitality, I would like to acknowledge John Carpenter and the CARMA staff, Remo Tilanus, Jan Wouterloot and others at the JCMT, the APEX and the SMA staff.

I am grateful to Paola, Malcolm and Daniele who helped me set my first steps into